Conductance of junctions of multiple interacting quantum wires and long Aharonov-Bohm-Kondo rings

by

Zheng Shi

B. Sc., Peking University, 2010

M. Sc., The University Of British Columbia, 2012

A THESIS SUBMITTED IN PARTIAL FULFILLMENT
OF THE REQUIREMENTS FOR THE DEGREE OF

Doctor of Philosophy

in

THE FACULTY OF GRADUATE AND POSTDOCTORAL STUDIES

(Physics)

The University Of British Columbia

(Vancouver)

July 2017

Abstract

In this thesis, we calculate the linear dc conductance of two types of multi-terminal interacting systems: junctions of interacting quantum wires attached to Tomonaga-Luttinger liquid (TLL) leads, and closed and open long Aharonov-Bohm-Kondo (ABK) rings. In both cases, we obtain corrections to the non-interacting Landauer formula, arising from interactions in the TLL leads and the quantum dot (QD) in the Kondo regime respectively.

In junctions of interacting quantum wires, if the wires are attached to Fermi liquid (FL) leads, the conductance is formally given by the Landauer formula with renormalized single-particle S-matrix elements. If, however, the wires are attached to TLL leads, i.e. the interaction does not vanish even in the leads, the conductance has an additional contribution dependent on the interaction strength in the leads. We calculate this additional contribution both at the first order in interaction and in the random phase approximation (RPA), and heuristically relate the FL conductance to the TLL conductance through a "contact resistance" between an FL lead and a TLL wire.

In long ABK rings, where the interaction is due to spin-flip scattering at a QD in the Kondo regime, the linear dc conductance consists of two parts: a disconnected part of the Landauer form, and a connected part that can be approximately eliminated at low temperatures. For a closed long ABK ring, where the electric current is conserved in the ring, the high-temperature conductance has qualitatively different behaviors for temperatures greater than and lower than the characteristic energy scale v_F/L, where v_F is the Fermi velocity and L is the ring circumference. Meanwhile, for an open long ABK ring where electrons may leak into the side leads coupled to ring arms, as long as the ring arms have both small transmission and small reflection, the ring behaves as a two-path Aharonov-Bohm (AB) interferometer, and we predict the observation of a $\pi/2$ phase shift due to scattering off the Kondo singlet formed at low energies around the impurity spin.

Lay Summary

In nanostructures such as quantum wires and quantum dots, electrons are spatially confined along the wire or inside the dot, and become much more likely to meet each other in their motion. Interactions between electrons are therefore especially important in nanostructures; combined with quantum mechanical laws, they can lead to many interesting properties that promise applications in quantum circuits and quantum computing. In this thesis, we theoretically study the effects of interactions between electrons on the electric current response to external voltages, focusing on two types of nanostructures: a junction connecting multiple quantum wires with interacting electrons, and also a nano-ring with an embedded quantum dot and a threading magnetic field. Our quantitative predictions are potentially applicable to quantum circuit design.

Preface

This thesis is based on notes I wrote during my PhD studies. The concept and scope of the research were developed collectively by my supervisor Prof. Ian Affleck, Dr. Yashar Komijani (for Chapter 3) and me. I performed all analytical and numerical calculations in consultation with my supervisor and (for Chapter 3) Dr. Yashar Komijani.

Section 1.2 and Sections 2.3 to 2.9 have been published in the following paper: Zheng Shi and Ian Affleck, Physics Review B **94**, 035106 (2016).

Section 1.3, Sections 3.2 to 3.8, Appendix B and most of Appendix C have been published in the following paper: Zheng Shi and Yashar Komijani, Physics Review B **95**, 075147 (2017).

Appendix A has been published in the following paper: Zheng Shi, Journal of Statistical Mechanics: Theory and Experiment (2016) 063106.

I verify that all hyperlinks in the bibliography are active as of July 10, 2017.

Table of Contents

Abstract . . . . . **ii**

Lay Summary . . . . . **iii**

Preface . . . . . **iv**

Table of Contents . . . . . **v**

List of Tables . . . . . **viii**

List of Figures . . . . . **ix**

List of Abbreviations . . . . . **xiv**

Acknowledgments . . . . . **xv**

1 Introduction **1**

1.1 Landauer formula for multi-terminal mesoscopic systems 2

1.2 Junctions of multiple interacting quantum wires 4

1.3 Linear dc conductance through ABK rings 5

1.4 This thesis 8

2 Conductance of junctions of multiple interacting quantum wires with TLL leads . . **10**

2.1 Bosonic approach to interacting quantum wires with TLL leads 11

2.1.1 Uniform wire 11

2.1.2 TLL leads 13

2.2 Bosonic approach to junctions of two wires and Y-junctions 16

2.2.1 2-lead junctions 16

2.2.2 Y-junctions 21

2.3 Fermionic formulation 23

2.4 Wilsonian approach to S-matrix renormalization 27

2.5 First-order perturbation theory conductance . . . 30
2.5.1 Zeroth order . . . 32
2.5.2 First order . . . 33
2.6 First-order Callan-Symanzik (CS) formulation of renormalization group (RG) . . . 39
2.7 RPA . . . 41
2.7.1 Details of the RPA conductance . . . 44
2.7.2 Real space integral Eq. (2.118) . . . 48
2.8 2-lead junctions and Y-junctions . . . 49
2.9 Conclusion and discussions . . . 51

3 Conductance of long ABK rings . . . 54
3.1 The spin-1/2 single-channel Kondo effect . . . 54
3.2 Anderson model and Kondo model . . . 57
3.2.1 Screening and non-screening channels . . . 58
3.2.2 Kondo model . . . 61
3.3 dc conductance . . . 63
3.3.1 Kubo formula in terms of screening and non-screening channels . . . 63
3.3.2 Disconnected part . . . 65
3.3.3 Connected part and its low-temperature elimination . . . 68
3.4 Perturbation theories . . . 72
3.4.1 Weak coupling perturbation theory . . . 72
3.4.2 FL perturbation theory . . . 77
3.5 Comparison with early results . . . 80
3.5.1 Short ABK ring . . . 80
3.5.2 Finite quantum wire . . . 81
3.6 Closed long ring . . . 82
3.6.1 Kondo temperature . . . 83
3.6.2 High-temperature conductance . . . 85
3.6.3 FL conductance . . . 89
3.7 Open long ring . . . 89
3.7.1 Wave function on a single lossy arm . . . 91
3.7.2 Background S-matrix and coupling site wave functions . . . 93
3.7.3 Kondo temperature and conductance . . . 96
3.8 Conclusion and open questions . . . 102

4 Conclusions . . . 106

Bibliography . . . 109

Appendices **122**

A S-matrix RG equation and fixed points for 2-lead junctions and Y-junctions **122**
A.1 First order in interaction 122
A.1.1 2-lead junction 122
A.1.2 Y-junction 123
A.2 RPA 128
A.2.1 2-lead junction 128
A.2.2 Y-junction 129

B Details of the disconnected contribution **134**
B.1 Properties of the S-matrix and the wave functions 135
B.2 Background transmission 136
B.3 Terms linear in T-matrix 139
B.4 Terms quadratic in T-matrix 141

C Details of weak-coupling and FL perturbation theory **144**
C.1 Weak-coupling perturbation theory 144
C.1.1 T-matrix 144
C.1.2 Connected contribution to the conductance 146
C.2 FL perturbation theory 149
C.2.1 T-matrix 149
C.2.2 Connected contribution to the conductance 151

List of Tables

Table 3.1 Different regimes of energy scales discussed in this chapter. T, T_K and E_V are respectively the temperature, the Kondo temperature, and the energy scale over which V_k^2 varies significantly. We also assume $E_{\text{conn}} \sim E_V$, where E_{conn} is the energy scale over which S and Γ vary significantly. For the low-temperature conductance in the small Kondo cloud regime, see discussion in Section 3.8. . . 105

List of Figures

Figure 2.1 Sketch of a quantum wire connected to two leads. The leads are modeled with Luttinger parameters K_L and K_R that are different from the Luttinger parameter of the wire, K_W. For FL leads $K_L = K_R = 1$. 13

Figure 2.2 a) The sketch of a 2-lead junction, with possibly different Luttinger parameters and speeds of sound in the two wires. The wires extend from $x = 0$ to ∞, and the junction is at $x = 0$. b) The RG fixed points of this model: D (smoothly connected wires) and N (decoupled wires). c) The RG flow diagram from the bosonic approach. RG flows are towards N when $K_e < 1$ (repulsive interactions) and towards D when $K_e > 1$ (attractive interactions); here K_e is the harmonic average of K_1 and K_2. 17

Figure 2.3 a) Typical RG fixed points of the Y-junction, as predicted by the bosonic approach (with the exception of the M fixed point): N (decoupled wires), χ^+ (chiral transmission which breaks time-reversal symmetry: 1 to 2, 2 to 3 and 3 to 1), M (electrons incident from any wire can be reflected or transmitted), D (Andreev reflection) and the asymmetric A_3 (1 and 2 are smoothly connected and 3 is decoupled). b) The RG flow diagram for a Z_3 symmetric Y-junction at $K < 1$. The horizontal axis measures the coupling strength between any two wires, so the N fixed point occupies the entire vertical axis. The vertical axis measures time-reversal symmetry breaking (e.g. due to an AB flux at the junction), which means the time-reversal symmetric M should be on the horizontal axis, but $\chi^\pm$ should not. RG flows are always towards N when $K < 1$, although it is found from the fermionic approach that M is more stable than $\chi^\pm$. c) Same as b) but with $1 < K < 3$. RG flows are towards $\chi^\pm$ whenever time-reversal symmetry is broken; in the time-reversal symmetric case, however, the RG flow is from N to M. 24

Figure 2.4 Sketch of a typical junction system with the number of quantum wires $N = 3$. The shaded junction area to the left is modeled by quadratic hopping terms between ends of the wires, which are all aligned at the origin $x = 0$. The electron-electron interaction strengths inside the wires are also plotted for comparison. The interaction strength in wire $j = 1$ is uniform, and that in wire $j = 2$ also goes to a constant nonzero value as $x \to \infty$; these two wires are said to be attached to TLL leads. In contrast, the wire $j = 3$ has a vanishing interaction strength far away from the junction, and is connected to an FL lead (the FL lead itself is too wide to be shown in full). 25
Figure 2.5 Diagrammatic representation of the electron-electron interaction. 28
Figure 2.6 Diagrams contributing to the linear dc conductance at the first order in interaction. The second line shows the self-energy dressed bubble diagrams, while vertex correction diagrams are in the third line. 32
Figure 2.7 Dressing of the first order vertex correction diagrams by the first order self-energy diagrams. 40
Figure 2.8 The RPA diagrammatics: (a) effective interaction in the RPA represented by thick wavy lines; (b) dressed propagator in the RPA, to $O(\delta D/D)$ in RG, represented by thick straight lines; and (c) diagrams contributing to the Kubo conductance in the RPA. The dressed propagator in (b) is calculated to $O(\delta D/D)$ only, because higher order terms in $\delta D/D$ do not contribute to the renormalization of the S-matrix [Eq. (2.106)]— see Section 2.6 for an explanation in the first order context. (a) and (c) do not involve truncation at $O(\delta D/D)$ because any renormalization of the interaction [Eq. (2.107)] and the conductance [Eqs. (2.105) and (2.109)] can be attributed to the renormalization of the S-matrix. Note that (c) features a thin interaction line (rather than a thick one) to avoid double-counting. 42
Figure 2.9 Schematic representation of the relation between the conductance of a junction with FL leads and that of a junction with TLL leads, through the "contact resistance"Eq. (2.30). 43

Figure 3.1 Sketch of a generic system which allows the application of our formalism. Here $N = 5$ and $M = 3$. 59

Figure 3.2 Disconnected (self-energy) and connected (vertex correction) contributions to the density-density correlation function, which is directly related to the conductance through the Kubo formula Eq. (3.31). The dashed lines represent external legs at times $\bar{t}$ and 0, the solid lines represent fully dressed Ψ fermion propagators, and the hatched circle represents all connected 4-point vertices of the screening channel. 64

Figure 3.3 Diagrammatics of weak-coupling perturbation theory. a) The vertices corresponding to the Kondo coupling and the potential scattering in Eq. (3.25a). b) Diagrams contributing to the T-matrix of the screening channel ψ electrons up to $O\left(J^2\right) \sim O\left(K^2\right)$. We have traced over the impurity spin so that the double dashed lines (impurity spin propagators) form loops, and arranged the internal time variables from left to right in increasing order. c) Connected diagrams contributing to the linear dc conductance up to $O\left(J^2\right)$. 73

Figure 3.4 Diagrammatics of FL perturbation theory. a) The two vertices given by the leading irrelevant operator, Eq. (3.87). b) Diagrams contributing to the T-matrix of $\tilde{\psi}$ electrons up to $O\left(1/T_K^2\right)$. The propagators are those of the phase-shifted screening channel operators $\tilde{\psi}$. 79

Figure 3.5 The short ABK ring studied in Refs. [66, 75]. 80

Figure 3.6 The finite quantum wire geometry studied in Ref. [116]. 81

Figure 3.7 Geometry of the long ABK ring with short upper arms and a pinched reference arm. 83

Figure 3.8 Kondo temperature T_K for the closed long ABK ring, calculated by numerical integration of the weak coupling RG equation Eq. (3.27), plotted against the AB phase φ. $T_K(\varphi)$ is an even function of φ and has a period of 2π, so only $0 \leq \varphi \leq \pi$ is shown. System parameters are: $d_{ref} = 60$, $\theta = \pi/2$, $|\tilde{r}| = 0$, $t_L = t_R$, $D_0 = 10$. The curves with $T_K \gg \Delta$ (small Kondo cloud regime) have a large bare Kondo coupling $\left(t_L^2 + t_R^2\right) j_0/\pi = 0.15$, whereas the curves with $T_K \ll \Delta$ (large Kondo cloud regime) have a much smaller bare Kondo coupling $\left(t_L^2 + t_R^2\right) j_0/\pi = 0.02$. In the small cloud regime T_K is almost independent of φ and k_F, as the curves are flat and overlapping with each other. In the large cloud regime, however, T_K highly sensitive to both φ and k_F. 85

Figure 3.9 Kondo-type correction to the conductance δG at $T \gg T_K$ for the closed long ABK ring with a particle-hole symmetric QD, calculated by RG improved perturbation theory Eq. (3.106), plotted against the AB phase φ. Again only $0 \leq \varphi \leq \pi$ is shown. System parameters are: $d_{ref} = 60$, $\theta = \pi/2$, $|\tilde{r}| = 0$, $t_L = t_R$, $\left(t_L^2 + t_R^2\right) j_0/\pi = 0.02$ at $D_0 = 10$ (i.e. the system is in the large cloud regime). $T/\Delta = 0.0955$ in panel a) and $T/\Delta = 19.1$ in panel b). For $T \ll \Delta$ the conductance shows considerable k_F dependence, while for $T \gg \Delta$ such dependence essentially vanishes and curves at different k_F overlap. Also, for $T \gg \Delta$ the first harmonic $\cos\varphi$ drops out as predicted by Eq. (3.109), and $\delta G(\varphi)$ has a period of π. 88

Figure 3.10 Geometry of the open long ABK ring. Side leads are appended to the QD arms and the reference arms, which are all of comparable lengths. 91

Figure 3.11 A single lossy arm attached to side leads. 92

Figure 3.12 Normalization factor V_k^2 from Eq. (3.19) as a function of k for different AB phases φ in the open long ABK ring, obtained by solving the full tight-binding model. We focus on a small slice of momentum $|k - \pi/3| < 0.05$. Two values of t_x are considered: $t_x = 0$ corresponding to the closed ring without electron leakage, and $t_x = 0.3t$ corresponding to strong leakage along and small transmission across the arms. System parameters are: $d_L = d_R = d_{ref}/2 = 100$, $t_{JL}^{L,R} = t_{JQ}^{L,R} = t_{JR}^{L,R} = t$, and symmetric QD coupling $t_L = t_R$. For comparison we have also plotted the analytic prediction Eq. (3.134) for $t_x = 0.3t$, which agrees quantitatively with the full tight-binding solution. While V_k^2 for the closed ring is extremely sensitive to k_F and φ, the sensitivity is strongly suppressed by electron leakage, and curves for different φ overlap when $t_x = 0.3t$. Since V_k^2 controls the renormalization of the Kondo coupling, the Kondo temperature of the open long ABK ring is not sensitive to mesoscopic details in the small transmission limit. 98

Figure 3.13 Low-temperature and high-temperature conductances G as functions of AB phase φ in the open long ABK ring with a particle-hole asymmetric QD, calculated with Eqs. (3.141a) and (3.145). We assume $T_K \ll t$ so that the thermal averaging in the high temperature case is trivial. System parameters are: $t_x = 0.3t$, $k_F = \pi/3$, $d_L = d_R = d_{ref}/2 = 100$, $t_{JL}^{L,R} = t_{JQ}^{L,R} = t_{JR}^{L,R} = t$, and particle-hole symmetry breaking phase shift $\delta_P = 0.1$. A phase shift of approximately $\pi/2$ is clearly visible as the temperature is lowered and Kondo correlations become important. 101

Figure C.1 The three connected diagrams at $O\left(T^2/T_K^2\right)$ contributing to the conductance. ZS, ZS' and BCS label only the topology of the diagrams and not necessarily the physics. 152

List of Abbreviations

RG renormalization group

FL Fermi liquid

TLL Tomonaga-Luttinger liquid

QD quantum dot

AB Aharonov-Bohm

ABK Aharonov-Bohm-Kondo

RPA random phase approximation

CS Callan-Symanzik

Acknowledgments

First of all, I am profoundly grateful to my supervisor, Professor Ian Affleck. He has been very considerate and supportive throughout my time at Vancouver, and has influenced me as a physicist more than anyone else does. I have benefited greatly from his deep insights and his extensive knowledge of condensed matter physics, and perhaps learned as much from his attitude toward work and life in general. I have been very fortunate to have the opportunity to work with him.

It is a pleasure to thank Dr. Yashar Komijani for his contribution to the work presented in Chapter 3, as well as many very enjoyable discussions. I would also like to thank my supervisory committee– Prof. Mona Berciu, Prof. Joshua Folk, and Prof. Ariel Zhitnitsky– whose questions and suggestions were immensely helpful in improving this thesis.

I want to thank the University of British Columbia. The Point Grey campus has been a wonderful place to live; also, the Department of Physics and Astronomy gave me a chance to meet many new friends, and granted me teaching experience that I find invaluable in shaping my character.

Finally, I cannot thank my parents enough for their support and encouragement. They are the best parents in the world and I dedicate my thesis to them.

Chapter 1

Introduction

Quantum wires and quantum dot (QD)s have received increasing attention from condensed matter theorists and experimentalists alike[53]. One realization of a quantum wire has electrons in a two-dimensional electron gas confined in a lateral direction, so that any motion of these electrons is effectively one-dimensional, taking place in the direction perpendicular to the confinement. A QD, which comprises a small droplet of electrons, can also be realized by confining a two-dimensional electron gas in both lateral directions. Such spatial confinement at mesoscopic length scales not only exposes interference effects, as demonstrated by the Aharonov-Bohm (AB) effect in one-dimensional rings, but also enhances interaction and correlation. In particular, an interacting quantum wire can behave as a paradigmic Tomonaga-Luttinger liquid (TLL), characterized by bosonic elementary excitations formed by electron-hole pairs, together with the power law decay of various correlation functions with interaction-dependent exponents[44]. In another example, tunneling through a QD features the Coulomb blockade phenomenon: unless the plunger gate voltage falls outside certain narrow intervals (the Coulomb peaks), the number of electrons in the QD is always an integer, and it takes a finite energy to add/remove an electron to/from the QD due to the Coulomb repulsion, which strongly suppresses tunneling. Meanwhile, when an odd number of electrons are on the QD, tunneling will be anomalously enhanced at low temperatures due to the Kondo effect[53].

Both quantum wires and QDs have a broad range of potential applications; in particular, they are conceived to be the building blocks of quantum computers. In quantum-circuit-based quantum computers, qubits can be realized by the spin states of the QDs[73], which are coupled to each other and manipulated externally through quantum wires; on the other hand, in topological quantum computers[31], the Majorana zero modes forming topological qubits are thought to live at the ends of quantum wires, and their braiding operations are achievable through quantum wire networks[8, 52].

In this thesis, we study two types of multi-terminal devices consisting of quantum wires and QDs, namely junctions of interacting quantum wires[111] and long Aharonov-Bohm-Kondo (ABK)

rings[112], with a focus on the influence of interactions on their transport properties. The former are an essential ingredient of any practical quantum circuit and may find utilization as nano-switches, while the latter prove useful in the quest for mesoscopic manifestations of Kondo physics. Before elaborating on our motivations, it is helpful to first revisit the non-interacting problem.

1.1 Landauer formula for multi-terminal mesoscopic systems

In this section, we illustrate a number of basic concepts by outlining the generic setup for a multi-terminal junction, and review the Landauer formula for the case without interactions[53, 54].

Consider N quantum wires meeting at a junction; each wire extends from $x = 0$ to $x \to \infty$, with the $x \to \infty$ part representing a reservoir (or a "lead"). We assume that each wire supports only a single channel and a single spin orientation; this is not a crucial assumption as we may view each channel/spin in a realistic setup effectively as a separate "wire". To define the linear dc conductance, we apply a weak bias voltage V_j to the reservoir connected to wire j, $j = 1, 2, ..., N$. The dc current (in the $+x$ direction) probed in wire j' is then given by

$$I_{j'} = \sum_{j=1}^{N} G_{j'j} V_j; \tag{1.1}$$

the conductance tensor $G_{jj'}$ obeys $\sum_j G_{jj'} = \sum_{j'} G_{jj'} = 0$, because the total current flowing out of the junction is zero, and a uniform voltage applied to all leads results in no current. We emphasize that here the conductance tensor is defined as the linear response coefficients to external bias voltages; it is possible that experimentally measured voltage drops also contain contributions from the electric polarization[55, 65, 91, 104, 125].

In the case where the junction, the wires and the reservoirs are all free from various interactions, the conductance tensor is directly related to the scattering S-matrix via the Landauer formula, whose derivation is sketched below.

The purely quadratic Hamiltonian consists of a kinetic term, and a potential scattering term confined in the junction region. The potential scattering vanishes inside the wires $x_j > 0$, so that the scattering state incident from wire j' at energy E has the following asymptotic wave function on wire j at $x_j > 0$:

$$\Phi_{j',E}(j,x_j) = \frac{1}{\sqrt{2\pi v_j(E)}} \left\{ \delta_{jj'} \exp\left[-ik_j(E)x_j\right] + S_{jj'}(E) \exp\left[ik_j(E)x_j\right] \right\}, \tag{1.2}$$

where $k_j(E)$ is the wave vector at energy E in wire j, and $v_j = (\partial k_j/\partial E)^{-1}$ is the corresponding group velocity. (Hereafter we let $\hbar = 1$.) The $N \times N$ scattering S-matrix $S(E)$ has diagonal elements representing reflection amplitudes and off-diagonal elements representing transmission amplitudes. $S(E)$ is a unitary matrix,

$$\sum_{j''} S_{jj''}(E) S^*_{j'j''}(E) = \delta_{jj'}, \tag{1.3}$$

due to current conservation and orthogonality between different scattering states.

The central assumption of the Landauer formula is that electrons leaving a reservoir ("source") retain their shifted Fermi distribution in that reservoir, until they are scattered into the reservoirs ("sinks") where they are immediately absorbed and reach local thermal equilibrium. If we let the equilibrium chemical potential be μ, in the presence of dc bias voltages V_j, the electrochemical potential in reservoir j becomes $\mu + eV_j$ where e is the electron charge. Consequently, taking the expectation value of the electric current operator $\hat{I}_j = e\hat{v}_j$ in the scattering state Eq. (1.2) where $\hat{v}_j$ is the velocity operator, we find the following contribution from electrons in the scattering state incident from wire j' to the current in wire j:

$$I_{j,j'} = -e \int dE v_j(E) \frac{1}{2\pi v_j(E)} \left[\delta_{jj'} - \left|S_{jj'}(E)\right|^2\right] f\left(E - \mu - eV_{j'}\right); \tag{1.4}$$

here $f(\varepsilon) = 1/\left(e^{\beta\varepsilon} + 1\right)$ is the Fermi function, with $\beta = 1/(k_B T)$. The $\delta_{jj'}$ part comes from the incident component in Eq. (1.2) and the $\left|S_{jj'}\right|^2$ part comes from the scattered component. We have neglected cross terms between the two components, which are associated with Friedel oscillations; contributions from these cross terms are suppressed by $O(T/(v_{Fj}k_{Fj}))$ relative to the terms that we have retained, where v_{Fj} and k_{Fj} are respectively the Fermi velocity and the Fermi wave vector in wire j. Summing over j' and expanding in powers of V_j, we find that the zeroth order term vanishes due to the unitarity of $S(E)$, i.e. there is no current in the absence of any bias voltage. We thus obtain the total current of the first order in V:

$$I_j = -\frac{e^2}{2\pi} \sum_{j'} \int dE \left[\delta_{jj'} - \left|S_{jj'}(E)\right|^2\right] \left[-f'(E-\mu)\right] V_{j'}. \tag{1.5}$$

Comparing with Eq. (1.1) we find the linear dc conductance tensor[53, 54]

$$G_{jj'} = -\frac{e^2}{2\pi} \int dE \left[-f'(E-\mu)\right] \left[\delta_{jj'} - \left|S_{jj'}(E)\right|^2\right]. \tag{1.6}$$

As expected, it follows from the unitarity of $S(E)$ that $G_{jj'}$ satisfies $\sum_j G_{jj'} = \sum_{j'} G_{jj'} = 0$.

The derivation above relies on the existence of noninteracting scattering states characterized by the scattering S-matrix, and their thermal equilibrium with quasiparticles in the Fermi liquid (FL) reservoirs. As we will see in this thesis, interactions can change the Landauer picture significantly whether they are in the reservoirs, in the wires or at the junction itself.

1.2 Junctions of multiple interacting quantum wires

A class of powerful theoretical approaches to junctions of interacting quantum wires models the quantum wires as conformally invariant bulk TLL[40, 41, 51, 60, 61, 93, 130]. In the spirit of boundary conformal field theory, at low energies the junction with its boundary operators should eventually renormalize to conformally invariant boundary conditions; it is these conformally invariant boundary conditions that control the low-energy physics of *any* realistic junction, regardless of their microscopic details. Possible fixed points of the renormalization group (RG) flow are then postulated, and their various properties, such as zero-temperature conductance and operator scaling dimensions, are explored. Details of the RG flow, however, are largely open to conjecture except in the vicinity of these fixed points. These approaches are often consolidated with the technique of bosonization, as the elementary excitations of TLLs are bosonic in nature, and various boundary conditions imposed by the junction are often conveniently expressed in bosonic field variables.

Alternate formalisms have been independently developed in the language of fermions. Consider first the junction system without bulk electron-electron interaction in the quantum wires; we further ignore local interactions so that this system becomes completely non-interacting. (For a free-fermion system, unless localized discrete states exist, local interactions are irrelevant in the RG sense and do not affect leading order physics.) A single-particle S-matrix determines the scattering basis, a new set of single-particle states which diagonalizes the non-interacting system. The bulk electron-electron interaction is then reintroduced and handled by perturbation theory, whose infrared divergence is resummed in an RG procedure. The S-matrix elements are now scale-dependent coupling constants. In the simplest approximation scheme, both the renormalized single-particle self-energy and the renormalized two-particle vertex depend only on the renormalized S-matrix at every point in the RG flow; the S-matrix elements (or the transmission probabilities) are thus treated as the only running coupling constants of the theory, and by solving their RG equations we gain information about the conductance. This scheme is first adopted by Refs. [28, 70, 77, 132] to the first order in interaction; various generalizations include resonant tunneling with an energy-dependent S-matrix[87, 99], second order perturbation theory in interaction in a setup with a tunnel electrode[16], random phase approximation (RPA) in interaction[11–15], superconducting junctions[27, 29, 30, 126], and refermionization of fixed points proposed by bosonic theory[45], to list a few. In particular, it has been found that the RPA in the Tomonaga-Luttinger model with a linear dispersion reproduces various scaling dimensions of the conductance known from bosonic methods. (The term RPA has been used interchangeably with "ladder approximation" in Refs. [11, 13, 15].) An improved approximation, known as the functional RG method[18, 19, 36, 78–81], explicitly studies the flows of single-particle self-energy and the two-particle vertex. Despite its basis on perturbation theory in interaction, the functional RG shows excellent agreement with analytic results at Luttinger parameter $K = 1/2$, and with numerical density matrix renormalization group data for fairly strong interactions. The merit of these formalisms

are that the crossover behavior between different fixed points can, in principle, be found to any order in interaction. Nevertheless, when the interaction becomes sufficiently strong in a junction of three wires (a "Y-junction"), the fixed points and the RG flow predicted by the RPA fermionic approach and the bosonic approach begin to differ qualitatively. Also a careful analysis reveals that, in the RPA approach, the β function of the S-matrix beyond one-loop order contains non-universal terms[11, 13] which depend on the precise cutoff scheme of the theory, and may potentially change its predictions.

To our knowledge, many aspects of the junction problem have not been explored in the fermionic formalism. One such example is the well-known distinction between a semi-infinite TLL wire and a finite TLL wire connected to a FL reservoir[10, 42, 55, 56, 61, 65, 68, 69, 76, 90, 91, 97, 100, 105, 106, 125]. There have been controversies on the nature of the conductance measured in a realistic experimental setup[55, 125]. However, if we consider the linear dc response to an externally applied bias voltage[65, 91], then it has been predicted that the corresponding linear response coefficients (which we have been referring to as the "conductances") with and without the FL reservoirs are generally different[104]. (These coefficients are well-defined and can be studied numerically.) For instance, the conductance of a finite TLL wire attached to FL leads on both sides is e^2/h, irrespective of the interaction strength; on the other hand, the conductance of an infinite spinless TLL wire is Ke^2/h, where K is the Luttinger parameter. The Landauer formula based on a perfectly transmitting S-matrix alone cannot recover the Ke^2/h result. In existing literature employing the fermionic formalism, the case of FL leads has been well studied, but the effects of TLL leads on the conductance are not discussed.

The reasons are twofold for our interest in the effects of TLL leads on the conductance from the fermionic perspective. At the fixed points well understood in the bosonic approach, such as the perfect transmission fixed point in the two-lead junction and the chiral fixed points in the Y-junction, the agreement of these results in both approaches is a necessary validation of the fermionic approach. On the other hand, for the fixed points eluding the bosonic treatment, such as the maximally open fixed point of the Y-junction (known as the "M fixed point"[13, 15, 19, 93, 99]), these results can be directly compared to numerics[104] where available.

1.3 Linear dc conductance through ABK rings

Another important ingredient in mesoscopic devices is the QD[26, 47, 48, 102, 114, 127]. The conductance through a QD can be measured by embedding it between two reservoirs. When the QD has a non-zero spin in its ground state, as is the case when there is an odd number of electrons, the conductance may undergo a strong enhancement as the temperature is reduced well below the charging energy. This is due to spin-flip cotunneling processes; for a spin-$1/2$ dot in e.g. the spin-down state, such a process can be a spin-up electron hopping onto the QD from one reservoir, and a spin-down electron hopping off the QD at the same time to the other reservoir. An effective model

thus features a localized impurity spin coupled with a Fermi sea of conduction electrons, in analogy with the famous Kondo problem[49, 67], which usually refers to the low-temperature resistivity minimum in a system of magnetic impurities embedded in a non-magnetic metallic host.

In the Kondo model, perturbation theory in the coupling constant is plagued by infrared divergence, but after much theoretical endeavor[9, 89, 129] it has been recognized that the model has a relatively simple low energy behavior. For the single-channel spin-$1/2$ model, at temperatures well below the Kondo temperature T_K, the impurity spin is "screened" by the conduction electrons, forming a local singlet state. The spatial extent of this singlet state, commonly termed the "Kondo screening cloud", is expected to be $L_K = v_F/T_K$ where v_F is the Fermi velocity. The remaining conduction electrons are well described by a FL theory at zero temperature, and acquire a phase shift ($\pi/2$ in the presence of particle-hole symmetry) upon being elastically scattered by the Kondo singlet. Moreover, at finite temperatures, scattering by the Kondo impurity can have both elastic and inelastic contributions[21, 134], and it has been suggested that the inelastic scattering can be the origin of decoherence in mesoscopic structure, as measured for example by weak localization[83, 98, 134]. The possibility of imitating the impurity spin by a QD has triggered renewed experimental and theoretical interest in mesoscopic manifestations of Kondo physics, such as the observation of the length scale L_K, the $\pi/2$ phase shift, and also decoherence effects of inelastic Kondo scattering.

Many mesoscopic configurations have been proposed in order to observe L_K. These include QD-terminated finite quantum wires[95], and also various geometries with an embedded QD, including finite quantum wires[25, 94, 116, 117], small metallic grains/larger QDs[24, 63, 64, 71, 72, 119, 124], and in particular, closed long AB rings with[118, 131] and without[4, 115] external electrodes. (A closed ring conserves the electric current and there is no leakage current.) Another motivation for quantum rings is that they may be used to answer the question of whether or not the inelastic scattering from the Kondo QD can cause decoherence by suppressing the amplitude of AB oscillations. A common feature of all these configurations is that they introduce at least one additional mesoscopic length scale L. When the bare Kondo coupling strength is adjusted so that L_K crosses the scale L, the dependence of observables on other control parameters changes qualitatively. In the closed long AB ring with an embedded QD [also known as the ABK ring], for instance, L is the circumference of the ring: it is known that both L_K itself and the conductance through the ring can have drastically different AB phase dependences for $L_K \gg L$ and $L_K \lesssim L$[118, 131]. In the "large Kondo cloud" regime $L_K \gg L$, corresponding to a relatively small bare Kondo coupling, the Kondo cloud "leaks" out of the ring and the size of the cloud becomes strongly influenced by the ring size and other mesoscopic details of the system. For a given bare Kondo coupling, L_K can be extremely sensitive to the AB phase at certain values of Fermi energy, varying by many orders of magnitude. This sensitivity is completely lost in the opposite "small Kondo cloud" regime $L_K \lesssim L$, where the bare Kondo coupling is relatively large.

The conductance calculation of ABK rings, however, involves an additional layer of complication[66] that went neglected in a number of early works. In mesoscopic Kondo problems with FL electrodes, it is usually convenient to work with the scattering states and rotate to the basis of the so-called screening and non-screening channels: the screening channel ψ is coupled to the QD and therefore has a nonzero T-matrix, while the non-screening channel ϕ is described by a decoupled non-interacting theory[22, 46, 75, 103, 131]. A careful evaluation by Kubo formula at finite temperatures reveals that, unlike a QD directly coupled to external leads, the interaction effects on the linear dc conductance of short ABK rings are generally *not* fully encoded by the screening channel T-matrix in the single-particle sector, or equivalently the two-point function. Instead, there exists a contribution from connected four-point diagrams, corresponding to two-particle scattering processes in the screening channel, which cannot be interpreted as resulting from a single-particle scattering amplitude[66]. This is not in contradiction with the famous Meir-Wingreen formula[57, 82] due to the violation of the proportionate coupling condition[33]. For the short ABK ring, the four-point contribution becomes comparable to the two-point contribution well above the Kondo temperature $T \gg T_K$, but can be approximately eliminated at temperatures low compared to the bandwidth and the on-site repulsion of the QD, $T \ll \min\{t, U\}$, by applying the bias voltage and probing the current in a particular fashion. (This does not mean the four-point contribution is negligible for $T \ll \min\{t, U\}$, however.) One naturally wonders how this result generalizes to the closed long ring at high and low temperatures, and how it possibly modifies early predictions on conductance[131], which is again expected to display qualitatively different behaviors for $L_K \gg L$ and $L_K \lesssim L$.

On the other hand, efforts to measure the $\pi/2$ phase shift are mainly concentrated on two-path AB interferometer devices[17, 58, 59, 108, 123, 133]. In these devices, electrons from the source lead propagate through two possible paths (QD path and reference path) to the drain lead; the two paths enclose a tunable AB phase φ, and a QD tuned into the Kondo regime is embedded in the QD path. Most importantly, the complex transmission amplitudes through the two paths $t_d e^{i\varphi}$ and t_{ref} should be independent of each other, and the total coherent transmission amplitude at zero temperature $t_{sd} = t_{ref} + t_d e^{i\varphi}$ is the sum of the individual amplitudes (the "two-slit condition"), meaning multiple traversals of the ring are negligible. Using a multi-particle scattering formalism, and assuming that only single-particle scattering processes are coherent, Ref. [23] calculates the conductance of such an interferometer with an embedded Kondo QD in terms of the single-particle T-matrix through the QD, and concludes that the AB oscillations are suppressed by inelastic multi-particle scattering processes due to the Kondo QD.

The two-path interferometer can in principle be realized through open AB rings, where in contrast to closed rings, the propagating electrons may leak into side leads attached to the ring. For a non-interacting QD, Ref. [7] presents the criteria for an open long ring to yield the intrinsic transmission phase through the QD: all lossy arms with side leads should have a small transmission and a small reflection. A small transmission suppresses multiple traversals of the ring and guarantees

the validity of the two-slit assumption, while a small reflection prevents electrons from "rattling" (tunneling back and forth) across the QD. However, when the QD is in the Kondo regime, as with the previously discussed closed AB rings, the transmission probability through the QD[6] and even the Kondo temperature[118] may be sensitive to the AB phase and other details of the geometry, hampering the detection of the intrinsic phase shift across the QD. In addition, since the screening channels in the open ABK ring and in the simple embedded QD geometry are usually not the same, it is not obvious that the single-particle sector T-matrices coincide in the two geometries. These issues are not addressed in Ref. [23], which simply assumes that the two-slit condition is obeyed by the coherent processes, and that the T-matrix of the open ABK ring is identical to that of the QD embedded between source and drain leads. To our knowledge, it has been a mystery whether in certain parameter regimes the open long ABK ring realizes the two-path interferometer with a Kondo QD, where the Kondo temperature and the transmission probability through the QD are independent of the details of other parts of the ring, and the T-matrix of the ring truthfully reflects the T-matrix of the QD.

The aforementioned problems in closed and open ABK rings prompt a unified treatment of linear dc conductance in different mesoscopic geometries containing an interacting QD. Much work has been done on generic mesoscopic geometries[33, 37, 62], but in the formalism to be presented in this thesis, we aim to take the connected contribution into account expressly, and refrain from making assumptions about the geometry in question (such as parity symmetry).

1.4 This thesis

In this thesis, we discuss how the linear dc transport through a multi-terminal system is affected by interactions, namely interacting quantum wires and reservoirs[111], and an interacting QD in the Kondo regime[112].

In the first part of the thesis, we adopt the RPA fermionic approach to study the conductance tensor for a generic multi-lead junction in the presence of TLL leads. Our theory makes extensive use of the scattering basis transformation of the non-interacting part of the system; as a result it is explicitly formulated on the basis of the single-particle S-matrix (much like that in Ref. [70]), and is formally independent of the number of wires. This stands in contrast to previous RPA treatments of junctions attached to FL leads, whose formulation heavily depends on the parametrization of the conductance tensors, different for two-lead junctions[11] and Y-junctions[13, 15]. We derive a Landauer-type conductance formula, appropriate for the renormalized S-matrix, and recover the additional contribution from the TLL leads to the conductance, absent in the naive Landauer formalism. Our theory is applied to the two-lead junction and Y-junction problems, where in addition to verifying existing results on the fixed points and the phase diagrams, the conductance of the M fixed point attached to TLL leads is calculated.

In the second part of this thesis, we study a QD represented by an Anderson impurity, which

is embedded in a junction connecting an arbitrary number of FL leads. The junction is regarded as a black box characterized only by its scattering S-matrix and its coupling with the QD, and all leads (including source, drain and possibly side leads) are treated on equal footing. In parallel with Ref. [66] we find that the linear dc conductance is given by the sum of a "disconnected" part and a "connected" part. The disconnected part has the appearance of a linear response Landauer formula, where the "transmission amplitude" is linear in the T-matrix of the screening channel in the single-particle sector, and indeed reduces at zero temperature to a non-interacting transmission amplitude appropriate for the local FL theory. The connected part is again a Fermi surface property, can be eliminated by proper application of bias voltages, and is calculated perturbatively at weak coupling $T \gg T_K$, as well as at strong coupling $T \ll T_K$ provided the local FL theory applies. Our formalism is subsequently applied to long ABK rings. In the case of closed rings, we show that for $T \gg T_K$, the high-temperature conductance exhibits qualitatively different behaviors as a function of the AB phase for $T \gg v_F/L$ and $T \ll v_F/L$. In the case of open rings, when the small transmission condition is met, we find the mesoscopic fluctuations are suppressed, and the two-path interferometer behavior is indeed recovered at low temperatures. If in addition the small reflection condition is satisfied, the Kondo temperature of the QD and the complex transmission amplitude through the QD are both unaffected by the details of the ring. We then find the conductance at $T \gg T_K$ and $T \ll T_K$, and in particular rigorously calculate the normalized visibility[23] of the AB oscillations in the FL regime. We show that while the deviation of normalized visibility from unity is indeed proportional to inelastic scattering as predicted by Ref. [66], the constant of proportionality depends on non-universal particle-hole symmetry breaking potential scattering. Our findings also suggest that the $\pi/2$ phase shift across the QD is measurable in our two-path interferometer when the criteria of small transmission and small reflection are fulfilled. While we focus on long ABK rings in this thesis, our general formalism is applicable to a Kondo impurity embedded in an arbitrary non-interacting multi-terminal mesoscopic structure.

Chapter 2

Conductance of junctions of multiple interacting quantum wires with TLL leads

This chapter is devoted to junctions of multiple interacting quantum wires[111]. We first review the bosonic approach to quantum wires in Section 2.1, and outline its application to 2-lead junctions and Y-junctions in Section 2.2. Switching to the fermionic approach, we then elaborate on our model for a generic multi-lead junction in Section 2.3. Viewing the single-particle S-matrix elements as running coupling constants, we derive an S-matrix RG equation à la Wilson in Section 2.4. This derivation does not directly shed light on the conductance, however, which prompts us to calculate the linear dc conductance of the junction to the first order in interaction in Section 2.5. Section 2.6 is based on perturbative RG, again to the first order in interaction. We recover the S-matrix RG equation from a Callan-Symanzik (CS) approach, using the Kubo conductance calculated in Section 2.5. This establishes a modified Landauer formula involving the renormalized S-matrix in the case of FL leads. An additional contribution to the conductance is shown to arise from TLL leads. In Section 2.7, the conductance is found in the RPA to arbitrary order in interaction; we derive an S-matrix RG equation in the RPA, and again find the conductance in terms of the renormalized S-matrix both with and without TLL leads. Section 2.8 applies our results to the fixed points of 2-lead junctions and Y-junctions at the first order and in the RPA. In particular, we find the conductance at the M fixed point of a Z_3 symmetric Y-junction attached to TLL leads. We discuss some open questions and summarize our findings in Section 2.9. Finally, a review of various RG fixed points in the fermionic approach is given in Appendix A.

2.1 Bosonic approach to interacting quantum wires with TLL leads

As a first example of how TLL leads may modify the Landauer formula in quasi one-dimensional mesoscopic structures, we examine a simple model of an interacting quantum wire of spinless electrons connected to TLL leads from the bosonization perspective[42, 61, 76, 100, 105, 106, 125].

2.1.1 Uniform wire

Let us begin by considering a uniform quantum wire with spinless electrons. Retaining the degrees of freedom in the vicinity of the Fermi wave vector $k \approx \pm k_F$ only, and approximating their dispersions by linear ones, we have the Hamiltonian

$$H = H_0 + H_{g_2} + H_{g_4}, \tag{2.1}$$

where

$$H_0 = \int_{-\infty}^{\infty} dx\,(iv_F)\left[\psi_L^\dagger(x)\,\partial_x\psi_L(x) - \psi_R^\dagger(x)\,\partial_x\psi_R(x)\right], \tag{2.2}$$

$$H_{g_2} = g_2\int_{-\infty}^{\infty} dx\rho_L(x)\,\rho_R(x), \tag{2.3}$$

$$H_{g_4} = \frac{g_4}{2}\int_{-\infty}^{\infty} dx\left[\rho_L^2(x) + \rho_R^2(x)\right]. \tag{2.4}$$

H_0 is a kinetic term describing right-moving and left-moving electrons ψ_R and ψ_L with velocities $\pm v_F$ and dispersions $\varepsilon_{\pm,k} = v_F(\pm k - k_F)$ respectively. The full electron annihilation operator is simply $\psi(x) = e^{ik_Fx}\psi_R(x) + e^{-ik_Fx}\psi_L(x)$. $\rho_{R/L} =: \psi_{R/L}^\dagger\psi_{R/L}:$ are the normal-ordered chiral density operators (i.e. with their ground state expectation value subtracted); H_{g_2} then accounts for the interaction between electrons of opposite chiralities, and H_{g_4} accounts for the interaction between electrons of the same chirality[122]. We ignore Umklapp processes [$e^{4ik_Fx}\psi_R^\dagger(x)\,\psi_R^\dagger(x+a)\,\psi_L(x)\,\psi_L(x+a)$+h.c. where a is a small distance] which do not play a significant role away from commensurate fillings, as well as backscattering processes ($\psi_R^\dagger\psi_L\psi_L^\dagger\psi_R$+h.c.) which can be absorbed into H_{g_2} for spinless fermions[42, 44].

The above model can be solved exactly by the bosonization technique[44], which takes advantage of the fact that the elementary excitations are density fluctuations. We introduce bosonic fields ϕ and θ such that

$$\partial_x\phi(x) = -\pi\left[\rho_R(x) + \rho_L(x)\right], \tag{2.5}$$

$$\partial_x\theta(x) = \pi\left[\rho_R(x) - \rho_L(x)\right]; \tag{2.6}$$

thus $\partial_x\phi$ is proportional to the zero-momentum piece of the density fluctuations (the other piece is $\psi_R^\dagger\psi_L$+h.c. of momentum $\pm 2k_F$), and $\partial_x\theta$ is proportional to the zero-momentum piece of the current operator. ϕ commutes with itself and so does θ, but they obey the commutation relation

$$[\phi(x), \theta(y)] = i\frac{\pi}{2}\operatorname{sgn}(y-x); \tag{2.7}$$

thus the canonical momentum conjugate to ϕ is

$$\Pi(x) = \frac{1}{\pi}\partial_x\theta(x). \tag{2.8}$$

The original fermion operators are solitons in the boson language:

$$\psi_{R/L}(x) = U_{R/L}\frac{1}{\sqrt{2\pi\alpha}}\exp[\mp i\phi(x) + i\theta(x)], \tag{2.9}$$

where the short-distance cutoff α mimics a finite bandwidth which scales as $1/\alpha$. $U_{R/L}$ are Klein factors encoding the Fermi statistics of $\psi_{R/L}$; they commute with both bosons and anticommute with each other. Their presence ensures that the application of $\psi_{R/L}$ on a state reduces the fermion number of that state by 1.

It turns out that both the kinetic part of the Hamiltonian H_0 and the interaction parts H_{g_2} and H_{g_4} are quadratic in bosons. Therefore, H_{g_2} and H_{g_4} does not change the linear spectrum other than renormalizing the speed of sound from v_F:

$$H_0 = \frac{v_F}{2\pi}\int dx\left[(\pi\Pi(x))^2 + (\partial_x\phi(x))^2\right], \tag{2.10}$$

$$H = H_0 + H_{g_2} + H_{g_4} = \frac{u}{2\pi}\int dx\left[K(\pi\Pi(x))^2 + \frac{1}{K}(\partial_x\phi(x))^2\right], \tag{2.11}$$

where

$$u = v_F\sqrt{\left(1+\frac{g_4}{2\pi v_F}\right)^2 - \left(\frac{g_2}{2\pi v_F}\right)^2} \tag{2.12}$$

is the renormalized speed of sound,

$$K = \sqrt{\frac{1+(g_4-g_2)/(2\pi v_F)}{1+(g_4+g_2)/(2\pi v_F)}} \tag{2.13}$$

is known as the Luttinger parameter. For repulsive interactions $g_2 > 0$, $K < 1$, while for attractive interactions $g_2 < 0$, $K > 1$; free electrons have $K = 1$. Also notice that, when $g_2 = 0$, g_4 alone does not change the Luttinger parameter from 1, which means a minimal model of interacting electrons requires the g_2 term but not the g_4 term.

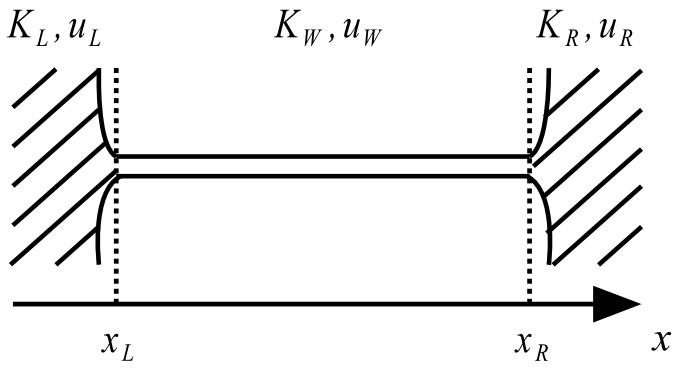

Figure 2.1: Sketch of a quantum wire connected to two leads. The leads are modeled with Luttinger parameters K_L and K_R that are different from the Luttinger parameter of the wire, K_W. For FL leads $K_L = K_R = 1$.

2.1.2 TLL leads

To investigate the effect of TLL leads on conductance, it is convenient to introduce a slightly more general model, with position-dependent speed of sound and Luttinger parameter:

$$H = \frac{1}{2\pi}\int dx \left[u(x)K(x)\left(\pi\Pi(x)\right)^2 + \frac{u(x)}{K(x)}\left(\partial_x\phi(x)\right)^2\right], \tag{2.14}$$

where

$$u(x) = \begin{cases} u_L, x < x_L \\ u_W, x_L < x < x_R \\ u_R, x > x_R \end{cases}, \tag{2.15}$$

$$K(x) = \begin{cases} K_L, x < x_L \\ K_W, x_L < x < x_R \\ K_R, x > x_R \end{cases}. \tag{2.16}$$

This model may result from e.g. a position-dependent g_2 interaction, which is stronger inside the quantum wire segment $x_L < x < x_R$ than in the reservoirs[42, 76, 105, 106, 125]; see Fig. 2.1. Note that the infinitely long wire limit $|x_R - x_L| \to \infty$ would not be well-defined if the asymptotic behavior of $K(x)$ as $x \to \pm\infty$ were not specified, because as we shall see momentarily, this asymptotic behavior is required to determine the Green's function which in turn determines the conductance.

Assuming the wire is subjected to an electric field which exists between reservoirs only and is

turned on slowly from $t \to -\infty$,

$$E = -\frac{\partial A}{\partial t} = E_0(x)\, e^{-i(\omega+i0)t}, \tag{2.17}$$

where $E_0(x) = 0$ for $x < x_L$ and $x > x_R$, the Hamiltonian is modified according to

$$\pi\Pi(x) \to \pi\Pi(x) - eA(x,t); \tag{2.18}$$

Thus the current is, in the linear response regime[44],

$$\begin{aligned} I(x,t) &= -\left\langle \frac{\delta H}{\delta A(x,t)} \right\rangle = eu(x)K(x)\langle\Pi(x,t)\rangle - \frac{e^2}{\pi}u(x)K(x)A(x,t) \\ &= -e^2u(x)K(x)\int dt'\int dx' u(x')K(x')A(x',t')\,G_{\Pi\Pi}(x,x',t-t') - \frac{e^2}{\pi}u(x)K(x)A(x,t), \end{aligned} \tag{2.19}$$

where the equilibrium retarded current-current correlation function is

$$G_{\Pi\Pi}(x,x',t-t') \equiv (-i)H(t-t')\left\langle\left[\Pi(x,t),\Pi(x',t')\right]\right\rangle. \tag{2.20}$$

Here we denote the Heaviside unit-step function by $H(t)$. It is useful to study similarly defined objects $G_{\Pi\phi}$ and $G_{\phi\phi}$; for instance,

$$G_{\phi\Pi}(x,x',t-t') \equiv (-i)H(t-t')\left\langle\left[\Pi(x,t),\phi(x',t')\right]\right\rangle. \tag{2.21}$$

From the quadratic Hamiltonian Eq. (2.14) we can work out the equations of motion for $G_{\Pi\phi}$ and $G_{\phi\phi}$:

$$\partial_{t'}G_{\Pi\phi}(x,x',t-t') = \delta(x-x')\,\delta(t-t') + \pi u(x')K(x')G_{\Pi\Pi}(x,x',t-t'), \tag{2.22}$$

$$\partial_t G_{\phi\phi}(x,x',t-t') = \pi u(x)K(x)G_{\Pi\phi}(x,x',t-t'). \tag{2.23}$$

With these two equations, we can remove the diamagnetic term and cast the current into the following form:

$$I(x,t) = -\frac{e^2}{\pi^2}\int dt' \int dx' A\left(x',t'\right)\partial_{t'}\partial_t G_{\phi\phi}\left(x,x',t-t'\right)$$
$$= \frac{e^2}{\pi^2}\int dx' E_0\left(x'\right) i\omega G_{\phi\phi}\left(x,x',\omega\right) e^{-i\omega t}. \tag{2.24}$$

In the second line we have performed Fourier transform $G_{\phi\phi}\left(x,x',t-t'\right) = \int \frac{d\omega}{2\pi} e^{-i\omega(t-t')} G_{\phi\phi}\left(x,x',\omega\right)$. For our particular choice of $u(x)$ and $K(x)$, it is not difficult to solve for $G_{\phi\phi}$. Writing down the equation of motion for $G_{\Pi\phi}$,

$$\partial_t G_{\Pi\phi}\left(x,x',t-t'\right) = -\delta\left(x-x'\right)\delta\left(t-t'\right) + \partial_x\left[\frac{1}{\pi}\frac{u(x)}{K(x)}\partial_x G_{\phi\phi}\left(x,x',t-t'\right)\right], \tag{2.25}$$

we may eliminate $G_{\Pi\phi}$ to find a closed equation for $G_{\phi\phi}$,

$$\omega^2 G_{\phi\phi}\left(x,x',\omega\right) = \pi u(x)K(x)\delta\left(x-x'\right) - u\left(x'\right)K\left(x'\right)\partial_{x'}\left[\frac{u(x')}{K(x')}\partial_{x'} G_{\phi\phi}\left(x,x',\omega\right)\right]. \tag{2.26}$$

$G_{\phi\phi}$ should be continuous everywhere, $\left[u\left(x'\right)/K\left(x'\right)\right]\partial_{x'} G_{\phi\phi}$ should be continuous everywhere except when $x' = x$, and as $x' \to \pm\infty$, $G_{\phi\phi}$ should describe purely outgoing wave. Choosing $x < x_L$ (because in the dc limit it is unimportant where we choose to measure the current), the aforementioned boundary conditions lead to the following solution:

$$G_{\phi\phi}\left(x,x',\omega\right) = \frac{\pi K_W K_L}{i\omega} e^{-i\frac{\omega}{u_L}x} \frac{\left(K_W+K_R\right)e^{i\frac{\omega}{u_W}x'} - \left(K_W-K_R\right)e^{2i\frac{\omega}{u_W}x_R}e^{-i\frac{\omega}{u_W}x'}}{\left(K_W+K_L\right)\left(K_W+K_R\right) - \left(K_W-K_L\right)\left(K_W-K_R\right)e^{2i\frac{\omega}{u_W}\left(x_R-x_L\right)}}. \tag{2.27}$$

Therefore, in the dc limit $\omega \to 0$,

$$I(x,t) = \frac{e^2}{2\pi}\frac{2K_L K_R}{K_L+K_R}\int dx' E_0\left(x'\right), \tag{2.28}$$

i.e. the linear dc conductance is

$$G = \frac{e^2}{2\pi}\frac{2K_L K_R}{K_L+K_R}. \tag{2.29}$$

Remarkably, G is independent of properties of the quantum wire, but does depend on the interaction strength in the reservoirs. In particular, for Fermi liquid reservoirs interactions become negligible ($K_L = K_R = 1$), and G reduces to the Landauer prediction $e^2/(2\pi)$; on the other hand, when an interacting quantum wire acts as its own reservoir ($K_L = K_R = K_W$), $G = K_W e^2/(2\pi)$ de-

viates from the Landauer prediction.

It is also worth mentioning that, in the limit of tunneling through a junction of two quantum wires with Luttinger parameters K_L and K_R (i.e. $x_L \to x_R$ so that the central segment becomes infinitely short), there exists a heuristic understanding of Eq. (2.29): a series connection between an infinite wire with Luttinger parameter K_L and a "contact resistance" G_c[32]. If we assume loss of coherence, we have $G_c^{-1} + \left[K_L e^2/(2\pi)\right]^{-1} = G^{-1}$. Solving for G_c, we find

$$G_c^{-1} = \left(\frac{e^2}{2\pi}\right)^{-1} \frac{1}{2}\left(\frac{1}{K_R} - \frac{1}{K_L}\right). \tag{2.30}$$

Note that here G_c is defined for the right wire relative to the left wire: the sign of G_c changes if it is defined for the left wire relative to the right wire.

2.2 Bosonic approach to junctions of two wires and Y-junctions

We now review the RG flow diagrams of junctions of two wires and Y-junctions[40, 41, 51, 60, 61, 93, 130]. The RG fixed points of these models control their low-energy behavior, and correspond to conformally invariant boundary conditions. The simplest way to identify the RG fixed points is the method of delayed evaluation of boundary condition[51, 93]. While bosonizing the electron operators at the junction according to Eq. (2.9), we keep both types of bosonic variables ϕ and θ without imposing any specific conformally invariant boundary condition on them, thus doubling the degrees of freedom in the system. The boundary conditions are reintroduced and the extraneous degrees of freedom eliminated only when we compute the scaling dimensions of various tunneling processes at the junction.

2.2.1 2-lead junctions

We illustrate the method through 2-lead junctions. Each wire extends from $x = 0$ to ∞, and the junction is located at $x = 0$, as shown in Fig. 2.2 panel a).

Introducing boson fields (ϕ_j, θ_j) for wire j, we further define rescaled fields $\left(\tilde{\phi}_j, \tilde{\theta}_j\right)$ such that

$$\tilde{\phi}_j = \frac{\phi_j}{\sqrt{K_j}},\ \tilde{\theta}_j = \theta_j \sqrt{K_j}, \tag{2.31}$$

where K_j is the Luttinger parameter for wire j; this transformation preserves the commutation

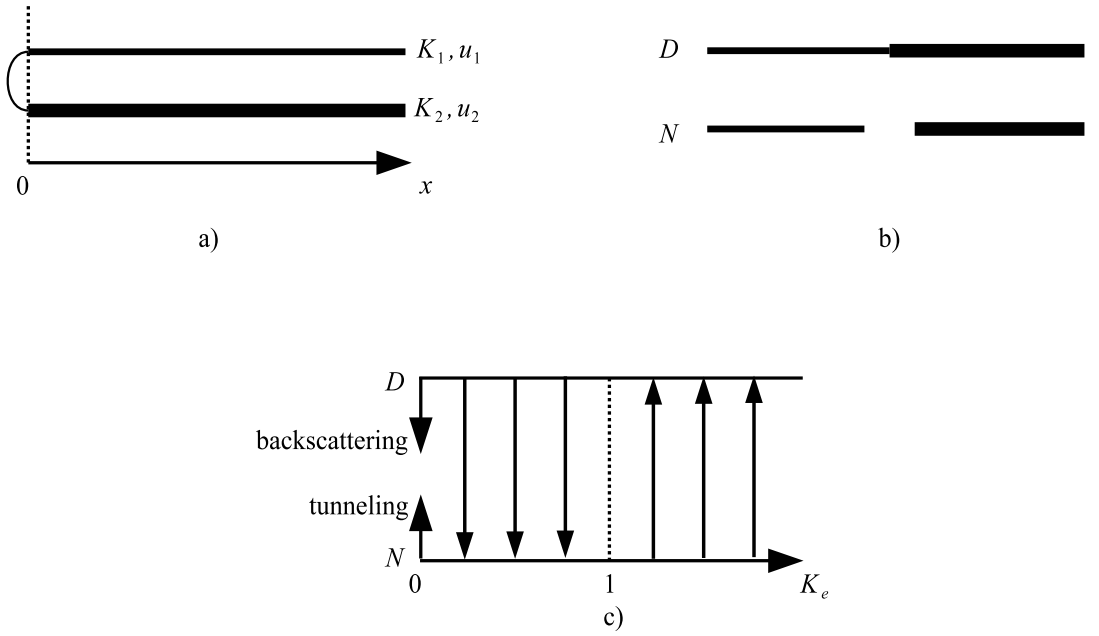

Figure 2.2: a) The sketch of a 2-lead junction, with possibly different Luttinger parameters and speeds of sound in the two wires. The wires extend from $x = 0$ to ∞, and the junction is at $x = 0$. b) The RG fixed points of this model: D (smoothly connected wires) and N (decoupled wires). c) The RG flow diagram from the bosonic approach. RG flows are towards N when $K_e < 1$ (repulsive interactions) and towards D when $K_e > 1$ (attractive interactions); here K_e is the harmonic average of K_1 and K_2.

relation. The imaginary time action of the bulk wires may then be written as a non-interacting form,

$$S_0 = \sum_{j=1,2} \frac{1}{2\pi} \int_0^\infty d\tilde{x} \int_0^\beta d\tau \left[\left(\partial_\tau \tilde{\phi}_j\right)^2 + \left(\partial_{\tilde{x}} \tilde{\phi}_j\right)^2 \right] \tag{2.32a}$$

$$= \sum_{j=1,2} \frac{1}{2\pi} \int_0^\infty d\tilde{x} \int_0^\beta d\tau \left[\left(\partial_\tau \tilde{\theta}_j\right)^2 + \left(\partial_{\tilde{x}} \tilde{\theta}_j\right)^2 \right], \tag{2.32b}$$

where we have also rescaled $x = u_j \tilde{x}$ for wire j.

For future convenience we define the following linear combinations of $\tilde{\theta}$:

$$\Theta_0 = \frac{\sqrt{K_1}\tilde{\theta}_1 + \sqrt{K_2}\tilde{\theta}_2}{\sqrt{K_1+K_2}}, \tag{2.33a}$$

$$\Theta_1 = \frac{\sqrt{K_2}\tilde{\theta}_1 - \sqrt{K_1}\tilde{\theta}_2}{\sqrt{K_1+K_2}}. \tag{2.33b}$$

The bulk action S_0 is also of a non-interacting form in terms of Θ_0 and Θ_1. We can similarly define conjugate variables Φ_0 and Φ_1. The right- and left-moving chiral fields for these linear combinations are

$$\varphi_{0R/L} = \Theta_0 \mp \Phi_0, \tag{2.34a}$$

$$\varphi_{1R/L} = \Theta_1 \mp \Phi_1. \tag{2.34b}$$

The right-movers depend only on $\tau - i\tilde{x}$ and the left-movers depend only on $\tau + i\tilde{x}$. The *LL* and *RR* correlation functions are unaffected by the boundary at $x = 0$:

$$\left\langle \varphi_{jL}(\tau,\tilde{x})\, \varphi_{j'L}(0,0) \right\rangle = \delta_{jj'} \ln \frac{\alpha}{\tau + i\tilde{x} + \alpha \operatorname{sgn}\tau}, \tag{2.35a}$$

$$\left\langle \varphi_{jR}(\tau,\tilde{x})\, \varphi_{j'R}(0,0) \right\rangle = \delta_{jj'} \ln \frac{\alpha}{\tau - i\tilde{x} + \alpha \operatorname{sgn}\tau}; \tag{2.35b}$$

the *LR* and *RL* correlation functions, however, are usually nonzero due to the junction.

Since the total current is conserved at the junction, from Eq. (2.6) we have the boundary condition

$$\partial_x (u_1 K_1 \theta_1 + u_2 K_2 \theta_2)|_{x=0} = \sqrt{K_1+K_2}\, \partial_{\tilde{x}} \Theta_0|_{\tilde{x}=0} = 0; \tag{2.36}$$

Thus $\partial_\tau \Phi_0|_{\tilde{x}=0} = \partial_{\tilde{x}} \Theta_0|_{\tilde{x}=0} = 0$, and Φ_0 is constant ("pinned") at the boundary. This corresponds to the following boundary condition on $\varphi_{0R/L}$:

$$\varphi_{0R}(\tilde{x}=0) = \varphi_{0L}(\tilde{x}=0) + \text{const.} \tag{2.37a}$$

We need an additional boundary condition for the remaining degrees of freedom, in this case $\varphi_{1R/L}$. A natural ansatz is

$$\varphi_{1R}(\tilde{x}=0) = \mathscr{R}_{11} \varphi_{1L}(\tilde{x}=0) + \text{const.}, \tag{2.37b}$$

where $\mathscr{R}$ is an orthogonal matrix; this is because all φ fields are real, and the correlation functions

$\langle \varphi_R \varphi_R \rangle$ and $\langle \varphi_L \varphi_L \rangle$ should have the same constant prefactor. For a junction of two wires, $\mathscr{R}$ is 1×1 and the only possibilities are $\mathscr{R}_{11} = \pm 1$.

We may view the right-movers as analytic continuation of the left-movers. For $\tilde{x} < 0$, based on the above boundary conditions, we have the following "unfolding" transformation:

$$\varphi_{0R}(\tilde{x}) = \varphi_{0L}(-\tilde{x}) + \text{const.}, \tag{2.38a}$$

$$\varphi_{1R}(\tilde{x}) = \mathscr{R}_{11} \varphi_{1L}(-\tilde{x}) + \text{const.} \tag{2.38b}$$

It then follows that, for instance,

$$\langle \varphi_{1R}(\tau, \tilde{x}) \, \varphi_{1L}(0,0) \rangle = \mathscr{R}_{11} \ln \frac{\alpha}{\tau - i\tilde{x} + \alpha \operatorname{sgn} \tau}.$$

Let us calculate the scaling dimensions of some tunneling processes. Defining K_e as the harmonic average of K_1 and K_2,

$$K_e = \frac{2K_1 K_2}{K_1 + K_2}, \tag{2.39}$$

we can write down the bosonized form of several typical processes using Eq. (2.9),

$$\psi_{2R}^\dagger \psi_{1L}\Big|_{x=0} \propto \exp\left[i(\phi_2 - \theta_2 + \phi_1 + \theta_1)\right] = \exp\left[i\left(\sqrt{K_1 + K_2}\Phi_0 + \sqrt{\frac{2}{K_e}}\Theta_1\right)\right], \tag{2.40a}$$

$$\psi_{1R}^\dagger \psi_{1L}\Big|_{x=0} \propto \exp(2i\phi_1) = \exp\left[i\left(\frac{2K_1\Phi_0}{\sqrt{K_1 + K_2}} + \sqrt{2K_e}\Phi_1\right)\right], \tag{2.40b}$$

$$\psi_{2R}^\dagger \psi_{1R}\Big|_{x=0} \propto \exp\left[i(\phi_2 - \theta_2 - \phi_1 + \theta_1)\right] = \exp\left[i\left(\frac{(K_2 - K_1)\Phi_0}{\sqrt{K_1 + K_2}} - \sqrt{2K_e}\Phi_1 + \sqrt{\frac{2}{K_e}}\Theta_1\right)\right], \tag{2.40c}$$

where all boson fields are evaluated at $\tilde{x} = 0$. We have discarded the Klein factors which do not contribute to the power law decay of the correlation functions. Neglecting the constant Φ_0, the correlation functions are easily evaluated:

$$\left\langle T_\tau \exp\left(i\sqrt{\frac{2}{K_e}}\left[\Theta_1(\tau,0) - \Theta_1(0,0)\right]\right)\right\rangle \propto \exp\left(\frac{2}{K_e}\langle T_\tau \Theta_1(\tau,0)\Theta_1(0,0)\rangle\right) = \left(\frac{\alpha}{\tau}\right)^{\frac{1+\mathscr{R}_{11}}{K_e}}, \tag{2.41}$$

meaning $\psi_{2R}^\dagger \psi_{1L}\Big|_{x=0}$ has scaling dimension $(1 + \mathscr{R}_{11})/(2K_e)$. Similarly, $\psi_{1R}^\dagger \psi_{1L}\Big|_{x=0}$ has dimen-

sion $(1-\mathscr{R}_{11})K_e/2$, and $\psi_{2R}^\dagger\psi_{1R}\Big|_{x=0}$ has dimension $(1+\mathscr{R}_{11})/(2K_e)+(1-\mathscr{R}_{11})K_e/2$.

We examine the two conformally invariant boundary conditions separately:

1) When $\mathscr{R}_{11}=1$, $\psi_{2R}^\dagger\psi_{1L}\Big|_{x=0}$ and $\psi_{2R}^\dagger\psi_{1R}\Big|_{x=0}$ have dimension $1/K_e$, whereas $\psi_{1R}^\dagger\psi_{1L}\Big|_{x=0}$ has dimension zero for any K_e, i.e. becomes the identity operator. The latter result implies that ψ_{1R} can be identified with ψ_{1L} up to a constant phase, indicative of an open boundary condition at $x=0$ for both wires. Thus, at this fixed point, the two wires are completely decoupled. Alternatively, note that Φ_0 and Φ_1 are both pinned at $\tilde{x}=0$, so ϕ_1 and ϕ_2 are also pinned; Eq. (2.6) then leads to zero current in each wire. This fixed point is known as the N (Neumann) fixed point in literature. It is stable when $K_e<1$, and unstable when $K_e>1$. The dimension of leading irrelevant operators is $1/K_e$; second-order perturbation theory thus implies that, when $K_e<1$, the conductance is proportional to T^{2/K_e-2} at low temperatures.

2) When $\mathscr{R}_{11}=-1$, $\psi_{1R}^\dagger\psi_{1L}\Big|_{x=0}$ and $\psi_{2R}^\dagger\psi_{1R}\Big|_{x=0}$ have dimension K_e, and $\psi_{2R}^\dagger\psi_{1L}\Big|_{x=0}$ becomes identity. The latter result implies that ψ_{2R} can be identified with ψ_{1L} up to a constant phase, which means the two wires are smoothly connected without backscattering. This fixed point is known as the D (Dirichlet) fixed point. For $K_1=K_2$ it further reduces to the case of a single infinite wire. The D fixed point is stable when $K_e>1$, and unstable when $K_e<1$. The dimension of leading irrelevant operators is K_e, so when $K_e>1$, the low-temperature correction to the zero-temperature conductance should scale as T^{2K_e-2}[51].

These two RG fixed points are shown in Fig. 2.2 panel b), and the RG flow diagram is shown in panel c).

Finally, we calculate the linear dc conductance, again using the Kubo formula. In the dc limit where the current is measured or how the external electric field is applied should be unimportant. Measuring the current at position x on wire j and applying a uniform electric field from 0 to L on wire j', we have the Kubo formula

$$G_{jj'}=\frac{e^2}{\pi^2}u_jK_ju_{j'}K_{j'}\lim_{\omega\to0}\frac{1}{i\omega L}\left[\int d\tau e^{i\omega\tau}\int_0^L dy\left\langle T_\tau\partial_y\theta_{j'}(\tau,y)\,\partial_x\theta_j(0,x)\right\rangle-(\omega\to0)\right]. \tag{2.42}$$

Taking G_{12} as an example,

$$\begin{aligned}G_{12}=\frac{e^2}{\pi^2}\frac{\sqrt{K_1K_2}}{K_1+K_2}\lim_{\omega\to0}\frac{1}{i\omega\frac{L}{u_2}}\Bigg[&\int d\tau e^{i\omega\tau}\int_0^{\frac{L}{u_2}}d\tilde{y}\\&\times\left\langle T_\tau\partial_{\tilde{y}}\left(\sqrt{K_2}\Theta_0-\sqrt{K_1}\Theta_1\right)(\tau,\tilde{y})\,\partial_{\tilde{x}}\left(\sqrt{K_1}\Theta_0+\sqrt{K_2}\Theta_1\right)(0,\tilde{x})\right\rangle-(\omega\to0)\Bigg];\end{aligned} \tag{2.43}$$

the $\langle\Theta_0\Theta_1\rangle$ and $\langle\Theta_1\Theta_0\rangle$ cross terms vanish as Θ_0 and Θ_1 are decoupled, and the $\langle\Theta_0\Theta_0\rangle$ contribution must also vanish since it corresponds to the conductance of a semi-infinite wire. The remaining $\langle\Theta_1\Theta_1\rangle$ contribution is straightforward to evaluate:

$$
\begin{aligned}
G_{12} &= -\frac{e^2}{\pi^2}\frac{K_1K_2}{K_1+K_2}\lim_{\omega\to 0}\frac{1}{4i\omega\frac{L}{u_2}}\left[\int d\tau e^{i\omega\tau}\int_0^{\frac{L}{u_2}} d\tilde{y}\partial_{\tilde{y}}\partial_{\tilde{x}}\left\langle T_\tau\left(\varphi_{1R}+\varphi_{1L}\right)(\tau,\tilde{y})\left(\varphi_{1R}+\varphi_{1L}\right)(0,\tilde{x})\right\rangle-(\omega\to 0)\right] \\
&= -\frac{e^2}{\pi^2}\frac{K_1K_2}{K_1+K_2}\lim_{\omega\to 0}\frac{1}{4i\omega\frac{L}{u_2}}\left\{\int d\tau e^{i\omega\tau}\int_0^{\frac{L}{u_2}} d\tilde{y}\partial_{\tilde{y}}\partial_{\tilde{x}}\left[\ln\frac{\alpha^2}{\tau^2+(\tilde{y}-\tilde{x})^2}+\mathscr{R}_{11}\ln\frac{\alpha^2}{\tau^2+(\tilde{y}+\tilde{x})^2}\right]-(\omega\to 0)\right\} \\
&= -\frac{e^2}{\pi^2}\frac{K_1K_2}{K_1+K_2}\lim_{\omega\to 0}\frac{1}{4i\omega\frac{L}{u_2}}\left\{(2\pi i)\left[e^{-\omega\left|\frac{L}{u_2}-\tilde{x}\right|}\operatorname{sgn}\left(\frac{L}{u_2}-\tilde{x}\right)+e^{-\omega\tilde{x}}-\mathscr{R}_{11}e^{-\omega\left(\frac{L}{u_2}+\tilde{x}\right)}+\mathscr{R}_{11}e^{-\omega\tilde{x}}\right]-(\omega\to 0)\right\} \\
&= \frac{1-\mathscr{R}_{11}}{2}K_e\frac{e^2}{2\pi}.
\end{aligned}
\tag{2.44}
$$

In other words, the conductance at the N fixed point is 0, and the conductance at the D fixed point is $K_e e^2/(2\pi)$. This is a special case of Eq. (2.29).

2.2.2 Y-junctions

We proceed to apply the method above to Y-junctions[51]. In this case, the "center-of-mass" field Θ_0 should be

$$
\Theta_0 = \frac{\sqrt{K_1}\tilde{\theta}_1+\sqrt{K_2}\tilde{\theta}_2+\sqrt{K_3}\tilde{\theta}_3}{\sqrt{K_1+K_2+K_3}}, \tag{2.45}
$$

while a convenient set of definitions of the remaining two Θ fields is

$$
\Theta_1 = \frac{\sqrt{K_2}\tilde{\theta}_1-\sqrt{K_1}\tilde{\theta}_2}{\sqrt{K_1+K_2}}, \tag{2.46}
$$

$$
\Theta_2 = \frac{\sqrt{K_1K_3}\tilde{\theta}_1+\sqrt{K_2K_3}\tilde{\theta}_2-(K_1+K_2)\tilde{\theta}_3}{\sqrt{K_1+K_2+K_3}\sqrt{K_1+K_2}}. \tag{2.47}
$$

(Other linear combinations are possible, as long as they are orthogonal to each other and to Θ_0.) Again Φ fields can be similarly defined, and their chiral fields are given as before. Φ_0 is pinned at the junction $\tilde{x}=0$ by current conservation, and $\varphi_{0R/L}$ obey an open boundary condition. We group the remaining fields as $\vec{\Theta}\equiv(\Theta_1,\Theta_2)$ and $\vec{\Phi}\equiv(\Phi_1,\Phi_2)$, and express the boundary condition for these fields as $\vec{\varphi}_R=\mathscr{R}\vec{\varphi}_L$. $\mathscr{R}$ is now a 2×2 rotation matrix which can be parametrized as

$$
\mathscr{R} = \begin{pmatrix} \cos\xi & \sin\xi \\ -\sin\xi & \cos\xi \end{pmatrix}. \tag{2.48}
$$

It is tedious but straightforward to enumerate all single-particle processes at the junction and express their scaling dimensions in terms of $\mathscr{R}$.

It turns out that there are at least four different types of fixed points, namely the N fixed point with three decoupled wires where $\xi=0$ and $\mathscr{R}=1$, the A_j fixed point with wire j ($j=1,2,3$)

decoupled from the other two wires which are smoothly connected, and also two types of fixed points with novel physics: D (Dirichlet) fixed point and $\chi^{\pm}$ (chiral) fixed points.

At the D fixed point, $\xi = \pi$ and $\mathscr{R} = -1$. None of the single-particle tunneling processes becomes identity, but some two-particle processes do, such as $\psi_{2R}^{\dagger}\psi_{1L}\psi_{2L}^{\dagger}\psi_{1R}$ which describes an electron pair tunneling from wire 1 to wire 2. This evinces Andreev reflection physics at the D fixed point. We can also look at the linear dc conductance

$$G_{jj'}^{D} = 2\frac{e^2}{2\pi}\left(-K_j\delta_{jj'} + \frac{K_jK_{j'}}{K_1+K_2+K_3}\right), \tag{2.49}$$

which indicates $G_{11} = -(4/3)\,e^2/(2\pi)$ in the case of non-interacting wires $K_1 = K_2 = K_3 = 1$. (In this case the D fixed point would only be possible for an interacting junction.) $|G_{11}|$ exceeds $e^2/(2\pi)$, and the enhancement can be attributed to Andreev reflection. The D fixed point cannot possibly be stable unless the interactions in all three wires are very strongly attractive.

At the $\chi^{\pm}$ fixed points, $\tan\xi = \pm\sqrt{(K_1+K_2+K_3)/(K_1K_2K_3)}$. At χ^{+}, $\psi_{2R}^{\dagger}\psi_{1L}$, $\psi_{3R}^{\dagger}\psi_{2L}$ and $\psi_{1R}^{\dagger}\psi_{3L}$ simultaneously become identity; heuristically, this means incident electrons are scattered from wire j into wire $j+1$ (here we identify $j+3 \equiv j$). Similarly, at χ^{-}, $\psi_{1R}^{\dagger}\psi_{2L}$, $\psi_{2R}^{\dagger}\psi_{3L}$ and $\psi_{3R}^{\dagger}\psi_{1L}$ simultaneously become identity. The linear dc conductance is given by

$$G_{jj'}^{\chi^{\pm}} = -2\frac{e^2}{2\pi}\frac{K_j(K_1+K_2+K_3)\,\delta_{jj'} + \left(\pm K_1K_2K_3\varepsilon_{jj'} - K_jK_{j'}\right)}{K_1+K_2+K_3+K_1K_2K_3}, \tag{2.50}$$

where the anti-symmetric tensor $\varepsilon_{jj'}$ is defined as follows: $\varepsilon_{12} = \varepsilon_{23} = \varepsilon_{31} = 1$, $\varepsilon_{21} = \varepsilon_{32} = \varepsilon_{13} = -1$, $\varepsilon_{jj} = 0$.

We now focus on the Z_3 symmetric Y-junction of three identical quantum wires, with Luttinger parameter $K_j = K$. The RG flow diagram is greatly simplified under this assumption[93].

1) At $K < 1$, the only stable fixed point is the N fixed point. Neither $\chi^{\pm}$ nor D is stable.

2) At $K = 1$, the system is non-interacting in the bulk and all single-particle processes are marginal in the RG sense. There is a manifold of fixed points, which contains both N and $\chi^{\pm}$, although not D.

3) At $1 < K < 3$, N becomes unstable, and the RG flows are eventually toward $\chi^{\pm}$ which become stable. However, while N preserves time-reversal symmetry, $\chi^{\pm}$ explicitly breaks it (since $G_{jj'}^{\chi^{\pm}} \neq G_{j'j}^{\chi^{\pm}}$ when $j \neq j'$). Therefore the most economic assumption is that there exists an intermediate fixed point (termed M for mysterious) that preserves time-reversal symmetry. M is stable against time-reversal symmetric perturbations, such as tunneling between any two wires; however, it is unstable against time-reversal symmetry breaking perturbations, such as an AB phase at the junction that is seen in either tunneling cycle ($1 \to 2 \to 3 \to 1$ or $1 \to 3 \to 2 \to 1$). It is not difficult to see from a non-interacting model that M also belongs to the fixed manifold when $K = 1$. D remains unstable.

4) At $K = 3$, the system again has non-interacting quasiparticles but they are not the bare elec-

trons. There is a manifold of fixed points, which contains $\chi^{\pm}$ but not N, M or D.

5) At $K > 3$, N remains unstable, $\chi^{\pm}$ becomes unstable once more, and D becomes stable. (There are in fact two types of D fixed points which have the same conductance tensor; however, only one type can be reached by an RG flow that preserves time-reversal symmetry. This type of D fixed point is stable when $K > 9$.)

We are particularly interested in the realistic case of K close to 1, when the interactions are not too strong. In this case the D fixed point is never stable, and important fixed points are N, $\chi^{\pm}$, M and also the asymmetric A_j if Z_3 asymmetry is allowed. The RG flow diagrams for $K < 1$ and $1 < K < 3$ are depicted in Fig. 2.3, along with schematic representations of N, χ^{+}, M, A_3 and D. Unfortunately, important as the M fixed point may be in the presence of time-reversal symmetry and Z_3 symmetry, we are unaware of its corresponding conformally invariant boundary condition in terms of bosonic variables. In the remainder of this chapter, we turn to the fermionic approach to junctions of quantum wires, which appears to be a more convenient description of the M fixed point.

2.3 Fermionic formulation

In this section, we establish the model Hamiltonian for a generic junction of interacting quantum wires, to be studied by the fermionic approach in the remainder of the chapter.

The system consists of N quantum wires of interacting spinless electrons, numbered $j = 1, 2, ..., N$, meeting at a junction which we choose as the origin $x = 0$. We align the wires so that they are parallel to the $+x$ axis; see Fig. 2.4.

In the continuum limit of the model, on each quantum wire we retain right- and left-movers in narrow bands of wave vectors around the Fermi points $\pm k_{Fj}$:

$$\psi_j(x) \approx e^{ik_{Fj}x}\psi_{jR}(x) + e^{-ik_{Fj}x}\psi_{jL}(x) = \int_{-D}^{D} \frac{dE}{\sqrt{2\pi v_{Fj}}} \left[\psi_{jR}(E)\, e^{i\left(\frac{E}{v_{Fj}} + k_{Fj}\right)x} + \psi_{jL}(E)\, e^{-i\left(\frac{E}{v_{Fj}} + k_{Fj}\right)x} \right], \tag{2.51}$$

where v_{Fj} is the Fermi velocity in wire j, the dispersion relation is linearized as $E = E_j(k) = v_{Fj}k$, and $D \ll v_{Fj}k_{Fj}$ is the high-energy cutoff. Left-movers ψ_{jL} are incident on the junction, scattered, and turned into right-movers $\psi_{j'R}$; ψ_{jL} and $\psi_{j'R}$ are not independent degrees of freedom, but related by the single-particle S-matrix of the junction $S_{jj'}$ [see also Eq. (2.57)].

The Hamiltonian consists of three parts:

$$H = \sum_{j=1}^{N} \left(H^j_{0,\text{wire}} + H^j_{\text{int}} \right) + H_{0,B}. \tag{2.52}$$

$H^j_{0,\text{wire}}$ is the non-interacting part of the Hamiltonian for wire j, quadratic in electron operators,

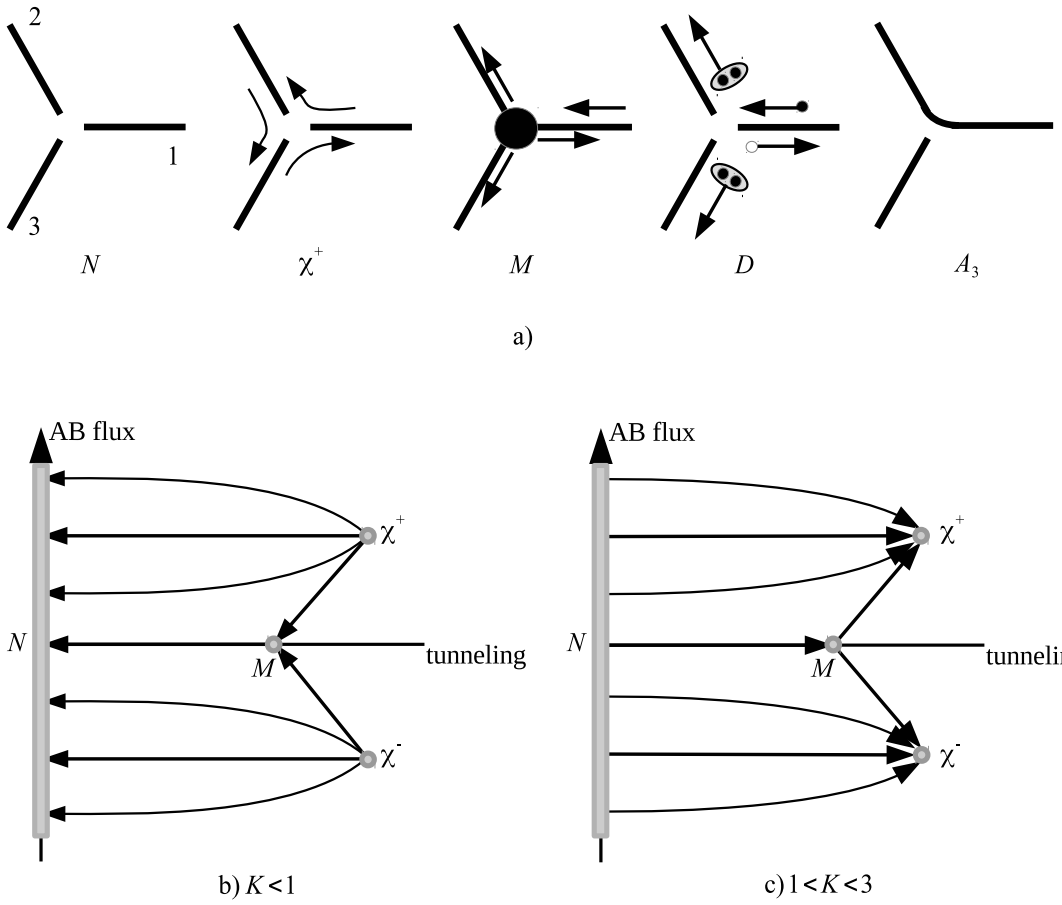

Figure 2.3: a) Typical RG fixed points of the Y-junction, as predicted by the bosonic approach (with the exception of the M fixed point): N (decoupled wires), χ^+ (chiral transmission which breaks time-reversal symmetry: 1 to 2, 2 to 3 and 3 to 1), M (electrons incident from any wire can be reflected or transmitted), D (Andreev reflection) and the asymmetric A_3 (1 and 2 are smoothly connected and 3 is decoupled). b) The RG flow diagram for a Z_3 symmetric Y-junction at $K < 1$. The horizontal axis measures the coupling strength between any two wires, so the N fixed point occupies the entire vertical axis. The vertical axis measures time-reversal symmetry breaking (e.g. due to an AB flux at the junction), which means the time-reversal symmetric M should be on the horizontal axis, but $\chi^\pm$ should not. RG flows are always towards N when $K < 1$, although it is found from the fermionic approach that M is more stable than $\chi^\pm$. c) Same as b) but with $1 < K < 3$. RG flows are towards $\chi^\pm$ whenever time-reversal symmetry is broken; in the time-reversal symmetric case, however, the RG flow is from N to M.

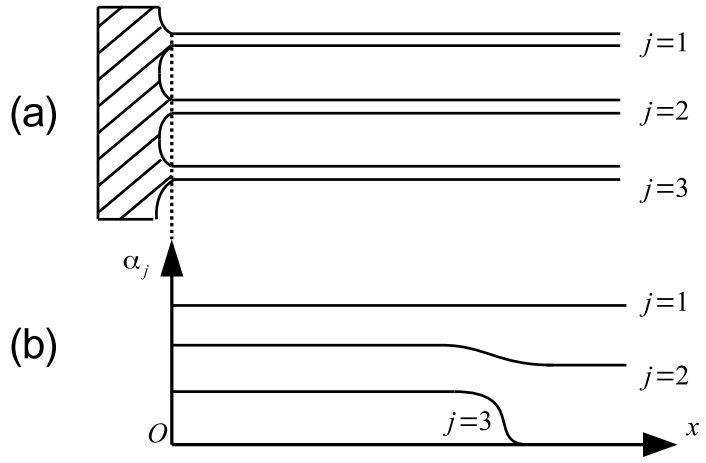

Figure 2.4: Sketch of a typical junction system with the number of quantum wires $N = 3$. The shaded junction area to the left is modeled by quadratic hopping terms between ends of the wires, which are all aligned at the origin $x = 0$. The electron-electron interaction strengths inside the wires are also plotted for comparison. The interaction strength in wire $j = 1$ is uniform, and that in wire $j = 2$ also goes to a constant nonzero value as $x \to \infty$; these two wires are said to be attached to TLL leads. In contrast, the wire $j = 3$ has a vanishing interaction strength far away from the junction, and is connected to an FL lead (the FL lead itself is too wide to be shown in full).

$$H^j_{0,\text{wire}} \approx iv_{Fj}\int_0^\infty dx\left[\psi^\dagger_{jL}\partial_x\psi_{jL} - \psi^\dagger_{jR}\partial_x\psi_{jR}\right](x) \approx \int_{-D}^{D} dE\,E\left(\psi^\dagger_{jR}(E)\,\psi_{jR}(E) - \psi^\dagger_{jL}(E)\,\psi_{jL}(E)\right), \tag{2.53}$$

while the quartic term H^j_{int} to be specified below describes the electron-electron interaction in wire j. The boundary term $H_{0,B}$ is quadratic, and is responsible for electron transfer between wires across the junction. For simplicity we again assume that each wire only supports one single channel, and ignore quartic interactions between wires, at the junction and between the junction and the wires.

To model the electron-electron interaction, we assume it is short-ranged and the system is away from half-filling, so that the Umklapp processes are unimportant. We further ignore processes where two chiral densities of the same chirality interact with one another, $\psi^\dagger_R\psi_R\psi^\dagger_R\psi_R$ or $\psi^\dagger_L\psi_L\psi^\dagger_L\psi_L$; as discussed in Section 2.1 these g_4 processes renormalize the Fermi velocity but do not change the Luttinger parameter by themselves. For spinless fermions, this leaves us with only processes involving two chiral densities of different chiralities (g_2 processes) $\psi^\dagger_R\psi_R\psi^\dagger_L\psi_L$. The electron-electron interaction is then represented by a spatially variant g_2 term:

$$H_{\text{int}}^{j}=\int_{0}^{\infty}dx g_{2}^{j}(x)\,\psi_{jR}^{\dagger}(x)\,\psi_{jR}(x)\,\psi_{jL}^{\dagger}(x)\,\psi_{jL}(x)\,. \tag{2.54}$$

$g_2^j(x\to\infty)$ is a constant. A finite $g_2^j(\infty)\neq 0$ corresponds to a TLL lead attached to wire j, while if $g_2^j(\infty)=0$ the junction is considered to be connected to an FL lead. We define a dimensionless interaction strength

$$\alpha_j(x)=g_2^j(x)/(2\pi v_{Fj})\,. \tag{2.55}$$

Along the lines of Refs. [77, 132], viewing the electron-electron interaction as a perturbation, we can first diagonalize the quadratic part of the Hamiltonian. The resultant eigenstates, which form the so-called scattering basis, can be related to the S-matrix in the low-energy theory. Note that such a scattering basis transformation is independent of the actual eigenstates of the fully interacting system; we are therefore always able to proceed with this transformation, regardless of whether the interaction is present at $x\to\infty$. For non-resonant scattering, which we assume throughout this chapter, the S-matrix elements $S_{jj'}(E)\equiv S_{jj'}$ are independent of the electron energy E at low energies, and the single-particle scattering state incident from wire j' with energy E' reads

$$\phi_{j'}^{\dagger}\left(E'\right)|0\rangle=\sum_{j}\int_{0}^{\infty}dx\frac{1}{\sqrt{2\pi v_{Fj}}}\left(\delta_{jj'}e^{-i\frac{E'}{v_{Fj}}x}\psi_{jL}^{\dagger}(x)+S_{jj'}e^{i\frac{E'}{v_{Fj}}x}\psi_{jR}^{\dagger}(x)\right)|0\rangle+\cdots, \tag{2.56}$$

where $|0\rangle$ corresponds to the filled Fermi sea, and the omitted terms represent the part of the wave function from the junction area. Under our assumption of non-resonant scattering, these omitted terms do not contribute to the renormalization of the interaction[132]. Inverting Eq. (2.56) we may express the original electrons ψ in terms of the scattering basis operators ϕ,

$$\begin{aligned}\psi_{jR}(E)&=\sum_{j'=1}^{N}\int dE'\int_{0}^{\infty}dx\left(\frac{1}{\sqrt{2\pi v_{Fj}}}e^{i\frac{E}{v_{Fj}}x}\right)^{*}\left(\frac{1}{\sqrt{2\pi v_{Fj}}}S_{jj'}e^{i\frac{E'}{v_{Fj}}x}\right)\phi_{j'}\left(E'\right)\\&=\sum_{j'}\int_{-D}^{D}\frac{dE'}{2\pi}\frac{-i}{E-E'-i0}S_{jj'}\phi_{j'}\left(E'\right).\end{aligned} \tag{2.57a}$$

Similarly

$$\psi_{jL}(E)=\int_{-D}^{D}\frac{dE'}{2\pi}\frac{i}{E-E'+i0}\phi_{j}\left(E'\right). \tag{2.57b}$$

The coefficients of this transformation would be δ-functions if the Fourier transform were performed on the real axis; however, they pick up a principal value part here because our system is defined on the positive x-axis.

Now recast the Hamiltonian in the scattering basis. By definition, the quadratic part of the Hamiltonian is diagonal:

$$\sum_{j=1}^{N} H^{j}_{0,\text{wire}} + H_{0,B} = \sum_{j} \int dE\, E \phi^{\dagger}_{j}(E)\, \phi_{j}(E). \tag{2.58}$$

We insert the scattering basis transformation into the interaction Eq. (2.54). Allowing the energies to run freely from $-\infty$ to ∞ and calculating the energy integrals using the method of residues[34], we find

$$H^{j}_{\text{int}} = \int_{0}^{\infty} dx g^{j}_{2}(x) \sum_{l_1 l_2 l_3 l_4} \int \frac{dE_1 dE_2 dE_3 dE_4}{(2\pi)^2 v^2_{Fj}} \phi^{\dagger}_{l_1}(E_1)\, \phi_{l_2}(E_2)\, \phi^{\dagger}_{l_3}(E_3)\, \phi_{l_4}(E_4)\, e^{i(-E_1+E_2+E_3-E_4)\frac{x}{v_{Fj}}} S^{*}_{jl_1} S_{jl_2} \delta_{jl_3} \delta_{jl_4} \tag{2.59}$$

This is a plausible manipulation, seeing that the scattering basis transformation should not introduce additional singularities at the band edge. Now

$$H^{j}_{\text{int}} = \int_{0}^{\infty} dx g^{j}_{2}(x) \sum_{l_1 l_2 l_3 l_4} \int \frac{dE_1 dE_2 dE_3 dE_4}{(2\pi)^2 v^2_{Fj}} \rho^{j}_{l_1 l_2 l_3 l_4}(E_1, E_2, E_3, E_4; x)\, \phi^{\dagger}_{l_1}(E_1)\, \phi_{l_2}(E_2)\, \phi^{\dagger}_{l_3}(E_3)\, \phi_{l_4}(E_4), \tag{2.60}$$

where we introduce the function

$$\rho^{j}_{l_1 l_2 l_3 l_4}(E_1, E_2, E_3, E_4; x) \equiv \frac{1}{2}\left[e^{i(-E_1+E_2+E_3-E_4)\frac{x}{v_{Fj}}} S^{*}_{jl_1} S_{jl_2} \delta_{jl_3} \delta_{jl_4} + e^{i(-E_3+E_4+E_1-E_2)\frac{x}{v_{Fj}}} S^{*}_{jl_3} S_{jl_4} \delta_{jl_1} \delta_{jl_2} \right]. \tag{2.61}$$

Note that we have symmetrized the function ρ so that $\rho^{j}_{l_1 l_2 l_3 l_4}(E_1, E_2, E_3, E_4; x) = \rho^{j}_{l_3 l_4 l_1 l_2}(E_3, E_4, E_1, E_2; x)$. This interaction is diagrammatically represented by the symmetric vertex in Fig. 2.5. We may well opt not to symmetrize ρ; however, the two created electrons $E_1 l_1$ and $E_3 l_3$ (or the two annihilated electrons $E_2 l_2$ and $E_4 l_4$) would be inequivalent in that case, and the diagrammatic bookkeeping would be more difficult.

2.4 Wilsonian approach to S-matrix renormalization

We now review the derivation of the S-matrix RG equation using the Wilsonian scaling approach in Ref. [132].

Starting from Eq. (2.60), we reduce the energy cutoff D to $D - \delta D$ ($\delta D \ll D$), and integrate out the so-called "fast modes" with energies in one of the two slices $(-D + \delta D, -D)$ and $(D - \delta D, D)$. This procedure generates corrections of $O(\alpha \delta D / D)$ to the quadratic part of the Hamiltonian [Eq. (2.58)] as well as the quartic part [Eq. (2.60)]. We assume that the corrections

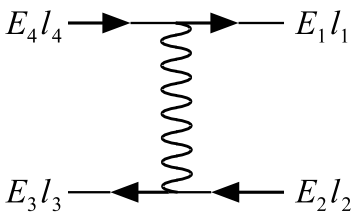

Figure 2.5: Diagrammatic representation of the electron-electron interaction.

to the quartic part are unimportant; the rationale is that the quartic part originates entirely from the bulk, so it should renormalize independently of the junction. In fact, since the quartic part is free of Umklapp processes, it should be exactly marginal in the RG sense[109]. Meanwhile, the renormalized quadratic part becomes off-diagonal and must be diagonalized with a new scattering basis, which is in turn associated with a running (i.e. cutoff-dependent) S-matrix.

The quadratic correction generated by Eq. (2.60) reads

$$\delta H_0^j = -2\int_0^\infty dx g_2^j(x) \sum_{l_1 l_2 l_3} \int_{\delta D} dE_1 \int_{-D}^{D} \frac{dE_2 dE_3}{(2\pi)^2 v_{Fj}^2} \rho^j_{l_1 l_2 l_3 l_1}(E_1, E_2, E_3, E_1; x) f(E_1) \phi^\dagger_{l_3}(E_3) \phi_{l_2}(E_2). \tag{2.62}$$

The E_2E_3 contraction is equivalent to the E_1E_4 contraction; hence the factor of 2. The E_1E_2 and E_3E_4 contractions are discarded because, once we sum over l taking into account the S-matrix unitarity $\sum_{l_1} \left|S_{jl_1}\right|^2 = 1$, we find the resulting "tadpole" diagrams only harmlessly shift the chemical potential[109].

We let ϕ' be the renormalized scattering basis after integrating out fast modes. ϕ' is related to ϕ by another S-matrix, $S^\delta_{jj'}$, which only weakly deviates from the $N \times N$ identity matrix:

$$\phi_j(E) = \int \frac{dE'}{2\pi} \left[\frac{i}{E - E' + i0} \phi'_j(E') + \frac{-i}{E - E' - i0} \sum_{j'} S^\delta_{jj'}(E'; E) \phi'_{j'}(E') \right] \tag{2.63}$$

The inverse transformation is obtained by calculating anti-commutators:

$$\left(\phi'_{j'}(E')\right)^\dagger = \sum_j \int \frac{dE}{2\pi} \left[\frac{i}{E - E' + i0} \delta_{jj'} + \frac{-i}{E - E' - i0} S^\delta_{jj'}(E'; E) \right] \phi^\dagger_j(E) \tag{2.64}$$

By definition ϕ' diagonalizes the renormalized quadratic Hamiltonian,

$$\left[\sum_j H^j_{0,\text{wire}} + H_{0,B} + \sum_j \delta H^j_0, \left(\phi'_{j'}\left(E'\right)\right)^\dagger\right] = E'\left(\phi'_{j'}\left(E'\right)\right)^\dagger \tag{2.65}$$

Substituting Eq. (2.64) into the above, we find to $O\left(\delta D/D\right)$

$$\begin{aligned} i\left[\delta_{jj'} - S^\delta_{jj'}\left(E';E\right)\right] = \delta D \int_0^\infty dx \Bigg\{ & f\left(D\right)\left[\frac{\alpha_j\left(x\right)}{v_{Fj}} S^*_{jj} S_{jj'} e^{-i\frac{2D-E-E'}{v_{Fj}}x} + \frac{\alpha_{j'}\left(x\right)}{v_{Fj'}} S_{j'j'} S^*_{j'j} e^{i\frac{2D-E-E'}{v_{Fj'}}x}\right] \\ & + f\left(-D\right)\left[\frac{\alpha_j\left(x\right)}{v_{Fj}} S^*_{jj} S_{jj'} e^{i\frac{2D+E+E'}{v_{Fj}}x} + \frac{\alpha_{j'}\left(x\right)}{v_{Fj'}} S_{j'j'} S^*_{j'j} e^{-i\frac{2D+E+E'}{v_{Fj'}}x}\right]\Bigg\}. \end{aligned} \tag{2.66}$$

We now perform the x integral in a simple model. Let us assume that the junction is connected through wire n to a TLL or FL lead at $x = L_n$; in other words, when $x \geq L_n$, $\alpha_n\left(x\right) = \alpha_n\left(\infty\right)$ becomes a constant independent of x and $d\alpha_n\left(x\right)/dx = 0$. We further assume that the interaction inside the wire is also uniform, i.e.

$$\alpha_j\left(x\right) = \alpha_j\left(0\right) + \left[\alpha_j\left(\infty\right) - \alpha_j\left(0\right)\right] H\left(x - L_j\right) \tag{2.67}$$

where $H\left(x\right)$ is the Heaviside unit-step function. Now

$$\begin{aligned} \delta_{jj'} - S^\delta_{jj'}\left(E';E\right) = \delta D \Bigg\{ & f\left(D\right)\left[S^*_{jj} S_{jj'} \frac{\left(\alpha_j\left(0\right) - \alpha_j\left(\infty\right)\right) e^{-i\frac{2D-E-E'}{v_{Fj}}L_j} - \alpha_j\left(0\right)}{2D-E-E'}\right. \\ & \left. + S_{j'j'} S^*_{j'j} \frac{\left(\alpha_{j'}\left(0\right) - \alpha_{j'}\left(\infty\right)\right) e^{i\frac{2D-E-E'}{v_{Fj'}}L_{j'}} - \alpha_{j'}\left(0\right)}{2D-E-E'}\right] + f\left(-D\right)\left[S^*_{jj} S_{jj'} \frac{\left(\alpha_j\left(0\right) - \alpha_j\left(\infty\right)\right) e^{i\frac{2D+E+E'}{v_{Fj}}L_j} - \alpha_j\left(0\right)}{-2D-E-E'}\right. \\ & \left. + S_{j'j'} S^*_{j'j} \frac{\left(\alpha_{j'}\left(0\right) - \alpha_{j'}\left(\infty\right)\right) e^{-i\frac{2D+E+E'}{v_{Fj'}}L_{j'}} - \alpha_{j'}\left(0\right)}{-2D-E-E'}\right]\Bigg\} \end{aligned} \tag{2.68}$$

If $D \gtrsim |E|, |E'|, \pm 2D - E - E'$ can be approximated as $\pm 2D$, thus giving rise to a scaling contribution $O\left(\delta D/D\right)$. If $D \gtrsim v_{Fn}/L_n$, $\exp\left(\pm i 2DL_n/v_{Fn}\right)$ oscillates rapidly with D and is negligible; on the other hand, when $D \lesssim v_{Fn}/L_n$, $\exp\left(\pm i 2DL_n/v_{Fn}\right) \approx 1$. Finally, if $D \gtrsim T$, the factors $f\left(D\right) \approx 0$ and $f\left(-D\right) \approx 1$ are approximately independent of D. Therefore, to $O\left(\delta D/D\right)$, Eq. (2.68) predicts that

$$S^\delta_{jj'}\left(E;E'\right) = \delta_{jj'} - \frac{\delta D}{2D}\left(\alpha_j\left(D\right) S^*_{jj} S_{jj'} - \alpha_{j'}\left(D\right) S_{j'j'} S^*_{j'j}\right) \tag{2.69}$$

independent of $|E|$, $|E'|$ and T as long as $D \gtrsim \max\left\{|E|, |E'|, T\right\}$. Here we have defined a cutoff-dependent interaction strength

$$\alpha_n(D) \equiv \begin{cases} \alpha_n(0), D \gtrsim v_{Fn}/L_n \\ \alpha_n(\infty), D \lesssim v_{Fn}/L_n \end{cases}. \tag{2.70}$$

This means the renormalization will stop at the energy scale of the incident/scattered electron or the temperature, whichever is higher. In addition, the energy scale associated with the inverse length of wire n, v_{Fn}/L_n, determines whether the renormalization due to that wire is controlled by interaction strength in the wire $\alpha_n(0)$ or that in the lead $\alpha_n(\infty)$: the effective interaction strength crosses over from $\alpha_n(0)$ to $\alpha_n(\infty)$ as the D is reduced below v_{Fn}/L_n.

The renormalized S-matrix $S+\delta S$ relates ϕ' to the original fermions ψ. Inserting Eq. (2.63) into Eq. (2.57) we find that δS and S^δ obey the simple matrix relation $\delta S = SS^\delta - S$, and according to Eq. (2.69), $\delta S_{jj'}$ is given by

$$\delta S_{jj'} = -\frac{\delta D}{2D}\left(\sum_n \alpha_n(D) S_{jn} S^*_{nn} S_{nj'} - \alpha_j(D) S_{jj}\delta_{jj'}\right). \tag{2.71}$$

We are now in a position to write down the RG equation for the S-matrix valid to $O(\alpha)$. Restoring the explicit cutoff dependence, we have

$$-\frac{dS_{jj'}(D)}{d\ln D} = -\frac{1}{2}\sum_n \alpha_n(D)\left[S_{jn}(D) S^*_{nn}(D) S_{nj'}(D) - \delta_{j'n} S_{nn}(D)\,\delta_{nj}\right] \tag{2.72}$$

where the RG flow is cut off at the temperature T. In the special case of α_n independent of D, this is the equation given in Refs. [70, 77]. It can be readily checked that Eq. (2.72) preserves the unitarity of the S-matrix.

We pause to remark that, as the cutoff is reduced below the inverse length of one of the wires, renormalization due to that wire is governed only by the lead to which that wire is attached. This is reasonable because a junction of finite-length TLL wires attached to FL leads should, at low energies, renormalize into a junction connected directly to FL leads[12, 42, 93].

2.5 First-order perturbation theory conductance

Intuitively, once the renormalization flow of the S-matrix is stopped by a physical infrared cutoff, the renormalized S-matrix should represent the non-interacting part of the low-energy theory of the junction, and can be taken as an input to the Landauer formalism. However, such an argument does not address the role of the low-energy residual interaction, which turns out to be especially important in the case of TLL leads. Also, in principle, the Landauer formalism is well-founded only in the absence of inelastic scattering. We are therefore motivated to study the conductance in the CS formulation, which fully exposes possible deviations from the Landauer predictions.

In the CS formulation of RG, we start from a field theory with a running cutoff D, and calculate low-energy physical observables (in our case the linear dc conductance tensor $G_{jj'}$) as a function of the running coupling constants of the theory [in our case the S-matrix elements $S_{jj'}(D)$]. This is

once again accomplished by perturbation theory in interaction. We require that when D is greater than the energy scales at which the system is probed, namely the finite temperature T, $G_{jj'}$ should be independent of D. Therefore, by allowing the cutoff to run from D to $D-\delta D$, where $\delta D \ll D$, we can find the RG equation satisfied by the coupling constants $S_{jj'}(D)$, and subsequently find the conductance. In this section and the next, we first compute the linear dc conductance in Kubo formalism to the first order in interaction, then apply the CS formulation to our perturbation theory results.

The current operator at coordinate x in wire j is first written in terms of the fermion fields:

$$\hat{I}_j(x) = ev_{Fj}\left(\psi_{jR}^{\dagger}\psi_{jR} - \psi_{jL}^{\dagger}\psi_{jL}\right)(x). \tag{2.73}$$

Note that $\hat{I}_j$ is not changed by the interaction; it is proportional to the commutator of the electron density with the Hamiltonian, but the interaction commutes with the electron density. Using Eq. (2.57) we find the imaginary time correlation function $\Omega_{jj'}(x,x';\tau-\tau') \equiv -\left\langle T_\tau I_j(x,\tau) I_{j'}(x',\tau')\right\rangle$ to be

$$\begin{aligned}
&\Omega_{jj'}\left(x,x';\tau-\tau'\right) \\
&= -\frac{e^2}{(2\pi)^2}\sum_{j_1 j_2 j_1' j_2'}\int d\varepsilon_1 d\varepsilon_2 d\varepsilon_1' d\varepsilon_2' \left[e^{i\frac{\varepsilon_2-\varepsilon_1}{v_{Fj}}x} S_{jj_1}^{*} S_{jj_2} - e^{-i\frac{\varepsilon_2-\varepsilon_1}{v_{Fj}}x}\delta_{jj_1}\delta_{jj_2}\right] \\
&\times\left[e^{i\frac{\varepsilon_2'-\varepsilon_1'}{v_{Fj'}}x'} S_{j'j_1'}^{*} S_{j'j_2'} - e^{-i\frac{\varepsilon_2'-\varepsilon_1'}{v_{Fj'}}x'}\delta_{j'j_1'}\delta_{j'j_2'}\right]\left\langle T_\tau \phi_{j_1}^{\dagger}(\varepsilon_1,\tau)\phi_{j_2}(\varepsilon_2,\tau)\phi_{j_1'}^{\dagger}\left(\varepsilon_1',\tau'\right)\phi_{j_2'}\left(\varepsilon_2',\tau'\right)\right\rangle_{\mathrm{H}}.
\end{aligned} \tag{2.74}$$

The imaginary time-ordered expectation value should be evaluated in the Heisenberg picture. The linear dc conductance $G_{jj'}$ is then given by the retarded current-current correlation function Ω,

$$G_{jj'}\left(x,x'\right) = \lim_{\omega\to 0}\lim_{\eta_\omega\to 0^+}\frac{1}{i\omega}\left[\Omega_{jj'}\left(x,x';\omega^+\right) - \Omega_{jj'}\left(x,x';0\right)\right], \tag{2.75}$$

where again $\omega^+ \equiv \omega + i\eta_\omega$. The coordinate dependence should vanish in the $\omega\to 0$ limit, since where exactly we apply the bias or measure the current is inconsequential in a dc experiment[42, 93].

Eq. (2.75) is now calculated in perturbation theory. Switching to the interaction picture, we perform a Wick decomposition of the time-ordered product, go to the frequency space and sum over the Matsubara frequencies. The retarded correlation function is then obtained by analytic continuation $i\omega_n \to \omega^+ \equiv \omega + i\eta_\omega$ where the $\eta_\omega \to 0^+$ limit is taken. The energy integrals are calculated afterwards, followed by real space integrals [which appear in Eq. (2.60)] in the end. Feynman diagrams involved to the first order are shown in Fig. 2.6, with the final results given by Eqs. (2.88) and (2.98).

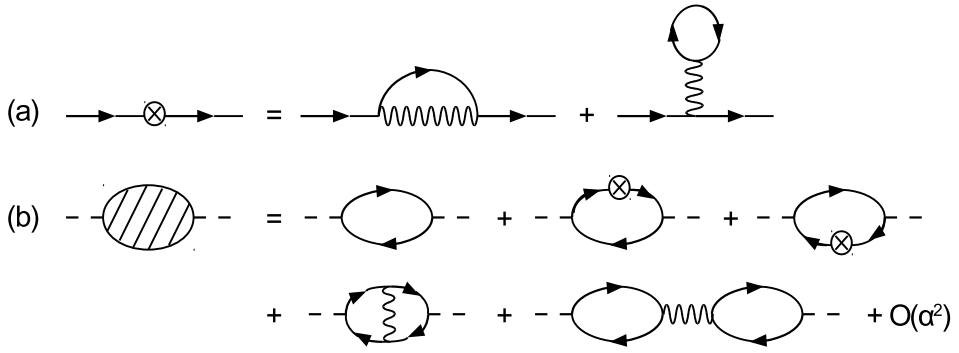

Figure 2.6: Diagrams contributing to the linear dc conductance at the first order in interaction. The second line shows the self-energy dressed bubble diagrams, while vertex correction diagrams are in the third line.

2.5.1 Zeroth order

At the zeroth order, there is only a single bubble diagram for the current-current correlation function[35, 38]. Wick's theorem gives

$$\begin{aligned}&\left\langle T_\tau \phi^\dagger_{j_1}(\varepsilon_1,\tau)\,\phi_{j_2}(\varepsilon_2,\tau)\,\phi^\dagger_{j'_1}(\varepsilon'_1,\tau')\,\phi_{j'_2}(\varepsilon'_2,\tau')\right\rangle \\ &= -\delta_{j_2 j'_1}\delta(\varepsilon_2-\varepsilon'_1)\,\mathscr{G}_{j_2}(\varepsilon_2,\tau-\tau')\,\delta_{j_1 j'_2}\delta(\varepsilon_1-\varepsilon'_2)\,\mathscr{G}_{j_1}(\varepsilon_1,\tau'-\tau).\end{aligned} \tag{2.76}$$

Here $\mathscr{G}$ is the free scattering basis Matsubara Green's function $\mathscr{G}_j(E,i\omega_n)=1/(i\omega_n-E)$, $\omega_n=(2n+1)\pi/\beta$. We have dropped the H subscript in Eq. (2.74) when switching to the interaction picture. Going to the frequency space, we have the standard Matsubara sum

$$\frac{1}{\beta}\sum_{i\omega_n}\mathscr{G}_{j_2}(E_2,i\omega_n)\mathscr{G}_{j_1}(E_1,i\omega_n-ip_m)=\frac{f(E_2)-f(E_1)}{-ip_m+E_2-E_1}, \tag{2.77}$$

where $p_m=2m\pi/\beta$ is a bosonic frequency and $f(\varepsilon)=1/\left(e^{\beta\varepsilon}+1\right)$ is the Fermi distribution at temperature $\beta=1/T$. Performing analytic continuation $ip_m\to\omega^+\equiv\omega+i\eta_\omega$ ($\eta_\omega\to 0^+$) then yields the zeroth order retarded correlation function,

$$\Omega^{(0)}_{jj'}\left(x,x';\omega^+\right)=\frac{e^2}{(2\pi)^2}\sum_{j_1j_2}\int d\varepsilon_1 d\varepsilon_2\frac{f(\varepsilon_2)-f(\varepsilon_1)}{-\omega^++\varepsilon_2-\varepsilon_1}\left[\delta_{jj'}e^{i(\varepsilon_2-\varepsilon_1)\left(\frac{x}{v_{Fj}}-\frac{x'}{v_{Fj'}}\right)}\right.$$
$$\left.+\delta_{jj'}e^{i(\varepsilon_1-\varepsilon_2)\left(\frac{x}{v_{Fj}}-\frac{x'}{v_{Fj'}}\right)}-\left|S_{j'j}\right|^2e^{i(\varepsilon_1-\varepsilon_2)\left(\frac{x}{v_{Fj}}+\frac{x'}{v_{Fj'}}\right)}-\left|S_{jj'}\right|^2e^{i(\varepsilon_2-\varepsilon_1)\left(\frac{x}{v_{Fj}}+\frac{x'}{v_{Fj'}}\right)}\right]. \tag{2.78}$$

We have done the j_1 and j_2 sums using unitarity of the S-matrix. Employing contour techniques, we integrate over ε_1 on $(-\infty,\infty)$ for the term proportional to $f(\varepsilon_2)$, and integrate over ε_2 on $(-\infty,\infty)$ for the term proportional to $f(\varepsilon_1)$:

$$\begin{aligned}&\Omega^{(0)}_{jj'}\left(x,x';\omega^+\right)\\&=\frac{e^2}{(2\pi)^2}\int d\varepsilon_2\,(2\pi i)\,f(\varepsilon_2)\left[\delta_{jj'}e^{i\omega^+\left|\frac{x}{v_{Fj}}-\frac{x'}{v_{Fj'}}\right|}-0-\left|S_{jj'}\right|^2e^{i\omega^+\left(\frac{x}{v_{Fj}}+\frac{x'}{v_{Fj'}}\right)}\right]\\&-\frac{e^2}{(2\pi)^2}\int d\varepsilon_1\,(2\pi i)\,f(\varepsilon_1)\left[\delta_{jj'}e^{i\omega^+\left|\frac{x}{v_{Fj}}-\frac{x'}{v_{Fj'}}\right|}-0-\left|S_{jj'}\right|^2e^{i\omega^+\left(\frac{x}{v_{Fj}}+\frac{x'}{v_{Fj'}}\right)}\right].\end{aligned} \tag{2.79}$$

We note that the $\left|S_{j'j}\right|^2$ term vanishes because the associated singularities are on the wrong side of the contour. Now combine the $f(\varepsilon_2)$ and $f(\varepsilon_1)$ terms and restore the cutoff D, recalling that $\varepsilon_2-\varepsilon_1=\omega^+$. This gives

$$\Omega^{(0)}_{jj'}\left(x,x';\omega^+\right)=i\frac{e^2}{2\pi}\int d\varepsilon_2\left[f(\varepsilon_2)-f\left(\varepsilon_2-\omega^+\right)\right]\left[\delta_{jj'}e^{i\omega^+\left|\frac{x}{v_{Fj}}-\frac{x'}{v_{Fj'}}\right|}-0-\left|S_{jj'}\right|^2e^{i\omega^+\left(\frac{x}{v_{Fj}}+\frac{x'}{v_{Fj'}}\right)}\right]. \tag{2.80}$$

Substituting into Eq. (3.31), taking the $\eta_\omega\to0^+$ limit and then the $\omega\to0$ limit, we obtain

$$G^{(0)}_{jj'}=-\frac{e^2}{2\pi}\left(\delta_{jj'}-\left|S_{jj'}\right|^2\right), \tag{2.81}$$

which is the usual linearized Landauer formula.

2.5.2 First order

Higher order diagrams can be classified into two basic types, namely self-energy diagrams and vertex corrections. They are discussed separately in the following.

Self-energy diagrams

At the first order, as shown in Fig. 2.6, the bubble diagram is dressed by two types of self-energies: contraction of E_1 with E_2 or E_3 with E_4 in Eq. (2.60) (the "tadpole"), and contraction of E_1 with E_4 or E_2 with E_3.

For the self-energy diagrams and the dressed conductance bubbles we need two more types of Matsubara frequency sums. The first one is

$$\frac{1}{\beta}\sum_{i\omega_n}\mathscr{G}_j\left(\varepsilon, i\omega_n\right) = f\left(\varepsilon\right). \tag{2.82}$$

The second one is

$$\begin{aligned}
&\frac{1}{\beta}\sum_{i\omega_n}\mathscr{G}_{j_1'}\left(\varepsilon_1', i\omega_n\right)\mathscr{G}_{j_1}\left(\varepsilon_1, i\omega_n\right)\mathscr{G}_{j_2}\left(\varepsilon_2, i\omega_n + ip_m\right) \\
&= f\left(\varepsilon_2\right)\frac{1}{\left(\varepsilon_2 - ip_m\right) - \varepsilon_1'}\frac{1}{\left(\varepsilon_2 - ip_m\right) - \varepsilon_1} - \int\frac{d\tilde{\varepsilon}}{2\pi i}f\left(\tilde{\varepsilon}\right) \\
&\times\frac{1}{\tilde{\varepsilon} + ip_m - \varepsilon_2}\left[\frac{1}{\tilde{\varepsilon} + i0 - \varepsilon_1'}\frac{1}{\tilde{\varepsilon} + i0 - \varepsilon_1} - \frac{1}{\tilde{\varepsilon} - i0 - \varepsilon_1'}\frac{1}{\tilde{\varepsilon} - i0 - \varepsilon_1}\right].
\end{aligned} \tag{2.83}$$

To compute this sum, we consider the following contour integral,

$$\oint\frac{dz}{2\pi i}f\left(z\right)\frac{1}{z - \varepsilon_1'}\frac{1}{z - \varepsilon_1}\frac{1}{z + ip_m - \varepsilon_2}, \tag{2.84}$$

where the integration contour is wrapped around the branch cut on the real axis[74], so that poles inside the contour are $z = i\omega_n$ (n running over all integers) and also $z = \varepsilon_2 - ip_m$. The $f\left(\varepsilon_2\right)$ term in Eq. (2.83) comes from $z = \varepsilon_2 - ip_m$, and the $f\left(\tilde{\varepsilon}\right)$ term comes from the branch cut $z = 0$.

We ignore the tadpole-type self-energy diagrams, again on the grounds that they only modify the chemical potential. The other type of self-energy diagrams turn out to dress the S-matrix. One instance of these diagrams reads

$$\Omega_{jj'}^{(1),\text{SE,non-tadpole,1}}\left(x,x';\tau-\tau'\right)=-\frac{e^2}{(2\pi)^2}\sum_{j_1j_2j_1'j_2'}\int d\varepsilon_1 d\varepsilon_2 d\varepsilon_1' d\varepsilon_2'$$
$$\times\left[e^{i\frac{(\varepsilon_2-\varepsilon_1)}{v_{Fj}}x}S_{jj_1}^*S_{jj_2}-e^{-i\frac{(\varepsilon_2-\varepsilon_1)}{v_{Fj}}x}\delta_{jj_1}\delta_{jj_2}\right]\left[e^{i\frac{(\varepsilon_2'-\varepsilon_1')}{v_{Fj'}}x'}S_{j'j_1'}^*S_{j'j_2'}-e^{-i\frac{(\varepsilon_2'-\varepsilon_1')}{v_{Fj'}}x'}\delta_{j'j_1'}\delta_{j'j_2'}\right]$$
$$\times(-)\int_0^\beta d\tau_1\sum_n\int dy\,g_2^n(y)\sum_{l_1l_2l_3l_4}\int\frac{dE_1dE_2dE_3dE_4}{(2\pi)^2v_{Fn}^2}\rho_{l_1l_2l_3l_4}^n(E_1,E_2,E_3,E_4;y)$$
$$\times\delta_{j_2j_1'}\delta\left(\varepsilon_2-\varepsilon_1'\right)\mathscr{G}_{j_2}\left(\varepsilon_2,\tau-\tau'\right)\delta_{j_2'l_1}\delta\left(\varepsilon_2'-E_1\right)\mathscr{G}_{j_2'}\left(\varepsilon_2',\tau'-\tau_1\right)$$
$$\times\delta_{l_2l_3}\delta\left(E_2-E_3\right)\mathscr{G}_{l_2}\left(E_2,0\right)\delta_{l_4j_1}\delta\left(E_4-\varepsilon_1\right)\mathscr{G}_{j_1}\left(\varepsilon_1,\tau_1-\tau\right).\tag{2.85}$$

Going to the frequency space, performing Matsubara sums and analytic continuation, we find

$$\Omega_{jj'}^{(1),\text{SE,non-tadpole,1}}\left(x,x';\omega^+\right)=-\frac{e^2}{(2\pi)^2}\sum_{j_1j_2j_2'}\int d\varepsilon_1 d\varepsilon_2 d\varepsilon_2'$$
$$\times\left[e^{i\frac{(\varepsilon_2-\varepsilon_1)}{v_{Fj}}x}S_{jj_1}^*S_{jj_2}-e^{-i\frac{(\varepsilon_2-\varepsilon_1)}{v_{Fj}}x}\delta_{jj_1}\delta_{jj_2}\right]\left[e^{i\frac{(\varepsilon_2'-\varepsilon_2)}{v_{Fj'}}x'}S_{j'j_2}^*S_{j'j_2'}-e^{-i\frac{(\varepsilon_2'-\varepsilon_2)}{v_{Fj'}}x'}\delta_{j'j_2}\delta_{j'j_2'}\right]$$
$$\times(-)\sum_n\int dy\,g_2^n(y)\int\frac{dE_2}{(2\pi)^2v_{Fn}^2}f(E_2)\,\rho_{j_2'nnj_1}^n\left(\varepsilon_2',E_2,E_2,\varepsilon_1;y\right)$$
$$\times\left[f(\varepsilon_2)\frac{1}{(\varepsilon_2-\omega^+)-\varepsilon_2'}\frac{1}{(\varepsilon_2-\omega^+)-\varepsilon_1}-\int\frac{d\tilde{\varepsilon}}{2\pi i}f(\tilde{\varepsilon})\frac{1}{\tilde{\varepsilon}+\omega^+-\varepsilon_2}\right.$$
$$\left.\times\left(\frac{1}{\tilde{\varepsilon}+i0-\varepsilon_2'}\frac{1}{\tilde{\varepsilon}+i0-\varepsilon_1}-\frac{1}{\tilde{\varepsilon}-i0-\varepsilon_2'}\frac{1}{\tilde{\varepsilon}-i0-\varepsilon_1}\right)\right].\tag{2.86}$$

Carrying out the ε_1 and ε_2' integrations, and also the ε_2 integration in the $f(\tilde{\varepsilon})$ term, this becomes in the $x,x'\to\infty$ limit

$$\Omega_{jj'}^{(1),\text{SE,non-tadpole,1}}\left(x,x';\omega^+\right)=-\frac{e^2}{2\pi}\int d\varepsilon_2\left[f(\varepsilon_2)-f\left(\varepsilon_2-\omega^+\right)\right]$$
$$\times(-)\sum_n\int dy\,\alpha_n(y)\int\frac{dE_2}{v_{Fn}}f(E_2)\frac{1}{2}e^{i\omega^+\left(\frac{x}{v_{Fj}}+\frac{x'}{v_{Fj'}}\right)}$$
$$\times S_{jj'}\left[S_{jn}^*S_{nn}S_{nj'}^*e^{2i(E_2-(\varepsilon_2-\omega^+))\frac{y}{v_{Fn}}}+\delta_{jn}S_{nn}^*\delta_{j'n}e^{-2i(E_2-(\varepsilon_2-\omega^+))\frac{y}{v_{Fn}}}\right].\tag{2.87}$$

This is just one of the four terms which contribute to the dressing of the S-matrix in Eq. (3.31). Another identical term comes from contracting E_1 with E_4 (completely equivalent to contracting E_2 with E_3 which we have done). The remaining two terms have all their electron propagators reverted, so that their contributions to the conductance are the complex conjugate of the first two terms. In

the end, contributions from first-order self-energy diagrams can be integrated into a Landauer-type formula:

$$G^{(0)}_{jj'} + G^{(1),\mathrm{SE}}_{jj'} = -\frac{e^2}{2\pi}\left(\delta_{jj'} - \int d\varepsilon\,[-f(\varepsilon)]\left|S^{\mathrm{d}(1)}_{jj'}(\varepsilon)\right|^2\right) \tag{2.88}$$

where the first order "dressed S-matrix" $S^{\mathrm{d}(1)}$ is given by

$$\begin{aligned} S^{\mathrm{d}(1)}_{jj'}(\varepsilon) = S_{jj'} - i\sum_n \int_0^\infty dy\,\alpha_n(y) \int \frac{d\varepsilon'}{v_{Fn}} f(\varepsilon') \\ \times S_{jn}S^*_{nn}S_{nj'}\exp\left(2i(\varepsilon-\varepsilon')\frac{y}{v_{Fn}}\right) + \delta_{jn}S_{nn}\delta_{j'n}\exp\left(-2i(\varepsilon-\varepsilon')\frac{y}{v_{Fn}}\right); \end{aligned} \tag{2.89}$$

$\alpha_n(y)$ has been defined in Eq. (2.55). For a non-interacting system $S^{\mathrm{d}(1)}_{jj'}(\varepsilon) = S_{jj'}$; this is in agreement with our intuitive expectation.

For the simple model Eq. (2.67), integrating over y:

$$\begin{aligned} S^{\mathrm{d}(1)}_{jj'}(\varepsilon) = S_{jj'}(\varepsilon) - \sum_n \int d\varepsilon' \frac{f(\varepsilon')}{2(\varepsilon'-\varepsilon)} \Big(S_{jn}S^*_{nn}S_{nj'}\left[(\alpha_n(\infty)-\alpha_n(0))\,e^{2i(\varepsilon-\varepsilon')\frac{L_n}{v_{Fn}}} + \alpha_n(0)\right] \\ -\delta_{jn}S_{nn}\delta_{j'n}\left[(\alpha_n(\infty)-\alpha_n(0))\,e^{-2i(\varepsilon-\varepsilon')\frac{L_n}{v_{Fn}}} + \alpha_n(0)\right]\Big). \end{aligned} \tag{2.90}$$

The ε' integral is infrared divergent, which prompts an RG resummation of leading logarithms. We will determine the renormalization of the S-matrix using Eq. (2.90) and discuss its implications in Section 2.6.

Vertex correction diagrams

There are two types of first order vertex correction diagrams, the "cracked egg" diagram and the ring diagram. Neither type of vertex corrections to the conductance requires Matsubara sums other than Eq. (2.77).

By summing over all dummy wire indices, we can show that the "cracked egg" contribution to the dc conductance is proportional to $\delta_{jj'}$. On the other hand, due to current conservation and the absence of equilibrium currents, the full dc conductance $G_{jj'}$ obeys

$$\sum_j G_{jj'} = \sum_{j'} G_{jj'} = 0; \tag{2.91}$$

this must also be true at $O(\alpha)$. Since Eq. (2.91) is already satisfied by the self-energy contribution Eq. (2.88), and also by the ring diagram contribution Eq. (2.98) as we shall see below, it must be separately satisfied by the "cracked egg" diagrams as well. But $\sum_j \delta_{jj'} = \sum_{j'} \delta_{jj'} = 1$, and we infer

that the "cracked egg" diagrams must be identically zero.

An example of the ring diagram is

$$\Omega^{(1),\mathrm{VC,ring},1}_{jj'}\left(x,x';\tau-\tau'\right)=-\frac{e^2}{(2\pi)^2}\sum_{j_1j_2j_1'j_2'}\int d\varepsilon_1 d\varepsilon_2 d\varepsilon_1' d\varepsilon_2'$$
$$\times\left[e^{i\frac{(\varepsilon_2-\varepsilon_1)}{v_{Fj}}x}S^*_{jj_1}S_{jj_2}-e^{-i\frac{(\varepsilon_2-\varepsilon_1)}{v_{Fj}}x}\delta_{jj_1}\delta_{jj_2}\right]\left[e^{i\frac{(\varepsilon_2'-\varepsilon_1')}{v_{Fj'}}x'}S^*_{j'j_1'}S_{j'j_2'}-e^{-i\frac{(\varepsilon_2'-\varepsilon_1')}{v_{Fj'}}x'}\delta_{j'j_1'}\delta_{j'j_2'}\right]$$
$$\times(-)\int_0^\beta d\tau_1\sum_n\int dy\,g_2^n(y)\sum_{l_1l_2l_3l_4}\int\frac{dE_1dE_2dE_3dE_4}{(2\pi)^2v_{Fn}^2}\rho^n_{l_1l_2l_3l_4}(E_1,E_2,E_3,E_4;y)$$
$$\times\delta_{j_2l_1}\delta\left(\varepsilon_2-E_1\right)\mathscr{G}_{j_2}\left(\varepsilon_2,\tau-\tau_1\right)\delta_{l_4j_1'}\delta\left(\varepsilon_1'-E_4\right)\mathscr{G}_{j_1'}\left(\varepsilon_1',\tau_1-\tau'\right)$$
$$\times\delta_{j_2'l_3}\delta\left(\varepsilon_2'-E_3\right)\mathscr{G}_{j_2'}\left(\varepsilon_2',\tau'-\tau_1\right)\delta_{j_1l_2}\delta\left(E_2-\varepsilon_1\right)\mathscr{G}_{j_1}\left(\varepsilon_1,\tau_1-\tau\right). \tag{2.92}$$

Going to the frequency space, performing Matsubara sums and analytic continuation:

$$\Omega^{(1),\mathrm{VC,ring},1}_{jj'}\left(x,x';\omega^+\right)=-\frac{e^2}{(2\pi)^2}\sum_{j_1j_2j_1'j_2'}\int d\varepsilon_1 d\varepsilon_2 d\varepsilon_1' d\varepsilon_2'$$
$$\times\left[e^{i\frac{(\varepsilon_2-\varepsilon_1)}{v_{Fj}}x}S^*_{jj_1}S_{jj_2}-e^{-i\frac{(\varepsilon_2-\varepsilon_1)}{v_{Fj}}x}\delta_{jj_1}\delta_{jj_2}\right]\left[e^{i\frac{(\varepsilon_2'-\varepsilon_1')}{v_{Fj'}}x'}S^*_{j'j_1'}S_{j'j_2'}-e^{-i\frac{(\varepsilon_2'-\varepsilon_1')}{v_{Fj'}}x'}\delta_{j'j_1'}\delta_{j'j_2'}\right]$$
$$\times\sum_n\int dy\,g_2^n(y)\frac{1}{(2\pi)^2v_{Fn}^2}\rho^n_{j_2j_1j_2'j_1'}\left(\varepsilon_2,\varepsilon_1,\varepsilon_2',\varepsilon_1';y\right)\frac{f(\varepsilon_2)-f(\varepsilon_1)}{\varepsilon_2-\varepsilon_1-\omega^+}\frac{f(\varepsilon_2')-f(\varepsilon_1')}{\varepsilon_2'-\varepsilon_1'+\omega^+}. \tag{2.93}$$

Integrating over the energies as before, we find

$$\Omega^{(1),\mathrm{VC,ring},1}_{jj'}\left(x,x';\omega^+\right)=-\frac{e^2}{2\pi}\int d\varepsilon_1 d\varepsilon_1'(-)\left[f\left(\varepsilon_1+\omega^+\right)-f(\varepsilon_1)\right]\left[f\left(\varepsilon_1'-\omega^+\right)-f\left(\varepsilon_1'\right)\right]$$
$$\times\sum_n\int dy\,\alpha_n(y_1)\frac{1}{v_{Fn}}\frac{1}{2}\Bigg[\left|S_{jn}\right|^2\delta_{j'n}e^{i\omega^+\left(\frac{x}{v_{Fj}}-\frac{x'}{v_{Fj'}}\right)}e^{2i\omega^+\frac{y}{v_{Fn}}}H\left(y-x'\right)$$
$$-\delta_{jn}\delta_{j'n}e^{-i\omega^+\left(\frac{x}{v_{Fj}}+\frac{x'}{v_{Fj'}}\right)}e^{2i\omega^+\frac{y}{v_{Fn}}}H(y-x)H\left(y-x'\right)$$
$$-\delta_{jn}\delta_{j'n}e^{i\omega^+\left(\frac{x}{v_{Fj}}+\frac{x'}{v_{Fj'}}\right)}e^{-2i\omega^+\frac{y}{v_{Fn}}}H(x-y)H\left(x'-y\right)$$
$$-\left|S_{jn}\right|^2\left|S_{nj'}\right|^2e^{i\omega^+\left(\frac{x}{v_{Fj}}+\frac{x'}{v_{Fj'}}\right)}e^{2i\omega^+\frac{y}{v_{Fn}}}+\delta_{jn}\left|S_{nj'}\right|^2e^{-i\omega^+\left(\frac{x}{v_{Fj}}-\frac{x'}{v_{Fj'}}\right)}e^{2i\omega^+\frac{y}{v_{Fn}}}H(y-x)\Bigg]. \tag{2.94}$$

There exists an analogous term with all electron lines reverted. Upon substitution into Eq. (3.31) these two terms produce

$$G^{(1),\mathrm{VC}}_{jj'}\left(x,x'\right)=\frac{e^2}{2\pi}i\sum_n\int_0^\infty\frac{dy}{v_{Fn}}\alpha_n\left(y\right)$$
$$\times\lim_{\omega\to0}\lim_{\eta_\omega\to0^+}\omega\left[\left|S_{jn}\right|^2\delta_{j'n}e^{i\omega^+\left(\frac{x}{v_{Fj}}-\frac{x'}{v_{Fj'}}\right)}e^{2i\omega^+\frac{y}{v_{Fn}}}H\left(y-x'\right)-\delta_{jn}\delta_{j'n}e^{-i\omega^+\left(\frac{x}{v_{Fj}}+\frac{x'}{v_{Fj'}}\right)}e^{2i\omega^+\frac{y}{v_{Fn}}}H\left(y-x\right)H\left(y-x'\right)\right.$$
$$-\delta_{jn}\delta_{j'n}e^{i\omega^+\left(\frac{x}{v_{Fj}}+\frac{x'}{v_{Fj'}}\right)}e^{-2i\omega^+\frac{y}{v_{Fn}}}H\left(x-y\right)H\left(x'-y\right)-\left|S_{jn}\right|^2\left|S_{nj'}\right|^2e^{i\omega^+\left(\frac{x}{v_{Fj}}+\frac{x'}{v_{Fj'}}\right)}e^{2i\omega^+\frac{y}{v_{Fn}}}$$
$$\left.+\delta_{jn}\left|S_{nj'}\right|^2e^{-i\omega^+\left(\frac{x}{v_{Fj}}+\frac{x'}{v_{Fj'}}\right)}e^{2i\omega^+\frac{y}{v_{Fn}}}H\left(y-x\right)\right]. \tag{2.95}$$

Integration by parts gives us

$$\frac{2i\omega^+}{v_{Fn}}\int_{y_l}^{y_u}dy\alpha_n\left(y\right)e^{2i\omega^+\frac{y}{v_{Fn}}}=\alpha_n\left(y_u\right)e^{2i\omega^+\frac{yu}{v_{Fn}}}-\alpha_n\left(y_l\right)e^{2i\omega^+\frac{y_l}{v_{Fn}}}-\int_{y_l}^{y_u}dye^{2i\omega^+\frac{y}{v_{Fn}}}\frac{d\alpha_n\left(y\right)}{dy}, \tag{2.96}$$

where y_u can be $v_{Fn}x/v_{Fj}$, $v_{Fn}x'/v_{Fj'}$ or ∞, and y_l can be $v_{Fn}x/v_{Fj}$, $v_{Fn}x'/v_{Fj'}$ or 0. We can let x and x' be sufficiently large so that $y_u>L_n$ is always satisfied; thus in the $d\alpha_n/dy$ term in Eq. (2.96), y_u may be replaced by L_n.

If $y_u\to\infty$, the $\alpha_n\left(y_u\right)$ term damps out due to the small imaginary part η_ω, and Eq. (2.96) becomes in the $\omega\to0$ and $\eta_\omega\to0$ limit

$$\frac{2i\omega^+}{v_{Fn}}\int_{y_l}^{y_u}dy\alpha_n\left(y\right)e^{2i\omega^+\frac{y}{v_{Fn}}}=-\alpha_n\left(y_l\right)-\int_{y_l}^{L_n}dy\frac{d\alpha_n\left(y\right)}{dy}=-\alpha_n\left(L_n\right)=-\alpha_n\left(\infty\right). \tag{2.97a}$$

On the other hand, if y_u is finite, the $\alpha_n\left(y_u\right)$ term will survive the $\omega\to0$ and $\eta_\omega\to0$ limit:

$$\frac{2i\omega^+}{v_{Fn}}\int_{y_l}^{y_u}dy\alpha_n\left(y\right)e^{2i\omega^+\frac{y}{v_{Fn}}}=\alpha_n\left(y_u\right)-\alpha_n\left(y_l\right)-\int_{y_l}^{L_n}dy\frac{d\alpha_n\left(y\right)}{dy}=\alpha_n\left(y_u\right)-\alpha_n\left(L_n\right)=0. \tag{2.97b}$$

Therefore, taking the dc limit explicitly in Eq. (2.95), we find wire n contributes to the vertex correction only when it is attached to a TLL lead, and the interaction inside the wire is immaterial:

$$G^{(1),\mathrm{VC}}_{jj'}\left(x,x'\right)=\frac{e^2}{2\pi}\sum_n\frac{1}{2}\alpha_n\left(\infty\right)\left(\delta_{jn}-\left|S_{jn}\right|^2\right)\left(\delta_{nj'}-\left|S_{nj'}\right|^2\right). \tag{2.98}$$

When $\alpha_n\left(\infty\right)=0$, as is the case for any wire n attached to an FL lead, the vertex correction due to n vanishes.

2.6 First-order CS formulation of RG

In this section, we analyze the result of Section 2.5 from the perspective of the CS formulation of RG[12], and present a modified Landauer formula involving the renormalized S-matrix in the case of FL leads, supplemented by vertex corrections from TLL leads.

Beginning from the simplest case where all leads are FL leads, i.e. $\alpha_n(\infty)=0$ for all n, the vertex correction Eq. (2.98) vanishes, and the full linear dc conductance to $O(\alpha)$ is given by Eq. (2.88). Reducing the cutoff from D to $D-\delta D$ and demanding the right-hand side of Eq. (2.88) be a scaling invariant, we have

$$\int_{\delta D} d\varepsilon \left[-f'(\varepsilon)\right] \left|S^{\mathrm{d}(1)}_{jj'}(\varepsilon,D)\right|^2 + \int_{-D}^{D} d\varepsilon \left[-f'(\varepsilon)\right] \left[\left(S^{\mathrm{d}(1)}_{jj'}(\varepsilon,D)\right)^* \delta S^{\mathrm{d}(1)}_{jj'}(\varepsilon,D) + \text{c.c.}\right] = 0 \tag{2.99}$$

where $\int_{\delta D} = \int_{(D-\delta D)}^{D} + \int_{-D}^{-(D-\delta D)}$ stands for integration over fast modes, and $\delta S^{\mathrm{d}(1)}$ is the renormalization of $S^{\mathrm{d}(1)}$:

$$\delta S^{\mathrm{d}(1)}_{jj'}(\omega,D) \equiv S^{\mathrm{d}(1)}_{jj'}(\omega,D) - S^{\mathrm{d}(1)}_{jj'}(\omega,D-\delta D). \tag{2.100}$$

Here $S^{\mathrm{d}(1)}_{jj'}(\varepsilon,D)$ is Eq. (2.90) with the ε' integral going from $-D$ to D. We have made the cutoff dependence explicit, and all S-matrix elements are understood to be cutoff-dependent, $S_{jj'} \to S_{jj'}(D)$.

Since the derivative of the Fermi function is peaked at the Fermi energy with width T, the $\int_{\delta D}$ integral in Eq. (2.99) approximately vanishes while $D \gtrsim T$; Eq. (2.99) is thus automatically satisfied if Eq. (2.100) vanishes. The implication is that, at least in the case of FL leads, the renormalization of the conductance can be fully accounted for by the renormalization of the S-matrix.

To the lowest order in δD, the condition that $\delta S^{\mathrm{d}(1)}_{jj'}(\omega,D)=0$ is equivalent to

$$\begin{aligned}
\delta S_{jj'}(\omega,D) &\equiv S_{jj'}(\omega,D) - S_{jj'}(\omega,D-\delta D) \\
&= \sum_n \int_{\delta D} d\varepsilon' \frac{f(\varepsilon')}{2(\varepsilon'-\omega)} \Big(S_{jn} S^*_{nn} S_{nj'} \left[(\alpha_n(\infty) - \alpha_n(0)) e^{2i(\omega-\varepsilon')\frac{L_n}{v_{Fn}}} + \alpha_n(0) \right] \\
&\quad - \delta_{jn} S_{nn} \delta_{j'n} \left[(\alpha_n(\infty) - \alpha_n(0)) e^{-2i(\omega-\varepsilon')\frac{L_n}{v_{Fn}}} + \alpha_n(0) \right] \Big).
\end{aligned} \tag{2.101}$$

When we assume $D \gtrsim \max\{|\omega|, T\}$, and apply the same considerations below Eq. (2.68), from Eq. (2.101) we recover none other than Eq. (2.71). Thus to the first order in interaction the CS approach and the Wilsonian approach predict the same S-matrix renormalization, Eq. (2.72).

Once the cutoff D is reduced to the order of T, the perturbative correction to the S-matrix $S^{\mathrm{d}(1)}_{jj'}(\varepsilon,D) - S_{jj'}(D)$ vanishes to the scaling accuracy; thus $S_{jj'}(D=T)$ may be used to approximate the dressed S-matrix in Eq. (2.88), and the conductance for a junction connected to FL leads is given

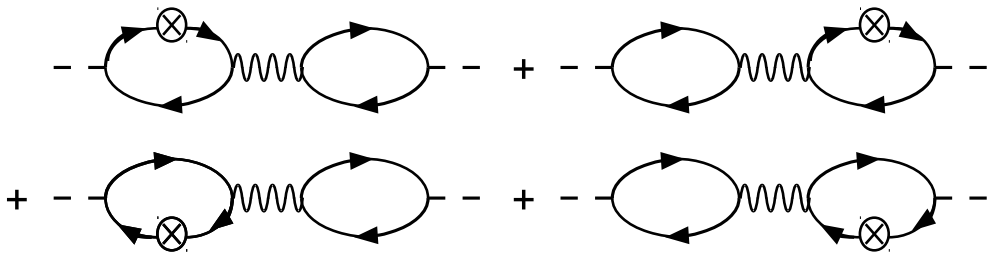

Figure 2.7: Dressing of the first order vertex correction diagrams by the first order self-energy diagrams.

by the modified Landauer formula,

$$G_{jj'}^{\mathrm{FL}} = -\frac{e^2}{2\pi}\left(\delta_{jj'} - \left|S_{jj'}(T)\right|^2\right), \tag{2.102}$$

where the S-matrix is now fully renormalized according to Eq. (2.72), with the cutoff reduced to the temperature T. This is the Landauer-type formula invoked in Refs. [70, 77, 132].

When some of the leads are TLL leads, corrections of Eq. (2.98) must also be taken into account. It is important to note, however, that in a CS analysis of the total conductance, Eq. (2.100) remains valid to $O(\alpha)$. This is because as the cutoff is lowered, Eq. (2.98) contributes additional terms of the form of $\alpha(\infty) S^* \delta S$ to Eq. (2.99). However, by Eq. (2.100), δS is $O(\alpha)$; hence $\alpha(\infty) S^* \delta S$ is $O\left(\alpha^2\right)$, and is negligible to $O(\alpha)$.

To calculate the total conductance at $D = T$ with TLL leads, we go slightly beyond the first order and dress the $O(\alpha)$ vertex correction diagrams with $O(\alpha)$ self-energy diagrams, shown in Fig. 2.7. The bare S-matrix in Eq. (2.98) is then replaced by the dressed S-matrix, $S^{\mathrm{d}(1)}$:

$$\begin{aligned} G_{jj'}^{\mathrm{d}(1),\mathrm{VC}}(x,x') = \frac{e^2}{2\pi}\sum_n \frac{1}{2}\alpha_n(\infty)\left(\delta_{jn} - \int d\varepsilon_1 \left[-f'(\varepsilon_1)\right]\left|S_{jn}^{\mathrm{d}(1)}(\varepsilon_1)\right|^2\right) \\ \times\left(\delta_{nj'} - \int d\varepsilon_2 \left[-f'(\varepsilon_2)\right]\left|S_{nj'}^{\mathrm{d}(1)}(\varepsilon_2)\right|^2\right). \end{aligned} \tag{2.103}$$

This allows us to repeat our previous analysis for the case of FL leads, and further approximate $S_{jj'}^{\mathrm{d}(1)}$ by $S_{jj'}(D = T)$. Thus the TLL leads contribute an additional conductance of

$$G_{jj'}^{\mathrm{TLL}} - G_{jj'}^{\mathrm{FL}} = \frac{e^2}{2\pi} \sum_n \frac{\alpha_n(\infty)}{2} \left(\delta_{jn} - \left|S_{jn}(T)\right|^2\right) \left(\delta_{nj'} - \left|S_{nj'}(T)\right|^2\right). \tag{2.104}$$

Eqs. (2.72), (2.102) and (2.104) provide a comprehensive first-order picture for non-resonant tunneling through a junction: the interaction renormalizes the S-matrix, the renormalized S-matrix determines the conductance through a Landauer-type formula if the junction is connected to FL leads, and the residual interaction further modifies the conductance if the junction is attached to TLL leads[111]. As will be demonstrated in Section 2.7, this picture is by no means limited to the first order.

2.7 RPA

In this section, we extend our first-order RG analysis in Section 2.6 to arbitrary order in interaction under the RPA[11, 13, 15]. The correlation function Eq. (2.74) is perturbatively evaluated for both self-energy diagrams and vertex corrections by the same procedures, except that the interaction is dressed with ring diagrams; see Fig. 2.8. We subsequently find the S-matrix RG equation in the CS scheme and express the conductance in terms of the renormalized S-matrix. This is once more a straightforward calculation, and we present the result first before laying out the details.

Introduce the shorthand $W_{jj'}(D) \equiv \left|S_{jj'}(D)\right|^2$. The RPA self-energy diagrams give rise to a modified Landauer formula:

$$G_{jj'}^{\mathrm{FL}} = -\frac{e^2}{2\pi} \left[\delta_{jj'} - W_{jj'}(T)\right], \tag{2.105}$$

where the renormalization of the S-matrix is governed by a generalization of Eq. (2.72)[111],

$$-\frac{dS_{jj'}(D)}{d\ln D} = -\frac{1}{2} \sum_{n_1 n_2} \left[S_{jn_1}(D)\, \Pi_{n_1 n_2}(D)\, S^*_{n_2 n_1}(D)\, S_{n_2 j'}(D) - \delta_{j' n_1} \Pi^*_{n_1 n_2}(D)\, S_{n_2 n_1}(D)\, \delta_{n_2 j}\right]. \tag{2.106}$$

The RPA-dressed interaction is

$$\Pi(D) \equiv 2\left[\mathscr{Q}(D) - W(D)\right]^{-1}, \tag{2.107}$$

where

$$\mathscr{Q}_{jj'} = Q_j(D)\, \delta_{jj'},\ Q_j(D) = \frac{1+K_j(D)}{1-K_j(D)}, \tag{2.108}$$

with $K_j(D) = \sqrt{\left(1-\alpha_j(D)\right)/\left(1+\alpha_j(D)\right)}$ being the cutoff-dependent "Luttinger parameter" for wire j; $\alpha_j(D)$ is given in Eq. (2.70). To lowest order in α_j, $\Pi_{ij} = \delta_{ij}\alpha_j$. When all wires of the junction are attached to FL leads, in parallel with the $O(\alpha)$ calculation, Eq. (2.105) captures the

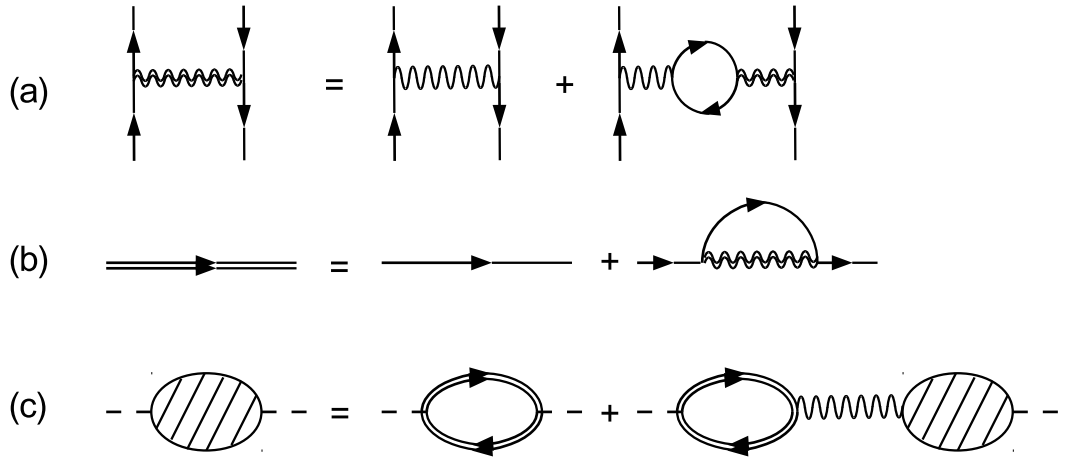

Figure 2.8: The RPA diagrammatics: (a) effective interaction in the RPA represented by thick wavy lines; (b) dressed propagator in the RPA, to $O(\delta D/D)$ in RG, represented by thick straight lines; and (c) diagrams contributing to the Kubo conductance in the RPA. The dressed propagator in (b) is calculated to $O(\delta D/D)$ only, because higher order terms in $\delta D/D$ do not contribute to the renormalization of the S-matrix [Eq. (2.106)]— see Section 2.6 for an explanation in the first order context. (a) and (c) do not involve truncation at $O(\delta D/D)$ because any renormalization of the interaction [Eq. (2.107)] and the conductance [Eqs. (2.105) and (2.109)] can be attributed to the renormalization of the S-matrix. Note that (c) features a thin interaction line (rather than a thick one) to avoid double-counting.

entirety of the conductance. This is in agreement with the Kubo formula calculation in Refs. [11–13, 15] in the language of chiral fermion densities.

When some wires are attached to TLL leads, they again provide important corrections to the dc conductance. All RPA vertex correction diagrams dressed with RPA self-energy evaluate to

$$G^{\mathrm{TLL}}_{jj'} - G^{\mathrm{FL}}_{jj'} = \frac{e^2}{2\pi} \sum\nolimits_{n_1 n_2} \left[\delta_{jn_1} - W_{jn_1}(T)\right] \frac{1}{2} \Pi^{\mathrm{L}}_{n_1 n_2} \left[\delta_{n_2 j'} - W_{n_2 j'}(T)\right], \tag{2.109}$$

where the residual effective interaction is

$$\Pi^{\mathrm{L}} = 2\left[\mathscr{Q}^{\mathrm{L}} - W(T)\right]^{-1}, \tag{2.110}$$

and $\mathscr{Q}^{\mathrm{L}}$ is given by Eq. (2.108) with K_j replaced by $K^{\mathrm{L}}_j = \sqrt{(1-\alpha_j(\infty))/(1+\alpha_j(\infty))}$, the Luttinger parameter of the lead.

Remarkably, if we follow Eq. (2.30) and introduce the dc "contact resistance" tensor between the wires and leads,

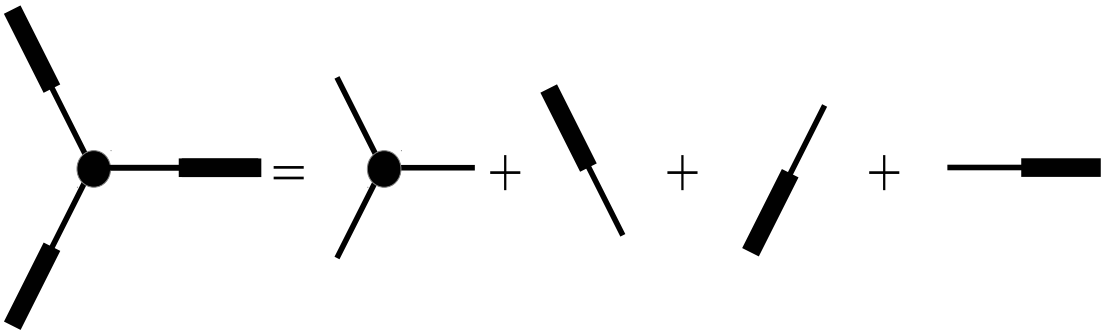

Figure 2.9: Schematic representation of the relation between the conductance of a junction with FL leads and that of a junction with TLL leads, through the "contact resistance"Eq. (2.30).

$$\left(G_c^{-1}\right)_{jj'} = \left(\frac{e^2}{2\pi}\right)^{-1} \frac{1}{2}\left[\left(K_j^{\mathrm{L}}\right)^{-1} - 1\right]\delta_{jj'}, \tag{2.111}$$

then Eq. (2.109) can be formally recast as

$$\mathbf{G}^{\mathrm{TLL}} = \left(\mathbf{1} - \mathbf{G}^{\mathrm{FL}}\mathbf{G}_c^{-1}\right)^{-1}\mathbf{G}^{\mathrm{FL}}, \tag{2.112}$$

where $\mathbf{1}$ is the $N \times N$ identity matrix. The same relation has been derived in Refs. [51, 93], which assume that the dc contact resistance between a finite TLL wire and an FL lead is not affected by the junction at the other end of the TLL wire. This assumption is reinforced by our RPA calculations. While it is tempting to further simplify Eq. (2.112) into $\left(\mathbf{G}^{\mathrm{TLL}}\right)^{-1} + \mathbf{G}_c^{-1} = \left(\mathbf{G}^{\mathrm{FL}}\right)^{-1}$, this simplification cannot be rigorous since neither $\mathbf{G}^{\mathrm{TLL}}$ nor $\mathbf{G}^{\mathrm{FL}}$ is invertible. Nevertheless, it does provide us with an intuitive understanding of Eq. (2.112); see Fig. 2.9.

We emphasize that the inclusion of the vertex correction diagrams does not change the RG equation of the S-matrix, Eq. (2.106). [The TLL leads do change the renormalization of the S-matrix through the scale-dependent interaction, Eq. (2.70).] The reason for this is as follows. Eq. (2.106) results from dressing the single particle propagator as shown in panel (b) of Fig. 2.8. The conductance is calculated in perturbation theory by replacing all bare single particle propagators (the thin lines) with the dressed ones (the thick lines) in the basic bubble diagram and the vertex correction diagrams; or equivalently, by replacing all bare S-matrix elements with the ones dressed with the RPA self-energy. As with the case at the first order, the RPA vertex correction diagrams do not introduce additional cutoff-sensitive integrals, and all cutoff-sensitive integrals originate from the dressed S-matrix. Therefore, the dressed S-matrix should be a cutoff-independent quantity when

we apply the CS scheme to the conductance, regardless of whether the vertex correction diagrams contribute to the conductance. The form of Eq. (2.106) is thus independent of vertex corrections.

An immediate consequence of the robustness of the S-matrix renormalization is that, in the temperature range above the inverse lengths of the wires, the leading universal scaling exponents of the conductance versus temperature are the same for FL leads and TLL leads to the accuracy of the RG method. Since the temperature dependence of the residual interaction ultimately results from that of the renormalized W matrix, Taylor-expanding Eq. (2.109) in the vicinity of a fixed point, we find that the leading scaling exponents of the TLL lead conductance are none other than those of the W matrix, i.e. those of the FL lead conductance; in this temperature range the TLL leads merely modify the non-universal multiplicative coefficients to the power law. Therefore, for the temperature dependence of the conductance in the introduction, we have directly quoted the FL lead results from Refs. [13, 15, 70].

Eqs. (2.105)–(2.112) are the central results of this chapter. They show that at least in the RPA, in addition to the Landauer-type formula, TLL leads give rise to important corrections to the linear dc conductance which are also given in terms of the renormalized S-matrix[111]. In the remaining sections of this chapter, we will implement these results in non-resonant tunneling through 2-lead junctions and Y-junctions.

We now expound the RPA calculations that lead to Eqs. (2.106) and (2.109).

2.7.1 Details of the RPA conductance

The RPA self-energy beyond the first order involves a new type of Matsubara sum. For instance, at the third order in interaction, we need

$$\begin{aligned}
&\frac{1}{\beta}\sum_{ip_m}\frac{f(E_4)-f(E_3)}{ip_m+E_4-E_3}\frac{f(E_8)-f(E_7)}{ip_m+E_8-E_7}\frac{1}{i(p_m+\omega_n)-E_2}\\
&=f(E_2)\frac{f(E_4)-f(E_3)}{E_2-i\omega_n+E_4-E_3}\frac{f(E_8)-f(E_7)}{E_2-i\omega_n+E_8-E_7}\\
&+\int\frac{d\tilde{\varepsilon}}{2\pi i}n_B(\tilde{\varepsilon})\frac{1}{\tilde{\varepsilon}+i\omega_n-E_2}\left(\frac{f(E_4)-f(E_3)}{(\tilde{\varepsilon}+i0)+E_4-E_3}\frac{f(E_8)-f(E_7)}{(\tilde{\varepsilon}+i0)+E_8-E_7}\right.\\
&\left.-\frac{f(E_4)-f(E_3)}{(\tilde{\varepsilon}-i0)+E_4-E_3}\frac{f(E_8)-f(E_7)}{(\tilde{\varepsilon}-i0)+E_8-E_7}\right)
\end{aligned}\tag{2.113}$$

where $n_B(\varepsilon)=1/\left(e^{\beta\varepsilon}-1\right)$ is the Bose distribution. To derive Eq. (2.113) we again wrap the integration contour around the branch cut at the real axis. The fraction with numerator $f(E_3)-f(E_4)$ originates from the fermion loop with loop energy E_3 and E_4; at the lth order there will be $l-1$ loops present. ip_m is the bosonic frequency carried by the interaction lines; after ip_m, $i\omega_n$ is also summed over following Eq. (2.83).

After we perform analytic continuation and integrate over the loop momenta, as x, $x' \to \infty$, the three most important terms in the correlation function at the third order are

$$\begin{aligned}
&\Omega^{(3),\mathrm{SE,RPA},E_2}_{jj'}\left(x,x';\omega^+\right) = \frac{e^2}{2\pi} e^{i\omega^+\left(\frac{x}{v_{Fj}}+\frac{x'}{v_{Fj'}}\right)} \int d\varepsilon_1' \left[f\left(\varepsilon_1'\right) - f\left(\varepsilon_1' - \omega^+\right)\right] S_{jj'} \\
&\times \sum_{n_1 n_2 n_3} \int_0^\infty d\tilde{y}_1 d\tilde{y}_2 d\tilde{y}_3 \alpha_{n_1}\left(v_{Fn_1}\tilde{y}_1\right) \alpha_{n_2}\left(v_{Fn_2}\tilde{y}_2\right) \alpha_{n_3}\left(v_{Fn_3}\tilde{y}_3\right) \int dE_2 f\left(E_2\right) \tilde{E}_2^2 \\
&\times \Big[S^*_{jn_3} S_{n_1 n_3} S^*_{n_1 j'} \left|S_{n_2 n_1}\right|^2 \left|S_{n_3 n_2}\right|^2 e^{2i\tilde{E}_2(\tilde{y}_1+\tilde{y}_2+\tilde{y}_3)} \\
&+ S^*_{jn_3} S_{n_1 n_3} S^*_{n_1 j'} \delta_{n_3 n_2} \delta_{n_2 n_1} H\left(\tilde{y}_1 - \tilde{y}_2\right) H\left(\tilde{y}_3 - \tilde{y}_2\right) e^{2i\tilde{E}_2(\tilde{y}_1-\tilde{y}_2+\tilde{y}_3)} \\
&+ \delta_{jn_3} \delta_{n_3 n_1} S^*_{n_1 j'} \delta_{n_3 n_2} \left|S_{n_2 n_1}\right|^2 H\left(\tilde{y}_2 - \tilde{y}_3\right) e^{2i\tilde{E}_2(\tilde{y}_1+\tilde{y}_2-\tilde{y}_3)} \\
&+ S^*_{jn_3} \delta_{n_3 n_1} \delta_{n_1 j'} \left|S_{n_3 n_2}\right|^2 \delta_{n_2 n_1} H\left(\tilde{y}_2 - \tilde{y}_1\right) e^{2i\tilde{E}_2(-\tilde{y}_1+\tilde{y}_2+\tilde{y}_3)} \\
&+ \delta_{jn_3} S^*_{n_3 n_1} \delta_{n_1 j'} \delta_{n_3 n_2} \delta_{n_2 n_1} H\left(\tilde{y}_2 - \tilde{y}_1\right) H\left(\tilde{y}_2 - \tilde{y}_3\right) e^{2i\tilde{E}_2(-\tilde{y}_1+\tilde{y}_2-\tilde{y}_3)} \Big]
\end{aligned} \tag{2.114a}$$

where we have substituted $\tilde{y}_n = y_n / v_{Fn}$ and $\tilde{E}_2 = E_2 - \varepsilon_1' + \omega^+$,

$$\begin{aligned}
&\Omega^{(3),\mathrm{SE,RPA},\tilde{\varepsilon}+}_{jj'}\left(x,x';\omega^+\right) = \frac{e^2}{2\pi} e^{i\omega^+\left(\frac{x}{v_{Fj}}+\frac{x'}{v_{Fj'}}\right)} \int d\varepsilon_1' \left[f\left(\varepsilon_1'\right) - f\left(\varepsilon_1' - \omega^+\right)\right] S_{jj'} \\
&\times \sum_{n_1 n_2 n_3} \int_0^\infty d\tilde{y}_1 d\tilde{y}_2 d\tilde{y}_3 \alpha_{n_1}\left(v_{Fn_1}\tilde{y}_1\right) \alpha_{n_2}\left(v_{Fn_2}\tilde{y}_2\right) \alpha_{n_3}\left(v_{Fn_3}\tilde{y}_3\right) \int d\tilde{\varepsilon} n_B\left(\tilde{\varepsilon}\right) \tilde{\varepsilon}^2 \\
&\times \Big[\delta_{jn_3} \delta_{n_3 n_1} S^*_{n_1 j'} \delta_{n_3 n_2} \left|S_{n_2 n_1}\right|^2 H\left(\tilde{y}_2 - \tilde{y}_3\right) H\left(\tilde{y}_3 - \tilde{y}_1\right) e^{2i(\tilde{\varepsilon}+i0)(\tilde{y}_1+\tilde{y}_2-\tilde{y}_3)} \\
&+ S^*_{jn_3} \delta_{n_3 n_1} \delta_{n_1 j'} \left|S_{n_3 n_2}\right|^2 \delta_{n_2 n_1} H\left(\tilde{y}_2 - \tilde{y}_1\right) H\left(\tilde{y}_1 - \tilde{y}_3\right) e^{2i(\tilde{\varepsilon}+i0)(-\tilde{y}_1+\tilde{y}_2+\tilde{y}_3)} \\
&+ \delta_{jn_3} S^*_{n_3 n_1} \delta_{n_1 j'} \delta_{n_3 n_2} \delta_{n_2 n_1} H\left(\tilde{y}_2 - \tilde{y}_1\right) H\left(\tilde{y}_2 - \tilde{y}_3\right) e^{2i(\tilde{\varepsilon}+i0)(-\tilde{y}_1+\tilde{y}_2-\tilde{y}_3)} \Big]
\end{aligned} \tag{2.114b}$$

and finally

$$\begin{aligned}
&\Omega^{(3),\mathrm{SE,RPA},\tilde{\varepsilon}-}_{jj'}\left(x,x';\omega^+\right) = \frac{e^2}{2\pi} e^{i\omega^+\left(\frac{x}{v_{Fj}}+\frac{x'}{v_{Fj'}}\right)} \int d\varepsilon_1' \left[f\left(\varepsilon_1'\right) - f\left(\varepsilon_1' - \omega^+\right)\right] S_{jj'} \\
&\times \sum_{n_1 n_2 n_3} \int_0^\infty d\tilde{y}_1 d\tilde{y}_2 d\tilde{y}_3 \alpha_{n_1}\left(v_{Fn_1}\tilde{y}_1\right) \alpha_{n_2}\left(v_{Fn_2}\tilde{y}_2\right) \alpha_{n_3}\left(v_{Fn_3}\tilde{y}_3\right) \int d\tilde{\varepsilon} n_B\left(\tilde{\varepsilon}\right) \tilde{\varepsilon}^2 \\
&\times \Big[-\delta_{jn_3} \delta_{n_3 n_1} S^*_{n_1 j'} \delta_{n_1 n_2} \left|S_{n_2 n_3}\right|^2 H\left(\tilde{y}_2 - \tilde{y}_1\right) H\left(\tilde{y}_3 - \tilde{y}_1\right) e^{2i(\tilde{\varepsilon}-i0)(\tilde{y}_1-\tilde{y}_2-\tilde{y}_3)} \\
&- \delta_{jn_3} S^*_{n_3 n_1} \delta_{n_1 j'} \delta_{n_1 n_2} \delta_{n_2 n_3} H\left(\tilde{y}_1 - \tilde{y}_2\right) H\left(\tilde{y}_3 - \tilde{y}_2\right) e^{2i(\tilde{\varepsilon}-i0)(-\tilde{y}_1+\tilde{y}_2-\tilde{y}_3)} \\
&- S^*_{jn_3} \delta_{n_3 n_1} \delta_{n_1 j'} \left|S_{n_1 n_2}\right|^2 \delta_{n_2 n_3} H\left(\tilde{y}_2 - \tilde{y}_3\right) H\left(\tilde{y}_1 - \tilde{y}_3\right) e^{2i(\tilde{\varepsilon}-i0)(-\tilde{y}_1-\tilde{y}_2+\tilde{y}_3)} \\
&- \delta_{jn_3} S^*_{n_3 n_1} \delta_{n_1 j'} \left|S_{n_1 n_2}\right|^2 \left|S_{n_2 n_3}\right|^2 e^{2i(\tilde{\varepsilon}-i0)(-\tilde{y}_1-\tilde{y}_2-\tilde{y}_3)} \Big]
\end{aligned} \tag{2.114c}$$

plus similar terms with all electron lines reverted. $\tilde{y}_j \equiv y_j/v_{Fj}$ runs between 0 and ∞, $j = 1, 2, 3$. These three terms come from lines 2, 3 and 4 of Eq. (2.113) respectively.

In the dc limit, the zeroth order contribution and the self-energy corrections to the conductance again constitute a Landauer-type formula with a dressed S-matrix, similar to Eq. (2.88). Now we reduce the cutoff and demand the conductance be cutoff-independent. Once the $\tilde{y}$ integrals are performed, it is obvious that the cutoff-sensitive integrals are the E_2 integral and the $\tilde{\varepsilon}$ integral.

We are in a position to discuss the real space integrals. We first focus on the simplest case where the interactions in wires and leads are uniform and identical, $\alpha_{n_1}(y) = \alpha_{n_1}$ for any n_1, so that all α's factor out. At the third order, we find the following integrals:

$$I_1\left(E^+\right) \equiv \int_0^\infty d\tilde{y}_1 d\tilde{y}_2 d\tilde{y}_3 e^{iE^+(\tilde{y}_1+\tilde{y}_3)} e^{iE^+(\tilde{y}_1-2\tilde{y}_2+\tilde{y}_3)} H(\tilde{y}_1-\tilde{y}_2) H(\tilde{y}_3-\tilde{y}_2) \tag{2.115}$$

which appears alongside the factors $\delta_{n_1 n_2}\delta_{n_2 n_3}$, and

$$\int_0^\infty d\tilde{y}_1 e^{2iE^+\tilde{y}_1} = \frac{i}{2E^+} \tag{2.116}$$

which appears alongside, for example, $W_{n_1 n_2} W_{n_2 n_3}$. (More accurately, Eq. (2.116) comes with each "node" n_2 as long as n_2 is not sandwiched between two Kronecker δ factors.) Here $E^+ \equiv E + i0$ may be replaced by $\tilde{E}_2$ or $(\pm\tilde{\varepsilon} + i0)$. At higher orders, we need to evaluate the integral

$$I_M\left(E^+\right) \equiv \prod_{l=1}^{2M+1}\left(\int_0^\infty d\tilde{y}_l\right) e^{iE^+(\tilde{y}_1+\tilde{y}_{2M+1})} \prod_{j=1}^{M}\left[e^{iE^+\left(\tilde{y}_{2j-1}+\tilde{y}_{2j+1}-2\tilde{y}_{2j}\right)} H(\tilde{y}_{2j-1}-\tilde{y}_{2j}) H(\tilde{y}_{2j+1}-\tilde{y}_{2j})\right] \tag{2.117}$$

This is accompanied by a string of $2M$ consecutive δ factors uninterrupted by W factors, $\delta_{n_1 n_2}\delta_{n_2 n_3}\cdots\delta_{n_{2M} n_{2M+1}}$. We will prove in Section 2.7.2 that

$$I_M\left(E^+\right) = \left(\frac{i}{2E^+}\right)^{2M+1} C_M \tag{2.118}$$

where $C_M = (2M)!/[M!(M+1)!]$ is the Mth Catalan number[120, 121]. The first few Catalan numbers $0 \le M \le 5$ are 1, 1, 2, 5, 14, 42.

At this stage we can combine the $(E^+)^{-1}$ factors in Eqs. (2.116) and (2.118) with the $\tilde{E}_2$ or $\tilde{\varepsilon}$ factors. At each order there will be a single $(E^+)^{-1}$ factor left unpaired, which gives the leading-log renormalization $\delta D/D$ as the cutoff is reduced from D to $D - \delta D$. Collecting terms of all orders we see the S-matrix RG equation is of the form of Eq. (2.106), but the interaction $\Pi(D)$ is given by

$$\frac{\Pi_{jj'}}{2} = \frac{\alpha_j}{2}\delta_{jj'} + \frac{\alpha_j}{2}\frac{\alpha_{j'}}{2}\Bigg\{ W_{jj'} + \sum_{n_1}\frac{\alpha_{n_1}}{2}\left[\delta_{jn_1}\delta_{n_1j'} + W_{jn_1}W_{n_1j'}\right] + \sum_{n_1n_2}\frac{\alpha_{n_1}}{2}\frac{\alpha_{n_2}}{2}\left[\delta_{jn_1}\delta_{n_1n_2}W_{n_2j'} + W_{jn_1}\delta_{n_1n_2}\delta_{n_2j'} + W_{jn_1}W_{n_1n_2}W_{n_2j'}\right] + \sum_{n_1n_2n_3}\frac{\alpha_{n_1}}{2}\frac{\alpha_{n_2}}{2}\frac{\alpha_{n_3}}{2}\left[2\delta_{jn_1}\delta_{n_1n_2}\delta_{n_2n_3}\delta_{n_3j'} + \delta_{jn_1}\delta_{n_1n_2}W_{n_2n_3}W_{n_3j'} + W_{jn_1}\delta_{n_1n_2}\delta_{n_2n_3}W_{n_3j'} + W_{jn_1}W_{n_1n_2}\delta_{n_2n_3}\delta_{n_3j'} + W_{jn_1}W_{n_1n_2}W_{n_2n_3}W_{n_3j'}\right] + \cdots \Bigg\} \tag{2.119}$$

The rules to write down terms in Eq. (2.119) are as follows. At $O(\alpha^m)$, there is a total number of $(m-1)$ factors of δ and W. The δ factors always appear in even-length strings separated by the W factors. Each string of δ of length $2M$ is associated with a multiplicative coefficient of the Mth Catalan number C_M. For instance, at $O(\alpha^{17})$ there is a term $W\delta\delta\delta\delta\delta\delta WWW\delta\delta\delta\delta\delta WW$, whose prefactor will be $C_3C_2 = 5\times 2 = 10$.

We can resum Eq. (2.119) by observing that we can uniquely construct every term containing a least one factor of W, by adding to an existing term a (possibly empty) even-length string of δ followed by one factor of W; e.g. the term $\delta\delta\delta\delta WW\delta\delta W$ is uniquely constructed as $\delta\delta\delta\delta/W/W\delta\delta W$. In other words, Π satisfies the relation

$$\frac{\Pi_{jj'}}{2} = \frac{\bar{\Pi}_{jj'}}{2} + \sum_{l_1l_2}\frac{\bar{\Pi}_{jl_1}}{2}W_{l_1l_2}\frac{\Pi_{l_2j'}}{2}. \tag{2.120}$$

Here $\bar{\Pi}$ is the part of Π which does not contain any factors of W:

$$\begin{aligned}\frac{\bar{\Pi}_{jj'}}{2} &= \frac{\alpha_j}{2}\delta_{jj'} + \frac{\alpha_j}{2}\frac{\alpha_{j'}}{2}\left[\sum_{n_1}\frac{\alpha_{n_1}}{2}\delta_{jn_1}\delta_{n_1j'} + \sum_{n_1n_2n_3}\frac{\alpha_{n_1}}{2}\frac{\alpha_{n_2}}{2}\frac{\alpha_{n_3}}{2}2\delta_{jn_1}\delta_{n_1n_2}\delta_{n_2n_3}\delta_{n_3j'} + \cdots\right] \\ &= \frac{\alpha_j}{2}\delta_{jj'}\sum_{M=0}^{\infty}C_M\left(\frac{\alpha_j}{2}\right)^{2M} = \frac{\alpha_j}{1+\sqrt{1-\alpha_j^2}}\delta_{jj'}.\end{aligned} \tag{2.121}$$

In the last line we have used the generating function of Catalan numbers[120],

$$\sum_{M=0}^{\infty}C_Mx^M = \frac{2}{1+\sqrt{1-4x}}. \tag{2.122}$$

Inserting Eq. (2.121) into Eq. (2.120) and solving for Π, we obtain Eq. (2.107) in the case of spatially uniform interactions, $\alpha_n(y) = \alpha_n$.

We now argue that the cutoff-dependence of the Luttinger parameter is through Eq. (2.70) as is the case with the first order calculation. To this end, notice that it is values of $\tilde{y}_n$ between 0 and

$O(1/E^+)$ that dominate the integral in Eq. (2.117). Therefore, when $D = \mathrm{Re}\, E^+ \gtrsim v_{Fn}/L_n$, the integral is governed by $v_{Fn}\tilde{y}_n \lesssim L_n$; in this range of $\tilde{y}_n$, $\alpha_n(v_{Fn}\tilde{y}_n) = \alpha_n(0)$. On the other hand, when $D \ll v_{Fn}/L_n$, the integral is controlled mainly by $v_{Fn}\tilde{y}_n \gg L_n$, where $\alpha_n(v_{Fn}\tilde{y}_n) = \alpha_n(\infty)$. This justifies the crossover behavior given by Eqs. (2.70) and (2.108), and concludes the calculation of the self-energy terms in the RPA conductance.

Calculations of the RPA vertex corrections, or the ring diagrams, are completely in parallel with the first-order vertex corrections except Eq. (2.117) appears in the real space integrals. Here E^+ in Eq. (2.117) should be substituted for ω^+. At the mth order, all m factors of $1/\omega^+$ in Eqs. (2.116) and (2.118) can be paired with the $m+1$ factors of ω^+ from loop energy integrals; the single unpaired ω^+ will be combined with the $1/\omega$ factor in Eq. (3.31) so that the conductance is finite in the dc limit. Also, all interaction strengths appearing here are those in the leads $\alpha_n(\infty)$; this is because in the dc limit $\omega \lesssim v_{Fn}/L_n$ for any lead n, and we may refer to our argument in the previous paragraph for $D \ll v_{Fn}/L_n$. Eventually, taking into account the dressing of the electron lines, we recover Eq. (2.109).

2.7.2 Real space integral Eq. (2.118)

To prove Eq. (2.118), we adopt the following change of variables in Eq. (2.117): $z_0 = \tilde{y}_1$, $z_{2j-1} = \tilde{y}_{2j-1} - \tilde{y}_{2j}$, $z_{2j} = \tilde{y}_{2j+1} - \tilde{y}_{2j}$, $1 \le j \le M$. The absolute value of the Jacobian of this change of variables is simply $\left|(-1)^M\right| = 1$. We also introduce the shorthand $s_j = \sum_{l=0}^{j}(-1)^l z_l$. Eq. (2.117) then becomes

$$I_M\left(E^+\right) = \int_0^\infty dz_0 \prod_{l=1}^{M}\left(\int_0^{s_{2l-2}} dz_{2l-1}\int_0^\infty dz_{2l}\right)\prod_{j=0}^{M} e^{2iE^+ z_{2j}} \tag{2.123}$$

Now consider the auxiliary object,

$$\tilde{I}_M\left(E^+, z_0\right) \equiv \prod_{l=1}^{M}\left(\int_0^{s_{2l-2}} dz_{2l-1}\int_0^\infty dz_{2l}\right)\prod_{j=0}^{M} e^{2iE^+ z_{2j}} \equiv \left(2iE^+\right)^{-2M} e^{2iE^+ z_0}\sum_{l=0}^{M}\frac{T_{M,l}}{l!}\left(-2iE^+ z_0\right)^l \tag{2.124}$$

where $T_{M,l}$ are dimensionless coefficients; obviously $\tilde{I}_0\left(E^+, z_0\right) = e^{2iE^+ z_0}$ and $T_{0,0} = 1$. $\tilde{I}_M$ obeys the recurrence relation

$$\tilde{I}_{M+1}\left(E^+, z_0\right) = \int_0^{z_0} dz_1 e^{2iE^+ z_1}\int_0^\infty dz_2 \tilde{I}_M\left(E^+, z_0 - z_1 + z_2\right). \tag{2.125}$$

Inserting Eq. (2.124) into Eq. (2.125), we find that $T_{M,l}$ satisfies the simple recurrence relation $T_{M+1,l} = \sum_{j=l-1}^{M} T_{M,j}$, and that $T_{M+1,0} = 0$ ($M \ge 0$). Such a recurrence relation leads to the Catalan's triangle[121],

$$T_{M,l} = \frac{(2M-l-1)!\,l}{M!\,(M-l)!}\ (M \geq 1)\,. \tag{2.126}$$

Therefore,

$$I_M\left(E^+\right) = \int_0^\infty dz_0 \tilde{I}_M\left(E^+, z_0\right) = -\left(2iE^+\right)^{-2M-1} \sum_{l=0}^{M} T_{M,l} \tag{2.127}$$

Noting that $\sum_{l=0}^{M} T_{M,l} = C_M$, which is a property of Catalan's triangle, we immediately recover Eq. (2.118).

2.8 2-lead junctions and Y-junctions

In this section we evaluate the conductance at several established fixed points of 2-lead junctions and Y-junctions attached to FL leads and TLL leads. The analysis is carried out at the first order in interaction [Eqs. (2.102) and (2.104)] and then in the RPA [Eqs. (2.105) and (2.112)]. In particular, we will examine the conductance of the maximally open M fixed point in the RPA for the Z_3 symmetric Y-junction. A more detailed discussion on RG fixed point S-matrices and their stability can be found in Appendix A.

For simplicity, the interactions are once more modeled by Eq. (2.67). We write $\alpha_j(0)$, the interaction strength in wire j, simply as α_j; also when the junction is connected to TLL leads, we assume the interactions in wires and leads are uniform and identical, i.e. $\alpha_j(\infty) = \alpha_j$. Of course, by definition $\alpha_j(\infty) = 0$ for FL leads.

2-lead junction

In a 2-lead junction of spinless fermions away from resonance, solving the S-matrix RG equations [Eq. (2.72) at the first order and Eq. (2.106) in the RPA], we find that the only fixed points are the complete reflection fixed point (the N fixed point) and the perfect transmission fixed point (the D fixed point)[11, 77, 132].

At the N fixed point $W_{12} = 0$, the two wires are decoupled from each other, and we find the obvious result that the conductance $G_{jj'}^{N,\mathrm{FL}} = G_{jj'}^{N,\mathrm{TLL}} = 0$, irrespective of what leads the junction is attached to.

On the other hand, at the D fixed point $W_{12} = 1$, the backscattering between the two wires vanishes. With FL leads $G_{jj'}^{D,\mathrm{FL}} = \left(e^2/2\pi\right)\left(1-2\delta_{jj'}\right)$, as predicted by the naive Landauer formula; with TLL leads, Eq. (2.104) predicts

$$G_{jj'}^{D,\mathrm{TLL}} = \left(1 - \frac{\alpha_1+\alpha_2}{2}\right)\frac{e^2}{2\pi}\left(1-2\delta_{jj'}\right) \tag{2.128}$$

at the first order, and Eq. (2.112) predicts

$$G_{jj'}^{D,\mathrm{TLL}} = \frac{2K_1K_2}{K_1+K_2}\frac{e^2}{2\pi}\left(1-2\delta_{jj'}\right) \tag{2.129}$$

in the RPA. Here the RPA has recovered the famous result for the conductance of two semi-infinite TLL wires, which takes the form of Eq. (2.29).

Y-junction

Even at the first order in interaction, the RG flow portrait for a Y-junction is more complicated than the two-lead junction[70]. Solving Eq. (2.72), we find a "non-geometrical" M fixed point whose existence and transmission probabilities generally depend on the interaction strengths, in addition to the "geometrical" fixed points N, A_j and $\chi^{\pm}$. Provided the interactions are not too strong, these are also the only fixed points allowed in the RPA[15]. N (complete reflection) and A_j (asymmetric) can be obtained by adding a third decoupled wire with label j to the N and D fixed points of the two-lead junction respectively. The conductances at N and A_j are therefore a trivial generalization of the two-lead case, and we will focus on $\chi^{\pm}$ and M alone.

At the chiral fixed points $\chi^{\pm}$, in the absence of interaction, an electron incident from wire j is perfectly transmitted to wire $j\pm1$ (here we identify $j+3\equiv j$); thus the time-reversal symmetry is broken. The W matrix is given by $W_{jj'}=\left(1-\delta_{jj}\mp\varepsilon_{jj'}\right)/2$, where the anti-symmetric tensor $\varepsilon_{jj'}$ is defined by $\varepsilon_{12}=\varepsilon_{23}=\varepsilon_{31}=1$, $\varepsilon_{21}=\varepsilon_{32}=\varepsilon_{13}=-1$ and $\varepsilon_{jj}=0$. At the first order, inserting the W matrix into Eqs. (2.102) and (2.104), we find $G_{jj'}^{\chi^{\pm},\mathrm{FL}}=-\left(e^2/2\pi\right)\left(3\delta_{jj'}-1\pm\varepsilon_{jj'}\right)/2$, and

$$G_{jj'}^{\chi^{\pm},\mathrm{TLL}}-G_{jj'}^{\chi^{\pm},\mathrm{FL}}=\frac{e^2}{2\pi}\frac{1}{2}\left[\left(\alpha_j+\alpha_{j'}\right)\left(\frac{3}{2}-\delta_{jj'}\right)+\frac{1}{2}\left(\alpha_1+\alpha_2+\alpha_3\right)\left(1-\delta_{jj'}\pm\varepsilon_{jj'}\right)\right]. \tag{2.130}$$

In the RPA, on the other hand, Eq. (2.112) gives the conductance at $\chi^{\pm}$ with TLL leads as

$$G_{jj'}^{\chi^{\pm},\mathrm{TLL}}=-2\frac{e^2}{2\pi}\frac{K_j\left(K_1+K_2+K_3\right)\delta_{jj'}+\left(\pm K_1K_2K_3\varepsilon_{jj'}-K_jK_{j'}\right)}{K_1+K_2+K_3+K_1K_2K_3}, \tag{2.131}$$

which again agrees with the bosonization result Eq. (2.50).

The presence of the M fixed point can be inferred in a Z_3 symmetric time-reversal invariant Y-junction with attractive interactions: in this system, N is unstable, A_j is forbidden by Z_3 symmetry, and $\chi^{\pm}$ are forbidden by time-reversal symmetry, so there must be at least one stable fixed point. The W matrix has generally interaction-dependent elements at M. At the first order,

$$W_{jj'}=\begin{cases}\left(\frac{\alpha_1\alpha_2\alpha_3/\alpha_j}{\alpha_1\alpha_2+\alpha_2\alpha_3+\alpha_3\alpha_1}\right)^2, & j=j'\\ \left(1-\frac{\alpha_1\alpha_2\alpha_3/\alpha_j}{\alpha_1\alpha_2+\alpha_2\alpha_3+\alpha_3\alpha_1}\right)\left(1-\frac{\alpha_1\alpha_2\alpha_3/\alpha_{j'}}{\alpha_1\alpha_2+\alpha_2\alpha_3+\alpha_3\alpha_1}\right), & j\neq j'\end{cases}. \tag{2.132}$$

We see explicitly that M obeys time-reversal symmetry, $W_{jj'}=W_{j'j}$. Demanding $0\leq W_{jj'}\leq 1$, we

find that at the first-order M can only exist in the following situations: 1) α_1, α_2, $\alpha_3 > 0$; 2) α_1, α_2, $\alpha_3 < 0$; 3) $\alpha_1 > 0$, $\alpha_2 > 0$, $\alpha_3 < -\alpha_1$, $\alpha_3 < -\alpha_2$; 4) $\alpha_1 < 0$, $\alpha_2 < 0$, $\alpha_3 > -\alpha_1$, $\alpha_3 > -\alpha_2$; and situations equivalent to 3) and 4) up to permuted subscripts (e.g. $(\alpha_1, \alpha_2, \alpha_3) \to (\alpha_3, \alpha_1, \alpha_2)$).

Substituting Eq. (2.132) into Eq. (2.104), we find that at the first-order the conductance at M obeys

$$G^{M,\mathrm{TLL}}_{jj'} - G^{M,\mathrm{FL}}_{jj'} = \begin{cases} \frac{e^2}{2\pi} \frac{(\alpha_1+\alpha_2)(\alpha_2+\alpha_3)(\alpha_1+\alpha_3)}{2(\alpha_1\alpha_2+\alpha_2\alpha_3+\alpha_3\alpha_1)^3} \alpha_j^2 \left(\alpha_1+\alpha_2+\alpha_3-\alpha_j\right)^2, & j = j' \\ -\frac{e^2}{2\pi} \frac{(\alpha_1+\alpha_2)(\alpha_2+\alpha_3)(\alpha_1+\alpha_3)}{2(\alpha_1\alpha_2+\alpha_2\alpha_3+\alpha_3\alpha_1)^3} \left[\alpha_j\alpha_{j'}\left(\alpha_1\alpha_2+\alpha_2\alpha_3+\alpha_3\alpha_1\right) - \frac{(\alpha_1\alpha_2\alpha_3)^2}{\alpha_j\alpha_{j'}}\right], & j \neq j' \end{cases}. \tag{2.133}$$

Note that for Z_3 symmetric interactions ($\alpha_j = \alpha$), $W_{jj'} = 1/9 + \delta_{jj'}/3$ becomes independent of the interaction strength. Now $W_{jj'}$ produces the maximal transmission probability $8/9$ allowed by unitarity in a Z_3 symmetric S-matrix, and at the first order $G^{M,\mathrm{TLL}}_{jj'} - G^{M,\mathrm{FL}}_{jj'} = -(8/27)\,\alpha\left(e^2/2\pi\right)\left(1-3\delta_{jj'}\right)$. Compared to FL leads, TLL leads enhance conductance for attractive interactions and reduce conductance for repulsive interactions, as with the two-lead D fixed point.

In the RPA, the W matrix of the M fixed point is generally cumbersome, but reduces to the aforementioned maximally transmitting W matrix for Z_3 symmetric interactions. Eq. (2.112) then gives[111]

$$G^{M,\mathrm{TLL}}_{jj'} = \frac{4K}{3K+6}\frac{e^2}{2\pi}\left(1-3\delta_{jj'}\right). \tag{2.134}$$

This result supports the findings of Ref. [104]. There the M fixed point conductance of a Y-junction of infinite TLL wires is computed numerically using density matrix renormalization group, and conjectured to be

$$G_{jj'} = \frac{2K\gamma}{2K+3\gamma-3K\gamma}\frac{e^2}{2\pi}\left(1-3\delta_{jj'}\right), \tag{2.135}$$

where it is suggested that the dimensionless parameter γ is $4/9$ based on the non-interacting limit $K = 1$.

2.9 Conclusion and discussions

We would like to discuss some of the questions left open in our approach.

First, we have assumed that scattering by the junction is fully described by operators which are quadratic in conduction fermions and independent of other degrees of freedom. Local operators quartic in fermions are ignored, among others. This does not pose a threat to the first-order calculations, because any quartic local operator has a scaling dimension of at least $4 \times 1/2 = 2$ in the non-interacting case, and is necessarily highly irrelevant. However, it has been shown that sufficiently

strong attractive bulk interactions can render quartic boundary operators relevant[93]. An example is the electron pair hopping operator at the Z_3 symmetric Y-junction, $\psi_{1L}^\dagger \psi_{1R}^\dagger \psi_3 \partial_x \psi_3 \,(x=0) + \text{h.c.}$: it is of dimension $3/K$ at the asymmetric fixed point A_3, where K is the Luttinger parameter of all three wires, and A_3 sees wire 3 decoupled from perfectly connected wires 1 and 2. Apparently, for very strong interactions $K > 3$, this operator becomes relevant and can potentially dominate the physical properties of the stable fixed point. Unfortunately, the present RPA analysis does not predict a scaling exponent consistent with this operator[15]; it is hence incomplete in this regard, and should not be carried too far into the regime of strongly attractive bulk interactions.

A related issue is the existence of the D fixed points in the Y-junction. Predicted by the bosonic approaches[51, 86, 93] but not the fermionic ones[13, 15], these fixed points are only stable for strong attractive interactions. They are most notably characterized by Andreev reflections, even when electron-electron interaction is absent in the bulk. This hints at multi-particle scattering at the junction, and rules out the possibility to represent the D fixed points by single-particle S-matrices. (Single-particle S-matrices with particle-hole channels are not feasible either since the D fixed points respect particle number conservation[93].) The D fixed points are not predicted by purely fermionic approaches, because the latter are based on the ansatz that the junction is always described by a single-particle S-matrix along the RG flow; but such an ansatz will likely be invalidated if, for instance, relevant quartic boundary operators are present. We are thus led to believe that the lack of D fixed points in the present RPA analysis does not refute their possible stability when the bulk interactions are strongly attractive. Indeed, the refermionization method adopted by Ref. [45] may be successfully used to describe the crossover from the "pair tunneling" D fixed point to the $\chi^\pm$ fixed points in the vicinity of Luttinger parameter $K = 3$, with an S-matrix of free fermions which are not the original electrons.

On the other hand, even when the bulk interactions are relatively weak, it is not a priori clear to what extent the RPA is successful. In the Tomonaga-Luttinger model (which we have adopted in our bulk quantum wires), the RPA is known to be exact due to the interaction which separately conserves the numbers of right- and left-movers[34]. This is no longer the case once right- and left-movers become mixed up by the scattering at the junction. It has been pointed out that going beyond the RPA changes the renormalization of the S-matrix away from the "geometrical" fixed points, although all universal scaling exponents stay the same[11–13]. As for the "non-geometrical" M fixed point in the Y-junction, its position is generally shifted when we go beyond the RPA. Remarkably, however, if the interaction is Z_3 symmetric, not only the W matrix but also the scaling exponents at the M fixed point remain identical with the RPA results up to the third order in interaction[13]. The agreement of our RPA result with the numerics of Ref. [104] is suggestive, but more work on vertex corrections is required to verify the validity of our RPA conductance at the Z_3 symmetric M fixed point with TLL leads, Eq. (2.134).

As a conclusion to this chapter, using the fermionic RG formalism, we calculated the linear dc

conductance tensor of a junction of multiple quantum wires. We showed, both at the first order and in the RPA, that a junction attached to FL leads has a conductance tensor which obeys a linearized Landauer-type formula with a renormalized S-matrix. TLL leads modify the conductance through vertex corrections, and the conductance with FL leads can be heuristically related to the conductance with TLL leads through the contact resistance between leads.

Chapter 3

Conductance of long ABK rings

This chapter tackles the problem of long ABK rings[112]. We begin by reviewing the spin-$1/2$ single-channel Kondo effect in Section 3.1, focusing on the size of the Kondo screening cloud and the $\pi/2$ phase shift from scattering by the Kondo singlet. To treat ABK rings, we introduce a generalized Anderson model with an interacting QD in Section 3.2; the screening channel is separated from the non-screening ones, and an effective Kondo model in the local moment regime is obtained. In Section 3.3 the linear dc conductance is calculated using Kubo formula. Disconnected and connected contributions are examined separately, and the approximate elimination of the connected contribution is discussed. Perturbation theories in the weak-coupling and FL regimes are employed in Section 3.4; weak-coupling results applicable at high temperatures formally resemble the short ring case. In Section 3.5, we make contact with earlier results by applying our formalism to a short ABK ring as well as a QD connected to two finite non-interacting quantum wires. Section 3.6 then applies the formalism to the closed long ring, and Section 3.7 studies open long rings and their potential utilization as two-path interferometers. Conclusions and open questions are presented in Section 3.8. Appendix B consists of details related to the calculation of disconnected contributions. Finally, Appendix C include technical details of the two perturbation theories, explicitly calculating the screening channel T-matrix and the connected contribution to the conductance.

3.1 The spin-$1/2$ single-channel Kondo effect

Let us go over properties of the spin-$1/2$ single-channel Kondo model[1]. For concreteness, we consider an impurity spin in a three-dimensional electron gas. If the system is spherically symmetric, only the s-wave harmonic is coupled to the impurity spin. Hence the low-energy effective Hamiltonian is one-dimensional:

$$H = \int_0^\infty dx\,(iv_F)\left[\psi_L^\dagger(x)\,\partial_x\psi_L(x) - \psi_R^\dagger(x)\,\partial_x\psi_R(x)\right] + J\psi_L^\dagger\frac{\vec{\sigma}}{2}\psi_L(0)\cdot\vec{S}, \tag{3.1}$$

where v_F is again the Fermi velocity of the conduction band, with the dispersion $\varepsilon_k = v_F k$ (we measure energies relative to the Fermi energy), $\vec{S}$ is the impurity spin, and J is the Kondo coupling constant. The right- and left-movers $\psi_{R/L}$ are respectively outgoing and incoming s-wave components, and obey the anticommutation relation

$$\left\{ \psi_{L/R}(x), \psi_{L,R}^{\dagger}(x') \right\} = \delta(x-x'). \tag{3.2}$$

Here we only let $\psi_L(0)$ couple to $\vec{S}$, because in absence of J, ψ_R and ψ_L satisfy the boundary condition at $x=0$:

$$\psi_R(0) = \psi_L(0); \tag{3.3}$$

thus coupling $\psi_R(0)$ to $\vec{S}$ merely amounts to redefining J. We can again unfold the system so that for $x>0$, $\psi_R(x) = \psi_L(-x)$; the Hamiltonian then becomes

$$H = \int_{-\infty}^{\infty} dx\,(iv_F)\,\psi_L^{\dagger}(x)\,\partial_x \psi_L(x) + J\psi_L^{\dagger}\frac{\vec{\sigma}}{2}\psi_L(0)\cdot\vec{S}. \tag{3.4}$$

The perturbation theory in J is infrared divergent; the energy scale associated with this divergence is the Kondo temperature T_K. To find T_K we can, for instance, calculate the β-function of J which describes how J renormalizes as the high-energy cutoff decreases. This is done by restricting the energy of ψ_L to $(-D,D)$, where the reduced bandwidth D is much smaller than the original bandwidth, and subsequently integrating out in the action the "fast" degrees of freedom with energies between $(-D,-D+\delta D)$ and $(D-\delta D,D)$, where $\delta D \ll D$. The high-energy cutoff in the resultant theory is thus reduced from D to $D-\delta D$.

The $O\left(J^2\right)$ fast-mode correction to the Euclidean action is

$$\frac{J^2}{2}\int d\tau d\tau' \left\langle T_\tau \psi_L^{\dagger}(\tau)\frac{\sigma_a}{2}\psi_L(\tau)\,\psi_L^{\dagger}(\tau')\frac{\sigma_b}{2}\psi_L(\tau')\right\rangle_f \left\langle T_\tau S^a(\tau) S^b(\tau')\right\rangle \tag{3.5}$$

where both expectation values are calculated in the interaction picture, $\langle\rangle_f$ indicates that only fast modes are integrated over (or, equivalently, contracted), all ψ_L operators are at $x=0$, and sums over repeated indices are implied. The impurity spin operator has no dynamics of its own in the absence of J; thus

$$\left\langle T_\tau S^a(\tau) S^b(\tau')\right\rangle = H(\tau-\tau') S^a S^b + H(\tau'-\tau) S^b S^a = \frac{1}{4}\delta_{ab} + \frac{1}{2} i\varepsilon_{abc} S^c \operatorname{sgn}(\tau-\tau'), \tag{3.6}$$

where $H(\tau)$ is again the Heaviside function, and ε_{abc} is the Levi-Civita symbol. It is the sign function term that makes the spin-flip Hamiltonian very different from normal potential scattering.

Meanwhile, each ψ_L can be decomposed into a "fast" component ψ_{Lf} and a "slow" one ψ_{Ls}, so

the correlation function of ψ_L has $2^4 = 16$ terms. Of these, the only two terms contributing to the renormalization of J are $\left\langle T_\tau \psi^\dagger_{Lf}(\tau)\,\sigma_a \psi_{Ls}(\tau)\,\psi^\dagger_{Ls}(\tau')\,\sigma_b \psi_{Lf}(\tau')\right\rangle_f$ and $\left\langle T_\tau \psi^\dagger_{Ls}(\tau)\,\sigma_a \psi_{Lf}(\tau)\,\psi^\dagger_{Lf}(\tau')\,\sigma_b \psi_{Ls}(\tau')\right\rangle_f$. The slow modes are not affected by the contraction, while the fast modes are contracted as follows:

$$\begin{aligned}-\left\langle T_\tau \psi_{Lf}(\tau)\,\psi^\dagger_{Lf}(\tau')\right\rangle_f &= -\left(\int_{-D}^{-D+\delta D} + \int_{D-\delta D}^{D}\right)\frac{d\varepsilon}{2\pi v_F} e^{-\varepsilon(\tau-\tau')}\left[H(\tau-\tau') - f(\varepsilon)\right] \\ &= -\frac{\delta D}{2\pi v_F} e^{-D|\tau-\tau'|}\,\mathrm{sgn}(\tau-\tau'). \end{aligned} \tag{3.7}$$

In the second line we are considering the zero temperature case (we expect the only effect of finite temperatures to be cutting off the RG flow). The sign function here cancels the sign function from time-ordering the impurity spin. Noting that $\sigma_a\sigma_b = \delta_{ab} + i\varepsilon_{abc}\sigma_c$, and that $\varepsilon_{abc}\varepsilon_{abd} = 2\delta_{cd}$, we find the overall $O(J^2)$ contribution to the action to be

$$\begin{aligned}&-\frac{J^2}{2}\int d\tau d\tau' \psi^\dagger_L(\tau)\frac{\vec{\sigma}}{2}\psi_L(\tau')\cdot\vec{S}\frac{\delta D}{2\pi v_F}e^{-D|\tau-\tau'|} \\ &\approx -J^2\frac{1}{2\pi v_F}\frac{\delta D}{D}\int d\tau \psi^\dagger_L(\tau)\frac{\vec{\sigma}}{2}\psi_L(\tau)\cdot\vec{S};\end{aligned} \tag{3.8}$$

in the second line we have neglected the slight retardation when integrating over τ', since only $|\tau'-\tau| \lesssim 1/D$ contributes significantly to the integral.

Therefore, the renormalization of J is given by $\delta J = (\delta \ln D) J^2/(2\pi v_F)$, and the RG equation for the dimensionless coupling constant $\lambda \equiv J/(2\pi v_F)$ is

$$-\frac{d\lambda}{d\ln D} = \lambda^2. \tag{3.9}$$

With the boundary condition $\lambda(D = D_0) = \lambda_0$, this equation has the solution

$$\lambda = \frac{1}{\ln \frac{D}{T_K}},$$

where the Kondo temperature is defined as

$$T_K \equiv D_0 \exp\left(-\frac{1}{\lambda_0}\right). \tag{3.10}$$

For ferromagnetic coupling $\lambda_0 < 0$, λ simply flows to zero as the cutoff is reduced. However, for antiferromagnetic coupling $\lambda > 0$, T_K is the energy scale at which λ becomes $O(1)$ and perturbation theory breaks down.

To obtain a qualitative picture of what happens in the antiferromagnetic case well below T_K, where apparently the Kondo coupling J flows to $+\infty$, it is useful to consider a lattice model. The

impurity spin is coupled to the end of a semi-infinite tight-binding chain of hopping strength t, and the Hamiltonian takes the form

$$H = -\sum_{n=0}^{\infty} t\left(c_n^\dagger c_{n+1} + \text{h.c.}\right) + J c_0^\dagger \frac{\vec{\sigma}}{2} c_0 \cdot \vec{S}. \tag{3.11}$$

In the naive strong coupling limit $J \gg t$, due to the second term, the impurity spin should be "screened", and form a singlet with one electron on site 0. Other electrons are essentially free except they are now forbidden to visit site 0, as doing so requires an energy penalty $\sim J$. Hence our strong coupling boundary condition is that the overall wave function should vanish at site 0; or, in terms of right- and left-movers,

$$\psi_R(0) + \psi_L(0) = 0. \tag{3.12}$$

Comparing Eq. (3.12) with Eq. (3.3), we see that the strong coupling boundary condition corresponds to an additional phase factor of $-1 = \exp(2i\pi/2)$, i.e. a $\pi/2$ phase shift due to the scattering by the Kondo singlet (together with the removal of the impurity spin from the effective Hamiltonian).

A question not addressed by the lattice model is the true length scale of the wave function of the screening electron L_K (or size of the "Kondo screening cloud") in the strong coupling limit[2, 85]. This length scale is one lattice spacing in the $J \gg t$ limit of the lattice model, but there is no lattice in our original effective model Eq. (3.1); the lattice of the underlying material has already dropped out upon taking the continuum limit. Since the screening cloud forms in the crossover from weak coupling to strong coupling, it is reasonable to expect that L_K is related to the crossover energy scale T_K, $L_K = v_F/T_K$.

3.2 Anderson model and Kondo model

Starting in this section, we study a generalized tight-binding Anderson model[112], in order to make contact with the long ABK ring geometries which will be our main interest. This model describes N FL leads meeting at a junction containing a QD with an on-site Coulomb repulsion. In addition to the QD, the junction comprises an arbitrary configuration of non-interacting tight-binding sites. The full Hamiltonian contains a non-interacting part, a QD part, and a coupling term between the two:

$$H = H_0 + H_T + H_d. \tag{3.13a}$$

The non-interacting part is made up of two terms,

$$H_0 = H_{0,\text{leads}} + H_{0,\text{junction}}; \tag{3.13b}$$

the lead term

$$H_{0,\text{leads}} = -t \sum_{j=1}^{N} \sum_{n=0}^{\infty} \sum_{\sigma} \left(c^{\dagger}_{j,n,\sigma} c_{j,n+1,\sigma} + \text{h.c.} \right) \tag{3.13c}$$

models the FL leads as semi-infinite nearest-neighbor tight-binding chains with hopping t, where j is the lead index, n is the site index and $\sigma = \uparrow, \downarrow$ is the spin index. For simplicity all leads are assumed to be identical. $H_{0,\text{junction}}$ is the non-interacting part of the junction; it glues all leads together and often includes additional sites (e.g. representing the arms of an ABK ring), but does not include coupling to the interacting QD. In a typical open ABK ring with electron leakage, two of the leads serve as source and drain electrodes, while the remaining $N-2$ leads mimic the base contacts thorough which electrons escape the junction. In experiments usually the current flowing through the source or the drain is monitored, but the leakage current can also be measured.

Assume that there are M sites in the junction to which the QD is directly coupled; hereafter we refer to these sites as the coupling sites. The coupling to the QD can be written as

$$H_T = -\sum_{r=1}^{M} \sum_{\sigma} \left[t_r c^{\dagger}_{C,r,\sigma} d_{\sigma} + \text{h.c.} \right] \tag{3.13d}$$

where d_σ annihilates an electron with spin σ on the QD, and $c^{\dagger}_{C,r,\sigma}$ creates a spin-σ electron on the rth coupling site. $c_{C,r}$ may coincide with $c_{j,0}$ (although not with $c_{j,n}$ for $n \geq 1$). In the simplest AB ring, there is only one physical AB phase, which may be incorporated in either $H_{0,\text{junction}}$ or H_T. In more complicated models both $H_{0,\text{junction}}$ and H_T can depend on AB phases.

Finally, the Hamiltonian of the interacting QD is given by

$$H_d = \sum_{\sigma} \varepsilon_d n_{d\sigma} + U n_{d\uparrow} n_{d\downarrow} \tag{3.13e}$$

where $n_{d\sigma} = d^{\dagger}_{\sigma} d_{\sigma}$. We assume $SU(2)$ spin symmetry throughout the chapter.

A generic system with $N = 5$ and $M = 3$ is sketched in Fig. 3.1, with details of the mesoscopic junction hidden. We will analyze more concrete realizations of this model, including ABK rings and QD attached to quantum wires[66, 75, 116], in Sections 3.5, 3.6 and 3.7.

3.2.1 Screening and non-screening channels

While it is $H_{0,\text{junction}}$ that ultimately determines the properties of the junction, its details are actually not important in our formalism. Instead, in the following we characterize the model by its background scattering S-matrix and coupling site wave functions. Both quantities are easily obtained from a given $H_{0,\text{junction}}$, and as we show in Section 3.3, they play a central role in our quest for the linear dc conductance.

To recast our model into the standard form of an interacting QD coupled to a continuum of states,

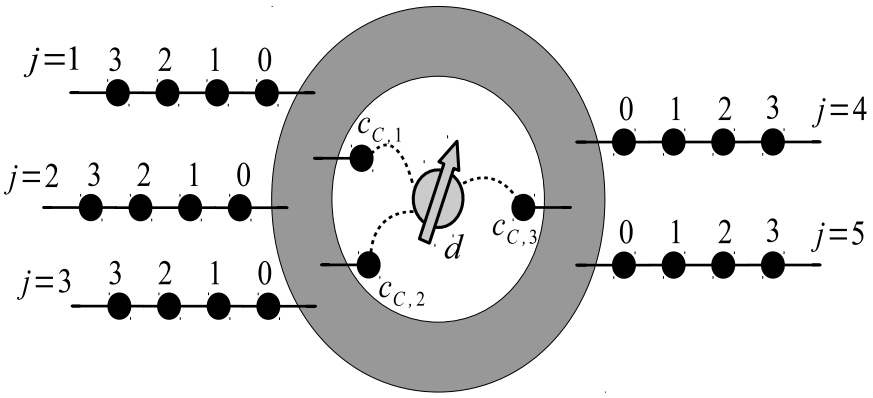

Figure 3.1: Sketch of a generic system which allows the application of our formalism. Here $N = 5$ and $M = 3$.

it is convenient to first diagonalize the non-interacting part of the Hamiltonian H_0 by introducing the scattering basis $q_{j,k,\sigma}$:

$$H_0 = \int_0^{\pi} \frac{dk}{2\pi} \sum_{j=1}^{N} \sum_{\sigma} \varepsilon_k q_{j,k,\sigma}^{\dagger} q_{j,k,\sigma}, \tag{3.14}$$

where $\varepsilon_k = -2t\cos k$ is the dispersion relation in the leads, and for simplicity we let the lattice constant $a = 1$. In addition to the scattering states $q_{j,k,\sigma}$, there may exist a number of bound states with their energies outside of the continuum, but since their wave functions decay exponentially away from the junction region, they do not affect linear dc transport properties.

The scattering basis operator $q_{j,k,\sigma}$ annihilates a scattering state electron incident from lead j with momentum k and spin σ, and obeys the anti-commutation relation $\left\{ q_{j,k,\sigma}, q_{j',k',\sigma'}^{\dagger} \right\} = 2\pi\delta_{jj'}\delta_{\sigma\sigma'}\delta(k-k')$. The corresponding wave function has the following form on site n in lead j',

$$\chi_{j,k}(j',n) = \delta_{jj'} e^{-ikn} + S_{j'j}(k) e^{ikn}; \tag{3.15a}$$

and on coupling site r,

$$\chi_{j,k}(r) = \Gamma_{rj}(k). \tag{3.15b}$$

In other words, for an electron incident from lead j, $S_{j'j}$ is the background reflection or transmission amplitude in lead j', and Γ_{rj} is the wave function on coupling site r. The scattering S-matrix S is unitary: $S^{\dagger}S = 1$.

From its wave function, $q_{j,k,\sigma}$ can be related to $c_{j,n,\sigma}$ and $c_{C,r,\sigma}$:

$$c_{j,n,\sigma} = \int_0^\pi \frac{dk}{2\pi} \sum_{j'=1}^{N} \left[\delta_{jj'} e^{-ikn} + S_{jj'}(k) e^{ikn} \right] q_{j',k,\sigma}, \tag{3.16a}$$

and

$$c_{C,r,\sigma} = \int_0^\pi \frac{dk}{2\pi} \sum_{j'=1}^{N} \Gamma_{rj'}(k) q_{j',k,\sigma}. \tag{3.16b}$$

We now express H_T in the scattering basis. Inserting Eq. (3.16b) into Eq. (3.13d), we find the QD is only coupled to one channel in the continuum, i.e. the screening channel:

$$H_T = -\sum_\sigma \int_0^\pi \frac{dk}{2\pi} V_k \left(\psi_{k,\sigma}^\dagger d_\sigma + \text{h.c.} \right), \tag{3.17}$$

where the screening channel operator $\psi_{k,\sigma}^\dagger$ is defined by

$$\psi_{k,\sigma}^\dagger = \frac{1}{V_k} \sum_{j=1}^{N} \sum_{r=1}^{M} t_r \Gamma_{r,j}^*(k) q_{j,k,\sigma}^\dagger, \tag{3.18}$$

and the normalization factor $V_k > 0$ is defined by

$$V_k^2 = \sum_{j=1}^{N} \sum_{r,r'=1}^{M} t_r t_{r'}^* \Gamma_{rj}^*(k) \Gamma_{r'j}(k) = \text{tr}\left[\Gamma^\dagger(k) \lambda \Gamma(k) \right]. \tag{3.19}$$

This ensures $\left\{ \psi_{k,\sigma}, \psi_{k',\sigma'}^\dagger \right\} = 2\pi \delta_{\sigma\sigma'} \delta(k-k')$. Here we also introduce the $M \times M$ Hermitian QD coupling matrix λ,

$$\lambda_{rr'} = t_r t_{r'}^*. \tag{3.20}$$

It will be useful to define a series of non-screening channels $\phi_{l,k,\sigma}$ orthogonal to ψ, where $l = 1, \cdots, N-1$. The ϕ channels are decoupled from the QD. In a compact notation we can write the transformation from the scattering basis to the screening–non-screening basis as

$$\Psi_{k,\sigma} \equiv \begin{pmatrix} \psi_{k,\sigma} \\ \phi_{1,k,\sigma} \\ \cdots \\ \phi_{N-1,k,\sigma} \end{pmatrix} = \mathbb{U}_k \begin{pmatrix} q_{1,k,\sigma} \\ q_{2,k,\sigma} \\ \cdots \\ q_{N,k,\sigma} \end{pmatrix}, \tag{3.21}$$

where $\mathbb{U}$ is a unitary matrix. The first row of $\mathbb{U}$ is known:

$$\mathbb{U}_{1,j,k} = \frac{1}{V_k} \sum_{r=1}^{M} t_r^* \Gamma_{rj}(k). \tag{3.22}$$

As long as $\mathbb{U}$ stays unitary, its remaining matrix elements can be chosen freely without affecting physical observables. Ψ now also diagonalizes H_0,

$$H_0 = \sum_\sigma \int_0^\pi \frac{dk}{2\pi} \varepsilon_k \left(\psi^\dagger_{k,\sigma} \psi_{k,\sigma} + \sum_{l=1}^{N-1} \phi^\dagger_{l,k,\sigma} \phi_{l,k,\sigma} \right); \tag{3.23}$$

we shall also need the inverse transformation,

$$q_{j,k,\sigma} = \mathbb{U}^*_{1,j,k} \psi_{k,\sigma} + \sum_{l=1}^{N-1} \mathbb{U}^*_{l+1,j,k} \phi_{l,k,\sigma}. \tag{3.24}$$

3.2.2 Kondo model

In the local moment regime of the Anderson model[49, 67], for $T \ll U$ we can perform the Schrieffer-Wolff transformation[107] on ψ to obtain an effective Kondo model with a reduced bandwidth and a momentum-dependent coupling:

$$H = H_0 + \int_{k_F-\Lambda_0}^{k_F+\Lambda_0} \frac{dk dk'}{(2\pi)^2} \left(J_{kk'} \psi^\dagger_k \frac{\vec{\sigma}}{2} \psi_{k'} \cdot \vec{S}_d + K_{kk'} \psi^\dagger_k \psi_{k'} \right), \tag{3.25a}$$

where the spin on the QD is given by $\vec{S}_d = d^\dagger (\vec{\sigma}/2) d$. $\Lambda_0 \ll k_F$ is the initial momentum cutoff, and the dispersion is linearized near the Fermi wave vector k_F as $\varepsilon_k = v_F (k - k_F)$; for the tight-binding model $v_F = 2t \sin k_F$.

The interaction consists of a spin-flip term J,

$$J_{kk'} = V_k V_{k'} (j_k + j_{k'}), \tag{3.25b}$$

$$j_k = \frac{1}{\varepsilon_k - \varepsilon_d} + \frac{1}{U + \varepsilon_d - \varepsilon_k} \approx j, \tag{3.25c}$$

and a particle-hole symmetry breaking potential scattering term K,

$$K_{kk'} = \frac{1}{4} V_k V_{k'} (\kappa_k + \kappa_{k'}), \tag{3.25d}$$

$$\kappa_k = \frac{1}{\varepsilon_k - \varepsilon_d} - \frac{1}{U + \varepsilon_d - \varepsilon_k} \approx \kappa. \tag{3.25e}$$

The energy cutoff is initially $D_0 \equiv v_F \Lambda_0$. When we reduce the running energy cutoff from D to $D + dD$ ($0 < -dD \ll D$) to integrate out the high-energy degrees of freedom in the narrow strips of energy $(-D, -D - dD)$ and $(D + dD, D)$, K is exactly marginal in the RG sense, whereas J is marginally relevant and obeys the following RG equation:

$$-\frac{d\left(\nu J_{kk'}\right)}{d\ln D}=\frac{1}{2}\left(\nu J_{k,k_F+\Lambda}\nu J_{k_F+\Lambda,k'}+\nu J_{k,k_F-\Lambda}\nu J_{k_F-\Lambda,k'}\right), \tag{3.26}$$

or equivalently

$$-\frac{dj}{d\ln D}=\nu j^2\left(V^2_{k_F+\Lambda}+V^2_{k_F-\Lambda}\right), \tag{3.27}$$

where ν is the density of states per channel per spin, $\nu=1/(2\pi v_F)$. Therefore, renormalization of the Kondo coupling is controlled by the momentum-dependent normalization factor V_k^2, defined in Eq. (3.19). j is the only truly independently renormalized coupling constant despite the appearance of Eq. (3.26); this follows from the fact that the screening channel is the only channel coupled to the QD[116].

The prototype Kondo model possesses a momentum-independent coupling function, $J_{kk'}\approx 2jV^2_{k_F}$. As a result, spin-charge separation occurs and the Kondo interaction is found to be exclusively in the spin sector[3]. The charge sector is nothing but a non-interacting theory with a particle-hole symmetry breaking phase shift due to the potential scattering term K, while at very low energy scales the spin sector renormalizes to a local FL theory with $\pi/2$ phase shift.

On the other hand, in a mesoscopic geometry V_k^2 often exhibit fluctuations on a mesoscopic energy scale E_V. (More precisely, E_V can be defined as the energy corresponding to the largest Fourier component in the spectrum of V_k^2, but for both specific models discussed in this chapter we can simply read it off the analytic expression.) In the presence of a characteristic length scale L, E_V may be of the order of the Thouless energy v_F/L, as is the case for the closed long ABK ring in Section 3.6; however this is not always true, with a counterexample provided by the open long ABK ring in Section 3.7 where E_V is of the order of the bandwidth $4t$. Well above E_V, V_k^2 appears featureless and can be approximated by its mean value $\overline{V_k^2}$ with respect to k. The Kondo temperature T_K can be loosely defined as the energy cutoff at which the dimensionless coupling $2\nu j\overline{V_k^2}$ becomes $O(1)$. As briefly sketched in Section 1.3, there are two very different parameter regimes of the Kondo temperature[112, 116, 131]:

a) The small Kondo cloud regime $T_K\gg E_V$. For $E_V\sim v_F/L$, the size of the Kondo screening cloud $L_K\equiv v_F/T_K\ll L$; hence the name. In this regime, the bare Kondo coupling is sufficiently large, so that $2\nu j\overline{V_k^2}$ renormalizes to $O(1)$ before it "senses" any mesoscopic fluctuation. By approximating $V_k^2\approx\overline{V_k^2}$, Eq. (3.27) has a solution

$$j(D)\approx\frac{j_0}{1+2\nu j_0\overline{V_k^2}\ln\frac{D}{D_0}}, \tag{3.28}$$

where j_0 is the bare Kondo coupling constant at the initial energy cutoff D_0. Eq. (3.28) gives the "background" Kondo temperature

$$T_K \approx T_K^0 \equiv D_0 \exp\left(-\frac{1}{2\nu j_0 \overline{V_k^2}}\right), \tag{3.29}$$

independent of the mesoscopic details of the geometry. For $T \ll T_K$, the low-energy effective theory is also conjectured to be a FL, but the T-matrix (or the phase shift) of the screening channel is not yet known with certainty[71, 116].

b) The very large Kondo cloud regime $T_K \ll E_V$. For $E_V \sim v_F/L$, $L_K \gg L$. In this regime, the bare Kondo coupling is very small, and j does not begin to renormalize significantly until the energy cutoff is well below E_V. The variation of V_k^2 is hence negligible in the resulting low energy theory, $V_k^2 \approx V_{k_F}^2$, but $V_{k_F}^2$ may be significantly different from $\overline{V_k^2}$, which means Kondo temperature is thus highly sensitive to the mesoscopic details of $V_{k_F}^2$. Because V_k^2 is almost independent of k, we may map the low-energy theory in question onto the conventional Kondo model, where conduction electrons are scattered by a point-like spin in real space. (We stress that this mapping would not be possible for a strongly k-dependent V_k^2, which is the case for the small cloud regime.) Following well-known results in the conventional Kondo model,[49] we see that the low-energy effective theory is a local FL theory, with parameters also sensitive to mesoscopic details.

3.3 dc conductance

In this section we calculate the dc conductance tensor of the system in linear response theory, generalizing the results in Ref. [66] to our multi-terminal setup. The result is presented as the sum of a disconnected contribution and a connected one (Fig. 3.2). By "disconnected" and "connected", we are referring to the topology of the corresponding Feynman diagrams: a disconnected contribution originates from a Feynman diagram without any cross-links, and can always be written as the product of two two-point functions. The disconnected contribution has a simple Landauer form, and is quadratic in the T-matrix of the screening channel ψ. The connected contribution is also shown to depend on properties near the Fermi surface only, but it is usually difficult to evaluate analytically except at high temperatures, or at low temperatures if the FL perturbation theory is applicable. Nevertheless, just as with the short ABK ring, the connected contribution can be approximately eliminated at temperatures low compared to another mesoscopic energy scale $T \ll E_{\text{conn}}$.

3.3.1 Kubo formula in terms of screening and non-screening channels

The linear dc conductance tensor $G_{jj'}$ is defined through $\langle I_j \rangle = \sum_{j'} G_{jj'} V_{j'}$, where I_j is the current operator in lead j, and $V_{j'}$ is the applied bias voltage on lead j'. I_j is given by $I_j = -edN_j/d\bar{t}$, where $\bar{t}$ is the real time variable, and

$$N_j \equiv \sum_\sigma \sum_{n=0}^{\infty} c_{j,n,\sigma}^\dagger c_{j,n,\sigma} \tag{3.30}$$

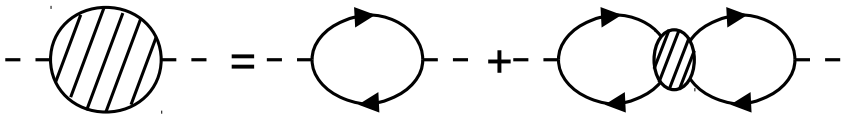

Figure 3.2: Disconnected (self-energy) and connected (vertex correction) contributions to the density-density correlation function, which is directly related to the conductance through the Kubo formula Eq. (3.31). The dashed lines represent external legs at times $\bar{t}$ and 0, the solid lines represent fully dressed Ψ fermion propagators, and the hatched circle represents all connected 4-point vertices of the screening channel.

is the density operator in lead j. $G_{jj'}$ is then given by the Kubo formula

$$G_{jj'} = \frac{e^2}{h} \lim_{\Omega \to 0} \left(-2\pi i \Omega\right) G'_{jj'}\left(\Omega\right), \tag{3.31}$$

where the retarded density-density correlation function is

$$G'_{jj'}\left(\Omega\right) \equiv -i \int_0^\infty d\bar{t} e^{i\Omega^+ \bar{t}} \left\langle \left[N_j\left(\bar{t}\right), N_{j'}\left(0\right)\right] \right\rangle \tag{3.32}$$

and $\Omega^+ \equiv \Omega + i0^+$. The retarded correlation function can be obtained by means of analytic continuation $i\omega_p \to \Omega^+$ from its imaginary time counterpart,

$$\mathscr{G}'_{jj'}\left(i\omega_p\right) = -\int_0^\beta d\tau e^{i\omega_p \tau} \left\langle T_\tau N_j\left(\tau\right) N_{j'}\left(0\right) \right\rangle, \tag{3.33}$$

where $\omega_p = 2p\pi/\beta$ is a bosonic Matsubara frequency, $\beta = 1/T$ is the inverse temperature, and T_τ is the imaginary time-ordering operator.

To calculate the correlation function we need the density operator N_j written as bilinears of Ψ. This is achieved by the insertion of Eq. (3.16a) and then Eq. (3.24) into Eq. (3.30). We find

$$N_j = \sum_\sigma \int_0^\pi \frac{dk_1 dk_2}{\left(2\pi\right)^2} \Psi^\dagger_{k_1,\sigma} \mathbb{M}^j_{k_1 k_2} \Psi_{k_2,\sigma}, \tag{3.34}$$

where for l_1, $l_2 = 1, ..., N$,

$$\begin{aligned}\left(\mathbb{M}^j_{k_1 k_2}\right)_{l_1 l_2} = \sum_{j_1 j_2} \mathbb{U}_{l_1, j_1, k_1} \mathbb{U}^*_{l_2, j_2, k_2} \Bigg[&\delta_{j j_1} \delta_{j j_2} \frac{1}{1 - e^{i(k_1 - k_2 + i0)}} + S^*_{j j_1}\left(k_1\right) \delta_{j j_2} \frac{1}{1 - e^{-i(k_1 + k_2 - i0)}} \\ &+ \delta_{j j_1} S_{j j_2}\left(k_2\right) \frac{1}{1 - e^{i(k_1 + k_2 + i0)}} + S^*_{j j_1}\left(k_1\right) S_{j j_2}\left(k_2\right) \frac{1}{1 - e^{i(k_2 - k_1 + i0)}} \Bigg].\end{aligned} \tag{3.35}$$

The matrix $\mathbb{M}$ obeys $\mathbb{M}^j_{k_1k_2} = \left(\mathbb{M}^j_{k_2k_1}\right)^\dagger$ which ensures N_j is Hermitian.

3.3.2 Disconnected part

We substitute Eq. (3.34) into Eq. (3.32). The disconnected part of the conductance is obtained by pairing up Ψ and $\Psi^\dagger$ operators to form two two-point Green's functions:

$$G'^D_{jj'}(\Omega) = -2i\int_0^\infty d\bar{t}e^{i\Omega^+\bar{t}}\int_0^\pi \frac{dk_1dk_2}{(2\pi)^2}\frac{dq_1dq_2}{(2\pi)^2}\,\mathrm{tr}\left[\mathbb{M}^j_{k_1k_2}\mathbb{G}^>_{k_2q_1}(\bar{t})\,\mathbb{M}^{j'}_{q_1q_2}\mathbb{G}^<_{q_2k_1}(-\bar{t}) - \mathbb{M}^{j'}_{q_1q_2}\mathbb{G}^>_{q_2k_1}(-\bar{t})\,\mathbb{M}^j_{k_1k_2}\mathbb{G}^<_{k_2q_1}(\bar{t})\right]. \tag{3.36}$$

Here the factor of 2 in the second line is due to the spin degeneracy. The greater and lesser Green's functions in the screening–non-screening basis are defined as

$$\mathbb{G}^>_{kq}(\bar{t}) \equiv -i\begin{pmatrix} \left\langle \psi_k(\bar{t})\,\psi^\dagger_q(0)\right\rangle & & & \\ & \left\langle \phi_{1,k}(\bar{t})\,\phi^\dagger_{1,q}(0)\right\rangle & & \\ & & \cdots & \\ & & & \left\langle \phi_{N-1,k}(\bar{t})\,\phi^\dagger_{N-1,q}(0)\right\rangle \end{pmatrix}, \tag{3.37a}$$

and

$$\mathbb{G}^<_{kq}(\bar{t}) \equiv +i\begin{pmatrix} \left\langle \psi^\dagger_q(0)\,\psi_k(\bar{t})\right\rangle & & & \\ & \left\langle \phi^\dagger_{1,q}(0)\,\phi_{1,k}(\bar{t})\right\rangle & & \\ & & \cdots & \\ & & & \left\langle \phi^\dagger_{N-1,q}(0)\,\phi_{N-1,k}(\bar{t})\right\rangle \end{pmatrix}. \tag{3.37b}$$

(The correlation functions are for either spin.) In equilibrium, fluctuation-dissipation theorem requires that $\mathbb{G}^>_{kq}(\omega) = 2i[1-f(\omega)]\,\mathrm{Im}\,\mathbb{G}^R_{kq}(\omega)$, and $\mathbb{G}^<_{kq}(\omega) = -2if(\omega)\,\mathrm{Im}\,\mathbb{G}^R_{kq}(\omega)$, where $f(\omega) = 1/\left(e^{\beta\omega}+1\right)$ is the Fermi function. These equilibrium relations result from the fact that $\mathbb{G}^R_{kq}(\omega) = \mathbb{G}^R_{qk}(\omega)$ for the Anderson model[66] [see Eq. (3.41) below]. With these relations Eq. (3.36) becomes

$$G'^D_{jj'}(\Omega) = 8\int\frac{d\omega d\omega'}{(2\pi)^2}\frac{f(\omega)-f(\omega')}{\omega-\omega'+\Omega^+}\int_0^\pi\frac{dk_1dk_2}{(2\pi)^2}\frac{dq_1dq_2}{(2\pi)^2}\,\mathrm{tr}\left[\mathbb{M}^j_{k_1k_2}\,\mathrm{Im}\,\mathbb{G}^R_{k_2q_1}(\omega')\,\mathbb{M}^{j'}_{q_1q_2}\,\mathrm{Im}\,\mathbb{G}^R_{q_2k_1}(\omega)\right]. \tag{3.38}$$

We note that, in contrast to the case of Ref. [66], the momentum integral here is not necessarily real. Instead, its complex conjugate takes the same form but with ω and ω' interchanged:

$$\int_0^\pi \frac{dk_1dk_2}{(2\pi)^2}\frac{dq_1dq_2}{(2\pi)^2}\,\mathrm{tr}\left[\mathbb{M}^j_{k_1k_2}\,\mathrm{Im}\,\mathbb{G}^R_{k_2q_1}\left(\omega'\right)\mathbb{M}^{j'}_{q_1q_2}\,\mathrm{Im}\,\mathbb{G}^R_{q_2k_1}\left(\omega\right)\right]^*$$
$$=\int_0^\pi \frac{dk_1dk_2}{(2\pi)^2}\frac{dq_1dq_2}{(2\pi)^2}\,\mathrm{tr}\left[\mathbb{M}^j_{k_1k_2}\,\mathrm{Im}\,\mathbb{G}^R_{k_2q_1}\left(\omega\right)\mathbb{M}^{j'}_{q_1q_2}\,\mathrm{Im}\,\mathbb{G}^R_{q_2k_1}\left(\omega'\right)\right]. \tag{3.39}$$

Making use of this property, we can show that $\left[G'^D_{jj'}\left(-\Omega\right)\right]^* = G'^D_{jj'}\left(\Omega\right)$. Thus the disconnected contribution to the dc conductance can be written as

$$G^D_{jj'} = \frac{e^2}{h}\lim_{\Omega\to 0}\left(2\pi\Omega\right)\mathrm{Im}\,G'^D_{jj'}\left(\Omega\right). \tag{3.40}$$

We should realize, however, that taking the imaginary part of $G'^D_{jj'}$ is generally not equivalent to taking the δ-function part of $1/\left(\omega-\omega'+\Omega^+\right)$ in Eq. (3.38).

For the Anderson model, since the interaction is restricted to the d electrons, it is not difficult to find the Dyson's equation for the retarded Green's function of ψ and ϕ by the equation-of-motion technique:

$$\mathbb{G}^R_{k_2q_1}\left(\omega\right) = 2\pi\delta\left(k_2-q_1\right)g^R_{k_2}\left(\omega\right)+\tau_\psi g^R_{k_2}\left(\omega\right)\mathrm{T}_{k_2q_1}\left(\omega\right)g^R_{q_1}\left(\omega\right), \tag{3.41}$$

where the free retarded Green's function for ψ and ϕ is

$$g^R_k\left(\omega\right) = \frac{1}{\omega^+-\varepsilon_k}, \tag{3.42}$$

and τ_ψ is the projection operator onto the screening channel subspace. Again, only the Green's function of the screening channel is modified by coupling to the QD. The retarded T-matrix of the screening channel in the single-particle sector is related to the retarded two-point function of the QD by

$$\mathrm{T}_{k_2q_1}\left(\omega\right) = V_{k_2}G^R_{dd}\left(\omega\right)V_{q_1}, \tag{3.43}$$

where $G^R_{dd}\left(\omega\right)\equiv -i\int_0^\infty d\bar{t}e^{i\omega^+\bar{t}}\left\langle\left\{d_\sigma\left(\bar{t}\right),d^\dagger_\sigma\left(0\right)\right\}\right\rangle$ is again the same for $\sigma = \uparrow,\downarrow$.

From Eqs. (3.38) and (3.41) we may express the disconnected contribution to the linear dc conductance in the Landauer form[112]:

$$G^D_{jj'} = -\frac{2e^2}{h}\int_{-2t}^{2t}d\varepsilon_p\left[-f'\left(\varepsilon_p\right)\right]\mathscr{T}^D_{jj'}\left(\varepsilon_p\right), \tag{3.44}$$

where the disconnected "transmission probability" $\mathscr{T}^D_{jj'}$ is written in terms of the absolute square of a "transmission amplitude",

$$\mathscr{T}^D_{jj'}(\varepsilon_p) = \delta_{jj'} - \left| \left\{ S(p) \left[1 - 2i\pi\nu_p \mathrm{T}_{pp}(\varepsilon_p) \mathbb{U}^\dagger_p \tau_\psi \mathbb{U}_p \right] \right\}_{jj'} \right|^2$$
$$= \delta_{jj'} - \left| S_{jj'}(p) + \frac{2i}{V_p^2} \left[S(p) \Gamma^\dagger(p) \lambda \Gamma(p) \right]_{jj'} \left[-\pi\nu_p \mathrm{T}_{pp}(\varepsilon_p) \right] \right|^2 . \tag{3.45}$$

Again λ is the QD coupling matrix defined in Eq. (3.20) and ν_p is the density of states per channel per spin for the tight-binding model

$$\nu_p = \frac{1}{4\pi t \sin p}. \tag{3.46}$$

The detailed derivation of Eq. (3.45) by contour methods is left for Appendix B.

At zero temperature, when the single-particle sector of the screening channel T-matrix is a pure phase shift, there is no connected contribution and Eq. (3.44) yields the full linear dc conductance[66]. In this case a clear picture emerges from Eq. (3.45): the conductance is given by the Landauer formula with an effective single-particle S-matrix, which is obtained from the original S-matrix simply by imposing a phase shift on the screening channel, corresponding to the particle-hole symmetry breaking potential scattering and the scattering by the Kondo singlet[75, 88].

Another useful representation of the disconnected probability, similar to that in Ref. [66], is obtained by expanding Eq. (3.45):

$$\mathscr{T}^D_{jj'}(\varepsilon_p) = \mathscr{T}_{0,jj'}(\varepsilon_p) + \mathscr{Z}_{R,jj'}(\varepsilon_p) \mathrm{Re}\left[-\pi\nu_p \mathrm{T}_{pp}(\varepsilon_p) \right]$$
$$+ \mathscr{Z}_{I,jj'}(\varepsilon_p) \mathrm{Im}\left[-\pi\nu_p \mathrm{T}_{pp}(\varepsilon_p) \right] + \mathscr{Z}_{2,jj'}(\varepsilon_p) \left| -\pi\nu_p \mathrm{T}_{pp}(\varepsilon_p) \right|^2, \tag{3.47a}$$

with a background transmission term

$$\mathscr{T}_{0,jj'}(\varepsilon_p) = \delta_{jj'} - \left| S_{jj'}(p) \right|^2, \tag{3.47b}$$

a term linear in the real part of the T-matrix, proportional to

$$\mathscr{Z}_{R,jj'}(\varepsilon_p) = \frac{4}{V_p^2} \mathrm{Im} \left\{ \left[S(p) \Gamma^\dagger(p) \lambda \Gamma(p) \right]_{jj'} S^*_{jj'}(p) \right\}, \tag{3.47c}$$

a term linear in the imaginary part, proportional to

$$\mathscr{Z}_{I,jj'}(\varepsilon_p) = \frac{4}{V_p^2} \mathrm{Re} \left\{ \left[S(p) \Gamma^\dagger(p) \lambda \Gamma(p) \right]_{jj'} S^*_{jj'}(p) \right\}, \tag{3.47d}$$

and a term quadratic in the T-matrix, proportional to

$$\mathscr{Z}_{2,jj'}(\varepsilon_p) = -\frac{4}{V_p^4}\left|\left[S(p)\Gamma^\dagger(p)\lambda\Gamma(p)\right]_{jj'}\right|^2. \tag{3.47e}$$

In the dc limit, the total current flowing out of the junction is zero, and a uniform voltage applied to all leads does not result in any current; hence the linear dc conductance satisfies current and voltage Kirchhoff's laws $\sum_j G_{jj'} = \sum_{j'} G_{jj'} = 0$. As a comparison it is interesting to consider the sum of the disconnected transmission probability, Eq. (3.47a), over j or j'. Using the unitarity of S and Eq. (3.20) it is not difficult to find that

$$\sum_j \mathscr{T}^D_{jj'}(\varepsilon_p) = \left\{\mathrm{Im}\left[-\pi\nu_p \mathrm{T}_{pp}(\varepsilon_p)\right] - \left|-\pi\nu_p \mathrm{T}_{pp}(\varepsilon_p)\right|^2\right\}\frac{4}{V_p^2}\left[\Gamma^\dagger(p)\lambda\Gamma(p)\right]_{j'j'}, \tag{3.48}$$

and

$$\sum_{j'} \mathscr{T}^D_{jj'}(\varepsilon_p) = \left\{\mathrm{Im}\left[-\pi\nu_p \mathrm{T}_{pp}(\varepsilon_p)\right] - \left|-\pi\nu_p \mathrm{T}_{pp}(\varepsilon_p)\right|^2\right\}\frac{4}{V_p^2}\left[S(p)\Gamma^\dagger(p)\lambda\Gamma(p)S^\dagger(p)\right]_{jj}. \tag{3.49}$$

As mentioned in Ref. [66], the quantity in curly brackets in Eqs. (3.48) and (3.49) measures the deviation of the single-particle sector of the T-matrix from the optical theorem[134]. In the case of a non-interacting QD or the $T = 0$ FL theory of the Kondo limit, where the connected contribution to the conductance vanishes, these row/column sum formulas conform to our expectations: the T-matrix obeys the optical theorem, leading to $\sum_j \mathscr{T}^D_{jj'} = \sum_{j'} \mathscr{T}^D_{jj'} = 0$, so that $\sum_j G_{jj'} = \sum_{j'} G_{jj'} = 0$ is ensured.

3.3.3 Connected part and its low-temperature elimination

In this subsection we show that the connected contribution to the conductance is again a Fermi surface contribution, and discuss how it can be approximately eliminated at low temperatures. Following Ref. [66] we construct a transmission probability for this contribution. After a partial insertion of Eq. (3.34) into Eq. (3.33), the connected part of the density-density correlation function can be written as

$$\mathscr{G}^{IC}_{jj'}(i\omega_p) = \int_0^\beta d\tau e^{i\omega_p\tau} P_{jj'}(\tau,\tau), \tag{3.50}$$

where the connected four-point function $P_{jj'}$ with two temporal arguments is

$$P_{jj'}(\tau_1,\tau_2) \equiv -\int_0^\pi \frac{dk_1 dk_2}{(2\pi)^2}\left(\mathbb{M}^j_{k_1k_2}\right)_{11}\sum_\sigma \left\langle T_\tau \psi^\dagger_{k_1\sigma}(\tau_1)\,\psi_{k_2\sigma}(\tau_2) N_{j'}(0)\right\rangle_C; \tag{3.51}$$

the subscript C denotes connected diagrams. Note that only the screening channel contributes to the connected part, as the non-screening channels are free fermions. Using the equation-of-motion technique, it is easy to relate $P_{jj'}$ to a partially amputated quantity:

$$P_{jj'}(\tau,\tau) = \int_0^\pi \frac{dk_1 dk_2}{(2\pi)^2} \left(\mathbb{M}^j_{k_1k_2}\right)_{11} V_{k_1} V_{k_2} \int d\tau_1 d\tau_2 g_{k_1}(\tau_1-\tau)\, g_{k_2}(\tau-\tau_2) \sum_\sigma \left\langle T_\tau d^\dagger_\sigma(\tau_1)\, d_\sigma(\tau_2) N_{j'}(0)\right\rangle_C, \tag{3.52}$$

where

$$g_k(\tau) \equiv [f(\tau) - H(\tau)]\, e^{-\varepsilon_k \tau} \tag{3.53}$$

is the imaginary time free Green's function and $H(\tau)$ is the Heaviside unit-step function. [Here "amputation" refers to the removal of the outermost $V\left(\psi^\dagger d + \text{h.c.}\right)$ vertices from the $\left\langle \psi^\dagger \psi \psi^\dagger \psi \right\rangle_C$ correlation function; recall that the ψ electrons only become interacting due to their interaction with d electrons.] With τ only appearing in free propagators, we can perform the Fourier transform explicitly,

$$\begin{aligned}
\mathscr{G}'^C_{jj'}(i\omega_p) &= \frac{1}{\beta}\sum_{\omega_m} P_{jj'}(i\omega_m, i\omega_m + i\omega_p) \\
&= \frac{1}{\beta}\sum_{\omega_m} \int_0^\pi \frac{dk_1 dk_2}{(2\pi)^2} \left(\mathbb{M}^j_{k_1k_2}\right)_{11} g_{k_1}(i\omega_m)\, g_{k_2}(i\omega_m + i\omega_p) V_{k_1} V_{k_2} \\
&\times \int d\tau_1 d\tau_2 e^{-i\omega_m\tau_1} e^{i(\omega_m+\omega_p)\tau_2} \sum_\sigma \left\langle T_\tau d^\dagger_\sigma(\tau_1)\, d_\sigma(\tau_2) N_{j'}(0)\right\rangle_C .
\end{aligned} \tag{3.54}$$

One may now use the contour integration argument in Ref. [66].[74] The final result is that the connected contribution to the dc conductance is expressed in terms of a transmission probability $\mathscr{T}^C$ related to $P_{jj'}$:

$$G^C_{jj'} = -\frac{2e^2}{h}\int_{-2t}^{2t} d\omega \left[-f'(\omega)\right] \mathscr{T}^C_{jj'}(\omega), \tag{3.55}$$

where

$$\mathscr{T}^C_{jj'}(\omega) = \lim_{\Omega\to 0} \frac{\Omega^2}{8} P_{jj'}(\omega - i\eta_1, \omega + \Omega + i\eta_2) + \text{c.c.} \tag{3.56}$$

and

$$P_{jj'}(\omega - i\eta_1, \omega + \Omega + i\eta_2)$$
$$= \int_0^\pi \frac{dk_1 dk_2}{(2\pi)^2} \left(\mathbb{M}^j_{k_1 k_2}\right)_{11} g^A_{k_1}(\omega)\, g^R_{k_2}(\omega+\Omega)\, V_{k_1} V_{k_2} \int d\tau_1 d\tau_2 e^{-i\omega^-\tau_1} e^{i(\omega^+ + \Omega)\tau_2} \sum_\sigma \left\langle T_\tau d^\dagger_\sigma(\tau_1)\, d_\sigma(\tau_2) N_{j'}(0)\right\rangle_C . \tag{3.57}$$

Here η_1, $\eta_2 \to 0^+$ are positive infinitesimal numbers.

It is in fact possible to do the k_1 and k_2 integrals. Using Eqs. (3.22), (3.35) and finally (B.6), we obtain

$$\begin{aligned}
&\int_0^\pi \frac{dk_1 dk_2}{(2\pi)^2} \left(\mathbb{M}^j_{k_1 k_2}\right)_{11} g^A_{k_1}(\varepsilon_p)\, g^R_{k_2}(\varepsilon_p+\Omega)\, V_{k_1} V_{k_2} \\
&= \sum_{r_1 r_2} t^*_{r_1} t_{r_2} \int_{-\pi}^\pi \frac{dk_1 dk_2}{(2\pi)^2} g^A_{k_1}(\varepsilon_p)\, g^R_{k_2}(\varepsilon_p+\Omega)\, \Gamma_{r_1 j}(k_1)\, \Gamma^*_{r_2 j}(k_2)\, \frac{1}{1 - e^{i(k_1 - k_2 + i0)}}.
\end{aligned} \tag{3.58}$$

Here domains of the momentum integrals are extended to $(-\pi, \pi)$ according to Eq. (B.6), which facilitates the application of the residue method. As explained in Appendix B, the poles of $\Gamma(k_1)$ and $\Gamma^*(k_2)$ are not important in the dc limit $\Omega \to 0$. Therefore, the $O(1/\Omega)$ contribution is dominated by the poles of the free Green's functions, and is given by

$$\int_0^\pi \frac{dk_1 dk_2}{(2\pi)^2} \left(\mathbb{M}^j_{k_1 k_2}\right)_{11} g^A_{k_1}(\varepsilon_p)\, g^R_{k_2}(\varepsilon_p+\Omega)\, V_{k_1} V_{k_2} = \frac{2\pi i}{\Omega} \nu_p \left[S(p')\, \Gamma^\dagger(p')\, \lambda\, \Gamma(p)\, S^\dagger(p)\right]_{jj} + O(1). \tag{3.59}$$

where $\varepsilon_p + \Omega \equiv \varepsilon_{p'}$, $0 \le p,\, p' \le \pi$. This leads to

$$\mathscr{T}^C_{jj'}(\varepsilon_p) = \nu_p \left[S(p)\, \Gamma^\dagger(p)\, \lambda\, \Gamma(p)\, S^\dagger(p)\right]_{jj} \left[\frac{i\pi}{4} \lim_{\Omega\to 0} \Omega \int d\tau_1 d\tau_2 e^{-i\omega^-\tau_1} e^{i(\omega^+ + \Omega)\tau_2} \sum_\sigma \left\langle T_\tau d^\dagger_\sigma(\tau_1)\, d_\sigma(\tau_2) N_{j'}(0)\right\rangle_C + \text{c.c.}\right]. \tag{3.60}$$

A similar manipulation can be done for the $N_{j'}$ part of the correlation function.

One can again consider the row and column sums of the tensor $\mathscr{T}^C$. Tracing over j immediately yields

$$\sum_j \mathscr{T}^C_{jj'}(\varepsilon_p) = \nu_p V_p^2 \left[\frac{i\pi}{4} \lim_{\Omega\to 0} \Omega \int d\tau_1 d\tau_2 e^{-i\omega^-\tau_1} e^{i(\omega^+ + \Omega)\tau_2} \sum_\sigma \left\langle T_\tau d^\dagger_\sigma(\tau_1)\, d_\sigma(\tau_2) N_{j'}(0)\right\rangle_C + \text{c.c.}\right]; \tag{3.61}$$

combining the last two equations, we have

$$\mathscr{T}^C_{jj'}(\varepsilon_p) - \frac{1}{V_p^2}\left[S(p)\Gamma^\dagger(p)\lambda\Gamma(p)S^\dagger(p)\right]_{jj}\sum_{j''}\mathscr{T}^C_{j''j'}(\varepsilon_p) = 0. \tag{3.62}$$

Let us now define E_{conn} as the characteristic energy scale below which both $S(p)$ and $\Gamma(p)$ vary slowly. By definition $E_{\text{conn}} \lesssim E_V$; while E_{conn} is not necessarily the same as E_V, for the two ABK ring geometries considered in this chapter $E_V \sim E_{\text{conn}}$. For a mesoscopic structure with characteristic length scale L, E_{conn} is usually the Thouless energy, $E_{\text{conn}} \sim v_F/L$; however, this is again not always the case, and the open long ABK ring in Section 3.7 provides a counterexample where E_{conn} is comparable to the bandwidth. Below E_{conn}, the function $\left[S(p)\Gamma^\dagger(p)\lambda\Gamma(p)S^\dagger(p)\right]_{jj}/V_p^2$ is only weakly dependent on p.

Eq. (3.62) suggests that we can approximately eliminate the connected part of $G_{jj'}$, provided[66] the temperature is low compared to E_{conn}. Consider the linear combination

$$G_{jj'} - \frac{1}{V_{k_F}^2}\left[S(k_F)\Gamma^\dagger(k_F)\lambda\Gamma(k_F)S^\dagger(k_F)\right]_{jj}\sum_{j''}G_{j''j'} \equiv G_{jj'}; \tag{3.63}$$

this corresponds to measuring the conductance by measuring the current in lead j, plus a constant times the total current in all leads. (Note that here we include both disconnected and connected contributions.) By Kirchhoff's law, this linear combination must equal $G_{jj'}$ itself. We write it as a sum of disconnected and connected contributions:

$$\begin{aligned} G_{jj'} = &\left(G^D_{jj'} - \frac{1}{V_{k_F}^2}\left[S(k_F)\Gamma^\dagger(k_F)\lambda\Gamma(k_F)S^\dagger(k_F)\right]_{jj}\sum_{j''}G^D_{j''j'}\right) \\ &- \int d\varepsilon_p\left[-f'(\varepsilon_p)\right]\left\{\mathscr{T}^C_{jj'}(\varepsilon_p) - \frac{1}{V_{k_F}^2}\left[S(k_F)\Gamma^\dagger(k_F)\lambda\Gamma(k_F)S^\dagger(k_F)\right]_{jj}\sum_{j''}\mathscr{T}^C_{j''j'}(\varepsilon_p)\right\}. \end{aligned} \tag{3.64}$$

For $T \ll E_{\text{conn}}$, by Eq. (3.62), the quantity in curly brackets approximately vanishes for $|\varepsilon_p - \varepsilon_{k_F}| \lesssim T$, whereas the Fermi factor approximately vanishes for $|\varepsilon_p - \varepsilon_{k_F}| \gg T$. Therefore

$$G_{jj'} \approx G^D_{jj'} - \frac{1}{V_{k_F}^2}\left[S(k_F)\Gamma^\dagger(k_F)\lambda\Gamma(k_F)S^\dagger(k_F)\right]_{jj}\sum_{j''}G^D_{j''j'}; \tag{3.65}$$

in other words, at $T \ll E_{\text{conn}}$ it is possible to write the conductance in terms of disconnected contributions alone.

Since Eq. (3.65) contains only the disconnected contribution, we may calculate it explicitly using Eqs. (3.47a) and (3.48). Since both $S(p)$ and $\Gamma(p)$ are slowly varying below the energy scale E_{conn}, we find the conductance is approximately linear in the T-matrix,

$$G_{jj'} \approx -\frac{2e^2}{h}\int d\varepsilon_p \left[-f'(\varepsilon_p)\right]\left\{\mathscr{T}_{0,jj'}(\varepsilon_{k_F}) + \mathscr{Z}_{R,jj'}(\varepsilon_{k_F})\,\mathrm{Re}\left[-\pi\nu_p \mathrm{T}_{pp}(\varepsilon_p)\right]\right.$$
$$\left. + \left[\mathscr{Z}_{I,jj'}(\varepsilon_{k_F}) + \mathscr{Z}_{2,jj'}(\varepsilon_{k_F})\right]\mathrm{Im}\left[-\pi\nu_p \mathrm{T}_{pp}(\varepsilon_p)\right]\right\}, \tag{3.66}$$

provided $T \ll E_{\mathrm{conn}}$. Eq. (3.66) can also be obtained by eliminating the connected part with the column sum Eq. (3.49) instead of the row sum,

$$G_{jj'} - \frac{1}{V_{k_F}^2}\left[\Gamma^\dagger(k_F)\,\lambda\,\Gamma(k_F)\right]_{j'j'}\sum_{j''} G_{jj''}, \tag{3.67}$$

which corresponds to measuring the conductance by applying a small uniform bias voltage in all leads, in addition to the small bias voltage in lead j'.

Eq. (3.66) is the first central result of this chapter. It generalizes the result of the two-lead short ABK ring in Ref. [66] to an arbitrary ABK ring, and expresses the linear dc conductance as a linear function of the scattering channel T-matrix, as long as the temperature is low compared to the mesoscopic energy scale E_{conn} at which $S(p)$ and $\Gamma(p)$ varies significantly[112].

3.4 Perturbation theories

3.4.1 Weak coupling perturbation theory

Although we now understand that the connected part of the conductance can be eliminated at low temperatures, this procedure may not be applicable in the weak-coupling regime $T \gg T_K$. In this subsection we calculate the linear dc conductance perturbatively in powers of V_k^2/U, again generalizing the short ring results of Ref. [66]; we expect the result to be valid in both small and large Kondo cloud regimes as long as $T \gg T_K$ and the renormalized Kondo coupling constant remains weak.

Disconnected part

We first find the disconnected part; the result is already given in Ref. [66], but for completeness we reproduce it here. (Technical notes can be found in Appendix C.) As implied by Eq. (3.45), our task amounts to calculating the retarded T-matrix of the screening channel in the single-particle sector, which is in turn achieved by calculating the two-point Green's function $-\left\langle T_\tau \psi_{k\sigma}(\tau)\,\psi^\dagger_{k'\sigma}(0)\right\rangle_{\mathrm{H}}$ in Heisenberg picture. The pertinent Feynman diagrams to $O\left(J^2\right)$ and $O\left(K^2\right)$ are depicted in Fig. 3.3, and we find

$$\nu \mathrm{T}_{kk'}(\Omega) = \nu K_{kk'} + \nu^2 \int d\varepsilon_q \frac{1}{\Omega^+ - \varepsilon_q}\left(K_{kq}K_{qk'} + \frac{3}{16}J_{kq}J_{qk'}\right), \tag{3.68}$$

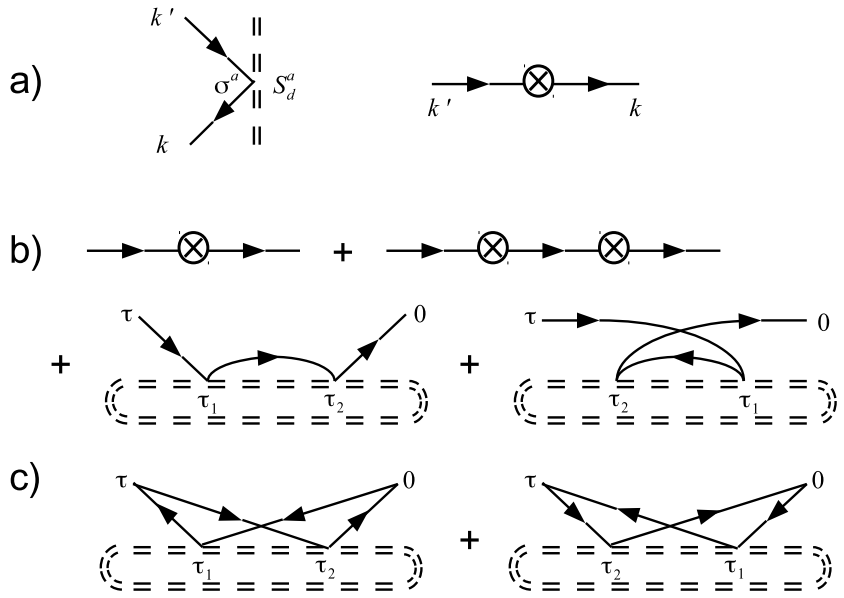

Figure 3.3: Diagrammatics of weak-coupling perturbation theory. a) The vertices corresponding to the Kondo coupling and the potential scattering in Eq. (3.25a). b) Diagrams contributing to the T-matrix of the screening channel ψ electrons up to $O\left(J^2\right) \sim O\left(K^2\right)$. We have traced over the impurity spin so that the double dashed lines (impurity spin propagators) form loops, and arranged the internal time variables from left to right in increasing order. c) Connected diagrams contributing to the linear dc conductance up to $O\left(J^2\right)$.

where again $\nu = 1/(2\pi v_F)$ for the model with a reduced band. The factor of $3/16$ results from time-ordering and tracing over the impurity spin, where we have used the following identity

$$\left\langle T_\tau S_d^a(\tau_1) S_d^b(\tau_2) \right\rangle = \frac{1}{4}\delta^{ab}. \tag{3.69}$$

The $O(K)$ and $O\left(K^2\right)$ terms, accounting for the particle-hole symmetry breaking potential scattering due to the QD, clearly obey the optical theorem $\mathrm{Im}\left[-\pi\nu_p \mathrm{T}_{pp}(\varepsilon_p)\right] = \left|-\pi\nu_p \mathrm{T}_{pp}(\varepsilon_p)\right|^2$. If κ is comparable to the renormalized value of j then the $O(K)$ term dominates the T-matrix.

On the other hand, if we tune the QD to be particle-hole symmetric, $\varepsilon_d = -U/2$ and $\kappa = 0$, both terms containing K will vanish, and the $O\left(J^2\right)$ term becomes the lowest order contribution to the T-matrix. For this term, one should also make a distinction between the real principal value part and the imaginary δ-function part. There are two different ways in which a screening channel electron incident onto the QD can be scattered[134]: either (i) elastically, where the energy and spin of the electron as well as the spin state of the QD are unchanged, or (ii) inelastically, where the scattered electron leaves behind particle-hole excitations and/or spin excitations. As noticed in Ref. [75]

and reiterated in Ref. [66], the principal value part of the $O\left(J^2\right)$ term introduces non-universalities due to its dependence on all energies in the reduced band $(-D,D)$; nevertheless it is merely an elastic potential scattering term that respects the optical theorem, and we neglect it in the following. Meanwhile, the δ-function part is an inelastic effect stemming from the Kondo physics, as can be seen from its violation of the optical theorem in the single-particle sector. (The T-matrix apparently disobeys the optical theorem because it is restricted to the single-particle sector, and the sum over intermediate states excludes many-particle states which appear in inelastic scattering.) Therefore, for a particle-hole symmetric QD, to $O\left(J^2\right)$ we have[66]

$$-\pi\nu \mathrm{T}_{pp}\left(\varepsilon_p\right)=i\frac{3\pi^2}{16}\nu^2 J_{pp}^2. \tag{3.70}$$

The weak-coupling perturbation theory is famous for being infrared divergent[67, 74] at $O\left(J^3\right)$, but as long as $T\gg T_K$, to logarithmic accuracy we verify in Appendix C that the $O\left(J^3\right)$ corrections to the T-matrix can be absorbed into our $O\left(J^2\right)$ result by reinterpreting the bare Kondo coupling constant J_{pp} as a renormalized one. The renormalization is governed by Eq. (3.26), and cut off at either the "electron energy" $|\varepsilon_p|$ or the temperature T, whichever is larger. In other words, the Kondo coupling J_{pp} in Eq. (3.70) should be replaced by $J_{pp}\left(\max\left\{|\varepsilon_p|,T\right\}\right)$, where the argument in round brackets stands for the energy cutoff D in Eq. (3.26) where the running coupling constant is evaluated.

Connected part

We now calculate the connected part to $O\left(J^2\right)$; the calculation follows Ref. [66] closely. Inserting Eq. (3.34) into Eq. (3.33), we write the connected part of the density-density correlation function in terms of a four-point correlation function of ψ:

$$\mathscr{G}'^{C}_{jj'}\left(i\omega_p\right)=\int_0^\pi \frac{dk_1dk_2dq_1dq_2}{\left(2\pi\right)^4}\left(\mathbb{M}^{j}_{k_1k_2}\right)_{11}\left(\mathbb{M}^{j'}_{q_1q_2}\right)_{11}\mathscr{G}^{C}_{k_1k_2q_1q_2}\left(i\omega_p\right), \tag{3.71}$$

where

$$\mathscr{G}^{C}_{k_1k_2q_1q_2}\left(i\omega_p\right)\equiv-\int_0^\beta d\tau e^{i\omega_p\tau}\sum_{\sigma\sigma'}\left\langle T_\tau\psi^\dagger_{k_1\sigma}\left(\tau\right)\psi_{k_2\sigma}\left(\tau\right)\psi^\dagger_{q_1\sigma'}\left(0\right)\psi_{q_2\sigma'}\left(0\right)\right\rangle_C. \tag{3.72}$$

We insert Eqs. (3.22) and (3.35) into Eq. (3.71), and take the continuum limit, which is appropriate for the Kondo model. Because in the wide band limit the most divergent contribution to $G'^{C}_{jj'}\left(\Omega\right)$ is from $k_1\approx k_2$ and $q_1\approx q_2$, we can expand the integrand around these points,

$$
\begin{aligned}
&\mathscr{G}'^{C}_{jj'}(i\omega_p)\\
&= O(1) + \int \frac{dk_1 dk_2 dq_1 dq_2}{(2\pi)^4} \frac{1}{V_{k_1}V_{k_2}V_{q_1}V_{q_2}} \mathscr{G}^{C}_{k_1k_2q_1q_2}(i\omega_p) \sum_{r_1r_2r_1'r_2'} t^*_{r_1}t_{r_2}t^*_{r_1'}t_{r_2'}\\
&\times \left\{ \Gamma_{r_1 j}(k_1)\Gamma^*_{r_2 j}(k_2) \frac{1}{-i(k_1-k_2+i0)} + \left[\Gamma S^\dagger(k_1)\right]_{r_1 j}\left[\Gamma S^\dagger(k_2)\right]^*_{r_2 j} \frac{1}{-i(k_2-k_1+i0)} \right\}\\
&\times \left\{ \Gamma_{r_1' j'}(q_1)\Gamma^*_{r_2' j'}(q_2) \frac{1}{-i(q_1-q_2+i0)} + \left[\Gamma S^\dagger(q_1)\right]_{r_1' j'}\left[\Gamma S^\dagger(q_2)\right]^*_{r_2' j'} \frac{1}{-i(q_2-q_1+i0)} \right\}. \quad (3.73)
\end{aligned}
$$

The only non-vanishing diagrams at $O\left(J^2\right)$ are shown in panel c) of Fig. 3.3:

$$
\begin{aligned}
\mathscr{G}^{C}_{k_1k_2q_1q_2}(i\omega_p) &= \frac{3}{8} J_{q_2k_1}J_{k_2q_1} \int_0^\beta d\tau e^{i\omega_p\tau} \int_0^\beta d\tau_1 d\tau_2 g_{q_2}(-\tau_1) g_{k_1}(\tau_1-\tau) g_{k_2}(\tau-\tau_2) g_{q_1}(\tau_2)\\
&= \frac{3}{8} J_{q_2k_1}J_{k_2q_1} \frac{1}{\beta} \sum_{\omega_{n_1}} g_{q_2}(i\omega_{n_1}) g_{k_1}(i\omega_{n_1}) g_{k_2}(i\omega_{n_1}+i\omega_p) g_{q_1}(i\omega_{n_1}+i\omega_p); \quad (3.74)
\end{aligned}
$$

we have again used Eq. (3.69). The frequency summation is performed by deforming the complex plane contour and wrapping it around the lines $\mathrm{Im}\, z = 0$ and $\mathrm{Im}\, z = -\omega_p$. Analytic continuation yields

$$
\begin{aligned}
G^{C}_{k_1k_2q_1q_2}(\Omega) = -\frac{3J_{q_2k_1}J_{k_2q_1}}{16\pi i} \int d\omega f(\omega) \big\{ &\left[g^R_{q_2}(\omega) g^R_{k_1}(\omega) - g^A_{q_2}(\omega) g^A_{k_1}(\omega)\right] g^R_{k_2}(\omega+\Omega) g^R_{q_1}(\omega+\Omega)\\
&+ g^A_{q_2}(\omega-\Omega) g^A_{k_1}(\omega-\Omega) \left[g^R_{k_2}(\omega) g^R_{q_1}(\omega) - g^A_{k_2}(\omega) g^A_{q_1}(\omega)\right] \big\}. \quad (3.75)
\end{aligned}
$$

Substituting Eqs. (3.75) and (3.25b) into Eq. (3.73), we are able to evaluate the momentum integrals in the $\Lambda \to \infty$ limit by contour methods. The *RRRR* and *AAAA* terms vanish, and the *AARR* terms combine to produce a Fermi surface factor $f'(\omega)$:

$$
\begin{aligned}
&G'^{C}_{jj'}(\Omega)\\
&= O(1) - \frac{1}{\Omega} \int d\omega \left[-f'(\omega)\right] \frac{3(2j)^2}{16\pi i} \sum_{r_1r_2r_1'r_2'} t^*_{r_1}t_{r_2}t^*_{r_1'}t_{r_2'} \left[\Gamma S^\dagger\left(k_F + \frac{\omega}{v_F}\right)\right]_{r_1 j}\\
&\times \left[\Gamma S^\dagger\left(k_F + \frac{\omega+\Omega}{v_F}\right)\right]^*_{r_2 j} \Gamma_{r_1' j'}\left(k_F + \frac{\omega+\Omega}{v_F}\right) \Gamma^*_{r_2' j'}\left(k_F + \frac{\omega}{v_F}\right) \frac{1}{v_F^2}\\
&= O(1) + \frac{1}{i\pi\Omega} \int d\varepsilon_p \left[-f'(\varepsilon_p)\right] \frac{3\pi^2\nu^2 J_{pp}^2}{16} \mathscr{Z}_{2,jj'}(\varepsilon_p), \quad (3.76)
\end{aligned}
$$

where we used Eq. (3.47e). The connected contribution to the conductance is now clearly a Fermi surface property:

$$G^C_{jj'} = -\frac{2e^2}{h}\int d\varepsilon_p \left[-f'(\varepsilon_p)\right] \mathscr{T}^{C(2)}_{jj'}(\varepsilon_p), \tag{3.77}$$

where the connected transmission probability is

$$\mathscr{T}^C_{jj'}(\varepsilon_p) = \mathscr{Z}_{2,jj'}(\varepsilon_p)\frac{3\pi^2}{16}\nu^2 J^2_{pp}. \tag{3.78}$$

This is formally identical to the short ring result, and is of the same order of magnitude $[O\left(J^2\right)]$ as the disconnected contribution for a particle-hole symmetric QD[66]. In fact, if leads j and j' are not directly coupled to each other (i.e. they become decoupled when their couplings with the QD are turned off; the simplest example is a QD embedded between source and drain leads[102]), we have $S_{jj'} = 0$, and the disconnected contribution for a particle-hole symmetric QD is $O\left(J^4\right)$. In this case the $O\left(J^2\right)$ connected contribution dominates.

Just as with the T-matrix, when we calculate the connected part further to $O\left(J^3\right)$ to logarithmic accuracy (as is done in Appendix C), the result can be absorbed into Eq. (3.78) if the coupling constant J is understood as fully renormalized according to Eq. (3.26), with its renormalization cut off by $|\varepsilon_p|$ or T.

Total conductance

We write the total conductance at $T \gg T_K$ as a background term and a correction due to the QD:

$$G_{jj'} = -\frac{2e^2}{h}\int d\varepsilon_p \left[-f'(\varepsilon_p)\right]\left[\mathscr{T}_{0,jj'}(\varepsilon_p) + \delta\mathscr{T}_{jj'}(\varepsilon_p)\right]. \tag{3.79}$$

If the QD is well away from particle-hole symmetry, κ can be of the same order of magnitude as $j(T)$ even when the latter is fully renormalized to the given temperature. In this case, the $T \gg T_K$ correction to the background conductance will be dominated by the potential scattering term; the connected contribution is negligible. The expression for $\delta\mathscr{T}$ is

$$\delta\mathscr{T}_{jj'}(\varepsilon_p) \approx -\mathscr{Z}_{R,jj'}(\varepsilon_p)\,\pi\nu K_{pp}. \tag{3.80}$$

If, however, the QD is particle-hole symmetric, the connected contribution becomes important. Inserting Eq. (3.70) into Eq. (3.47a) and combining with (3.78), we find the Kondo-type correction to $O\left(J^2\right)$ at $T \gg T_K$

$$\delta\mathscr{T}_{jj'}(\varepsilon_p) = \left[\mathscr{Z}_{I,jj'}(\varepsilon_p) + \mathscr{Z}_{2,jj'}(\varepsilon_p)\right]\frac{3\pi^2}{16}\nu^2 J^2_{pp}. \tag{3.81}$$

Again, in the RG improved perturbation theory, J_{pp} in Eq. (3.81) should be replaced by $J_{pp}\left(\max\left(|\varepsilon_p|, T\right)\right)$,

indicating that J_{pp} is the renormalized value at the running energy cutoff $\max(|\varepsilon_p|, T)$. This expression is valid as long as $T \gg T_K$, irrespective of whether the system is in small or large Kondo cloud regime.

Eq. (3.81) is formally similar to the previously obtained short ring result[66]. It should be noted, however, that the energy dependence of $\mathscr{Z}_I$, $\mathscr{Z}_2$ and J^2 is possibly much stronger than the short ring case, and the thermal averaging in Eq. (3.79) can lead to very different results in small and large Kondo cloud regimes. For instance, if $E_{\text{conn}} \ll T_K \ll T$ (which may happen in the small cloud regime), the Fermi factor in Eq. (3.79) averages over many peaks in $\mathscr{T}$, $\mathscr{Z}_I$, $\mathscr{Z}_2$ and V^2 that are associated with the underlying mesoscopic structure. In this case connected part elimination is not applicable. On the other hand, if $T_K \ll T \ll E_{\text{conn}}$, the variation of $\mathscr{T}$, $\mathscr{Z}_I$, $\mathscr{Z}_2$ or V^2 is negligible on the scale of T, and the Fermi factor in Eq. (3.79) may be approximated by a δ function. This leads to

$$G_{jj'} = -\frac{2e^2}{h}\left\{\mathscr{T}_{0,jj'}(\varepsilon_{k_F}) + \left[\mathscr{Z}_{I,jj'}(\varepsilon_{k_F}) + \mathscr{Z}_{2,jj'}(\varepsilon_{k_F})\right]\frac{3\pi^2}{16}\nu^2 J^2_{k_F k_F}\right\}, \tag{3.82}$$

which agrees with our prescription of eliminating the connected part, Eq. (3.66).

We mention that Eq. (3.81) can be interpreted as a completely inelastic contribution to the conductance, since in obtaining it we have retained only the $O(J^2)$ inelastic part of the single-particle T-matrix Eq. (3.70), and the connected contribution comes from two-particle processes which are again inelastic.

3.4.2 FL perturbation theory

It is also interesting to consider temperatures low compared to the Kondo temperature $T \ll T_K$. Since our formalism does not by itself provide a low-energy effective theory of the small cloud regime for $T_K \gg E_V$, we focus on the very large Kondo cloud regime $T_K \ll E_V$, where as explained in Section 3.2 the low-energy effective theory is simply a FL theory. If we further assume $T \ll E_{\text{conn}}$, then we can simply eliminate the connected contribution to the conductance with Eq. (3.66).

To use Eq. (3.66) we need the low-energy T-matrix for the screening channel in the single-particle sector in the FL regime, which is again well known[3, 5]. As discussed in Section 3.1, the strong-coupling single particle wave function at zero temperature is obtained by imposing a phase shift on the weak-coupling wave function. This phase shift $\delta_{\psi\psi}$ results from both elastic scattering off the Kondo singlet and particle-hole symmetry breaking potential scattering:

$$\delta_{\psi\psi,\sigma} = \sigma\frac{\pi}{2} + \delta_P, \tag{3.83}$$

where $\sigma = \pm 1$ for spin-up/spin-down electrons. To the lowest order in potential scattering $O(K)$, we have[75]

$$\tan\delta_P = -\pi\nu K_{k_F k_F}. \tag{3.84}$$

Let us introduce the phase-shifted screening channel $\tilde{\psi}$, which is then related to the original screening channel ψ via a scattering basis transformation:

$$\psi_{k,\sigma} = \int_{k_F-\Lambda}^{k_F+\Lambda} \frac{dp}{2\pi}\left(\frac{i}{k-p+i0} - e^{2i\delta_{\psi\psi,\sigma}}\frac{i}{k-p-i0}\right)\tilde{\psi}_{p,\sigma}. \tag{3.85}$$

Using the definition of the T-matrix in the single-particle sector Eq. (3.41) and the transformation Eq. (3.85) one can show that retarded T-matrices for ψ and $\tilde{\psi}$ are related by

$$\mathrm{T}_{kk',\sigma}(\omega) = \frac{i}{2\pi\nu}\left(e^{2i\delta_{\psi\psi,\sigma}} - 1\right) + e^{2i\delta_{\psi\psi,\sigma}}\tilde{\mathrm{T}}_{kk',\sigma}(\omega). \tag{3.86}$$

Since $\tilde{\psi}$ diagonalizes the strong-coupling fixed point Hamiltonian, by definition $\tilde{\mathrm{T}}_{k_F k_F,\sigma}(\omega=0)=0$ at zero temperature.

The leading irrelevant operator perturbing the strong-coupling fixed point is localized at the QD (with a spatial extent of v_F/T_K), and quadratic in spin current[3, 47]. It is most conveniently written in terms of $\tilde{\psi}$:

$$\begin{aligned} H_{int} = {} & \frac{2\pi v_F^2}{T_K} :\, \tilde{\psi}_\alpha^\dagger \tilde{\psi}_\alpha \tilde{\psi}_\beta^\dagger \tilde{\psi}_\beta :\, (x=0) \\ & - \frac{v_F^2}{T_K}\left[:\, \tilde{\psi}_\alpha^\dagger \left(i\frac{d}{dx} - k_F\right)\tilde{\psi}_\alpha + \left(-i\frac{d}{dx} - k_F\right)\tilde{\psi}_\alpha^\dagger \tilde{\psi}_\alpha :\, \right](x=0). \end{aligned} \tag{3.87}$$

Here :: denotes normal ordering, and sums over repeated spin indices α and β are implied. The $\tilde{\psi}$ operators have been unfolded, so that their wave functions are now defined on the entire real axis instead of the positive real axis. The two terms in H_{int} are illustrated in panel a) of Fig. 3.4 as a four-point vertex and a two-point one. Both terms share a single coupling constant of $O(1/T_K)$, because the leading irrelevant operator written in the $\tilde{\psi}$ basis must be particle-hole symmetric by definition. The on-shell retarded T-matrix for $\tilde{\psi}$ in the single-particle sector is calculated to $O\left(1/T_K^2\right)$ in Ref. [3]:

$$-\pi\nu\tilde{\mathrm{T}}_{pp}(\varepsilon_p) = \frac{\varepsilon_p}{T_K} + i\frac{3\varepsilon_p^2+\pi^2T^2}{2T_K^2}. \tag{3.88}$$

For completeness we give a derivation of this result in Appendix C. It is diagramatically represented by Fig. 3.4 panel b).

Substituting Eqs. (3.83), (3.86) and (3.88) into Eq. (3.66), we eliminate the connected contribution, and obtain the $T \ll T_K$ conductance in the very large Kondo cloud regime[112]:

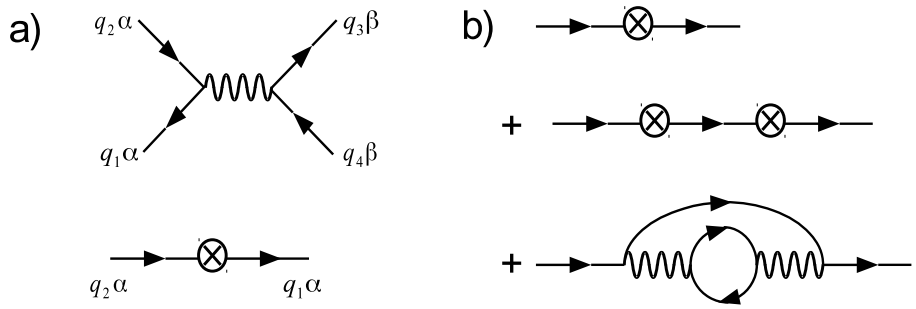

Figure 3.4: Diagrammatics of FL perturbation theory. a) The two vertices given by the leading irrelevant operator, Eq. (3.87). b) Diagrams contributing to the T-matrix of $\tilde{\psi}$ electrons up to $O\left(1/T_K^2\right)$. The propagators are those of the phase-shifted screening channel operators $\tilde{\psi}$.

$$G_{jj'} \approx -\frac{2e^2}{h}\left\{\mathscr{T}_{0,jj'}\left(\varepsilon_{k_F}\right) - \mathscr{Z}_{R,jj'}\left(\varepsilon_{k_F}\right)\left(\frac{1}{2} - \frac{\pi^2 T^2}{T_K^2}\right)\sin 2\delta_P \right.$$
$$\left. + \left[\mathscr{Z}_{I,jj'}\left(\varepsilon_{k_F}\right) + \mathscr{Z}_{2,jj'}\left(\varepsilon_{k_F}\right)\right]\left(\cos^2\delta_P - \frac{\pi^2 T^2}{T_K^2}\cos 2\delta_P\right)\right\}. \tag{3.89}$$

We note that the connected contribution can in fact be evaluated directly in the FL theory. This is also done in Appendix C, and provides further verification of our scheme of eliminating the connected contribution.

Predictions of the conductance at high temperatures [Eq. (3.79)] and at low temperatures [Eq. (3.89)] together constitute the second main result of this chapter. We emphasize once more that, while Eq. (3.79) is valid as long as $T \gg T_K$, Eq. (3.89) is expected to be justified provided $T \ll T_K \ll E_V$, so that the FL theory applies, and also $T \ll E_{\text{conn}}$, so that the connected contribution can be eliminated.

For clarity we tabulate various regimes of energy scales discussed so far (Table 3.1). Note again that the connected contribution to conductance can be eliminated when $T \ll E_{\text{conn}}$. In general we have $E_{\text{conn}} \lesssim E_V$, but we assume in this table that $E_{\text{conn}} \sim E_V$, which is the case with the systems to be discussed in this chapter.

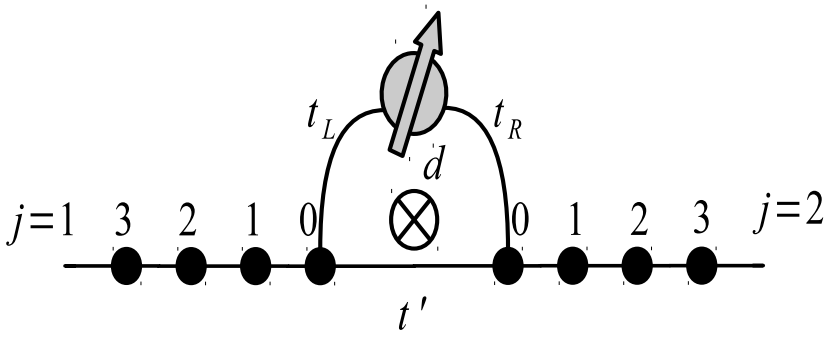

Figure 3.5: The short ABK ring studied in Refs. [66, 75].

3.5 Comparison with early results

3.5.1 Short ABK ring

Our formalism can be applied to the short ABK ring[66, 75] shown in Fig. 3.5. There are two leads ($N = 2$) and two coupling sites ($M = 2$); $H_{0,\text{junction}} = -t'\left(c^{\dagger}_{1,0}c_{2,0} + \text{h.c.}\right)$. The coupling sites coincide with the 0th sites of the leads, $c_{C,r=1} \equiv c_{1,0}$, $c_{C,r=2} \equiv c_{2,0}$; also the AB phase is on the couplings to the QD, $t_1 = t_L e^{i\frac{\varphi}{2}}$ and $t_2 = t_R e^{-i\frac{\varphi}{2}}$. We again let $\tilde{\tau} = t'/t$.

It is straightforward to obtain the background S-matrix and coupling site wave function matrix:

$$S(k) = -\frac{1}{1-\tilde{\tau}^2 e^{2ik}} \begin{pmatrix} e^{2ik}\left(1-\tilde{\tau}^2\right) & e^{ik}\tilde{\tau}\left(e^{2ik}-1\right) \\ e^{ik}\tilde{\tau}\left(e^{2ik}-1\right) & e^{2ik}\left(1-\tilde{\tau}^2\right) \end{pmatrix}, \tag{3.90}$$

$$\Gamma(k) = -\frac{1}{1-\tilde{\tau}^2 e^{2ik}} \begin{pmatrix} e^{2ik}-1 & 2ie^{2ik}\tilde{\tau}\sin k \\ 2ie^{2ik}\tilde{\tau}\sin k & e^{2ik}-1 \end{pmatrix}. \tag{3.91}$$

With Eqs. (3.27), (3.81) and (3.89), one reproduces all analytic results in Refs. [66, 75], including the Kondo temperature, the high- and low-temperature conductance, and the elimination of connected contribution at low temperatures.

The limit $t' = 0$ is useful as a benchmark against long ring geometries so we study it in some more detail. In this limit we recover the simplest geometry where a QD is embedded between source and drain leads[102]. The normalization factor is

$$V_k^2 = 4\left(t_L^2 + t_R^2\right)\sin^2 k, \tag{3.92}$$

and the zero-temperature transmission amplitude through the QD is given by Eqs. (3.45), (3.83),

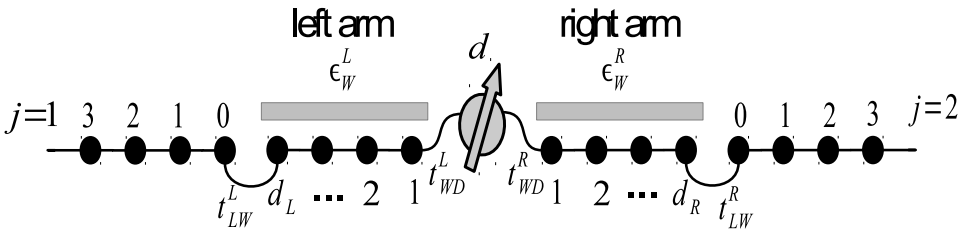

Figure 3.6: The finite quantum wire geometry studied in Ref. [116].

(3.86) and (3.88):

$$\begin{aligned} t_{QD} &\equiv \frac{2i}{V_k^2}\left[S(k)\Gamma^{\dagger}(k)\lambda\Gamma(k)\right]_{12}\left[-\pi\nu \mathrm{T}_{kk}(\varepsilon_k)\right] \\ &= e^{2ik}\frac{2t_L t_R}{t_L^2+t_R^2}\frac{1}{2}\left(e^{2i\delta_P}+1\right). \end{aligned} \tag{3.93}$$

3.5.2 Finite quantum wire

Another special case is the finite wire (or semi-transparent Kondo box) geometry in Fig. 3.6 where the reference arm is absent[116]; again $N = M = 2$. The left and right QD arms and coupling sites are subject to gate voltages:

$$\begin{aligned} H_{0,\text{junction}} = &-t\left(\sum_{n=1}^{d_L-1} c_{L,n}^{\dagger}c_{L,n+1} + \sum_{n=1}^{d_R-1} c_{R,n}^{\dagger}c_{R,n+1} + \text{h.c.}\right) \\ &+ \left(\varepsilon_W^L \sum_{n=1}^{d_L} c_{L,n}^{\dagger}c_{L,n} + \varepsilon_W^R \sum_{n=1}^{d_R} c_{R,n}^{\dagger}c_{R,n}\right) \\ &- \left(t_{LW}^L c_{L,d_L}^{\dagger}c_{1,0} + t_{LW}^R c_{R,d_R}^{\dagger}c_{2,0} + \text{h.c.}\right). \end{aligned} \tag{3.94}$$

The coupling sites are the first sites of the QD arms, $c_{C,r=1} \equiv c_{L,1}$, $c_{C,r=2} \equiv c_{R,1}$; $t_1 = t_{WD}^L$ and $t_2 = t_{WD}^R$.

The two leads are decoupled without the QD, so S and Γ are both diagonal. In this system we have

$$S_{11}(k) = -\frac{e^{ik}\sin k_L(d_L+1) - \gamma_L^2 \sin k_L d_L}{e^{-ik}\sin k_L(d_L+1) - \gamma_L^2 \sin k_L d_L}, \tag{3.95}$$

and

$$\Gamma_{11}(k) = -\frac{2i\gamma_L \sin k \sin k_L}{e^{-ik}\sin k_L (d_L+1) - \gamma_L^2 \sin k_L d_L}, \tag{3.96}$$

where k_L is determined by the gate voltage ε_W^L,

$$-2t\cos k_L + \varepsilon_W^L = -2t\cos k, \tag{3.97}$$

and $\gamma_L = t_{LW}^L/t$. S_{22} and Γ_{22} can be obtained simply by substituting L with R. Again, these results allow us to reproduce the (weak coupling) Kondo temperature, the high-temperature conductance, as well as the low-temperature conductance in the large Kondo cloud regime. (We do not quantitatively discuss the low-temperature conductance in the small cloud regime in this thesis; see Section 3.8.)

3.6 Closed long ring

In this section we apply our general formalism to the simplest model of a closed long ABK ring, studied in Ref. [131] (Fig. 3.7): the QD is coupled directly to the source and drain leads, and a long reference arm connects the two leads smoothly. A weak link with hopping t' splits the reference arm into two halves of equal length $d_{ref}/2$ where d_{ref} is an even integer. As opposed to Ref. [131], however, we use gauge invariance to assign the AB phase to the QD tunnel couplings rather than the weak link: $t_1 \equiv t_L e^{i\varphi/2}$ and $t_2 \equiv t_R e^{-i\varphi/2}$. We assume no additional non-interacting long arms connecting the QD with the source and drain leads, because multiple traversal processes in such long QD arms will lead to interference effects[84] independent of the AB phase, complicating the problem[131]. The Hamiltonian representing this model takes the form

$$\begin{aligned} H_{0,\text{junction}} = &-t\left[\left(\sum_{n=1}^{d_{ref}/2-1} + \sum_{n=d_{ref}/2+1}^{d_{ref}-1}\right) c_{ref,n}^\dagger c_{ref,n+1} + \text{h.c.}\right] \\ &-t\left(c_{ref,1}^\dagger c_{1,0} + c_{ref,d_{ref}}^\dagger c_{2,0} + \text{h.c.}\right) \\ &-t'\left(c_{ref,d_{ref}/2}^\dagger c_{ref,d_{ref}/2+1} + \text{h.c.}\right); \end{aligned} \tag{3.98}$$

the coupling sites are $c_{C,r=1} \equiv c_{1,0}$ and $c_{C,r=2} \equiv c_{2,0}$.

We first repeat the Kondo temperature analysis in Ref. [131] in order to distinguish between small and large Kondo cloud regimes, then carefully study the conductance at high and low temperatures, taking into account the previously neglected connected contribution.

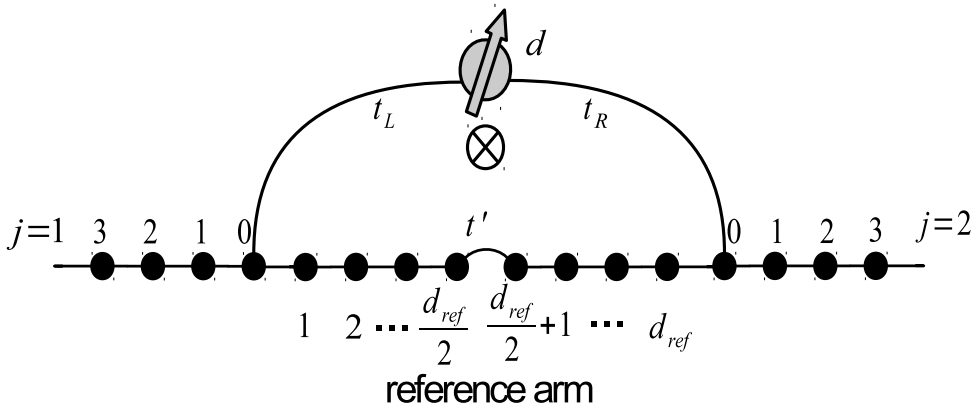

Figure 3.7: Geometry of the long ABK ring with short upper arms and a pinched reference arm.

3.6.1 Kondo temperature

The background S-matrix for this model is identical to the short ABK ring[75] up to overall phases, due to the smooth connection between reference arm and leads:

$$S(k) = e^{ikd_{ref}} \begin{pmatrix} \tilde{r}(k) & \tilde{t}(k) \\ \tilde{t}(k) & \tilde{r}(k) \end{pmatrix}; \tag{3.99}$$

where the S-matrix elements $\tilde{r}$ and $\tilde{t}$ for the weak link are

$$\tilde{r}(k) = -\frac{1-\tilde{\tau}^2}{e^{-2ik}-\tilde{\tau}^2}, \tilde{t}(k) = -\frac{2i\tilde{\tau}\sin k}{e^{-2ik}-\tilde{\tau}^2}, \tag{3.100}$$

and we introduce the shorthand $\tilde{\tau} = t'/t$. The wave function is also straightforward to find:

$$\Gamma_{jj'}(k) = \delta_{jj'} + S_{jj'}(k). \tag{3.101}$$

In the wide band limit, $\tilde{r}$ and $\tilde{t}$ are approximately independent of k in the reduced band $k_F - \Lambda_0 < k < k_F + \Lambda_0$ where the momentum cutoff $\Lambda_0 \ll 1$. This allows us to approximate them by their Fermi surface values, $\tilde{r}(k) \approx \tilde{r} = |\tilde{r}| e^{i\theta}$ and $\tilde{t}(k) \approx \tilde{t} = \pm i|\tilde{t}| e^{i\theta}$ (the $\pm\pi/2$ phase difference is required by unitarity of S); without loss of generality we focus on the $\tilde{t} = i|\tilde{t}| e^{i\theta}$ case.

From Eq. (3.101) one conveniently obtains the normalization factor

$$V_k^2 = 2\left(t_L^2+t_R^2\right)\left[1+|\tilde{r}|\cos\left(kd_{ref}+\theta\right)-\gamma|\tilde{t}|\cos\varphi\sin\left(kd_{ref}+\theta\right)\right]$$
$$= 2\left(t_L^2+t_R^2\right)\left[1+\sqrt{1-|\tilde{t}|^2\left(1-\gamma^2\cos^2\varphi\right)}\cos\left(kd_{ref}+\theta'\right)\right], \tag{3.102}$$

where $\gamma = 2t_L t_R/\left(t_L^2+t_R^2\right)$ measures the degree of symmetry of coupling to the QD. In the second line we have used $|\tilde{t}|^2+|\tilde{r}|^2=1$ and introduced another phase θ', where $\theta'-\theta$ is a function of γ, $|\tilde{t}|$ and φ but independent of k. We note that this expression is also applicable in the continuum limit, where the lattice constant $a\to 0$ (we have previously set $a=1$) but the arm length $d_{ref}a$ is fixed. In that case d_{ref} should be understood as the arm length $d_{ref}a$.

For long rings and filling factors not too small $k_F d_{ref} \gg 1$, V_k^2 oscillates around $2\left(t_L^2+t_R^2\right)$ as a function of k, and has its extrema at $k_n = \left(n\pi-\theta'\right)/d_{ref}$ where n takes integer values. The only characteristic energy scale for V_k^2 is therefore the peak/valley spacing $\Delta = v_F\pi/d_{ref}$, and $E_V \sim E_{\text{conn}} \sim \Delta$. As in Ref. [131] we define the reduced band such that $\Delta \ll D_0 \equiv v_F\Lambda_0$, and the reduced band initially contains many oscillations.

In the small Kondo cloud regime $T_K \gg \Delta$, one may assume the oscillations of V_k^2 are smeared out when the energy cutoff is being reduced from D_0, which is still well above T_K: $V_k^2 \simeq \overline{V_k^2} = 2\left(t_L^2+t_R^2\right)$. This means T_K in this regime is approximately the background Kondo temperature T_K^0 defined in Eq. (3.29), independent of the position of the Fermi level at the energy scale Δ, and also independent of the magnetic flux.

On the other hand, in the large cloud regime $T_K \lesssim \Delta$, now that the Kondo temperature is largely determined by the value of V_k^2 in a very narrow range of energies around the Fermi level, the mesoscopic k oscillations become much more important. When the running energy cutoff D is above the peak/valley spacing Δ, the renormalization of j is controlled by $\overline{V_k^2}$ as in Eq. (3.28). Once D is reduced below Δ, we may approximate the renormalization of j as being dominated by $V_{k_F}^2$. This leads to the following estimation of the Kondo temperature:

$$T_K \simeq \Delta\exp\left[-\frac{1}{2V_{k_F}^2\nu j(\Delta)}\right] = \Delta\left(\frac{T_K^0}{\Delta}\right)^{\left[1+\sqrt{1-|\tilde{t}|^2\left(1-\gamma^2\cos^2\varphi\right)}\cos\left(k_F d_{ref}+\theta'\right)\right]^{-1}}. \tag{3.103}$$

It is clear that T_K can be significantly dependent on the AB phase φ in this regime. In particular, T_K varies from $\sim\sqrt{T_K^0\Delta}$ ("on resonance") to practically 0 ("off resonance") as φ is tuned between 0 and π[131], when the Fermi energy is located on a peak or in a valley $k_F = k_n$, the background transmission is perfect $|\tilde{t}|=1$, and coupling to the QD is symmetric $\gamma=1$; see Fig. 3.8. (The special case $V_{k_F}^2 = 0$ corresponds to a pseudogap problem $\nu V_k^2 \propto (k-k_F)^2$, and the stable RG fixed point can be the local moment fixed point or the asymmetric strong coupling fixed point, depending on

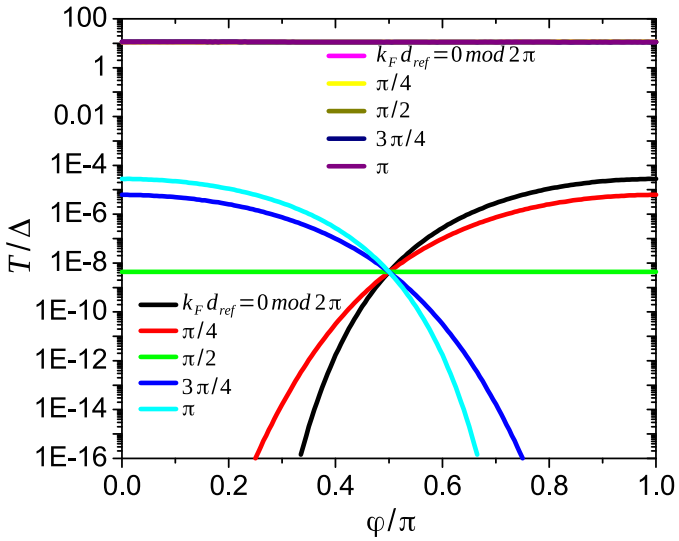

Figure 3.8: Kondo temperature T_K for the closed long ABK ring, calculated by numerical integration of the weak coupling RG equation Eq. (3.27), plotted against the AB phase φ. $T_K(\varphi)$ is an even function of φ and has a period of 2π, so only $0 \leq \varphi \leq \pi$ is shown. System parameters are: $d_{ref} = 60$, $\theta = \pi/2$, $|\tilde{r}| = 0$, $t_L = t_R$, $D_0 = 10$. The curves with $T_K \gg \Delta$ (small Kondo cloud regime) have a large bare Kondo coupling $\left(t_L^2 + t_R^2\right) j_0/\pi = 0.15$, whereas the curves with $T_K \ll \Delta$ (large Kondo cloud regime) have a much smaller bare Kondo coupling $\left(t_L^2 + t_R^2\right) j_0/\pi = 0.02$. In the small cloud regime T_K is almost independent of φ and k_F, as the curves are flat and overlapping with each other. In the large cloud regime, however, T_K highly sensitive to both φ and k_F.

the degree of particle-hole symmetry[39, 128].) As a general rule, stronger transmission through the pinch $|\tilde{t}|$ and greater symmetry of coupling γ result in stronger interference between the two tunneling paths through the device, and hence increases the tunability of the Kondo temperature by the magnetic flux.

3.6.2 High-temperature conductance

We now calculate the conductance at $T \gg T_K$ by perturbation theory. Following the discussion in Ref. [131], we consider the case of a particle-hole symmetric QD $\kappa = 0$ and $K_{kk'} = 0$, and also ignore the elastic real part of the potential scattering generated[66] at $O\left(J^2\right)$. These assumptions allow us to adopt Eq. (3.81) for the $O\left(J^2\right)$ correction to the transmission probability:

$$\delta \mathscr{T}_{jj'}(\varepsilon_k) = 3\pi^2 \nu^2 j^2 \left(V_k^2 \, \mathrm{Re} \left\{ \left[S(k) \Gamma^\dagger(k) \lambda \Gamma(k) \right]_{jj'} S^*_{jj'}(k) \right\} - \left| \left[S(k) \Gamma^\dagger(k) \lambda \Gamma(k) \right]_{jj'} \right|^2 \right), \tag{3.104}$$

where we have used Eqs. (3.47d) and (3.47e).

Note that Eq. (3.104) does not depend on details of the non-interacting part of the ring Hamiltonian $H_{0,\text{junction}}$. For a parity-symmetric geometry with two leads and two coupling sites ($N=M=2$), when coupling to the QD is also symmetric ($t_L=t_R$) and time-reversal symmetry is present ($\varphi=0$ or π), we can further show that the sign of the $O\left(J^2\right)$ transmission probability correction is determined by the sign of $1-2\left|\mathscr{T}_{0,12}\right|$, a property discussed in Ref. [66] at the end of Section IV C. Indeed, parity symmetry implies that $S_{11}=S_{22}$, $S_{12}=S_{21}$, $\Gamma_{11}=\Gamma_{22}$, $\Gamma_{12}=\Gamma_{21}$; hence it is not difficult to find from Eq. (3.104) that

$$\frac{1}{4}\left[\delta\mathscr{T}_{11}\left(\varepsilon_k\right)+\delta\mathscr{T}_{22}\left(\varepsilon_k\right)-\delta\mathscr{T}_{12}\left(\varepsilon_k\right)-\delta\mathscr{T}_{21}\left(\varepsilon_k\right)\right]=\frac{3}{8}\pi^2\nu^2J_{kk}^2\left[1-2\left|S_{12}\left(k\right)\right|^2\right]. \tag{3.105}$$

The left-hand side correspond to a particular way to measure the conductance, namely parity-symmetric bias voltage and parity-symmetric current probes, or $y=1/2$ in Section V of Ref. [66].

We now return to the long ring geometry without assumptions about t_L, t_R and φ. Plugging Eqs. (3.99) and (3.101) into Eq. (3.104) we find

$$\delta\mathscr{T}_{11}\left(\varepsilon_k\right)=-3\pi^2\nu^2j^2\left[C_0\left(k\right)+C_1\left(k\right)\cos\varphi+C_2\left(k\right)\cos 2\varphi\right], \tag{3.106}$$

where the coefficients $C_0\left(k\right)$, $C_1\left(k\right)$ and $C_2\left(k\right)$ are independent of φ but are usually complicated functions of k:

$$\begin{aligned}C_0\left(k\right)=&\left(t_L^4+t_R^4\right)\left|\tilde{t}\right|^2\left[1+2\left|\tilde{r}\right|\cos\left(kd_{ref}+\theta\right)+\left|\tilde{r}\right|^2\cos 2\left(kd_{ref}+\theta\right)\right]\\&-2t_L^2t_R^2\left[3-4\left|\tilde{t}\right|^2+4\left|\tilde{r}\right|^3\cos\left(kd_{ref}+\theta\right)+\left(\left|\tilde{r}\right|^4+\left|\tilde{t}\right|^4\right)\cos 2\left(kd_{ref}+\theta\right)\right],\end{aligned} \tag{3.107a}$$

$$\begin{aligned}C_1\left(k\right)=&\,4\left|\tilde{t}\right|t_Lt_R\left(t_L^2+t_R^2\right)\sin\left(kd_{ref}+\theta\right)\\&\times\left[\left|\tilde{r}\right|^2\cos 2\left(kd_{ref}+\theta\right)+\left|\tilde{r}\right|\left(\left|\tilde{r}\right|^2-\left|\tilde{t}\right|^2\right)\cos\left(kd_{ref}+\theta\right)-\left|\tilde{t}\right|^2\right],\end{aligned} \tag{3.107b}$$

$$C_2\left(k\right)=2\left|\tilde{t}\right|^2t_L^2t_R^2\left\{1+2\left|\tilde{r}\right|\cos\left(kd_{ref}+\theta\right)+\left|\tilde{r}\right|^2\cos 2\left(kd_{ref}+\theta\right)\right\}. \tag{3.107c}$$

In the special case of a smooth reference arm $\left|\tilde{r}\right|=0$ and $\left|\tilde{t}\right|=1$, the Kondo-type correction becomes especially simple:

$$\delta\mathscr{T}_{11}(\varepsilon_k) = -3\pi^2\nu^2 j^2 \left[t_L^2 + t_R^2 - 2t_L t_R \sin(kd_{ref} + \theta + \varphi)\right] \times \left[t_L^2 + t_R^2 - 2t_L t_R \sin(kd_{ref} + \theta - \varphi)\right]. \tag{3.108}$$

As in Refs. [66, 131], only the first and the second harmonics of the AB phase φ appear in the correction to the transmission probability $\delta\mathscr{T}_{11}$.

We may perform the thermal averaging in Eq. (3.79) at this stage. The Fermi factor $-f'(\varepsilon_k)$ ensures only the energy range $|\varepsilon_k| \lesssim T$ contributes significantly to the conductance; in this energy range the renormalization of j is cut off by T.

In the small Kondo cloud regime, $T \gg T_K$ means $T \gg \Delta$ so that we can average over many peaks of $\delta\mathscr{T}_{jj'}(\varepsilon_k)$, so we may drop all rapidly oscillating Fourier components in Eq. (3.106). This leads to

$$\delta G \approx -\frac{2e^2}{h} 3\pi^2\nu^2 [j(T)]^2 \left[\left(t_L^4 + t_R^4\right)|\tilde{t}|^2 - 2t_L^2 t_R^2 \left(3 - 4|\tilde{t}|^2\right) + 2|\tilde{t}|^2 t_L^2 t_R^2 \cos 2\varphi\right]. \tag{3.109}$$

We see that the first harmonic in φ approximately drops out upon thermal averaging.

On the other hand, in the large Kondo cloud regime, for $T \gg T_K$ it is possible to have either $T \gg \Delta$ or $T \ll \Delta$. In the former case Eq. (3.109) continues to hold. In the latter case $\delta\mathscr{T}_{jj'}(\varepsilon_k)$ has little variation in the energy range $|\varepsilon_k| \lesssim T$, so it is appropriate to replace $-f'(\varepsilon_k)$ with a δ function at the Fermi level; thus

$$\delta G \approx -\frac{2e^2}{h} 3\pi^2\nu^2 [j(T)]^2 [C_0(k_F) + C_1(k_F)\cos\varphi + C_2(k_F)\cos 2\varphi]. \tag{3.110}$$

Fig. 3.9 illustrates these two different cases for the large Kondo cloud regime[112]. We note that our $T \gg T_K$ results, Eq. (3.109) for $T \gg \Delta$ and Eq. (3.110) for $T \ll \Delta$, are different from those of Ref. [131]. We believe the discrepancy is due to the fact that only single-particle scattering processes are taken into consideration by Ref. [131]; the connected contribution to the conductance is omitted, despite being of comparable magnitude with the disconnected contribution.

It should be noted that our $T \gg T_K$ results do not constitute evidence in favor of the Kondo screening cloud per se, as they do not involve a direct comparison between T_K and Δ. Indeed, the difference between $T \gg \Delta$ and $T \ll \Delta$ is also present even if we replace the Kondo QD with a non-interacting QD. Nevertheless, our results may be experimentally relevant as they reveal the qualitatively different interplay between the AB flux and the Kondo scattering.

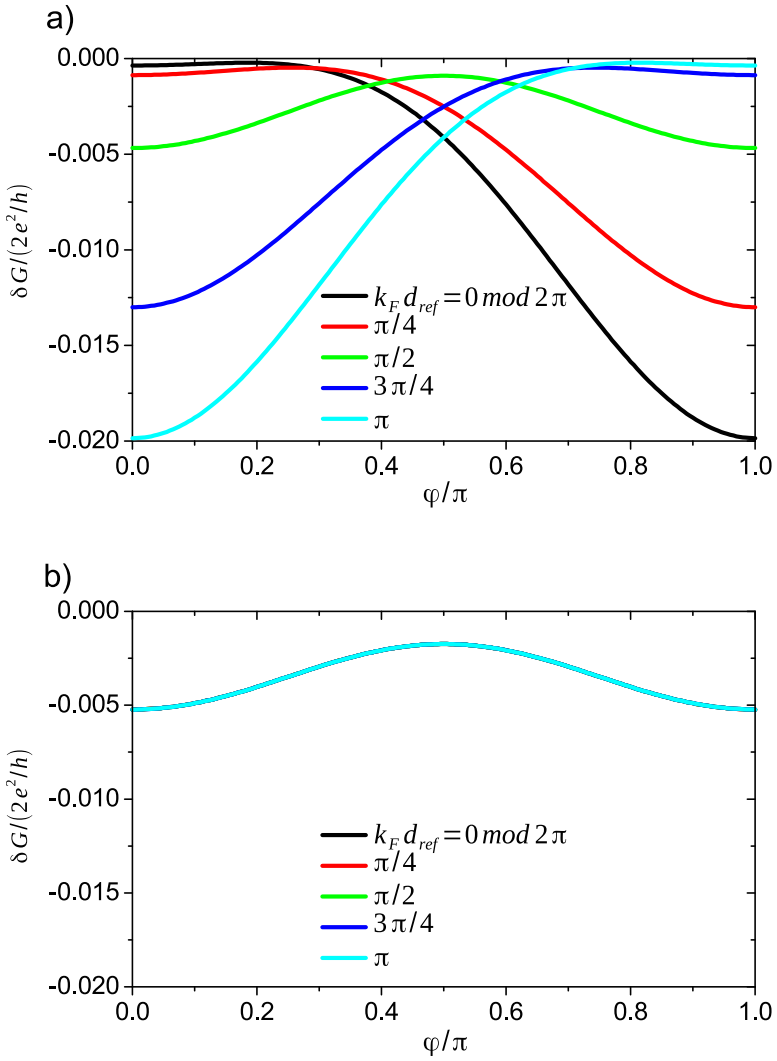

Figure 3.9: Kondo-type correction to the conductance δG at $T \gg T_K$ for the closed long ABK ring with a particle-hole symmetric QD, calculated by RG improved perturbation theory Eq. (3.106), plotted against the AB phase φ. Again only $0 \leq \varphi \leq \pi$ is shown. System parameters are: $d_{ref} = 60$, $\theta = \pi/2$, $|\tilde{r}| = 0$, $t_L = t_R$, $\left(t_L^2 + t_R^2\right) j_0/\pi = 0.02$ at $D_0 = 10$ (i.e. the system is in the large cloud regime). $T/\Delta = 0.0955$ in panel a) and $T/\Delta = 19.1$ in panel b). For $T \ll \Delta$ the conductance shows considerable k_F dependence, while for $T \gg \Delta$ such dependence essentially vanishes and curves at different k_F overlap. Also, for $T \gg \Delta$ the first harmonic $\cos\varphi$ drops out as predicted by Eq. (3.109), and $\delta G(\varphi)$ has a period of π.

3.6.3 FL conductance

It is also interesting to calculate the conductance in the $T \ll T_K$ limit in the very large Kondo cloud regime, starting from Eq. (3.89). We make the assumption that the particle-hole symmetry breaking potential scattering is negligible, $\delta_P = 0$, as in Ref. [131]. Inserting Eqs. (3.99) and (3.101) into Eqs. (3.47d) and (3.47e), we find the total conductance has the form

$$G = \frac{2e^2}{h}\left[T_s + \left(|\tilde{t}|^2 - T_s\right)\left(\frac{\pi T}{T_K}\right)^2\right], \tag{3.111}$$

where the $T = 0$ transmission probability is

$$\begin{aligned} T_s = \Bigg| & e^{ik_F d_{ref}}\tilde{t} - \frac{2}{V_{k_F}^2}\left[t_L e^{i\frac{\varphi}{2}}\left(e^{ik_F d_{ref}}\tilde{r}+1\right) + t_R e^{-i\frac{\varphi}{2}} e^{ik_F d_{ref}}\tilde{t}\right] \\ & \times\left[t_L e^{-i\frac{\varphi}{2}} e^{ik_F d_{ref}}\tilde{t} + t_R e^{i\frac{\varphi}{2}}\left(1+e^{ik_F d_{ref}}\tilde{r}\right)\right]\Bigg|^2. \end{aligned} \tag{3.112}$$

While Eq. (3.111) is ostensibly in agreement with Eq. (69) of Ref. [131], we suspect that there are two oversights in the derivation of the latter: at finite temperature, Ref. [131] neglects the connected contribution to the conductance, and also replaces the thermal factor $-f'(\varepsilon_p)$ with a δ function in Eq. (3.66). These two discrepancies cancel each other, leading to the same $T \ll T_K$ result as ours.

3.7 Open long ring

We turn to the open long ABK ring, with strong electron leakage due to side leads coupled to the arms of the ring, where our multi-terminal formalism shows its full capacity.

In our geometry shown in Fig. 3.10, the source lead branches into two paths at the left Y-junction, a QD path of length $d_L + d_R$ and a reference path of length d_{ref}. These two paths converge at the right Y-junction at the end of the drain lead. An embedded QD in the Kondo regime separates the QD path into two arms of lengths d_L and d_R. To open up the ring we attach additional non-interacting side leads to all sites inside the ring other than the two central sites in the Y-junctions and QD[6, 7, 23, 118]. The side leads, numbering $d_L + d_R + d_{ref}$ in total, are assumed to be identical to the main leads (source and drain), except that the first link on every side lead (connecting site 0 of the side lead to its base site in the ring) is assumed to have a hopping strength t_x which is generally different than the bulk hopping t. The Hamiltonian representing this model is therefore

$$
\begin{aligned}
H_{0,\text{junction}} = -t & \left(\sum_{n=0}^{d_L-2} c^\dagger_{L,n} c_{L,n+1} + \sum_{n=0}^{d_R-2} c^\dagger_{R,n} c_{R,n+1} + \sum_{n=1}^{d_{ref}-1} c^\dagger_{ref,n} c_{ref,n+1} + \text{h.c.} \right) \\
& - \left[\left(t^L_{JL} c^\dagger_{1,0} + t^L_{JQ} c^\dagger_{L,d_L-1} + t^L_{JR} c^\dagger_{ref,1} \right) c_{JL} + \text{h.c.} \right] \\
& - \left[\left(t^R_{JL} c^\dagger_{2,0} + t^R_{JQ} c^\dagger_{R,d_R-1} + t^R_{JR} c^\dagger_{ref,d_{ref}} \right) c_{JR} + \text{h.c.} \right] \\
& - t_x \left(\sum_{n=0}^{d_L-1} c^\dagger_{L,n} c^{(L)}_{n,0} + \sum_{n=0}^{d_R-1} c^\dagger_{R,n} c^{(R)}_{n,0} + \sum_{n=1}^{d_{ref}} c^\dagger_{ref,n} c^{(ref)}_{n,0} + \text{h.c.} \right),
\end{aligned} \tag{3.113}
$$

where $c_{JL(R)}$ is the annihilation operator on the central site of the left (right) Y-junction, and $c^{(\alpha)}_{n,0}$ is the annihilation operator on site 0 of the side lead attached to the nth site on arm α, $\alpha = L, R$ and ref. The coupling sites are $c_{C,r=1} \equiv c_{L,0}$ and $c_{C,r=2} \equiv c_{R,0}$, and again we let the couplings to the QD be $t_1 = t_L e^{i\frac{\varphi}{2}}$ and $t_2 = t_R e^{-i\frac{\varphi}{2}}$.

Our hope is that in certain parameter regimes the open long ring provides a realization of the two-path interferometer, where the two-slit interference formula applys:

$$
G_{sd} = G_{ref} + G_d + 2\sqrt{\eta_v}\sqrt{G_{ref} G_d} \cos(\varphi + \varphi_t), \tag{3.114}
$$

where G_{ref} is the conductance through the reference arm with the QD arm sealed off, and G_d is the conductance through the QD with the reference arm sealed off. φ is as before the AB phase, and φ_t is the accumulated non-magnetic phase difference of the two paths (*including* the $\pi/2$ transmission phase through the QD). η_v is the unit-normalized visibility of the AB oscillations; $\eta_v = 1$ at zero temperature if all transport processes are coherent[23]. In the two-path interferometer regime, φ_t reflects the intrinsic transmission phase through the QD, provided that the geometric phases of the two paths are the same (e.g. identical path lengths in a continuum model), no external magnetic field is applied to the QD, and the particle-hole symmetry breaking phase shift is zero.

For non-interacting embedded QDs well outside of the Kondo regime, small transmission through the lossy arms is known to suppress multiple traversals of the ring and ensure that the transmission amplitudes in two paths are mutually independent[7]. We show below that in our interferometer with a Kondo QD, the same criterion renders the mesoscopic fluctuations of the normalization factor V_k^2 negligible, and paves the way to the two-slit condition $t_{sd} = t_{ref} + t_d e^{i\varphi}$. If we additionally have small reflection by the lossy arms, then both the Kondo temperature of the system and the intrinsic transmission amplitude through the QD are the same as their counterparts for a QD directly embedded between the source and the drain. At finite temperature $T \ll T_K$, we recover and generalize the single-channel Kondo results of Ref. [23] for the normalized visibility η_v and the transmission phase φ_t.

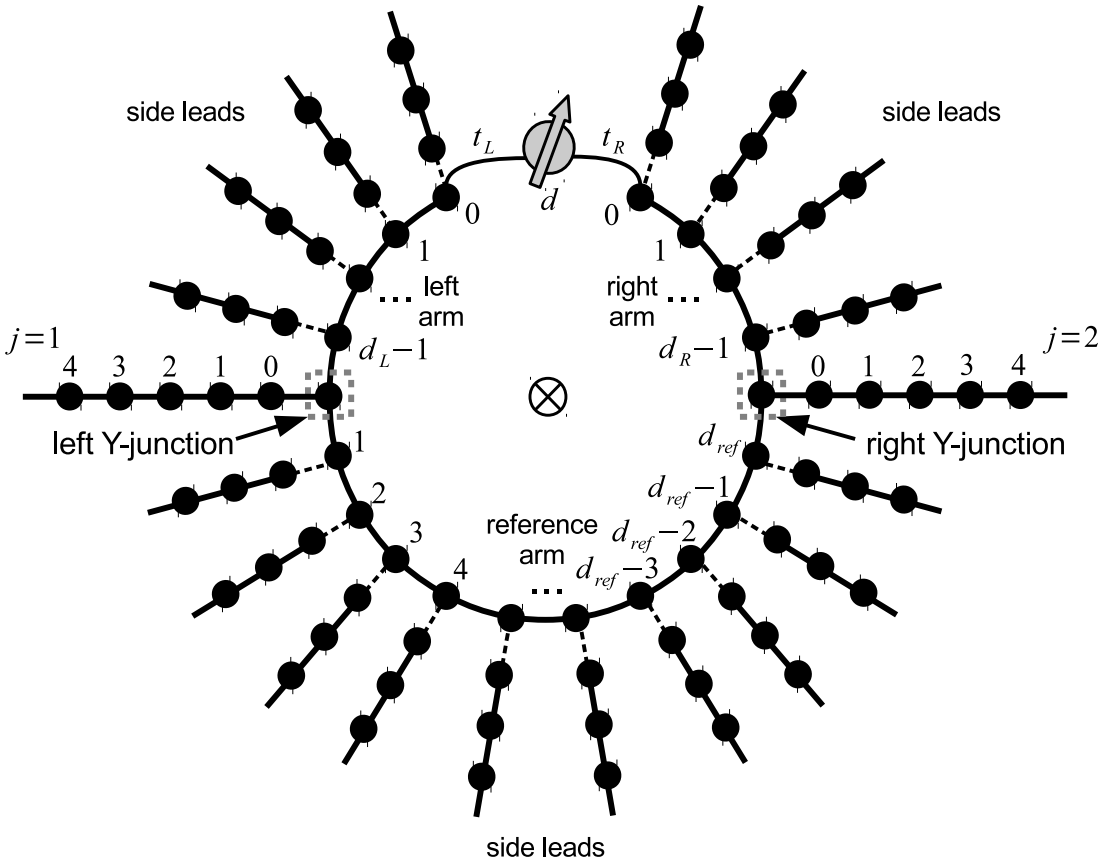

Figure 3.10: Geometry of the open long ABK ring. Side leads are appended to the QD arms and the reference arms, which are all of comparable lengths.

3.7.1 Wave function on a single lossy arm

To solve for the background S-matrix S and the wave function matrix Γ of the open ring, we first analyze a single lossy arm attached to side leads[7], depicted in Fig. 3.11.

Consider an arbitrary site labeled n on this arm; let the wave function on this site be ϕ_n, and let incident and scattered amplitudes on the side lead attached to this site be A_n^s and B_n^s. The wave function on site l ($l \geq 0$) on the side lead (also with bulk hopping t) is then written as $A_n^s e^{-ikl} + B_n^s e^{ikl}$, which gives the usual energy $-2t\cos k$. The Schroedinger's equations are

$$(-2t\cos k)\,(A_n^s + B_n^s) = -t_x\phi_n - t\left(A_n^s e^{-ik} + B_n^s e^{ik}\right), \tag{3.115a}$$

$$(-2t\cos k)\,\phi_n = -t\phi_{n-1} - t\phi_{n+1} - t_x\,(A_n^s + B_n^s)\,. \tag{3.115b}$$

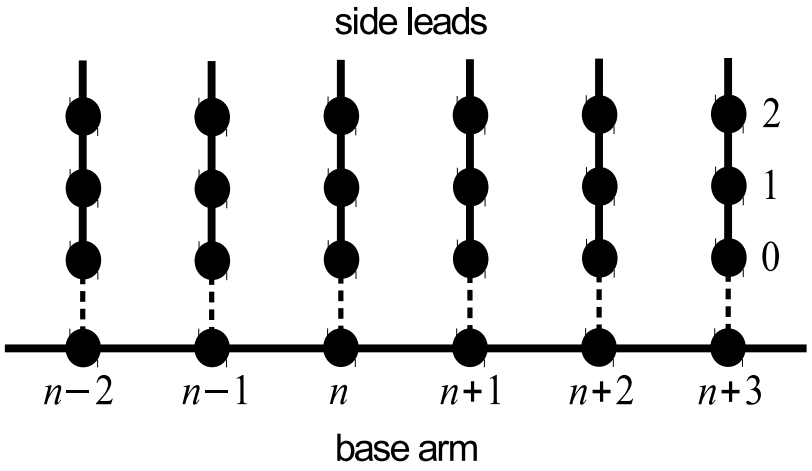

Figure 3.11: A single lossy arm attached to side leads.

Eliminating B_n^s, we find

$$\left(-2\cos k+\frac{t_x^2}{t^2}e^{ik}\right)\phi_n=-\phi_{n-1}-\phi_{n+1}+e^{ik}\,(2i\sin k)\,\frac{t_x}{t}A_n^s. \tag{3.116}$$

This means if $A_n^s=0$, i.e. no electron is incident from the side lead n, we can write the wave function on the nth site on the arm as

$$\phi_n=C_L\eta_1^n+C_R\eta_2^n, \tag{3.117}$$

where $C_{L,R}$ are constants independent of n and k. $\eta_{1,2}$ are roots of the characteristic equation

$$\eta^2+\left(-2\cos k+\frac{t_x^2}{t^2}e^{ik}\right)\eta+1=0, \tag{3.118}$$

so that $\eta_1\eta_2=1$. Hereafter we choose the convention $|\eta_1|<1$. When $t_x/t\ll\sin k$, to the lowest nontrivial order in t_x/t,

$$\eta_1\approx e^{ik}\left(1-\frac{t_x^2}{t^2}\frac{e^{ik}}{2i\sin k}\right), \tag{3.119}$$

and thus $|\eta_1|^2\approx 1-t_x^2/t^2$.

Eq. (3.117) bypasses the difficulty of solving for each ϕ_n individually: on the same arm the constants C_L and C_R only change where the side lead incident amplitude $A_n^s\neq 0$.

Let us now quantify the conditions of small transmission and small reflection. Connecting

external leads smoothly to both ends of a lossy arm of length $d_A \gg 1$, we may write the scattering state wave function incident from one end as

$$\begin{cases} e^{-ikn} + \tilde{R}e^{ikn} \text{ (left lead, } n = 0,1,2,\cdots) \\ C_L\eta_1^n + C_R\eta_1^{-n} \text{ (lossy arm, } n = 1,\cdots,d_A) \\ \tilde{T}e^{ikn} \text{ (right lead, } n = 0,1,2,\cdots) \end{cases}; \tag{3.120}$$

the Schroedinger's equation then yields

$$1 + \tilde{R} = C_L + C_R, \tag{3.121a}$$

$$e^{ik} + \tilde{R}e^{-ik} = C_L\eta_1 + C_R\eta_1^{-1}, \tag{3.121b}$$

$$\tilde{T} = C_L\eta_1^{d_A+1} + C_R\eta_1^{-d_A-1}, \tag{3.121c}$$

$$\tilde{T}e^{-ik} = C_L\eta_1^{d_A} + C_R\eta_1^{-d_A}. \tag{3.121d}$$

It is now straightforward to find the transmission and reflection coefficients:

$$\tilde{T} = \frac{e^{ik}\left(e^{2ik}-1\right)\eta_1^{d_A}\left(\eta_1^2-1\right)}{1-\eta_1^{2d_A+2}+2e^{ik}\eta_1\left(\eta_1^{2d_A}-1\right)+e^{2ik}\left(\eta_1^2-\eta_1^{2d_A}\right)}, \tag{3.122a}$$

$$\tilde{R} = \frac{e^{ik}\left(\eta_1^{2d_A}-1\right)\left[e^{ik}\left(1+\eta_1^2\right)-\left(e^{2ik}+1\right)\eta_1\right]}{1-\eta_1^{2d_A+2}+2e^{ik}\eta_1\left(\eta_1^{2d_A}-1\right)+e^{2ik}\left(\eta_1^2-\eta_1^{2d_A}\right)}. \tag{3.122b}$$

At $k = 0$ or π we always have trivially $\left|\tilde{R}\right| = 1$ and $\left|\tilde{T}\right| = 0$; we therefore focus on energies that are not too close to the band edges, so that $\sin k$ is not too small. In this case, under the long arm assumption $d_A \gg 1$, the small transmission condition $\left|\tilde{T}\right| \ll 1$ is satisfied if and only if $|\eta_1|^{d_A} \ll 1$, and the small reflection condition $\left|\tilde{R}\right| \ll 1$ is satisfied if and only if $t_x \ll t$[7].

3.7.2 Background S-matrix and coupling site wave functions

We now return to the open long ring model to solve for S and Γ with the aid of Eq. (3.117). Let us denote the incident amplitude vector by

$$\left(A_1, A_2, A_0^{(L)}, \cdots, A_{d_L-1}^{(L)}, A_1^{(ref)}, \cdots, A_{d_L}^{(ref)}, A_0^{(R)}, \cdots, A_{d_R-1}^{(R)}\right)^T; \tag{3.123}$$

here $A_n^{(\alpha)}$ is the incident amplitude in the side lead attached to the nth site on arm α. We are interested in the normalization factor V_k^2 and the source-lead component of the conductance tensor

G_{12}; for this purpose, according to Eqs. (3.19) and (3.89), the first two rows of the S-matrix S and the full coupling site wave function matrix Γ must be found. In other words, we need to express the scattered amplitudes in the main leads B_1, B_2, as well as the wave functions at the coupling sites Γ_1 and Γ_2, in terms of incident amplitudes. Because the Schroedinger equation is linear and all incident amplitudes are independent, we can let all but one of the incident amplitudes be zero at a time, and obtain the full solution by means of linear superposition.

When the incident amplitudes from the side leads are all zero $A_n^{(\alpha)} = 0$, according to Eq. (3.117) the wave function at wave vector k takes the form

$$\begin{cases} A_j e^{-ikn} + B_j e^{ikn} \,(\text{main lead } j = 1,2,\, n = 0,1,2,\cdots) \\ D_L^{(L)} \eta_1^n + D_R^{(L)} \eta_1^{-n} \,(\text{left QD arm},\, n = 0,1,\cdots,d_L - 1) \\ D_L^{(ref)} \eta_1^n + D_R^{(ref)} \eta_1^{-n} \,(\text{reference arm},\, n = 1,2,\cdots,d_{ref}) \\ D_L^{(R)} \eta_1^n + D_R^{(R)} \eta_1^{-n} \,(\text{right QD arm},\, n = 0,1,\cdots,d_R - 1) \end{cases} . \tag{3.124}$$

To characterize the two Y-junctions in the AB ring, it is convenient to introduce the auxiliary objects S'_L and S'_R:

$$\begin{pmatrix} B_1 \\ D_R^{(L)} \eta_1^{-d_L+1} \\ D_L^{(ref)} \eta_1 \end{pmatrix} = S'_L \begin{pmatrix} A_1 \\ D_L^{(L)} \eta_1^{d_L-1} \\ D_R^{(ref)} \eta_1^{-1} \end{pmatrix}, \tag{3.125}$$

$$\begin{pmatrix} B_2 \\ D_R^{(R)} \eta_1^{-d_R+1} \\ D_R^{(ref)} \eta_1^{-d_{ref}} \end{pmatrix} = S'_R \begin{pmatrix} A_2 \\ D_L^{(R)} \eta_1^{d_R-1} \\ D_L^{(ref)} \eta_1^{d_{ref}} \end{pmatrix}. \tag{3.126}$$

The 3×3 matrices S'_L and S'_R are generally not unitary. They are properties of the Y-junctions, and are independent of the amplitudes (A, B etc.) and arm lengths (d_L, d_R and d_{ref}). In the limit $t_x/t \to 0$, $\eta_1 \to e^{ik}$, and S'_L and S'_R turn into the usual unitary S-matrices, which we denote as $S_{L,R} \equiv S'_{L,R}(t_x \to 0)$. For our model we can find S'_L and S'_R explicitly by solving the Schroedinger's equations below:

$$t_{JL}^L \phi_L = t\left(A_1 e^{ik} + B_1 e^{-ik}\right), \tag{3.127a}$$

$$t_{JQ}^L \phi_L = t\left(D_L^{(L)} \eta_1^{d_L} + D_R^{(L)} \eta_1^{-d_L}\right), \tag{3.127b}$$

$$t_{JR}^L \phi_L = t\left(D_L^{(ref)} + D_R^{(ref)}\right), \tag{3.127c}$$

$$(-2t\cos k)\,\phi_L = -t_{JL}^L\,(A_1+B_1) - t_{JQ}^L\left(D_L^{(L)}\eta_1^{d_L-1} + D_R^{(L)}\eta_1^{-d_L+1}\right) - t_{JR}^L\left(D_L^{(ref)}\eta_1 + D_R^{(ref)}\eta_1^{-1}\right), \tag{3.127d}$$

where ϕ_L is the wave function on the central site of the left Y-junction. We can solve for S'_R in a similar fashion.

For given A_1 and A_2, Eq. (3.124) has 8 unknowns. Now that S'_L and S'_R are known, Eqs. (3.125) and (3.126) provide us with 6 equations. The remaining two equations are the open boundary conditions at the ends of the two QD arms, appropriate when the QD is decoupled:

$$D_L^{(L)}\eta_1^{-1} + D_R^{(L)}\eta_1 = 0, \tag{3.128}$$

$$D_L^{(R)}\eta_1^{-1} + D_R^{(R)}\eta_1 = 0. \tag{3.129}$$

It is straightforward to solve the closed set of equations.

On the other hand, when we let one of the incident amplitudes in the side leads be nonzero, there are two additional amplitudes in the wave function. For instance, if $A_m^{(L)} \neq 0$ for a given m, we need to effectuate the following changes to the wave function on the left QD arm in Eq. (3.124):

$$\begin{cases} D_L^{(L1)}\eta_1^n + D_R^{(L1)}\eta_1^{-n}\,(\text{left QD arm}, n = 0,1,\cdots,m) \\ D_L^{(L2)}\eta_1^n + D_R^{(L2)}\eta_1^{-n}\,(\text{left QD arm}, n = m,m+1,\cdots,d_L-1) \end{cases}; \tag{3.130}$$

$D_{L,R}^{(L)}$ should be replaced by $D_{L,R}^{(L1)}$ in Eq. (3.128) and by $D_{L,R}^{(L2)}$ in Eq. (3.125). Furthermore, we should have two boundary conditions at site m:

$$D_L^{(L1)}\eta_1^m + D_R^{(L1)}\eta_1^{-m} = D_L^{(L2)}\eta_1^m + D_R^{(L2)}\eta_1^{-m}, \tag{3.131}$$

$$\begin{aligned} &-\left(\eta_1 + \frac{1}{\eta_1}\right)\left(D_L^{(L1)}\eta_1^m + D_R^{(L1)}\eta_1^{-m}\right) \\ &= -\left(D_L^{(L1)}\eta_1^{m-1} + D_R^{(L1)}\eta_1^{-m+1}\right) - \left(D_L^{(L2)}\eta_1^{m+1} + D_R^{(L2)}\eta_1^{-(m+1)}\right) + e^{ik}\,(2i\sin k)\,\frac{t_x}{t}A_m^{(L)}, \end{aligned} \tag{3.132}$$

thus closing the set of equations. The last equation is none other than Eq. (3.116).

We are now in a position to present the solutions for B_1, B_2 and Γ_1, Γ_2 in terms of incident amplitudes. If we assume $d_L \sim d_R \sim d_{ref}/2 \gg 1$ (comparable arm lengths and path lengths in the long ring) and $|\eta_1|^{d_L} \ll 1$ (small transmission criterion), we have to $O\left(|\eta_1|^{d_L}\right)$

$$B_1 = S'_{L11}A_1 + S'_{L13}S'_{R31}\eta_1^{d_{ref}-1}A_2 - \sum_{n=0}^{d_L-1} e^{ik}\,(2i\sin k)\,\frac{t_x}{t}\,\frac{\eta_1^{n+1}-\eta_1^{-n-1}}{\eta_1-\eta_1^{-1}}S'_{L12}\eta_1^{d_L}A_n^{(L)}$$
$$+\sum_{n=1}^{d_{ref}} e^{ik}\,(2i\sin k)\,\frac{t_x}{t}\,\frac{S'_{R33}\eta_1^{d_{ref}-n}+\eta_1^{-d_{ref}+n}}{\eta_1-\eta_1^{-1}}S'_{L13}\eta_1^{d_{ref}-1}A_n^{(ref)}, \tag{3.133a}$$

$$B_2 = S'_{L31}S'_{R13}\eta_1^{d_{ref}-1}A_1 + S'_{R11}A_2 + \sum_{n=1}^{d_{ref}} e^{ik}\,(2i\sin k)\,\frac{t_x}{t}\,\frac{\eta_1^{-n+1}+S'_{L33}\eta_1^{n-1}}{\eta_1-\eta_1^{-1}}S'_{R13}\eta_1^{d_{ref}-1}A_n^{(ref)}$$
$$-\sum_{n=0}^{d_R-1} e^{ik}\,(2i\sin k)\,\frac{t_x}{t}\,\frac{\eta_1^{n+1}-\eta_1^{-n-1}}{\eta_1-\eta_1^{-1}}S'_{R12}\eta_1^{d_R}A_n^{(R)}, \tag{3.133b}$$

$$\Gamma_1 = S'_{L21}\eta_1^{(d_L-1)}\left(1-\eta_1^2\right)A_1 - \sum_{n=0}^{d_L-1} e^{ik}\,(2i\sin k)\,\frac{t_x}{t}\left(\eta_1^{-d_L+n+1}+S'_{L22}\eta_1^{d_L-n-1}\right)\eta_1^{d_L}A_n^{(L)}$$
$$-\sum_{n=1}^{d_{ref}} e^{ik}\,(2i\sin k)\,\frac{t_x}{t}\left(S'_{R33}\eta_1^{d_{ref}-n}+\eta_1^{-d_{ref}+n}\right)S'_{L23}\eta_1^{d_L}\eta_1^{d_{ref}-1}A_n^{(ref)}, \tag{3.133c}$$

$$\Gamma_2 = S'_{R21}\eta_1^{(d_R-1)}\left(1-\eta_1^2\right)A_2 - \sum_{n=1}^{d_{ref}} e^{ik}\,(2i\sin k)\,\frac{t_x}{t}\left(\eta_1^{-n+1}+S'_{L33}\eta_1^{n-1}\right)S'_{R23}\eta_1^{d_R}\eta_1^{d_{ref}-1}A_n^{(ref)}$$
$$-\sum_{n=0}^{d_R-1} e^{ik}\,(2i\sin k)\,\frac{t_x}{t}\left(\eta_1^{-d_R+n+1}+S'_{R22}\eta_1^{d_R-n-1}\right)\eta_1^{d_R}A_n^{(R)}. \tag{3.133d}$$

3.7.3 Kondo temperature and conductance

To the lowest nontrivial order in $|\eta|^{d_L}$, Eq. (3.133d) leads to the following simple results after some algebra:

$$V_k^2 = -\left(\eta_1-\eta_1^*\right)(2i\sin k)\left(t_L^2+t_R^2\right), \tag{3.134}$$

$$S_{12}(k) = S'_{L13}S'_{R31}\eta_1^{d_{ref}-1}, \tag{3.135}$$

$$\left[S(k)\,\Gamma^\dagger(k)\,\lambda\Gamma(k)\right]_{12} = t_L t_R e^{i\varphi}\,(2i\sin k)\left(\eta_1-\eta_1^{-1}\right)S'_{L12}S'_{R21}\eta_1^{d_L+d_R}. \tag{3.136}$$

In obtaining Eq. (3.136) we have used the algebraic identity

$$S'^{*}_{L21}S'_{L11}\left|\left(1-\eta_1^2\right)\right|^2=\left(4\sin^2 k\right)\left(\frac{t_x}{t}\right)^2\left[\frac{|\eta_1|^2\,\eta_1^* S'_{L12}}{\eta_1-\eta_1^*}-\frac{|\eta_1|^2}{1-|\eta_1|^2}\left(S'^{*}_{L22}S'_{L12}+S'^{*}_{L23}S'_{L13}\right)\right]; \tag{3.137}$$

in the limit $t_x \to 0$ this is just a statement of the S-matrix unitarity.

Eq. (3.134) tells us that, in the small transmission limit, the normalization factor V_k^2 exhibits little mesoscopic fluctuation, so that $E_V \sim t$; furthermore, it does not depend on the AB phase φ at all (see Fig. 3.12). When we also impose the small reflection condition $t_x \ll t$, $\eta_1 \approx e^{ik}$ and we find $V_k^2 \approx \left(4\sin^2 k\right)\left(t_L^2+t_R^2\right)$; this is precisely the normalization factor for a QD embedded between source and drain leads. We recall from Eq. (3.27) that the normalization of Kondo coupling is governed by V_k^2. Therefore, at least for our simple model of an interacting QD, the conditions of small transmission and small reflection combine to reduce the Kondo temperature of the open long ABK ring to that of the simple embedded geometry, independent of the details of the ring or the AB flux.

Proceeding with the small transmission assumption, we observe that since $E_V \sim t$, the distinction between small and large Kondo cloud regimes is no longer applicable. This is presumably because the Kondo cloud leaks into the side leads in the open ring, and is no longer confined in a mesoscopic region as in the closed ring. The low-energy theory of our model is therefore the usual local FL. At zero temperature, the connected contribution to the conductance vanishes, and the conductance G_{12} is proportional to the disconnected transmission probability Eq. (3.45) at the Fermi energy:

$$-\mathscr{T}_{12}^{D}\left(\varepsilon_{k_F}\right)=\left|S'_{L13}S'_{R31}\eta_1^{d_{ref}-1}+\frac{2t_Lt_R}{t_L^2+t_R^2}e^{i\varphi}\frac{\eta_1-\eta_1^{-1}}{\eta_1-\eta_1^*}S'_{L12}S'_{R21}\eta_1^{d_L+d_R}\frac{1}{2}\left(e^{2i\delta_P}+1\right)\right|^2, \tag{3.138}$$

where η_1, S'_L and S'_R are all evaluated at the Fermi surface, and we have used Eqs. (3.83) and (3.86). In the small reflection limit, Eq. (3.138) becomes

$$-\mathscr{T}_{12}^{D}\left(\varepsilon_{k_F}\right)=\left|S_{L13}S_{R31}\eta_1^{d_{ref}-1}+e^{i\varphi}S_{L12}S_{R21}\eta_1^{d_L+d_R-2}t_{QD}\right|^2, \tag{3.139}$$

where $S_{L,R}\equiv S'_{L,R}\left(t_x\to 0\right)$ are the aforementioned S-matrices of the Y-junctions, and

$$t_{QD}\equiv e^{2ik}\frac{2t_Lt_R}{t_L^2+t_R^2}\frac{1}{2}\left(e^{2i\delta_P}+1\right) \tag{3.140}$$

is the transmission amplitude through an embedded QD in the Kondo limit [see Eq. (3.93)].

It is clear from Eq. (3.138) that the two-slit condition $t_{sd}=t_{ref}+t_de^{i\varphi}$ is satisfied at zero temperature. Furthermore, under the small reflection condition, both $t_{ref}=S_{L13}S_{R31}\eta_1^{d_{ref}-1}$ and $t_d=S_{L12}S_{R21}\eta_1^{d_L+d_R-2}t_{QD}$ have straightforward physical interpretations; in particular t_d can be fac-

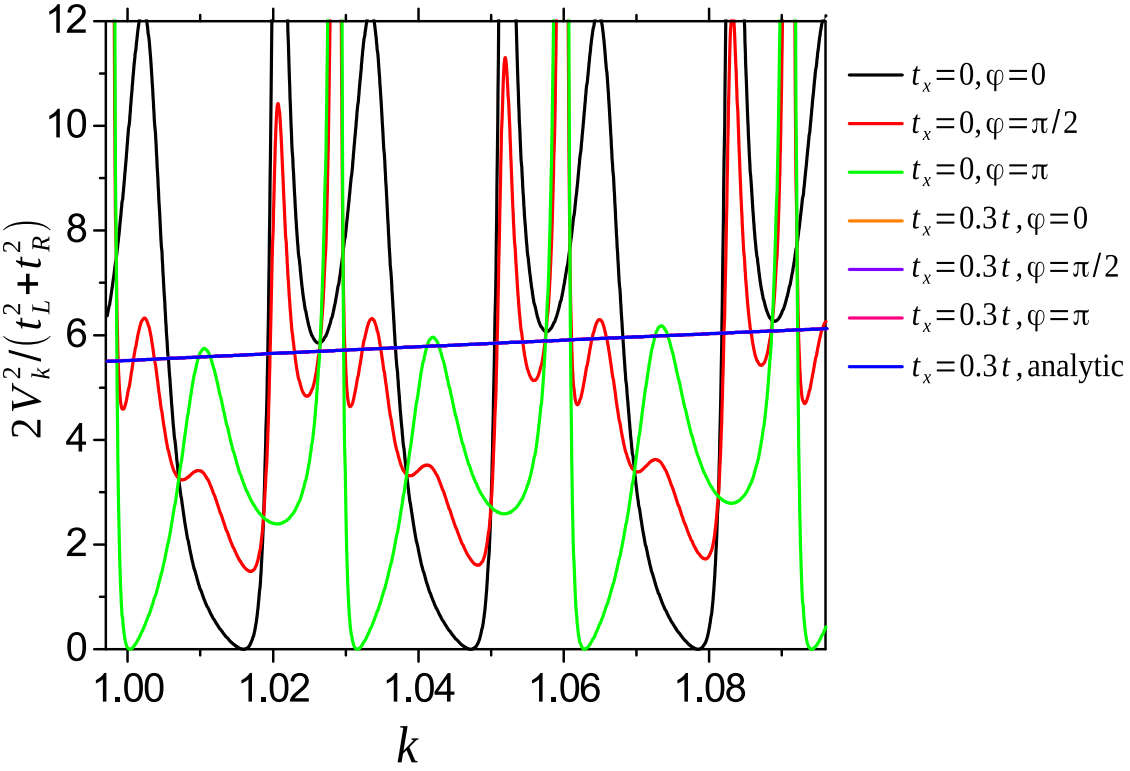

Figure 3.12: Normalization factor V_k^2 from Eq. (3.19) as a function of k for different AB phases φ in the open long ABK ring, obtained by solving the full tight-binding model. We focus on a small slice of momentum $|k-\pi/3|<0.05$. Two values of t_x are considered: $t_x=0$ corresponding to the closed ring without electron leakage, and $t_x=0.3t$ corresponding to strong leakage along and small transmission across the arms. System parameters are: $d_L=d_R=d_{ref}/2=100$, $t_{JL}^{L,R}=t_{JQ}^{L,R}=t_{JR}^{L,R}=t$, and symmetric QD coupling $t_L=t_R$. For comparison we have also plotted the analytic prediction Eq. (3.134) for $t_x=0.3t$, which agrees quantitatively with the full tight-binding solution. While V_k^2 for the closed ring is extremely sensitive to k_F and φ, the sensitivity is strongly suppressed by electron leakage, and curves for different φ overlap when $t_x=0.3t$. Since V_k^2 controls the renormalization of the Kondo coupling, the Kondo temperature of the open long ABK ring is not sensitive to mesoscopic details in the small transmission limit.

torized into a part t_{QD} which is the intrinsic transmission amplitude through QD, and a part due completely to the rest of the QD arm and the two Y-junctions.

We now consider the finite temperature conductance, assuming realistically that $T \ll t$ and $T_K \ll t$. If we further assume that the two Y-junctions are non-resonant, so that S'_L and S'_R change significantly as functions of energy only on the scale of the bandwidth $4t$, then mesoscopic fluctuations are entirely absent from Eq. (3.136), i.e. $E_{\rm conn} \sim t$. (It is worth mentioning that $E_{\rm conn}$ can be much less than t if the Y-junctions allow resonances, e.g. when the central site of each Y-junction is weakly coupled to all three legs; however, $E_V \sim t$ even in this case.) Since $T \ll E_{\rm conn}$, we can comfortably eliminate the connected contribution and use Eq. (3.89). At $T \ll T_K$ the total FL regime conductance $G(T,\varphi) \equiv -G_{12}$ is found to $O(T/T_K)^2$[112]:

$$G(T,\varphi) \equiv G_{ref} + G_d + 2\sqrt{G_{ref}G_d}\left\{\cos(\varphi+\theta+\delta_P) - \left(\frac{\pi T}{T_K}\right)^2 \times \left[\frac{\cos(\varphi+\theta+\delta_P)}{2\cos^2\delta_P} - \tan\delta_P \sin(\varphi+\theta+\delta_P)\right]\right\}. \tag{3.141a}$$

Here the conductance through the reference path is defined as

$$G_{ref} \equiv \frac{2e^2}{h}\left|S'_{L13}S'_{R31}\eta_1^{d_{ref}-1}\right|^2, \tag{3.141b}$$

the conductance through the QD path is defined as

$$G_d(T) = G_d^{(0)}\left[\cos^2\delta_P - \left(\frac{\pi T}{T_K}\right)^2 \cos 2\delta_P\right] \tag{3.141c}$$

with its $T=0$ and $\delta_P = 0$ value

$$G_d^{(0)} \equiv \frac{2e^2}{h}\frac{4t_L^2 t_R^2}{\left(t_L^2+t_R^2\right)^2}\left|\frac{\eta_1-\eta_1^{-1}}{\eta_1-\eta_1^*}S'_{L12}S'_{R21}\eta_1^{d_L+d_R}\right|^2, \tag{3.141d}$$

and finally the non-magnetic phase difference between the QD path and the reference path (*including* the QD) in the absence of δ_P is

$$\theta = \arg\left(\frac{\eta_1-\eta_1^{-1}}{\eta_1-\eta_1^*}\eta_1^{d_L+d_R-d_{ref}+1}\frac{S'_{L12}S'_{R21}}{S'_{L13}S'_{R31}}\right). \tag{3.141e}$$

Once again, η_1, S'_L and S'_R are all evaluated at the Fermi surface.

For $T \gg T_K$, we discuss two different scenarios: the particle-hole symmetric case and the strongly particle-hole asymmetric case. In the particle-hole symmetric case, as explained in Section 3.4, the potential scattering term K vanishes, and the $O\left(J^2\right)$ connected contribution plays an

important role. Inserting Eqs. (3.134)–(3.136) into Eqs. (3.81) and (3.79), we find the total high-temperature conductance in the particle-hole symmetric case to be

$$G(T,\varphi) = G_{ref} + G_d + 2\frac{\sqrt{3}}{4}\frac{\pi}{\ln\frac{T}{T_K}}\sqrt{G_{ref}G_d}\cos(\varphi+\theta). \tag{3.142}$$

Here the conductance through the reference path G_{ref} is given as before, while the conductance through the QD path has the usual logarithmic temperature dependence,

$$G_d(T) \equiv \frac{3}{16}\frac{\pi^2}{\ln^2\frac{T}{T_K}}G_d^{(0)}. \tag{3.143}$$

We have taken into account the renormalization of the Kondo coupling, Eq. (3.28); thermal averaging cuts off the logarithm at T. For our slowly varying V_k^2 given by Eq. (3.134), $\overline{V_k^2}$ is simply the Fermi surface value $V_{k_F}^2$, and the Kondo temperature is defined by Eq. (3.29).

Comparing Eqs. (3.141a) and (3.142) and noting that $\delta_P = 0$, we find that there is no phase shift between $T \ll T_K$ and $T \gg T_K$ in the presence of particle-hole symmetry, which is consistent with e.g. Fig. 4(d) of Ref. [43]. We also observe that the particle-hole symmetric normalized visibility η_v, defined in Eq. (3.114), has a characteristic logarithmic behavior at $T \gg T_K$:

$$\eta_v = \frac{3}{16}\frac{\pi^2}{\ln^2\frac{T}{T_K}}. \tag{3.144}$$

On the other hand, to demonstrate the $\pi/2$ phase shift due to Kondo physics, it is more useful to consider the case of relatively strong particle-hole asymmetry $\kappa \sim j(T)$ at $T \gg T_K$. The leading contribution to the conductance from potential scattering is $O(K)$, and the leading contribution from the Kondo coupling is $O\left(J^2\right)$; therefore, $\kappa \sim j(T)$ indicates that we may neglect the Kondo coupling altogether at temperature T. To the lowest order in potential scattering $O(K)$, Eq. (3.80) applies; also, since $T \ll t$, the thermal averging in Eq. (3.79) becomes trivial. Using the relation between K and δ_P, Eq. (3.84), we finally obtain

$$G(T,\varphi) = G_{ref} + 2\sqrt{G_{ref}G_d^{(0)}}\tan\delta_P\sin(\varphi+\theta). \tag{3.145}$$

Comparing Eqs. (3.141a) and (3.145), it becomes evident that transmission through the QD undergoes a $\pi/2+\delta_P$ phase shift from $T \gg T_K$ to $T \ll T_K$ as the Kondo correlations are switched on; see Fig. 3.13. We remark that the strongly particle-hole asymmetric case represents the situation without Kondo correlation whereas the particle-hole symmetric case does not. This is because in the latter case the leading QD contribution to the conductance is $O\left(J^2\right)$, which is of Kondo origin as we have discussed above Eq. (3.70).

We can again make a direct comparison with Eq. (3.114). While θ itself is not necessarily $\pi/2$, φ_t is experimentally observed with respect to its value with Kondo correlations turned off, so we

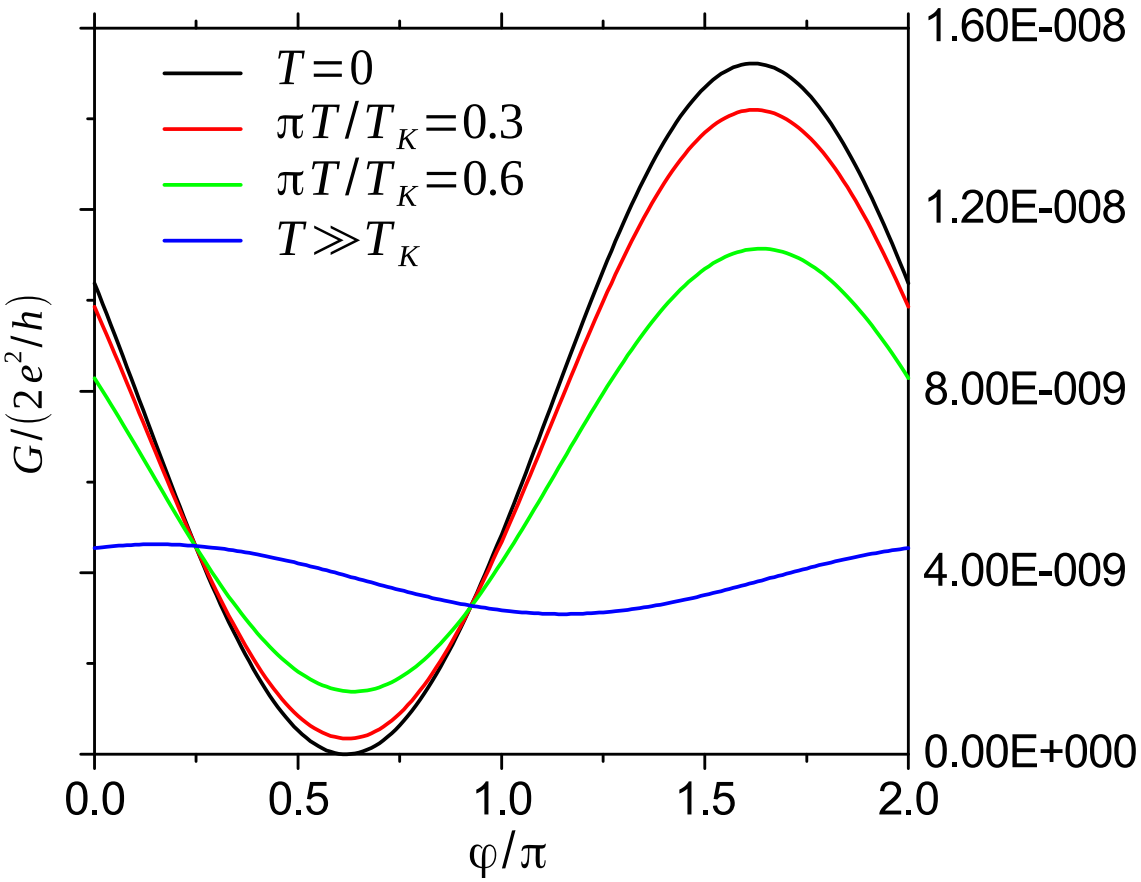

Figure 3.13: Low-temperature and high-temperature conductances G as functions of AB phase φ in the open long ABK ring with a particle-hole asymmetric QD, calculated with Eqs. (3.141a) and (3.145). We assume $T_K \ll t$ so that the thermal averaging in the high temperature case is trivial. System parameters are: $t_x = 0.3t$, $k_F = \pi/3$, $d_L = d_R = d_{ref}/2 = 100$, $t_{JL}^{L,R} = t_{JQ}^{L,R} = t_{JR}^{L,R} = t$, and particle-hole symmetry breaking phase shift $\delta_P = 0.1$. A phase shift of approximately $\pi/2$ is clearly visible as the temperature is lowered and Kondo correlations become important.

should define the reference value $\varphi_t^{(0)}$ by e.g. comparing with Eq. (3.145):

$$\varphi_t^{(0)} = \theta - \frac{\pi}{2}. \tag{3.146}$$

Therefore, to $O(T/T_K)^2$ we readily obtain the following results for the $T \ll T_K$ transmission phase and the normalized visibility[112]:

$$\varphi_t - \varphi_t^{(0)} = \frac{\pi}{2} + \delta_P - \left(\frac{\pi T}{T_K}\right)^2 \tan\delta_P, \tag{3.147}$$

$$\eta_v = 1 - \left(\frac{\pi T}{T_K}\right)^2 \frac{1}{\cos^2 \delta_P}. \tag{3.148}$$

These are in agreement with the $|\delta_P| \ll 1$, $T = 0$ and $\delta_P = 0$, $T \ll T_K$ results of Ref. [23], which assumes $\varphi_t^{(0)} = 0$, i.e. the non-magnetic phase difference between the two paths is zero without Kondo correlations. Note that in obtaining the T dependence in Eq. (3.148) it is crucial to include the connected contribution to conductance.

We stress that our $O(T/T_K)^2$ results for the transmission phase across the QD and the normalized visibility, Eqs. (3.147) and (3.148), are both exact in δ_P, which is non-universal and encompasses the effects of all particle-hole symmetry breaking perturbation. In particular, the $(T/T_K)^2$ coefficients were not reported previously.

3.8 Conclusion and open questions

One question we have not so far addressed is the low-energy physics in the small Kondo cloud regime, $T \ll T_K$ and $E_V \ll T_K$; here E_V is the energy scale below which the normalization factor V_k^2 controlling the Kondo temperature varies slowly, and $E_V \gtrsim E_{\text{conn}}$. We assume E_V and E_{conn} are of the same order of magnitude, a condition satisfied by both the closed ring ($E_V \sim E_{\text{conn}} \sim v_F/L$) and the open ring with non-resonant Y-junctions ($E_V \sim E_{\text{conn}} \sim t$). For temperatures above the mesoscopic energy scale $E_V \ll T \ll T_K$, we are no longer able to eliminate the connected contribution. However, because $T \gg E_V$ one can argue that physics associated with the energy scale E_V is smeared out by thermal fluctuations, and the mesoscopic system behaves as a bulk system with parameters showing no mesoscopic fluctuations[71]. On the other hand, below the mesoscopic energy scale $T \ll E_V \ll T_K$, since for $T \ll E_{\text{conn}}$ our formalism predicts that the connected part can be eliminated, the knowledge of the screening channel T-matrix in the single-particle sector alone is adequate for us to predict the conductance. Ref. [71] again offers an appealing hypothesis: the low-energy effective theory is again a FL theory, with the T-matrix governed by Kondo physics at short range $\sim O(L_K) = O(v_F/T_K)$ and modulated by mesoscopic fluctuations at long range $\sim O(L)$. This scenario leads to a quasiparticle spectrum which is in qualitative agreement with slave boson mean field theory[71]. The FL picture is often analyzed by a renormalized perturbation theory of the quasiparticles, where the bare parameters of the QD are replaced by renormalized values; in particular the large U between bare electrons is replaced by a small renormalized $\tilde{U}$ between quasiparticles[49]. In the small Kondo cloud regime, we expect that the real space geometry in the renormalized perturbation theory resembles that of the bare theory[116]; thus a perturbation theory calculation in U in our formalism is potentially useful in understanding the low-energy physics, as long as U is interpreted as the effective $\tilde{U}$. It will be interesting to test this $E_V \ll T_K$ picture, along with our perturbative predictions on conductance in other parameter regimes in this chapter, against results obtained from the numerical RG algorithm[5, 43, 50].

There is also an issue regarding the assumption of a single-level QD in the Kondo regime. To experimentally detect the $\pi/2$ phase shift in an AB interferometer, one typically sweeps the plunger gate voltage on the QD, and monitors the phase shift between consecutive Coulomb blockade peaks. A $\pi/2$ plateau should be observed at $T \lesssim T_K$ near the center of each Coulomb valley deep in the local moment regime, with an odd number of electrons on the QD[43, 123]. However, one needs to adopt a multi-level QD model to quantitatively reproduce the experimental results, in particular the phase shift lineshape asymmetry relative to the center of a valley, and also possibly a phase lapse inside the valley[113, 123]. A generalization of the current formalism to the multi-level case is necessary in order to quantify the influence of the interferometer on the measured transmission phase shift through a realistic QD.

Another natural open problem is the extension to the multi-channel Kondo physics. In our generalized Anderson model, separation of screening and non-screening channels is achieved in a single-level QD, and there is only one effective screening channel. Exotic physics emerges in the presence of two or more screening channels, realizable in e.g. a many-QD system[3, 92, 101]. In the 2-channel Kondo effect with identical couplings to two channels, for example, the low-energy physics is governed by a non-FL RG fixed point: at zero temperature a single particle scattered by the impurity can only enter a many-body state, and there are no elastic single-particle scattering events[134]. Ref. [23] discusses the manifestations of the 2-channel Kondo physics in the two-path interferometer, but again makes the two-slit assumption without examining its validity. Therefore an extension of our approach to the multi-channel case will be useful to justify the two-slit assumption in the open long ring and thus the 2-channel predictions of Ref. [23].

To conclude this chapter, we generalized the method developed in Ref. [66] to calculate the linear dc conductance tensor of a generic multi-terminal Anderson model with an interacting QD. The linear dc conductance of the system has a disconnected contribution of the Landauer form, and a connected contribution which is also a Fermi surface property. At temperatures low compared to the mesoscopic energy scale below which the background S-matrix and the coupling site wave functions vary slowly, $T \ll E_{\text{conn}}$, the connected contribution can be approximately eliminated using properties of the conductance tensor; the elimination procedure physically corresponds to probing the current response or applying the bias voltages in a particular manner. At temperatures high compared to the Kondo temperature $T \gg T_K$ this connected part is computed explicitly to $O\left(J^2\right)$, and found to be of the same order of magnitude as the disconnected part in the case of a particle-hole symmetric QD.

With this method we scrutinize both closed and open long ABK ring models. We find modifications to early results on the closed ring with a long reference arm of length L: the high-temperature conductance at $T \gg T_K$ should have qualitatively distinct behaviors for $T \gg v_F/L$ and $T \ll v_F/L$. In the open ring we conclude that the two-path interferometer is realized when the arms on the ring have weak transmission and weak reflection, and demonstrate the possibility to observe in this de-

vice the $\pi/2$ phase shift due to Kondo physics, and the suppression of AB oscillation visibility due to inelastic scattering.

Table 3.1: Different regimes of energy scales discussed in this chapter. T, T_K and E_V are respectively the temperature, the Kondo temperature, and the energy scale over which V_k^2 varies significantly. We also assume $E_{\text{conn}} \sim E_V$, where E_{conn} is the energy scale over which S and Γ vary significantly. For the low-temperature conductance in the small Kondo cloud regime, see discussion in Section 3.8.

	Weak-coupling perturbation theory applies	T_K depends on mesoscopic details	Connected part elimination possible
$T \gg T_K \gg E_V$	Yes	No	No
$T \gg E_V \gg T_K$	Yes	Yes	No
$E_V \gg T \gg T_K$	Yes	Yes	Yes

	FL perturbation theory applies	T_K depends on mesoscopic details	Connected part elimination possible
$T \ll T_K \ll E_V$	Yes	Yes	Yes
$T \ll E_V \ll T_K$	?	No	Yes
$E_V \ll T \ll T_K$	?	No	No

Chapter 4

Conclusions

In this thesis, we have discussed the transport properties of two types of multi-terminal interacting systems: junctions of interacting quantum wires attached to TLL leads, and closed and open long ABK rings. In both cases, we obtain corrections to the non-interacting Landauer formula, arising from interactions in the TLL leads and the QD in the Kondo regime respectively.

In Chapter 2 we examine junctions of multiple interacting quantum wires, focusing on the case without resonances. The significance of these systems derives from their pervasiveness in quantum circuits and also their demonstration of strongly-correlated TLL physics. Working in the fermionic language, we treat the interaction in the wires and the leads as a perturbation. In the absence of interactions, the Hamiltonian is fully determined by the single-particle scattering S-matrix, which defines the behavior of scattering state wave functions away from the junction. When the interactions are introduced, we may continue to diagonalize the quadratic part of the Hamiltonian and characterize its eigenstates (the scattering basis) in terms of a single-particle S-matrix. This also allows us to represent the interactions in the scattering basis. Treating the S-matrix elements as running coupling constants, it is possible to perform a Wilsonian RG calculation that determines the renormalization of the S-matrix.

If the quantum wires are attached to TLL leads, i.e. the interaction does not vanish even at $x \to \infty$, it is known from bosonization that the Landauer description of the conductance is inadequate. To directly investigate the linear dc conductance with TLL leads in the fermionic formalism, we employ the CS formulation of the RG, computing the conductance as a function of the renormalized S-matrix using the Kubo formula, and demanding that the conductance be independent of the ultraviolet cutoff.

We confirm that the S-matrix RG equation from the Wilsonian RG is reproduced in the CS approach at the first order in interaction, and generalize the RG equation to the RPA in a form independent of the number of leads to which the junction is connected. Meanwhile, the conductance itself depends on whether there is a residual interaction in the leads. If the wires are attached to FL

leads, i.e. the interaction becomes negligible far from the junction, our calculations justify the formal use of the Landauer formula, with the renormalized S-matrix elements as its input parameters. On the other hand, if the wires are attached to TLL leads, we find an additional contribution to the conductance, which depends on the interaction strength in the leads. This is true both at the first order in interaction and in the RPA; in particular, introducing a "contact resistance" between an FL lead and a TLL lead, we are able to justify the heuristic relation between the FL conductance and the TLL conductance, previously proposed in the context of bosonization. Our calculations recover the conductance of a single quantum wire connected to either FL leads or TLL leads, and furthermore provide an explanation for the conductance at the M fixed point of a spinless Y-junction connected to TLL leads, which was obtained numerically through density matrix renormalization group.

In Chapter 3 we discuss long ABK rings, where the interaction is assumed to be limited to the QD. Our motivation is rooted in the prospect of probing the Kondo physics in mesoscopic structures, such as the elusive Kondo screening cloud and the famous $\pi/2$ phase shift associated with scattering by the Kondo singlet. We introduce a very generic multi-terminal single-impurity Anderson model, with a background S-matrix and a coupling site wave function matrix as its input parameters. Our model is not only suitable for describing closed and long ABK rings, but also capable of reproducing many previously studied single-QD devices, including the QD embedded between source and drain leads, the QD embedded in a finite-length quantum wire, as well as the short ABK ring.

We first rewrite the model in terms of non-screening channels and a single screening channel, where only the screening channel interacts with the Anderson impurity, and the non-screening channels are merely free electrons. In the local moment regime, a Schrieffer-Wolff transformation leads to a Kondo model for the screening channel; it contains a Kondo coupling term and a potential scattering term, both of which may be strongly momentum-dependent. This momentum dependence can result in two different parameter regimes for the Kondo temperature T_K: the small Kondo cloud regime $T_K \gg E_V$ and the large Kondo cloud regime $T_K \ll E_V$, where E_V is the characteristic energy scale of the function that controls the renormalization of the Kondo coupling.

Turning to the linear dc conductance, we find that as in the short ABK ring case, the linear dc conductance consists of two parts: a "disconnected part" of the Landauer form coming from both screening and non-screening channels, and a "connected part" for the interacting screening channel only. The disconnected contribution involves the screening channel single-particle T-matrix, and at low temperatures can be intuitively understood as the result of imposing a QD-induced phase shift on the screening channel. The connected contribution is shown to be a Fermi surface property (as is the disconnected contribution), and can be eliminated at temperatures low relative to the characteristic energy scale of the background S-matrix and the coupling site wave function matrix. We are also able to compute the linear dc conductance explicitly when perturbation theories apply; these include the weak-coupling perturbation theory valid at high temperatures $T \gg T_K$, and the FL perturbation theory valid *in the large cloud regime* at low temperatures $T \ll T_K$.

Applying our formalism to closed long ABK rings, where the electric current is conserved along each ring arm, we reproduce earlier results on the AB flux dependence of T_K in both the small cloud regime and the large cloud regime. We also find that at high temperatures $T \gg T_K$, the conductance shows qualitatively different flux and Fermi energy dependences for temperatures higher than and lower than the characteristic energy scale v_F/L, where v_F is the Fermi velocity of the conduction band and L is the circumference of the ring. On the other hand, in an open long ABK ring where electrons may leak out of the ring from side leads, we find that the model simulates an AB interferometer which inherits the T_K of the QD when it is embedded directly between source and drain leads, provided the lossy ring arms have both small transmission and small reflection. Furthermore, as we turn on Kondo correlations on the QD by changing the temperature from well above the Kondo temperature to well below, the AB-flux-dependent conductance of the interferometer is predicted to truthfully reflect the $\pi/2$ Kondo phase shift.

Bibliography

[1] I. Affleck. Conformal field theory approach to the kondo effect. *Acta Physica Polonica. Series B*, 26(12):1869–1932, 1995. → pages 54

[2] I. Affleck. The kondo screening cloud: What it is and how to observe it. In *Perspectives Of Mesoscopic Physics: Dedicated to Yoseph Imry's 70th Birthday*, pages 1–44. World Scientific, 2010. → pages 57

[3] I. Affleck and A. W. W. Ludwig. Exact conformal-field-theory results on the multichannel kondo effect: Single-fermion green's function, self-energy, and resistivity. *Phys. Rev. B*, 48: 7297–7321, Sep 1993. doi:10.1103/PhysRevB.48.7297. URL http://link.aps.org/doi/10.1103/PhysRevB.48.7297. → pages 62, 77, 78, 103, 149

[4] I. Affleck and P. Simon. Detecting the kondo screening cloud around a quantum dot. *Phys. Rev. Lett.*, 86:2854–2857, Mar 2001. doi:10.1103/PhysRevLett.86.2854. URL http://link.aps.org/doi/10.1103/PhysRevLett.86.2854. → pages 6

[5] I. Affleck, L. Borda, and H. Saleur. Friedel oscillations and the kondo screening cloud. *Phys. Rev. B*, 77:180404, May 2008. doi:10.1103/PhysRevB.77.180404. URL http://link.aps.org/doi/10.1103/PhysRevB.77.180404. → pages 77, 102

[6] A. Aharony and O. Entin-Wohlman. Measuring the kondo effect in the aharonov-bohm interferometer. *Phys. Rev. B*, 72:073311, Aug 2005. doi:10.1103/PhysRevB.72.073311. URL http://link.aps.org/doi/10.1103/PhysRevB.72.073311. → pages 8, 89

[7] A. Aharony, O. Entin-Wohlman, B. I. Halperin, and Y. Imry. Phase measurement in the mesoscopic aharonov-bohm interferometer. *Phys. Rev. B*, 66:115311, Sep 2002. doi:10.1103/PhysRevB.66.115311. URL http://link.aps.org/doi/10.1103/PhysRevB.66.115311. → pages 7, 89, 90, 91, 93

[8] J. Alicea, Y. Oreg, G. Refael, F. von Oppen, and M. P. A. Fisher. Non-abelian statistics and topological quantum information processing in 1d wire networks. *Nature Phys.*, 7:412, 2011. doi:10.1038/nphys1915. → pages 1

[9] P. W. Anderson. A poor man's derivation of scaling laws for the kondo problem. *J. Phys. C*, 3(12):2436, 1970. URL http://stacks.iop.org/0022-3719/3/i=12/a=008. → pages 6

[10] W. Apel and T. M. Rice. Combined effect of disorder and interaction on the conductance of a one-dimensional fermion system. *Phys. Rev. B*, 26:7063–7065, Dec 1982.

doi:10.1103/PhysRevB.26.7063. URL http://link.aps.org/doi/10.1103/PhysRevB.26.7063. → pages 5

[11] D. N. Aristov and P. Wölfle. Transport of interacting electrons through a potential barrier: Nonperturbative rg approach. *Europhys. Lett.*, 82(2):27001, 2008. URL http://stacks.iop.org/0295-5075/82/i=2/a=27001. → pages 4, 5, 8, 41, 42, 49, 52, 122, 129

[12] D. N. Aristov and P. Wölfle. Conductance through a potential barrier embedded in a luttinger liquid: Nonuniversal scaling at strong coupling. *Phys. Rev. B*, 80:045109, Jul 2009. doi:10.1103/PhysRevB.80.045109. URL http://link.aps.org/doi/10.1103/PhysRevB.80.045109. → pages 30, 39, 129

[13] D. N. Aristov and P. Wölfle. Transport properties of a y junction connecting luttinger liquid wires. *Phys. Rev. B*, 84:155426, Oct 2011. doi:10.1103/PhysRevB.84.155426. URL http://link.aps.org/doi/10.1103/PhysRevB.84.155426. → pages 4, 5, 8, 41, 42, 44, 52, 123, 124, 125, 126, 127, 131

[14] D. N. Aristov and P. Wölfle. Transport through asymmetric two-lead junctions of luttinger liquid wires. *Lith. J. Phys.*, 52:2353, 2012. doi:10.3952/physics.v52i2.2353. URL http://dx.doi.org/10.3952/physics.v52i2.2353. → pages 129

[15] D. N. Aristov and P. Wölfle. Chiral y junction of luttinger liquid wires at strong coupling: Fermionic representation. *Phys. Rev. B*, 88:075131, Aug 2013. doi:10.1103/PhysRevB.88.075131. URL http://link.aps.org/doi/10.1103/PhysRevB.88.075131. → pages 4, 5, 8, 41, 42, 44, 50, 52, 122, 123, 124, 125, 126, 127, 130, 131, 132

[16] D. N. Aristov, A. P. Dmitriev, I. V. Gornyi, V. Y. Kachorovskii, D. G. Polyakov, and P. Wölfle. Tunneling into a luttinger liquid revisited. *Phys. Rev. Lett.*, 105:266404, Dec 2010. doi:10.1103/PhysRevLett.105.266404. URL http://link.aps.org/doi/10.1103/PhysRevLett.105.266404. → pages 4

[17] M. Avinun-Kalish, M. Heiblum, O. Zarchin, D. Mahalu, and V. Umansky. Crossover from 'mesoscopic' to 'universal' phase for electron transmission in quantum dots. *Nature*, 436: 529–533, Jul 2005. doi:10.1038/nature03899. → pages 7

[18] X. Barnabé-Thériault, A. Sedeki, V. Meden, and K. Schönhammer. Junctions of one-dimensional quantum wires: Correlation effects in transport. *Phys. Rev. B*, 71:205327, May 2005. doi:10.1103/PhysRevB.71.205327. URL http://link.aps.org/doi/10.1103/PhysRevB.71.205327. → pages 4

[19] X. Barnabé-Thériault, A. Sedeki, V. Meden, and K. Schönhammer. Junction of three quantum wires: Restoring time-reversal symmetry by interaction. *Phys. Rev. Lett.*, 94: 136405, Apr 2005. doi:10.1103/PhysRevLett.94.136405. URL http://link.aps.org/doi/10.1103/PhysRevLett.94.136405. → pages 4, 5

[20] B. Bellazzini, M. Mintchev, and P. Sorba. Bosonization and scale invariance on quantum wires. *J. Phys. A*, 40(10):2485, 2007. URL http://stacks.iop.org/1751-8121/40/i=10/a=017. → pages 135

[21] L. Borda, L. Fritz, N. Andrei, and G. Zaránd. Theory of inelastic scattering from quantum impurities. *Phys. Rev. B*, 75:235112, Jun 2007. doi:10.1103/PhysRevB.75.235112. URL http://link.aps.org/doi/10.1103/PhysRevB.75.235112. → pages 6

[22] C. Bruder, R. Fazio, and H. Schoeller. Aharonov-bohm oscillations and resonant tunneling in strongly correlated quantum dots. *Phys. Rev. Lett.*, 76:114–117, Jan 1996. doi:10.1103/PhysRevLett.76.114. URL http://link.aps.org/doi/10.1103/PhysRevLett.76.114. → pages 7

[23] A. Carmi, Y. Oreg, M. Berkooz, and D. Goldhaber-Gordon. Transmission phase shifts of kondo impurities. *Phys. Rev. B*, 86:115129, Sep 2012. doi:10.1103/PhysRevB.86.115129. URL http://link.aps.org/doi/10.1103/PhysRevB.86.115129. → pages 7, 8, 9, 89, 90, 102, 103

[24] P. S. Cornaglia and C. A. Balseiro. Kondo impurities in nanoscopic systems: Confinement-induced regimes. *Phys. Rev. B*, 66:115303, Sep 2002. doi:10.1103/PhysRevB.66.115303. URL http://link.aps.org/doi/10.1103/PhysRevB.66.115303. → pages 6

[25] P. S. Cornaglia and C. A. Balseiro. Transport through quantum dots in mesoscopic circuits. *Phys. Rev. Lett.*, 90:216801, May 2003. doi:10.1103/PhysRevLett.90.216801. URL http://link.aps.org/doi/10.1103/PhysRevLett.90.216801. → pages 6

[26] S. M. Cronenwett, T. H. Oosterkamp, and L. P. Kouwenhoven. A tunable kondo effect in quantum dots. *Science*, 281(5376):540–544, 1998. ISSN 0036-8075. doi:10.1126/science.281.5376.540. URL http://science.sciencemag.org/content/281/5376/540. → pages 5

[27] S. Das and S. Rao. Duality between normal and superconducting junctions of multiple quantum wires. *Phys. Rev. B*, 78:205421, Nov 2008. doi:10.1103/PhysRevB.78.205421. URL http://link.aps.org/doi/10.1103/PhysRevB.78.205421. → pages 4

[28] S. Das, S. Rao, and D. Sen. Renormalization group study of the conductances of interacting quantum wire systems with different geometries. *Phys. Rev. B*, 70:085318, Aug 2004. doi:10.1103/PhysRevB.70.085318. URL http://link.aps.org/doi/10.1103/PhysRevB.70.085318. → pages 4

[29] S. Das, S. Rao, and A. Saha. Renormalization group study of transport through a superconducting junction of multiple one-dimensional quantum wires. *Phys. Rev. B*, 77: 155418, Apr 2008. doi:10.1103/PhysRevB.77.155418. URL http://link.aps.org/doi/10.1103/PhysRevB.77.155418. → pages 4

[30] S. Das, S. Rao, and A. Saha. Systematic stability analysis of the renormalization group flow for the normal-superconductor-normal junction of luttinger liquid wires. *Phys. Rev. B*, 79: 155416, Apr 2009. doi:10.1103/PhysRevB.79.155416. URL http://link.aps.org/doi/10.1103/PhysRevB.79.155416. → pages 4

[31] S. Das Sarma, M. Freedman, and C. Nayak. Majorana zero modes and topological quantum computation. *Npj Quantum Inform.*, 1:15001, 2015. doi:10.1038/npjqi.2015.1. → pages 1

[32] C. de C. Chamon and E. Fradkin. Distinct universal conductances in tunneling to quantum hall states: The role of contacts. *Phys. Rev. B*, 56:2012–2025, Jul 1997. doi:10.1103/PhysRevB.56.2012. URL https://link.aps.org/doi/10.1103/PhysRevB.56.2012. → pages 16

[33] I. V. Dinu, M. Ţolea, and A. Aldea. Transport through a multiply connected interacting mesoscopic system using the keldysh formalism. *Phys. Rev. B*, 76:113302, Sep 2007. doi:10.1103/PhysRevB.76.113302. URL http://link.aps.org/doi/10.1103/PhysRevB.76.113302. → pages 7, 8

[34] I. Dzyaloshinskii and A. Larkin. Correlation functions for a one-dimensional fermi system with long-range interaction (tomonaga model). *Sov. Phys. JETP*, 38:202, Jan 1974. URL http://www.jetp.ac.ru/cgi-bin/e/index/e/38/1/p202?a=list. → pages 27, 52

[35] E. N. Economou and C. M. Soukoulis. Static conductance and scaling theory of localization in one dimension. *Phys. Rev. Lett.*, 46:618–621, Mar 1981. doi:10.1103/PhysRevLett.46.618. URL http://link.aps.org/doi/10.1103/PhysRevLett.46.618. → pages 32

[36] T. Enss, V. Meden, S. Andergassen, X. Barnabé-Thériault, W. Metzner, and K. Schönhammer. Impurity and correlation effects on transport in one-dimensional quantum wires. *Phys. Rev. B*, 71:155401, Apr 2005. doi:10.1103/PhysRevB.71.155401. URL http://link.aps.org/doi/10.1103/PhysRevB.71.155401. → pages 4

[37] O. Entin-Wohlman, A. Aharony, and Y. Meir. Kondo effect in complex mesoscopic structures. *Phys. Rev. B*, 71:035333, Jan 2005. doi:10.1103/PhysRevB.71.035333. URL http://link.aps.org/doi/10.1103/PhysRevB.71.035333. → pages 8

[38] D. S. Fisher and P. A. Lee. Relation between conductivity and transmission matrix. *Phys. Rev. B*, 23:6851–6854, Jun 1981. doi:10.1103/PhysRevB.23.6851. URL http://link.aps.org/doi/10.1103/PhysRevB.23.6851. → pages 32

[39] L. Fritz and M. Vojta. Phase transitions in the pseudogap anderson and kondo models: Critical dimensions, renormalization group, and local-moment criticality. *Phys. Rev. B*, 70: 214427, Dec 2004. doi:10.1103/PhysRevB.70.214427. URL http://link.aps.org/doi/10.1103/PhysRevB.70.214427. → pages 85

[40] A. Furusaki and N. Nagaosa. Resonant tunneling in a luttinger liquid. *Phys. Rev. B*, 47: 3827–3831, Feb 1993. doi:10.1103/PhysRevB.47.3827. URL http://link.aps.org/doi/10.1103/PhysRevB.47.3827. → pages 4, 16

[41] A. Furusaki and N. Nagaosa. Single-barrier problem and anderson localization in a one-dimensional interacting electron system. *Phys. Rev. B*, 47:4631–4643, Feb 1993. doi:10.1103/PhysRevB.47.4631. URL http://link.aps.org/doi/10.1103/PhysRevB.47.4631. → pages 4, 16

[42] A. Furusaki and N. Nagaosa. Tunneling through a barrier in a tomonaga-luttinger liquid connected to reservoirs. *Phys. Rev. B*, 54:R5239–R5242, Aug 1996.

doi:10.1103/PhysRevB.54.R5239. URL
http://link.aps.org/doi/10.1103/PhysRevB.54.R5239. → pages 5, 11, 13, 30, 31

[43] U. Gerland, J. von Delft, T. A. Costi, and Y. Oreg. Transmission phase shift of a quantum dot with kondo correlations. *Phys. Rev. Lett.*, 84:3710–3713, Apr 2000. doi:10.1103/PhysRevLett.84.3710. URL
http://link.aps.org/doi/10.1103/PhysRevLett.84.3710. → pages 100, 102, 103

[44] T. Giamarchi. *Quantum Physics in One Dimension*. International Series of Monographs on Physics. Clarendon Press, 2004. ISBN 9780198525004. → pages 1, 11, 14

[45] D. Giuliano and A. Nava. Dual fermionic variables and renormalization group approach to junctions of strongly interacting quantum wires. *Phys. Rev. B*, 92:125138, Sep 2015. doi:10.1103/PhysRevB.92.125138. URL
http://link.aps.org/doi/10.1103/PhysRevB.92.125138. → pages 4, 52

[46] L. Glazman and M. Raikh. Resonant kondo transparency of a barrier with quasilocal impurity states. *JETP Lett.*, 47:452, 1988. URL
http://www.jetpletters.ac.ru/ps/1095/article_16538.shtml. → pages 7

[47] L. I. Glazman and M. Pustilnik. *Nanophysics: Coherence and Transport*, pages 427–478. Elsevier, 2005. → pages 5, 78

[48] D. Goldhaber-Gordon, H. Shtrikman, D. Mahalu, D. Abusch-Magder, U. Meirav, and M. A. Kastner. Kondo effect in a single-electron transistor. *Nature*, 391:156–159, Jan 1998. doi:10.1038/34373. → pages 5

[49] A. Hewson. *The Kondo Problem to Heavy Fermions*. Cambridge Studies in Magnetism. Cambridge University Press, 1997. ISBN 9780521599474. → pages 6, 61, 63, 102

[50] W. Hofstetter, J. König, and H. Schoeller. Kondo correlations and the fano effect in closed aharonov-bohm interferometers. *Phys. Rev. Lett.*, 87:156803, Sep 2001. doi:10.1103/PhysRevLett.87.156803. URL
http://link.aps.org/doi/10.1103/PhysRevLett.87.156803. → pages 102

[51] C.-Y. Hou, A. Rahmani, A. E. Feiguin, and C. Chamon. Junctions of multiple quantum wires with different luttinger parameters. *Phys. Rev. B*, 86:075451, Aug 2012. doi:10.1103/PhysRevB.86.075451. URL
http://link.aps.org/doi/10.1103/PhysRevB.86.075451. → pages 4, 16, 20, 21, 43, 52, 130

[52] T. Hyart, B. van Heck, I. C. Fulga, M. Burrello, A. R. Akhmerov, and C. W. J. Beenakker. Flux-controlled quantum computation with majorana fermions. *Phys. Rev. B*, 88:035121, Jul 2013. doi:10.1103/PhysRevB.88.035121. URL
https://link.aps.org/doi/10.1103/PhysRevB.88.035121. → pages 1

[53] T. Ihn. *Electronic Quantum Transport in Mesoscopic Semiconductor Structures*. Springer Tracts in Modern Physics. Springer New York, 2004. ISBN 9780387218281. → pages 1, 2, 3

[54] Y. Imry. *Introduction to Mesoscopic Physics*. Mesoscopic physics and nanotechnology. Oxford University Press, 2002. ISBN 9780198507383. → pages 2, 3

[55] K.-I. Imura, K.-V. Pham, P. Lederer, and F. Piéchon. Conductance of one-dimensional quantum wires. *Phys. Rev. B*, 66:035313, Jul 2002. doi:10.1103/PhysRevB.66.035313. URL http://link.aps.org/doi/10.1103/PhysRevB.66.035313. → pages 2, 5

[56] K. Janzen, V. Meden, and K. Schönhammer. Influence of the contacts on the conductance of interacting quantum wires. *Phys. Rev. B*, 74:085301, Aug 2006. doi:10.1103/PhysRevB.74.085301. URL http://link.aps.org/doi/10.1103/PhysRevB.74.085301. → pages 5

[57] A.-P. Jauho, N. S. Wingreen, and Y. Meir. Time-dependent transport in interacting and noninteracting resonant-tunneling systems. *Phys. Rev. B*, 50:5528–5544, Aug 1994. doi:10.1103/PhysRevB.50.5528. URL http://link.aps.org/doi/10.1103/PhysRevB.50.5528. → pages 7

[58] Y. Ji, M. Heiblum, D. Sprinzak, D. Mahalu, and H. Shtrikman. Phase evolution in a kondo-correlated system. *Science*, 290(5492):779–783, 2000. ISSN 0036-8075. doi:10.1126/science.290.5492.779. URL http://science.sciencemag.org/content/290/5492/779. → pages 7

[59] Y. Ji, M. Heiblum, and H. Shtrikman. Transmission phase of a quantum dot with kondo correlation near the unitary limit. *Phys. Rev. Lett.*, 88:076601, Jan 2002. doi:10.1103/PhysRevLett.88.076601. URL http://link.aps.org/doi/10.1103/PhysRevLett.88.076601. → pages 7

[60] C. L. Kane and M. P. A. Fisher. Transmission through barriers and resonant tunneling in an interacting one-dimensional electron gas. *Phys. Rev. B*, 46:15233–15262, Dec 1992. doi:10.1103/PhysRevB.46.15233. URL http://link.aps.org/doi/10.1103/PhysRevB.46.15233. → pages 4, 16

[61] C. L. Kane and M. P. A. Fisher. Transport in a one-channel luttinger liquid. *Phys. Rev. Lett.*, 68:1220–1223, Feb 1992. doi:10.1103/PhysRevLett.68.1220. URL http://link.aps.org/doi/10.1103/PhysRevLett.68.1220. → pages 4, 5, 11, 16

[62] V. Kashcheyevs, A. Aharony, and O. Entin-Wohlman. Applicability of the equations-of-motion technique for quantum dots. *Phys. Rev. B*, 73:125338, Mar 2006. doi:10.1103/PhysRevB.73.125338. URL http://link.aps.org/doi/10.1103/PhysRevB.73.125338. → pages 8

[63] R. K. Kaul, D. Ullmo, S. Chandrasekharan, and H. U. Baranger. Mesoscopic kondo problem. *Europhys. Lett.*, 71(6):973, 2005. URL http://stacks.iop.org/0295-5075/71/i=6/a=973. → pages 6

[64] R. K. Kaul, G. Zaránd, S. Chandrasekharan, D. Ullmo, and H. U. Baranger. Spectroscopy of the kondo problem in a box. *Phys. Rev. Lett.*, 96:176802, May 2006. doi:10.1103/PhysRevLett.96.176802. URL http://link.aps.org/doi/10.1103/PhysRevLett.96.176802. → pages 6

[65] A. Kawabata. On the renormalization of conductance in tomonaga-luttinger liquid. *J. Phys. Soc. Japan*, 65(1):30–32, 1996. doi:10.1143/JPSJ.65.30. → pages 2, 5

[66] Y. Komijani, R. Yoshii, and I. Affleck. Interaction effects in aharonov-bohm˘kondo rings. *Phys. Rev. B*, 88:245104, Dec 2013. doi:10.1103/PhysRevB.88.245104. URL http://link.aps.org/doi/10.1103/PhysRevB.88.245104. → pages xi, 7, 9, 58, 63, 65, 67, 68, 69, 71, 72, 74, 76, 77, 80, 85, 86, 87, 103, 134, 143

[67] J. Kondo. Resistance minimum in dilute magnetic alloys. *Prog. Theor. Phys.*, 32(1):37–49, 1964. doi:10.1143/PTP.32.37. → pages 6, 61, 74

[68] S. Lal, S. Rao, and D. Sen. Transport through quasiballistic quantum wires: The role of contacts. *Phys. Rev. Lett.*, 87:026801, Jun 2001. doi:10.1103/PhysRevLett.87.026801. URL http://link.aps.org/doi/10.1103/PhysRevLett.87.026801. → pages 5

[69] S. Lal, S. Rao, and D. Sen. Conductance through contact barriers of a finite-length quantum wire. *Phys. Rev. B*, 65:195304, Apr 2002. doi:10.1103/PhysRevB.65.195304. URL http://link.aps.org/doi/10.1103/PhysRevB.65.195304. → pages 5

[70] S. Lal, S. Rao, and D. Sen. Junction of several weakly interacting quantum wires: A renormalization group study. *Phys. Rev. B*, 66:165327, Oct 2002. doi:10.1103/PhysRevB.66.165327. URL http://link.aps.org/doi/10.1103/PhysRevB.66.165327. → pages 4, 8, 30, 40, 44, 50, 122, 124, 127

[71] D. E. Liu, S. Burdin, H. U. Baranger, and D. Ullmo. From weak- to strong-coupling mesoscopic fermi liquids. *Europhys. Lett.*, 97(1):17006, 2012. URL http://stacks.iop.org/0295-5075/97/i=1/a=17006. → pages 6, 63, 102

[72] D. E. Liu, S. Burdin, H. U. Baranger, and D. Ullmo. Mesoscopic anderson box: Connecting weak to strong coupling. *Phys. Rev. B*, 85:155455, Apr 2012. doi:10.1103/PhysRevB.85.155455. URL http://link.aps.org/doi/10.1103/PhysRevB.85.155455. → pages 6

[73] D. Loss and D. P. DiVincenzo. Quantum computation with quantum dots. *Phys. Rev. A*, 57: 120–126, Jan 1998. doi:10.1103/PhysRevA.57.120. URL https://link.aps.org/doi/10.1103/PhysRevA.57.120. → pages 1

[74] G. Mahan. *Many-Particle Physics*. Physics of Solids and Liquids. Springer, 2000. ISBN 9780306463389. → pages 34, 69, 74, 150, 153

[75] J. Malecki and I. Affleck. Influence of interference on the kondo effect in a quantum dot. *Phys. Rev. B*, 82:165426, Oct 2010. doi:10.1103/PhysRevB.82.165426. URL http://link.aps.org/doi/10.1103/PhysRevB.82.165426. → pages xi, 7, 58, 67, 73, 77, 80, 83

[76] D. L. Maslov and M. Stone. Landauer conductance of luttinger liquids with leads. *Phys. Rev. B*, 52:R5539–R5542, Aug 1995. doi:10.1103/PhysRevB.52.R5539. URL http://link.aps.org/doi/10.1103/PhysRevB.52.R5539. → pages 5, 11, 13

[77] K. A. Matveev, D. Yue, and L. I. Glazman. Tunneling in one-dimensional non-luttinger electron liquid. *Phys. Rev. Lett.*, 71:3351–3354, Nov 1993. doi:10.1103/PhysRevLett.71.3351. URL http://link.aps.org/doi/10.1103/PhysRevLett.71.3351. → pages 4, 26, 30, 40, 49, 122

[78] V. Meden and U. Schollwöck. Conductance of interacting nanowires. *Phys. Rev. B*, 67: 193303, May 2003. doi:10.1103/PhysRevB.67.193303. URL http://link.aps.org/doi/10.1103/PhysRevB.67.193303. → pages 4

[79] V. Meden, W. Metzner, U. Schollwöck, and K. Schönhammer. A single impurity in a luttinger liquid: How it "cuts" the chain. *J. Low Temp. Phys.*, 126(3):1147–1163. ISSN 1573-7357. doi:10.1023/A:1013823514926. URL http://dx.doi.org/10.1023/A:1013823514926. → pages

[80] V. Meden, W. Metzner, U. Schollwöck, and K. Schönhammer. Scaling behavior of impurities in mesoscopic luttinger liquids. *Phys. Rev. B*, 65:045318, Jan 2002. doi:10.1103/PhysRevB.65.045318. URL http://link.aps.org/doi/10.1103/PhysRevB.65.045318. → pages

[81] V. Meden, S. Andergassen, W. Metzner, U. Schollwöck, and K. Schönhammer. Scaling of the conductance in a quantum wire. *Europhys. Lett.*, 64(6):769–775, 2003. doi:10.1209/epl/i2003-00624-x. URL http://dx.doi.org/10.1209/epl/i2003-00624-x. → pages 4

[82] Y. Meir and N. S. Wingreen. Landauer formula for the current through an interacting electron region. *Phys. Rev. Lett.*, 68:2512–2515, Apr 1992. doi:10.1103/PhysRevLett.68.2512. URL http://link.aps.org/doi/10.1103/PhysRevLett.68.2512. → pages 7

[83] T. Micklitz, A. Altland, T. A. Costi, and A. Rosch. Universal dephasing rate due to diluted kondo impurities. *Phys. Rev. Lett.*, 96:226601, Jun 2006. doi:10.1103/PhysRevLett.96.226601. URL http://link.aps.org/doi/10.1103/PhysRevLett.96.226601. → pages 6

[84] A. E. Miroshnichenko, S. Flach, and Y. S. Kivshar. Fano resonances in nanoscale structures. *Rev. Mod. Phys.*, 82:2257–2298, Aug 2010. doi:10.1103/RevModPhys.82.2257. URL http://link.aps.org/doi/10.1103/RevModPhys.82.2257. → pages 82

[85] A. K. Mitchell, M. Becker, and R. Bulla. Real-space renormalization group flow in quantum impurity systems: Local moment formation and the kondo screening cloud. *Phys. Rev. B*, 84:115120, Sep 2011. doi:10.1103/PhysRevB.84.115120. URL https://link.aps.org/doi/10.1103/PhysRevB.84.115120. → pages 57

[86] C. Nayak, M. P. A. Fisher, A. W. W. Ludwig, and H. H. Lin. Resonant multilead point-contact tunneling. *Phys. Rev. B*, 59:15694–15704, Jun 1999. doi:10.1103/PhysRevB.59.15694. URL http://link.aps.org/doi/10.1103/PhysRevB.59.15694. → pages 52

[87] Y. V. Nazarov and L. I. Glazman. Resonant tunneling of interacting electrons in a one-dimensional wire. *Phys. Rev. Lett.*, 91:126804, Sep 2003. doi:10.1103/PhysRevLett.91.126804. URL http://link.aps.org/doi/10.1103/PhysRevLett.91.126804. → pages 4

[88] T. K. Ng and P. A. Lee. On-site coulomb repulsion and resonant tunneling. *Phys. Rev. Lett.*, 61:1768–1771, Oct 1988. doi:10.1103/PhysRevLett.61.1768. URL http://link.aps.org/doi/10.1103/PhysRevLett.61.1768. → pages 67

[89] P. Nozières. A "fermi-liquid" description of the kondo problem at low temperatures. *J. Low Temp. Phys.*, 17(1):31–42, 1974. ISSN 1573-7357. doi:10.1007/BF00654541. URL http://dx.doi.org/10.1007/BF00654541. → pages 6, 151

[90] M. Ogata and H. Fukuyama. Collapse of quantized conductance in a dirty tomonaga-luttinger liquid. *Phys. Rev. Lett.*, 73:468–471, Jul 1994. doi:10.1103/PhysRevLett.73.468. URL http://link.aps.org/doi/10.1103/PhysRevLett.73.468. → pages 5

[91] Y. Oreg and A. M. Finkel'stein. dc transport in quantum wires. *Phys. Rev. B*, 54: R14265–R14268, Nov 1996. doi:10.1103/PhysRevB.54.R14265. URL http://link.aps.org/doi/10.1103/PhysRevB.54.R14265. → pages 2, 5

[92] Y. Oreg and D. Goldhaber-Gordon. Two-channel kondo effect in a modified single electron transistor. *Phys. Rev. Lett.*, 90:136602, Apr 2003. doi:10.1103/PhysRevLett.90.136602. URL http://link.aps.org/doi/10.1103/PhysRevLett.90.136602. → pages 103

[93] M. Oshikawa, C. Chamon, and I. Affleck. Junctions of three quantum wires. *J. Stat. Mech.*, 2006(02):P02008, 2006. URL http://stacks.iop.org/1742-5468/2006/i=02/a=P02008. → pages 4, 5, 16, 22, 30, 31, 43, 52, 127

[94] J. Park, S.-S. B. Lee, Y. Oreg, and H.-S. Sim. How to directly measure a kondo cloud's length. *Phys. Rev. Lett.*, 110:246603, Jun 2013. doi:10.1103/PhysRevLett.110.246603. URL http://link.aps.org/doi/10.1103/PhysRevLett.110.246603. → pages 6

[95] R. G. Pereira, N. Laflorencie, I. Affleck, and B. I. Halperin. Kondo screening cloud and charge staircase in one-dimensional mesoscopic devices. *Phys. Rev. B*, 77:125327, Mar 2008. doi:10.1103/PhysRevB.77.125327. URL http://link.aps.org/doi/10.1103/PhysRevB.77.125327. → pages 6

[96] A. Perelomov, Â. Zel'dovič, and I. Zeldovich. *Quantum Mechanics: Selected Topics*. Selected Topics Series. World Scientific, 1998. ISBN 9789810235505. → pages 135

[97] K.-V. Pham, F. Piéchon, K.-I. Imura, and P. Lederer. Tomonaga-luttinger liquid with reservoirs in a multiterminal geometry. *Phys. Rev. B*, 68:205110, Nov 2003. doi:10.1103/PhysRevB.68.205110. URL http://link.aps.org/doi/10.1103/PhysRevB.68.205110. → pages 5

[98] F. Pierre and N. O. Birge. Dephasing by extremely dilute magnetic impurities revealed by aharonov-bohm oscillations. *Phys. Rev. Lett.*, 89:206804, Oct 2002.

doi:10.1103/PhysRevLett.89.206804. URL http://link.aps.org/doi/10.1103/PhysRevLett.89.206804. → pages 6

[99] D. G. Polyakov and I. V. Gornyi. Transport of interacting electrons through a double barrier in quantum wires. *Phys. Rev. B*, 68:035421, Jul 2003. doi:10.1103/PhysRevB.68.035421. URL http://link.aps.org/doi/10.1103/PhysRevB.68.035421. → pages 4, 5

[100] V. V. Ponomarenko. Renormalization of the one-dimensional conductance in the luttinger-liquid model. *Phys. Rev. B*, 52:R8666–R8667, Sep 1995. doi:10.1103/PhysRevB.52.R8666. URL http://link.aps.org/doi/10.1103/PhysRevB.52.R8666. → pages 5, 11

[101] R. M. Potok, I. G. Rau, H. Shtrikman, Y. Oreg, and D. Goldhaber-Gordon. Observation of the two-channel kondo effect. *Nature*, 446:167–171, Mar 2007. doi:10.1038/nature05556. → pages 103

[102] M. Pustilnik and L. Glazman. Kondo effect in quantum dots. *J. Phys. Condens. Matter*, 16 (16):R513, 2004. URL http://stacks.iop.org/0953-8984/16/i=16/a=R01. → pages 5, 76, 80

[103] M. Pustilnik and L. I. Glazman. Kondo effect induced by a magnetic field. *Phys. Rev. B*, 64: 045328, Jul 2001. doi:10.1103/PhysRevB.64.045328. URL http://link.aps.org/doi/10.1103/PhysRevB.64.045328. → pages 7

[104] A. Rahmani, C.-Y. Hou, A. Feiguin, M. Oshikawa, C. Chamon, and I. Affleck. General method for calculating the universal conductance of strongly correlated junctions of multiple quantum wires. *Phys. Rev. B*, 85:045120, Jan 2012. doi:10.1103/PhysRevB.85.045120. URL http://link.aps.org/doi/10.1103/PhysRevB.85.045120. → pages 2, 5, 51, 52

[105] I. Safi. Conductance of a quantum wire: Landauer's approach versus the kubo formula. *Phys. Rev. B*, 55:R7331–R7334, Mar 1997. doi:10.1103/PhysRevB.55.R7331. URL http://link.aps.org/doi/10.1103/PhysRevB.55.R7331. → pages 5, 11, 13

[106] I. Safi and H. J. Schulz. Transport in an inhomogeneous interacting one-dimensional system. *Phys. Rev. B*, 52:R17040–R17043, Dec 1995. doi:10.1103/PhysRevB.52.R17040. URL http://link.aps.org/doi/10.1103/PhysRevB.52.R17040. → pages 5, 11, 13

[107] J. R. Schrieffer and P. A. Wolff. Relation between the anderson and kondo hamiltonians. *Phys. Rev.*, 149:491–492, Sep 1966. doi:10.1103/PhysRev.149.491. URL http://link.aps.org/doi/10.1103/PhysRev.149.491. → pages 61

[108] R. Schuster, E. Buks, M. Heiblum, D. Mahalu, V. Umansky, and H. Shtrikman. Phase measurement in a quantum dot via a double-slit interference experiment. *Nature*, 385: 417–420, Jan 1997. doi:10.1038/385417a0. → pages 7

[109] R. Shankar. Renormalization-group approach to interacting fermions. *Rev. Mod. Phys.*, 66: 129–192, Jan 1994. doi:10.1103/RevModPhys.66.129. URL http://link.aps.org/doi/10.1103/RevModPhys.66.129. → pages 28, 152

[110] Z. Shi. Impurity entropy of junctions of multiple quantum wires. *J. Stat. Mech.*, 2016(6): 063106, 2016. URL http://stacks.iop.org/1742-5468/2016/i=6/a=063106. → pages 122

[111] Z. Shi and I. Affleck. Fermionic approach to junctions of multiple quantum wires attached to tomonaga-luttinger liquid leads. *Phys. Rev. B*, 94:035106, Jul 2016. doi:10.1103/PhysRevB.94.035106. URL https://link.aps.org/doi/10.1103/PhysRevB.94.035106. → pages 1, 8, 10, 41, 44, 51

[112] Z. Shi and Y. Komijani. Conductance of closed and open long aharonov-bohm-kondo rings. *Phys. Rev. B*, 95:075147, Feb 2017. doi:10.1103/PhysRevB.95.075147. URL https://link.aps.org/doi/10.1103/PhysRevB.95.075147. → pages 2, 8, 54, 57, 62, 66, 72, 78, 87, 99, 101, 134, 144

[113] P. G. Silvestrov and Y. Imry. Enhanced sensitivity of the transmission phase of a quantum dot to kondo correlations. *Phys. Rev. Lett.*, 90:106602, Mar 2003. doi:10.1103/PhysRevLett.90.106602. URL http://link.aps.org/doi/10.1103/PhysRevLett.90.106602. → pages 103

[114] F. Simmel, R. H. Blick, J. P. Kotthaus, W. Wegscheider, and M. Bichler. Anomalous kondo effect in a quantum dot at nonzero bias. *Phys. Rev. Lett.*, 83:804–807, Jul 1999. doi:10.1103/PhysRevLett.83.804. URL http://link.aps.org/doi/10.1103/PhysRevLett.83.804. → pages 5

[115] P. Simon and I. Affleck. Persistent currents through a quantum dot. *Phys. Rev. B*, 64: 085308, Aug 2001. doi:10.1103/PhysRevB.64.085308. URL http://link.aps.org/doi/10.1103/PhysRevB.64.085308. → pages 6

[116] P. Simon and I. Affleck. Finite-size effects in conductance measurements on quantum dots. *Phys. Rev. Lett.*, 89:206602, Oct 2002. doi:10.1103/PhysRevLett.89.206602. URL http://link.aps.org/doi/10.1103/PhysRevLett.89.206602. → pages xi, 6, 58, 62, 63, 81, 102

[117] P. Simon and I. Affleck. Kondo screening cloud effects in mesoscopic devices. *Phys. Rev. B*, 68:115304, Sep 2003. doi:10.1103/PhysRevB.68.115304. URL http://link.aps.org/doi/10.1103/PhysRevB.68.115304. → pages 6

[118] P. Simon, O. Entin-Wohlman, and A. Aharony. Flux-dependent kondo temperature in an aharonov-bohm interferometer with an in-line quantum dot. *Phys. Rev. B*, 72:245313, Dec 2005. doi:10.1103/PhysRevB.72.245313. URL http://link.aps.org/doi/10.1103/PhysRevB.72.245313. → pages 6, 8, 89

[119] P. Simon, J. Salomez, and D. Feinberg. Transport spectroscopy of a kondo quantum dot coupled to a finite size grain. *Phys. Rev. B*, 73:205325, May 2006. doi:10.1103/PhysRevB.73.205325. URL http://link.aps.org/doi/10.1103/PhysRevB.73.205325. → pages 6

[120] N. J. A. Sloane. Sequence a000108. *The On-Line Encyclopedia of Integer Sequences*, page Sequence A000108, 2010. URL http://oeis.org/A000108. → pages 46, 47

[121] N. J. A. Sloane. Sequence a008315. *The On-Line Encyclopedia of Integer Sequences*, page Sequence A008315, 2010. URL http://oeis.org/A008315. → pages 46, 48

[122] J. Sólyom. *Fundamentals of the Physics of Solids: Volume 3 - Normal, Broken-Symmetry, and Correlated Systems*. Theoretical Solid State Physics: Interaction Among Electrons. Springer Berlin Heidelberg, 2010. ISBN 9783642045189. → pages 11

[123] S. Takada, C. Bäuerle, M. Yamamoto, K. Watanabe, S. Hermelin, T. Meunier, A. Alex, A. Weichselbaum, J. von Delft, A. Ludwig, A. D. Wieck, and S. Tarucha. Transmission phase in the kondo regime revealed in a two-path interferometer. *Phys. Rev. Lett.*, 113: 126601, Sep 2014. doi:10.1103/PhysRevLett.113.126601. URL http://link.aps.org/doi/10.1103/PhysRevLett.113.126601. → pages 7, 103

[124] W. B. Thimm, J. Kroha, and J. von Delft. Kondo box: A magnetic impurity in an ultrasmall metallic grain. *Phys. Rev. Lett.*, 82:2143–2146, Mar 1999. doi:10.1103/PhysRevLett.82.2143. URL http://link.aps.org/doi/10.1103/PhysRevLett.82.2143. → pages 6

[125] R. Thomale and A. Seidel. Minimal model of quantized conductance in interacting ballistic quantum wires. *Phys. Rev. B*, 83:115330, Mar 2011. doi:10.1103/PhysRevB.83.115330. URL http://link.aps.org/doi/10.1103/PhysRevB.83.115330. → pages 2, 5, 11, 13

[126] M. Titov, M. Müller, and W. Belzig. Interaction-induced renormalization of andreev reflection. *Phys. Rev. Lett.*, 97:237006, Dec 2006. doi:10.1103/PhysRevLett.97.237006. URL http://link.aps.org/doi/10.1103/PhysRevLett.97.237006. → pages 4

[127] W. G. van der Wiel, S. D. Franceschi, T. Fujisawa, J. M. Elzerman, S. Tarucha, and L. P. Kouwenhoven. The kondo effect in the unitary limit. *Science*, 289(5487):2105–2108, 2000. ISSN 0036-8075. doi:10.1126/science.289.5487.2105. URL http://science.sciencemag.org/content/289/5487/2105. → pages 5

[128] M. Vojta and L. Fritz. Upper critical dimension in a quantum impurity model: Critical theory of the asymmetric pseudogap kondo problem. *Phys. Rev. B*, 70:094502, Sep 2004. doi:10.1103/PhysRevB.70.094502. URL http://link.aps.org/doi/10.1103/PhysRevB.70.094502. → pages 85

[129] K. G. Wilson. The renormalization group: Critical phenomena and the kondo problem. *Rev. Mod. Phys.*, 47:773–840, Oct 1975. doi:10.1103/RevModPhys.47.773. URL http://link.aps.org/doi/10.1103/RevModPhys.47.773. → pages 6

[130] E. Wong and I. Affleck. Tunneling in quantum wires: A boundary conformal field theory approach. *Nucl. Phys. B*, 417(3):403 – 438, 1994. ISSN 0550-3213. doi:http://dx.doi.org/10.1016/0550-3213(94)90479-0. URL http://www.sciencedirect.com/science/article/pii/0550321394904790. → pages 4, 16

[131] R. Yoshii and M. Eto. Scaling analysis of kondo screening cloud in a mesoscopic ring with an embedded quantum dot. *Phys. Rev. B*, 83:165310, Apr 2011. doi:10.1103/PhysRevB.83.165310. URL http://link.aps.org/doi/10.1103/PhysRevB.83.165310. → pages 6, 7, 62, 82, 84, 85, 87, 89

[132] D. Yue, L. I. Glazman, and K. A. Matveev. Conduction of a weakly interacting one-dimensional electron gas through a single barrier. *Phys. Rev. B*, 49:1966–1975, Jan

1994. doi:10.1103/PhysRevB.49.1966. URL
http://link.aps.org/doi/10.1103/PhysRevB.49.1966. → pages 4, 26, 27, 40, 49, 122

[133] M. Zaffalon, A. Bid, M. Heiblum, D. Mahalu, and V. Umansky. Transmission phase of a singly occupied quantum dot in the kondo regime. *Phys. Rev. Lett.*, 100:226601, Jun 2008. doi:10.1103/PhysRevLett.100.226601. URL
http://link.aps.org/doi/10.1103/PhysRevLett.100.226601. → pages 7

[134] G. Zaránd, L. Borda, J. von Delft, and N. Andrei. Theory of inelastic scattering from magnetic impurities. *Phys. Rev. Lett.*, 93:107204, Sep 2004. doi:10.1103/PhysRevLett.93.107204. URL
http://link.aps.org/doi/10.1103/PhysRevLett.93.107204. → pages 6, 68, 73, 103

Appendices

Appendix A

S-matrix RG equation and fixed points for 2-lead junctions and Y-junctions

In this appendix we explicitly write down the S-matrix RG equations specific to 2-lead junctions and Y-junctions, both at the first order[70, 77, 132] (Eq. (2.72)) and in the RPA[11–15] (Eq. (2.106)). We show that in all these cases it is possible to eliminate the phases, resulting in a set of equations containing only the transmission/reflection probability matrix W (again $W_{jj'} \equiv \left|S_{jj'}\right|^2$). The fixed points of these equations are then listed and their stability analyzed, for comparison with the bosonization results in Section 2.2[110]. For simplicity, unless otherwise stated, we assume throughout this appendix that the interactions in the wires and leads are uniform and identical, $\alpha_n(x) = \alpha_n$ for any n.

A.1 First order in interaction

A.1.1 2-lead junction

For the transmission amplitude S_{12}, Eq. (2.72) becomes

$$-\frac{dS_{12}}{d\ln D} = -\frac{1}{2}\left(\alpha_1 W_{11} + \alpha_2 W_{22}\right) S_{12}. \tag{A.1}$$

In the 2-lead junction, unitarity implies $W_{11} = W_{22} = 1 - W_{12}$. Therefore, we have the following equation for $W_{12} \equiv |S_{12}|^2$,

$$-\frac{dW_{12}}{d\ln D} = -(\alpha_1+\alpha_2)\,W_{12}\,(1-W_{12}). \tag{A.2}$$

In the vicinity of the complete reflection fixed point N ($W_{12}=0$), linearizing Eq. (A.2), we find $-dW_{12}/d\ln D \approx -(\alpha_1+\alpha_2)\,W_{12}$; thus the N fixed point has a scaling exponent for the conductance $-(\alpha_1+\alpha_2)$, and is stable if $-(\alpha_1+\alpha_2)<0$ and unstable if $-(\alpha_1+\alpha_2)>0$. Similarly, the perfect transmission fixed point D ($W_{12}=1$) has a conductance scaling exponent $\alpha_1+\alpha_2$, and is stable if $\alpha_1+\alpha_2<0$ and unstable if $\alpha_1+\alpha_2>0$.

A.1.2 Y-junction

For a Y-junction, from Eq. (2.72)

$$-\frac{dS_{12}}{d\ln D} = -\frac{1}{2}\left(\alpha_1 W_{11}S_{12} + \alpha_2 W_{22}S_{12} + \alpha_3 S_{13}S^*_{33}S_{32}\right). \tag{A.3}$$

To reduce this to an equation involving W only, we need to relate the product $S^*_{12}S_{13}S^*_{33}S_{32}$ to W. This is achieved by taking advantage of unitarity of the S-matrix:

$$S^*_{12}S_{13}S^*_{33}S_{32} + \text{c.c.} = W_{23}W_{22} - W_{13}W_{12} - W_{33}W_{32}. \tag{A.4}$$

Thus, the RG equation obeyed by W_{12} takes the form

$$-\frac{dW_{12}}{d\ln D} = -(\alpha_1 W_{11} + \alpha_2 W_{22})\,W_{12} - \frac{1}{2}\alpha_3\left(W_{23}W_{22} - W_{13}W_{12} - W_{33}W_{32}\right). \tag{A.5}$$

Unitarity dictates that there are only 4 independent matrix elements of W. Following Refs. [13, 15], we parametrize the W matrix by four real numbers $(a,b,c,\bar{c})$ as follows:

$$W = \frac{1}{6}\begin{pmatrix} 2+3a+b-\sqrt{3}\,(c+\bar{c}) & 2-3a+b-\sqrt{3}\,(c-\bar{c}) & 2\left(1-b+\sqrt{3}c\right) \\ 2-3a+b+\sqrt{3}\,(c-\bar{c}) & 2+3a+b+\sqrt{3}\,(c+\bar{c}) & 2\left(1-b-\sqrt{3}c\right) \\ 2\left(1-b+\sqrt{3}\bar{c}\right) & 2\left(1-b-\sqrt{3}\bar{c}\right) & 2\,(1+2b) \end{pmatrix}. \tag{A.6}$$

In the presence of time-reversal symmetry, $c=\bar{c}$. If wires 1 and 2 are symmetrically coupled to the junction, $c=-\bar{c}$; we further find $a=b$ if Z_3 symmetry exists for the non-interacting system.

Eq. (2.72) and Eq. (A.6) now lead to a closed set of equations for a, b, c and $\bar{c}$,

$$-\frac{da}{d\ln D} = \frac{1}{12}\left[(\alpha_1+\alpha_2)\left(3+a+3b-6a^2-ab-c\bar{c}\right)-(\alpha_1-\alpha_2)\sqrt{3}\,(1-2a)\,(c+\bar{c})\right] + \frac{1}{3}\alpha_3\,(a-ab-c\bar{c}), \tag{A.7a}$$

$$-\frac{db}{d\ln D} = \frac{1}{12}\left[(\alpha_1+\alpha_2)\left(1+3a+b-2b^2-3ab-3c\bar{c}\right)+(\alpha_1-\alpha_2)\sqrt{3}\,(1+2b)\,(c+\bar{c})\right] + \frac{1}{3}\alpha_3\left(1+b-2b^2\right), \tag{A.7b}$$

$$-\frac{dc}{d\ln D} = \frac{1}{12}\left[-(\alpha_1+\alpha_2)\,(c\,(1+2b+6a)-3\bar{c})+\sqrt{3}\,(\alpha_1-\alpha_2)\left(-1-a+b+ab+2c^2+c\bar{c}\right)\right] - \frac{1}{3}\alpha_3\,(1+2b)\,c, \tag{A.7c}$$

$$-\frac{d\bar{c}}{d\ln D} = \frac{1}{12}\left[-(\alpha_1+\alpha_2)\,(\bar{c}\,(1+2b+6a)-3c)+\sqrt{3}\,(\alpha_1-\alpha_2)\left(-1-a+b+ab+2\bar{c}^2+c\bar{c}\right)\right] - \frac{1}{3}\alpha_3\,(1+2b)\,\bar{c}. \tag{A.7d}$$

After finding a fixed point $(a_0, b_0, c_0, \bar{c}_0)$ of Eq. (A.7d), we can again linearize the equations[13, 15] by expanding in terms of small deviations from the fixed point, $\mathbf{x} \equiv (a-a_0, b-b_0, c-c_0, \bar{c}-\bar{c}_0)$:

$$-\frac{d\mathbf{x}}{d\ln D} = \mathbf{M}\mathbf{x}. \tag{A.8}$$

The 4×4 matrix $\mathbf{M}$ have eigenvalues λ_l with corresponding left eigenvectors $\mathbf{v}_l$, $l = 1, 2, 3, 4$. For an RG flow starting in the vicinity of the fixed point in question, the solution to Eq. (A.8) takes the form

$$\mathbf{x}(D) = \sum_{j=1}^{4} C_l \left(\frac{D_0}{D}\right)^{\lambda_l} \mathbf{v}_l, \tag{A.9}$$

where C_j are constants and D_0 is the ultraviolet cutoff. λ_l thus controls the stability of the fixed point: $\mathbf{v}_l$ is a stable scaling direction if $\lambda_l < 0$, and an unstable one if $\lambda_l > 0$. For a junction attached to FL leads, replacing D by the temperature T in Eq. (A.9), we will find the low temperature conductance at a stable fixed point with all $\lambda_l < 0$, or the high temperature conductance at a completely unstable fixed point with all $\lambda_l > 0$; thus λ_l are the scaling exponents of the conductance. (λ_l are generally not the same with the S-matrix scaling exponents discussed in Ref. [70].)

In the following we list λ_l for the first order fixed points and discuss their physical meanings.

N **fixed point**: $(a_0, b_0, c_0, \bar{c}_0) = (1,1,0,0)$; $\lambda_{N,1} = -(\alpha_2+\alpha_3)$, $\lambda_{N,2} = -(\alpha_3+\alpha_1)$, $\lambda_{N,3} = -(\alpha_1+\alpha_2)$ and $\lambda_{N,4} = -(\alpha_1+\alpha_2+\alpha_3)$, with eigenvectors $\mathbf{v}_{N,1} = (1,-1/3,0,0)$, $\mathbf{v}_{N,2} = \left(0,-2/\sqrt{3},1,1\right)$, $\mathbf{v}_{N,3} = \left(0,2/\sqrt{3},1,1\right)$ and $\mathbf{v}_{N,4} = (0,0,1,-1)$ respectively. $\lambda_{N,1}$ corresponds to the process where a single electron tunnels between wires 2 and 3; thus we know from the 2-lead junction problem that it controls the RG flow between N and A_1. (By a flow "between" two fixed points, we refer to a flow which, starting sufficiently close to either of the two fixed points, can come into arbitrary proximity to the other.) Similarly, depending on the attractive or repulsive nature of the interactions, $\lambda_{N,2}$ and $\lambda_{N,3}$ control the RG flow from/to A_2 and A_3, respectively. The flow between N and M is jointly controlled by $\lambda_{N,1}$, $\lambda_{N,2}$ and $\lambda_{N,3}$. On the other hand, along the direction of $\mathbf{v}_{N,4}$, $c = -\bar{c} \neq 0$; thus $\mathbf{v}_{N,4}$ represents a chiral perturbation, and $\lambda_{N,4}$ controls the flows from/to $\chi_\pm$ which are the only fixed points breaking time-reversal symmetry at the first order.

We note that a, b, c and $\bar{c}$ are subject to additional constraints imposed by the S-matrix unitarity[13, 15]. By considering physically allowed S-matrices, it can be shown that $C_{N,4} = 0$ in Eq. (A.9) (i.e. $\mathbf{v}_{N,4}$ is not allowed) unless $C_{N,1}$, $C_{N,2}$ and $C_{N,3}$ are all nonzero. For this reason, $\lambda_{N,4}$ has not been regarded as an independent conductance scaling exponent in Refs. [13, 15]. Intuitively, this can also be understood from the fact that the breaking of time-reversal symmetry ($\mathbf{v}_{N,4}$) requires the presence of single electron tunneling between all three wires ($\mathbf{v}_{N,1}$, $\mathbf{v}_{N,2}$ and $\mathbf{v}_{N,3}$), so that a magnetic flux threaded into the junction cannot be trivially gauged away. It should be also mentioned that $\lambda_{N,4}$ is never the leading scaling exponent in either the high temperature or the low temperature limit. For instance, if we assume $\lambda_{N,4}$ is the leading exponent at low temperatures, then $\lambda_{N,4}$ must be greater than all remaining λ's, and we find all α's are negative and N is unstable in all directions, which contradicts our assumption.

A_j **fixed points**: At $A_{1,2}$, $(a_0, b_0, c_0, \bar{c}_0) = \left(1/2, -1/2, \mp\sqrt{3}/2, \mp\sqrt{3}/2\right)$; at A_3, $(a_0, b_0, c_0, \bar{c}_0) = (-1,1,0,0)$. We now focus on A_3 where wire 3 is decoupled, and wires 1 and 2 are perfectly connected.

At A_3, $\lambda_{A_3,1} = \lambda_{A_3,2} = -\alpha_3$, $\lambda_{A_3,3} = \alpha_1+\alpha_2$ and $\lambda_{A_3,4} = (\alpha_1+\alpha_2-2\alpha_3)/2$, with eigenvectors

$$\mathbf{v}_{A_3,1} = (0,0,1,-1), \tag{A.10a}$$

$$\mathbf{v}_{A_3,2} = \left(0, -\left(2/\sqrt{3}\right)(\alpha_1+\alpha_2), \alpha_1-\alpha_2, \alpha_1-\alpha_2\right), \tag{A.10b}$$

$$\mathbf{v}_{A_3,3} = \left(-\sqrt{3}(\alpha_1+\alpha_2+2\alpha_3), -(\alpha_1+\alpha_2+2\alpha_3)/\sqrt{3}, \alpha_1-\alpha_2, \alpha_1-\alpha_2\right), \tag{A.10c}$$

$$\mathbf{v}_{A_3,4} = (0,0,1,1) \tag{A.10d}$$

respectively. Again $\lambda_{A_3,1}$ corresponds to the single-electron tunneling between wires 2 and 3, $\lambda_{A_3,2}$ to that between 3 and 1, and $\lambda_{A_3,3}$ to that between 1 and 2. As before $\lambda_{A_3,3}$ controls the flow from/to N, and we see from the eigenvector $\mathbf{v}_{A_3,1}$ that $\lambda_{A_3,1} = \lambda_{A_3,2}$ controls the flows from/to $\chi_\pm$.

In the special case of 1-2 symmetric interaction, $\alpha_1 = \alpha_2$, it is clear that $\mathbf{v}_{A_3,4}$ is the only scaling direction breaking the 1-2 symmetry. Now the flows from/to A_1 and A_2 are controlled by $\lambda_{A_3,4}$ alone, and the flow from/to M is controlled by $\lambda_{A_3,1} = \lambda_{A_3,2}$ and $\lambda_{A_3,3}$ together but not $\lambda_{A_3,4}$.

We observe that $\mathbf{v}_{A_3,1}$ and $\mathbf{v}_{A_3,4}$ break the time-reversal symmetry and the 1-2 symmetry of the junction respectively without changing a or b. This is again forbidden by unitarity[13, 15] at A_3, i.e. $C_{A_3,1} = C_{A_3,4} = 0$ in Eq. (A.9) unless either $C_{A_3,2}$ or $C_{A_3,3}$ is nonzero. Physically it reflects the fact that any time-reversal asymmetry or 1-2 asymmetry at the junction should introduce perturbations that interrupt the perfectly connected wire. $\lambda_{A_3,4}$ is therefore not treated as a scaling exponent in Refs. [13, 15].

$\chi^\pm$ fixed points: At $\chi^\pm$, $(a_0, b_0, c_0, \bar{c}_0) = \left(-1/2, -1/2, \pm\sqrt{3}/2, \mp\sqrt{3}/2\right)$; $\lambda_{\chi^\pm,1} = \alpha_1$, $\lambda_{\chi^\pm,2} = \alpha_2$, $\lambda_{\chi^\pm,3} = \alpha_3$ and $\lambda_{\chi^\pm,4} = (\alpha_1+\alpha_2+\alpha_3)/2$, with eigenvectors

$$\begin{aligned}\mathbf{v}_{\chi^\pm,1} = \Big(&-\sqrt{3}\alpha_1, -(\alpha_1 + 2(\alpha_2+\alpha_3))/\sqrt{3}, (\alpha_1 - (\alpha_2+\alpha_3) \mp (\alpha_2+\alpha_3)),\\ &(\alpha_1 - (\alpha_2+\alpha_3) \pm (\alpha_2+\alpha_3))\Big),\end{aligned} \tag{A.11a}$$

$$\begin{aligned}\mathbf{v}_{\chi^\pm,2} = \Big(&\sqrt{3}\alpha_2, (\alpha_2 + 2(\alpha_1+\alpha_3))/\sqrt{3}, (\alpha_2 - (\alpha_1+\alpha_3) \pm (\alpha_1+\alpha_3)),\\ &(\alpha_2 - (\alpha_1+\alpha_3) \mp (\alpha_1+\alpha_3))\Big),\end{aligned} \tag{A.11b}$$

$$\mathbf{v}_{\chi^\pm,3} = \left(\sqrt{3}(\alpha_1+\alpha_2), -(\alpha_1+\alpha_2-4\alpha_3)/\sqrt{3}, \pm(\alpha_1+\alpha_2), \mp(\alpha_1+\alpha_2)\right), \tag{A.11c}$$

$$\mathbf{v}_{\chi^\pm,4} = \left(\sqrt{3}, \sqrt{3}, \pm 1, \mp 1\right) \tag{A.11d}$$

respectively. $\lambda_{\chi^\pm,1}$ corresponds to the single-electron tunneling between wires 2 and 3, and controls the flows from/to A_1; similarly $\lambda_{\chi^\pm,2}$ and $\lambda_{\chi^\pm,3}$ controls the flows from/to A_2 and A_3 respectively. $\lambda_{\chi^\pm,4}$ controls the RG flows from/to N and M.

The scaling direction $\mathbf{v}_{\chi^\pm,4}$ is forbidden by unitarity at $\chi^\pm$ ($C_{\chi^\pm,4} = 0$ in Eq. (A.9) unless $C_{\chi^\pm,1}$, $C_{\chi^\pm,2}$ and $C_{\chi^\pm,3}$ are all nonzero), so once more $\lambda_{\chi^\pm,4}$ is not treated as a scaling exponent

in Refs. [13, 15]. In terms of the mapping to the dissipative Hofstadter model[93], $\chi^{\pm}$ correspond to the localized phase of a quantum Brownian particle subject to a magnetic field and a triangular-lattice potential; $\lambda_{\chi^{\pm},1}$, $\lambda_{\chi^{\pm},2}$ and $\lambda_{\chi^{\pm},3}$ are then due to instantons tunneling back and forth between the three inequivalent nearest neighbor pairs of potential minima, while $\lambda_{\chi^{\pm},4}$ arises from instantons tunneling along the edges of elementary triangles formed by the potential minima. It is therefore reasonable that $\mathbf{v}_{\chi^{\pm},4}$ is allowed only if there exist deviations from $\chi^{\pm}$ along all three remaining scaling directions $\mathbf{v}_{\chi^{\pm},1}$, $\mathbf{v}_{\chi^{\pm},2}$ and $\mathbf{v}_{\chi^{\pm},3}$.

M **fixed point**: Due to time-reversal symmetry $c_0 = \bar{c}_0 = 0$; it is straightforward to find a_0 and b_0 from Eqs. (2.132) and (A.6). There are 4 scaling exponents at *M*:

$$\lambda_{M,1} = -\frac{\alpha_1\alpha_2\alpha_3}{\alpha_1\alpha_2+\alpha_2\alpha_3+\alpha_3\alpha_1}, \tag{A.12a}$$

$$\lambda_{M,2} = \frac{\alpha_1^2(\alpha_2+\alpha_3)+\alpha_2^2(\alpha_3+\alpha_1)+\alpha_3^2(\alpha_1+\alpha_2)}{\alpha_1\alpha_2+\alpha_2\alpha_3+\alpha_3\alpha_1}, \tag{A.12b}$$

$$\lambda_{M,3(4)} = \frac{1}{4}(\alpha_1\alpha_2+\alpha_2\alpha_3+\alpha_3\alpha_1)^{-1}\{(\alpha_1+\alpha_2)(\alpha_2+\alpha_3)(\alpha_3+\alpha_1) \pm\sqrt{(\alpha_1+\alpha_2)^2(\alpha_2+\alpha_3)^2(\alpha_3+\alpha_1)^2-8\alpha_1\alpha_2\alpha_3(\alpha_1+\alpha_2)(\alpha_2+\alpha_3)(\alpha_3+\alpha_1)}\}. \tag{A.12c}$$

Whenever *M* exists (see the conditions below Eq. (2.132)), $\lambda_{M,3}$, $\lambda_{M,4}$ are both real. Note that, unlike the situations at *N*, A_j and $\chi^{\pm}$, at *M* the four scaling directions are fully independent of each other. In the special case of Z_3 symmetric interactions ($\alpha_j = \alpha$), $\lambda_{M,1} = -\alpha/3$, $\lambda_{M,2} = 2\alpha$, $\lambda_{M,3} = \lambda_{M,4} = 2\alpha/3$, in agreement with the conductance predictions of Ref. [70]. The corresponding left eigenvectors are

$$\mathbf{v}_{M,1} = (0,0,1,-1), \tag{A.13a}$$

$$\mathbf{v}_{M,2} = \left(-\sqrt{3}(\alpha_1+\alpha_2), -(\alpha_1+\alpha_2+4\alpha_3)/\sqrt{3}, \alpha_1-\alpha_2, \alpha_1-\alpha_2\right). \tag{A.13b}$$

We can infer from the form of $\mathbf{v}_{M,1}$ that $\lambda_{M,1}$ controls the flows from/to $\chi^{\pm}$. $\mathbf{v}_{M,3}$ and $\mathbf{v}_{M,4}$ are too complicated to be given here in general.

In the case of 1-2 symmetric interactions ($\alpha_1 = \alpha_2$), significant simplifications occur:

$$\lambda_{M,1} = -\frac{\alpha_1\alpha_3}{\alpha_1+2\alpha_3}, \lambda_{M,2} = \frac{2\left(\alpha_1^2+\alpha_1\alpha_3+\alpha_3^2\right)}{\alpha_1+2\alpha_3}; \tag{A.14a}$$

$$\lambda_{M,3} = \frac{\alpha_3(\alpha_1+\alpha_3)}{\alpha_1+2\alpha_3}, \lambda_{M,4} = \frac{\alpha_1(\alpha_1+\alpha_3)}{\alpha_1+2\alpha_3}; \tag{A.14b}$$

$$\mathbf{v}_{M,3} = (3\alpha_3(\alpha_1+\alpha_3), -2\alpha_1(\alpha_1+2\alpha_3), 0, 0), \tag{A.15a}$$

$$\mathbf{v}_{M,4} = (0,0,1,1). \tag{A.15b}$$

In this case we find $\operatorname{sgn}\lambda_{M,2} = \operatorname{sgn}\lambda_{M,3} = \operatorname{sgn}\alpha_3$ and $\operatorname{sgn}\lambda_{M,4} = \operatorname{sgn}\alpha_1$. $\lambda_{M,2}$ and $\lambda_{M,3}$ control the flows from/to A_3 and N, and $\lambda_{M,4}$ controls the flows from/to A_1 and A_2.

We are now in a position to give the directions of RG flows based on the local scaling exponents. The results are summarized below.

1. The flow between N and A_3 is toward N if $\alpha_1+\alpha_2>0$, and toward A_3 if $\alpha_1+\alpha_2<0$;

2. The flows between N and $\chi^{\pm}$ are toward N if $\alpha_1+\alpha_2+\alpha_3>0$, and toward $\chi^{\pm}$ if $\alpha_1+\alpha_2+\alpha_3<0$;

3. If $\alpha_1=\alpha_2$, the flows between A_3 and $A_{1,2}$ are toward A_3 if $\alpha_1<\alpha_3$, and toward A_1 and A_2 if $\alpha_1>\alpha_3$;

4. The flows between A_3 and $\chi^{\pm}$ are toward A_3 if $\alpha_3>0$, and toward $\chi^{\pm}$ if $\alpha_3<0$.

In addition, if the non-geometrical fixed point M exists:

5. The flows between M and $\chi^{\pm}$ are toward M if $\lambda_{M,1}<0$, and toward $\chi^{\pm}$ if $\lambda_{M,1}>0$;

6. If $\alpha_1=\alpha_2$, the flows between M and $A_{1,2}$ are toward M if $\alpha_1<0$, and toward A_1 and A_2 if $\alpha_1>0$.

7. If $\alpha_1=\alpha_2$, the flow between M and A_3 is toward M if $\alpha_3<0$, and toward A_3 if $\alpha_3>0$.

8. If $\alpha_1=\alpha_2$, the flow between M and N is toward M if $\alpha_3<0$, and toward N if $\alpha_3>0$.

A.2 RPA

A.2.1 2-lead junction

Calculating Eq. (2.107) explicitly we find the cutoff-dependent RPA interaction

$$\Pi_{jj'} = \frac{\left(K_1^{-1}-1\right)\left(K_2^{-1}-1\right)\left(2\delta_{jj'}-1\right)W_{12}+2\left(K_j^{-1}-1\right)\delta_{jj'}}{2+\left(K_1^{-1}+K_2^{-1}-2\right)W_{12}}, \tag{A.16}$$

and the RPA RG equation for S_{12},

$$-\frac{dS_{12}}{d\ln D} = -\frac{2(1-W_{12})}{\gamma-1+2W_{12}}S_{12}, \tag{A.17}$$

where

$$\gamma = \frac{K_1^{-1} + K_2^{-1} + 2}{K_1^{-1} + K_2^{-1} - 2}; \tag{A.18}$$

or, in terms of W_{12},

$$-\frac{dW_{12}}{d\ln D} = -\frac{4W_{12}(1-W_{12})}{\gamma - 1 + 2W_{12}}, \tag{A.19}$$

in agreement with the RPA RG equation for conductance in Refs. [11, 12, 14].

As with the first order equation Eq. (A.2), Eq. (A.19) has two fixed points, the N fixed point $W_{12} = 0$ and the D fixed point $W_{12} = 1$. In this case the N fixed point has a conductance scaling exponent of $-4/(\gamma - 1) = 2 - 2/K_e$, and the D fixed point has a scaling exponent of $4/(\gamma + 1) = 2 - 2K_e$, where $K_e = 2/\left(K_1^{-1} + K_2^{-1}\right)$. Both exponents conform to the predictions of bosonic methods[11, 12, 14] as has been verified in Section 2.2.

A.2.2 Y-junction

Starting from Eq. (2.106) and following the same prescription which transforms Eq. (2.72) to Eq. (A.7d), we find the RG equations obeyed by a, b, c and $\bar{c}$ in the RPA:

$$\begin{aligned}
-\frac{da}{d\ln D} = Q_A^{-1}\Big\{ & 2\left[(1-b)\left(1+a+b-3a^2\right) - (1+3a)\,c\bar{c} + c^2 + \bar{c}^2\right](Q_1+Q_2+Q_3-3) \\
& + \left(3+a+3b-6a^2-ab-c\bar{c}\right)(Q_1+Q_2-2)(Q_3-1) \\
& + \sqrt{3}(1-2a)(c+\bar{c})(Q_1-Q_2)(Q_3-1) + 4\left[a(1-b)-c\bar{c}\right](Q_1-1)(Q_2-1)\Big\},
\end{aligned} \tag{A.20a}$$

$$\begin{aligned}
-\frac{db}{d\ln D} = Q_A^{-1}\{ & 2\left[(1-b)(1+2b-3ab) - 3(1+b)\,c\bar{c}\right](Q_1+Q_2+Q_3-3) \\
& + \left[(1-b)(1+3a+2b) - 3c\bar{c}\right](Q_1+Q_2-2)(Q_3-1) \\
& - \sqrt{3}(1+2b)(c+\bar{c})(Q_1-Q_2)(Q_3-1) + 4(1-b)(1+2b)(Q_1-1)(Q_2-1)\Big\},
\end{aligned} \tag{A.20b}$$

$$\begin{aligned}
-\frac{dc}{d\ln D} = Q_A^{-1}\Big\{ & 2\left[-c(1+2b-3ab) + \bar{c}\left(2-2b-3c^2\right)\right](Q_1+Q_2+Q_3-3) \\
& + \left[-c(1+6a+2b) + 3\bar{c}\right](Q_1+Q_2-2)(Q_3-1) \\
& + \sqrt{3}\left[(1+a)(1-b) - 2c^2 - c\bar{c}\right](Q_1-Q_2)(Q_3-1) - 4c(1+2b)(Q_1-1)(Q_2-1)\Big\},
\end{aligned} \tag{A.20c}$$

$$-\frac{d\bar{c}}{d\ln D} = Q_A^{-1}\left\{2\left[-\bar{c}\left(1+2b-3ab\right)+c\left(2-2b-3\bar{c}^2\right)\right]\left(Q_1+Q_2+Q_3-3\right)\right.$$
$$+\left[-\bar{c}\left(1+6a+2b\right)+3c\right]\left(Q_1+Q_2-2\right)\left(Q_3-1\right)$$
$$\left.+\sqrt{3}\left[\left(1+a\right)\left(1-b\right)-2\bar{c}^2-c\bar{c}\right]\left(Q_1-Q_2\right)\left(Q_3-1\right)-4\bar{c}\left(1+2b\right)\left(Q_1-1\right)\left(Q_2-1\right)\right\}, \tag{A.20d}$$

where

$$Q_A = 2\left[\left(1-a\right)\left(1-b\right)-c\bar{c}\right]\left(Q_1+Q_2+Q_3-3\right)+4\left(1-b\right)\left(Q_1-1\right)\left(Q_2-1\right)$$
$$+\left(4-3a-b\right)\left(Q_1+Q_2-2\right)\left(Q_3-1\right)-\sqrt{3}\left(c+\bar{c}\right)\left(Q_1-Q_2\right)\left(Q_3-1\right)$$
$$+6\left(Q_1-1\right)\left(Q_2-1\right)\left(Q_3-1\right). \tag{A.20e}$$

In the special case of 1-2 symmetric interaction $K_1 = K_2$, Eq. (A.20e) is reduced to the RG equations of Ref. [15]. The fully 1-2 symmetric case with both $K_1 = K_2$ and $c = -\bar{c}$ has been extensively analyzed there.

Eq. (A.20e) may once again be linearized to extract the scaling exponents. We first enumerate the scaling exponents at the geometrical fixed points N, A_j and $\chi^{\pm}$; their physical meanings are identical to their first order counterparts, and have been explained in detail in Appendix A.1.

N **fixed point**: At N, $\lambda_{N,1} = 2-K_2^{-1}-K_3^{-1}$, $\lambda_{N,2} = 2-K_3^{-1}-K_1^{-1}$, $\lambda_{N,3} = 2-K_1^{-1}-K_2^{-1}$, and $\lambda_{N,4} = 3-K_1^{-1}-K_2^{-1}-K_3^{-1}$.

A_j **fixed points**: At e.g. A_3, $\lambda_{A_3,1} = \lambda_{A_3,2} = 2-K_3^{-1}-\left(1+K_1K_2\right)/\left(K_1+K_2\right)$, $\lambda_{A_3,3} = 2-4K_1K_2/\left(K_1+K_2\right)$, and $\lambda_{A_3,4} = 3-K_3^{-1}-\left(1+3K_1K_2\right)/\left(K_1+K_2\right)$.

$\chi^{\pm}$ **fixed points**: At $\chi^{\pm}$,

$$\lambda_{\chi,j} = 2-\frac{4\left(K_1+K_2+K_3-K_j\right)K_j}{K_1+K_2+K_3+K_1K_2K_3},\ j=1,2,3; \tag{A.21a}$$

$$\lambda_{\chi,4} = 3-\frac{4\left(K_1K_2+K_2K_3+K_3K_1\right)}{K_1+K_2+K_3+K_1K_2K_3}. \tag{A.21b}$$

All scaling exponents above are in agreement with predictions of bosonization[51].

As for the non-geometrical fixed points, on account of mathematical simplicity we follow Ref. [15] and only give their positions and scaling exponents in the fully 1-2 symmetric case, $K_1 = K_2$ and $c_0 = -\bar{c}_0$. We introduce the quantities

$$\zeta = \frac{3Q_1Q_3-Q_1-2Q_3}{2Q_1+Q_3-3}, \tag{A.22}$$

$$\tau_0 = \sqrt{1+Q_1^2+2\zeta}; \tag{A.23}$$

where Q_1 and Q_3 are related to K_1 and K_3 by Eq. (2.108). ζ and τ_0 are identical to Q_1 and τ in Ref. [15] respectively.

M **and** *Q* **fixed points**: At these two fixed points

$$(a_0, b_0, c_0) = \left(\frac{1}{3}\left(Q_1 \mp \tau_0 \operatorname{sgn} Q_1\right), \frac{1}{6}\left(\left(|Q_1| \mp \tau_0\right)^2 - 3\right), 0\right), \tag{A.24}$$

where the upper signs are for M and the lower signs for Q. The two fixed points merge when $\tau_0 = 0$, or in terms of the Luttinger parameters,

$$K_3 = \frac{2K_1\left(K_1^2 - K_1 + 1\right)}{(K_1+1)(2K_1-1)}. \tag{A.25}$$

We note that Q also exists for Z_3 symmetric interactions but its W matrix remains Z_3 asymmetric; thus Q cannot be reached when the RG flow starts from a Z_3 symmetric S-matrix. The M fixed point again corresponds to the maximally open S-matrix in the Z_3 symmetric case, while the Q fixed point only appears when the interactions are sufficiently strongly attractive[13, 15]. The conditions for M and Q to appear are $\tau_0^2 = 1 + Q_1^2 + 2\zeta \geq 0$ and $||Q_1| \mp \tau_0| \leq 3$ (the latter is due to S-matrix unitarity), and for Z_3 symmetric interactions Q only starts to exist when the Luttinger parameter of all three wires $K \geq 3$. Both M and Q are time-reversal symmetric.

For attractive interaction in wire 1 ($K_1 > 1$), the 4 scaling exponents at either M or Q are

$$\lambda_{M(Q),1} = -\frac{3\left(Q_1 \pm \tau_0 + 3\right)\left(Q_1^2 + 2Q_1 - \tau_0^2 \pm 2\tau_0 - 3\right)}{2\left(Q_1 \pm \tau_0\right)\left(2Q_1 \mp \tau_0\right)^2}, \tag{A.26a}$$

$$\lambda_{M(Q),2} = -\frac{3\left(\left(Q_1 \pm \tau_0\right)^2 + 3\right)}{\left(Q_1 \pm \tau_0\right)\left(2Q_1 \mp \tau_0\right)}, \tag{A.26b}$$

$$\lambda_{M(Q),3} = -\frac{3\left(Q_1 \pm \tau_0 - 3\right)\left(Q_1^2 - 2Q_1 - \tau_0^2 \mp 2\tau_0 - 3\right)}{2\left(Q_1 \pm \tau_0\right)\left(2Q_1 \mp \tau_0\right)^2}, \tag{A.26c}$$

$$\lambda_{M(Q),4} = \mp\frac{3\tau_0\left(\left(Q_1 \pm \tau_0\right)^2 - 9\right)}{2\left(Q_1 \pm \tau_0\right)\left(2Q_1 \mp \tau_0\right)^2}; \tag{A.26d}$$

again the upper signs are for M and the lower signs for Q. For repulsive interaction in wire 1 ($K_1 < 1$), the lower signs should be taken to obtain the scaling exponents at M. When expanded to the first order in α_1 and α_3, Eq. (A.26d) agrees with Eq. (A.12c).

$C^{\pm}$ **fixed points**: As with the Q fixed point, the non-geometrical chiral fixed points $C^{\pm}$ only exist when the interaction is strongly attractive. At these fixed points

$$(a_0,b_0,c_0)=\left(\frac{1}{6}\left(2Q_1\left(\zeta+2\right)-\zeta^2+1\right),\frac{1}{6}\left(\zeta^2+4\zeta+1\right),\pm\frac{\left(\zeta-1\right)}{6}\sqrt{3-\left(2Q_1-\zeta\right)\left(2+\zeta\right)}\right). \tag{A.27}$$

The conditions for $C^{\pm}$ to appear are $-5\leq\zeta\leq 1$ and

$$0\leq 3-\left(2Q_1-\zeta\right)\left(2+\zeta\right)\leq\frac{1}{3}\left(5+\zeta\right)^2. \tag{A.28}$$

In the Z_3 symmetric Y-junction, these conditions are satisfied when the Luttinger parameter of all three wires $K\geq 2$. $C^{\pm}$ and $\chi^{\pm}$ merge when $\zeta=-2$, or in terms of the Luttinger parameters, $K_1^{-1}+2K_3^{-1}=1$.

There are again 4 scaling exponents at $C^{\pm}$,

$$\lambda_{C,1}=\frac{12Q_1}{\left(Q_1-1\right)\left(3Q_1-\zeta-2\right)}+\frac{12}{\left(Q_1-1\right)\left(\zeta-1\right)}, \tag{A.29a}$$

$$\lambda_{C,2}=-\frac{12}{3Q_1-\zeta-2}-\frac{12}{\zeta-1}-6, \tag{A.29b}$$

$$\lambda_{C,3(4)}=-\frac{3\left(3Q_1-\zeta+4\right)\left(\zeta+5\right)}{2\left(3Q_1-\zeta-2\right)\left(\zeta-1\right)}\left(\frac{\zeta+1}{\zeta+5}\pm\frac{1}{3}\sqrt{1+\frac{8\left(\zeta+2\right)\left(3Q_1-\zeta-2\right)}{\left(\zeta-1\right)\left(3Q_1-\zeta+4\right)}}\right). \tag{A.29c}$$

We conclude this appendix with a discussion of the RG flows in the Y-junction.

In the generic Z_3 asymmetric case, for simplicity we only focus on the RG flows when K_1, K_2 and K_3 are all close to unity, so that the only allowed non-geometrical fixed point is M. We focus on the flows between the geometrical fixed points. The results are listed below.

1. The flow between N and A_3 is toward N if $K_1^{-1}+K_2^{-1}>2$, and toward A_3 if $K_1^{-1}+K_2^{-1}<2$;

2. The flows between N and $\chi^{\pm}$ are toward N if $K_1^{-1}+K_2^{-1}+K_3^{-1}>3$ and $\lambda_{\chi,4}>0$, and toward $\chi^{\pm}$ if $K_1^{-1}+K_2^{-1}+K_3^{-1}<3$ and $\lambda_{\chi,4}<0$.

3. The flows between A_3 and $\chi^{\pm}$ are toward A_3 if $K_3^{-1}+\left(1+K_1K_2\right)/\left(K_1+K_2\right)>2$, and toward $\chi^{\pm}$ if $K_3^{-1}+\left(1+K_1K_2\right)/\left(K_1+K_2\right)<2$.

Finally, following Ref. [15] we detail the RG flows in a fully Z_3 symmetric junction with Luttinger parameter K for all three wires. Only the fixed points consistent with Z_3 symmetry, namely N, $\chi^{\pm}$, M, and $C^{\pm}$, need to be considered.

When $0<K<1$, N is the most stable fixed point, M is stable against chiral perturbations but otherwise unstable, and $\chi^{\pm}$ are completely unstable; $C^{\pm}$ do not exist. The flows are from $\chi^{\pm}$ to M or N, and from M to N.

When $1<K<2$, $\chi^{\pm}$ are the most stable fixed points, M is stable against time-reversal symmet-

ric perturbations and unstable against chiral perturbations, and N is completely unstable; $C^{\pm}$ do not exist. The flows are from N to M or $\chi^{\pm}$, and from M to $\chi^{\pm}$.

When $2 < K < 3$, $\chi^{\pm}$ remain stable, N remains completely unstable, while M becomes fully stable. $C^{\pm}$ emerge as the unstable fixed points separating $\chi^{\pm}$ and M, approaching $\chi^{\pm}$ as K approaches 3. The flows are from N to M, $\chi^{\pm}$ or $C^{\pm}$, and from $C^{\pm}$ to M or $\chi^{\pm}$.

When $K > 3$, $\chi^{\pm}$ become completely unstable, N remains completely unstable and M remains fully stable. $C^{\pm}$ remain unstable, moving toward $a_0 = b_0 = -1/3$ and $c_0 = -\bar{c}_0 = \pm 2/3$ as $K \to \infty$. The flows are from N to M or $C^{\pm}$, from $\chi^{\pm}$ to M or $C^{\pm}$, and from $C^{\pm}$ to M.

Appendix B

Details of the disconnected contribution

In this appendix we present the detailed derivation of Eq. (3.45) [or equivalently Eq. (3.47a)] from Eq. (3.38)[112]. The calculations are similar to those in Appendix B of Ref. [66], but an important difference is that here we cannot simply take the δ-function part and neglect the principal value part in Eq. (3.38). Instead, most of the momentum integrals are evaluated by means of contour integration.

From Eq. (3.41)

$$\begin{aligned} -2\,\mathrm{Im}\,\mathbb{G}^R_{k_2q_1}(\omega) &= (2\pi)^2\,\delta(k_2-q_1)\,\delta(\omega-\varepsilon_{k_2})+i\tau_\psi \\ &\quad\times\left[g^R_{k_2}(\omega)\,V_{k_2}\,G^R_{dd}(\omega)\,V_{q_1}\,g^R_{q_1}(\omega)-g^A_{k_2}(\omega)\,V_{k_2}\,G^A_{dd}(\omega)\,V_{q_1}\,g^A_{q_1}(\omega)\right]. \end{aligned} \tag{B.1}$$

We denote the three terms above as 0, R and A respectively. Inserting into Eq. (3.38), we find 3 types of contributions to the disconnected part:

$$\begin{aligned} G'^D_{jj'}(\Omega) &= G'^D_{jj',00}(\Omega)+\left[G'^D_{jj',0R}(\Omega)+G'^D_{jj',0A}(\Omega)+G'^D_{jj',R0}(\Omega)+G'^D_{jj',A0}(\Omega)\right] \\ &\quad+\left[G'^D_{jj',RA}(\Omega)+G'^D_{jj',RR}(\Omega)+G'^D_{jj',AR}(\Omega)+G'^D_{jj',AA}(\Omega)\right]; \end{aligned} \tag{B.2}$$

The 00 term is the background transmission, the first pair of square brackets is linear in the T-matrix of the screening channel, and the second pair of square brackets is quadratic in the T-matrix.

Due to the multiplying factor of Ω in Eq. (3.31), $O(1/\Omega)$ terms in $G'^D_{jj'}$ contribute to the linear dc conductance, while $O(1)$ and other terms which are regular in the dc limit $\Omega\to 0$ do not contribute. (We can check explicitly that there are no $O\left(1/\Omega^2\right)$ or higher-order divergences.) Therefore, in the dc limit we are only interested in the $O(1/\Omega)$ part of $G'^D_{jj'}$.

B.1 Properties of the S-matrix and the wave functions

Before actually doing the calculations it is useful to examine the properties of the background S-matrix and the wave functions in our tight-binding model, since we rely on these properties to transform the momentum integrals into contour integrals and evaluate them.

First consider the analytic continuation $k \to -k$. The wave function "incident" from lead j at momentum $-k$ takes the following form on lead j' [cf. Eq. (3.15a)],

$$\chi_{j,-k}\left(j',n\right) = \delta_{jj'}e^{ikn} + S_{j'j}\left(-k\right)e^{-ikn}; \tag{B.3}$$

and on coupling site r,

$$\chi_{j,-k}\left(r\right) = \Gamma_{rj}\left(-k\right).$$

This wave function should be a linear combination of the scattering state wave functions at momentum k which form a complete basis. The linear coefficients are obtained from S-matrix unitarity:

$$\chi_{j,-k}\left(j',n\right) = \sum_{j''} S^{*}_{jj''}\left(k\right)\chi_{j'',k}\left(j',n\right) = \delta_{jj'}e^{ikn} + S^{*}_{jj'}\left(k\right)e^{-ikn}, \tag{B.4}$$

and the same coefficients apply to the coupling sites:

$$\chi_{j,-k}\left(r\right) = \sum_{j''} S^{*}_{jj''}\left(k\right)\Gamma_{rj''}\left(k\right).$$

Hence

$$S\left(-k\right) = S^{\dagger}\left(k\right), \tag{B.5}$$

$$\Gamma\left(-k\right) = \Gamma\left(k\right)S^{\dagger}\left(k\right). \tag{B.6}$$

Eq. (B.5) is known as the Hermitian analyticity of the S-matrix[20].

Another useful property is the location of poles of $S\left(k\right) \equiv S\left(z = e^{ik}\right)$ on the z complex plane. Our analysis closely follows Ref. [96] which deals with the case of quadratic dispersion.

Consider one pole of the S-matrix $k \equiv k_1 + ik_2$, where for certain values of j and j', $\left|S_{j'j}\left(k\right)\right| \to \infty$. In the scattering state $\left|q_{j,k}\right\rangle \equiv q^{\dagger}_{j,k}\left|0\right\rangle$, where $\left|0\right\rangle$ is the Fermi sea ground state, the incident component of the wave function at momentum k becomes negligible relative to the scattered component. Therefore, the time-dependent wave function on lead j' at site n reads

$$\chi_{j,k}\left(j',n,\bar{t}\right) \approx S_{j'j}\left(k\right)e^{ikn}e^{-i\varepsilon_k\bar{t}} = S_{j'j}\left(k\right)e^{ikn}e^{2it\bar{t}\cos k_1\cosh k_2}e^{2t\bar{t}\sin k_1\sinh k_2}. \tag{B.7}$$

This expression is valid for any j' where $\left|S_{j'j}\left(k\right)\right|$ is divergent; for other j' the wave function is

negligible.

We define the "junction area" to include any tight-binding site that is not part of a lead, together with the 0th site of each lead. The total probability of the electron being inside the junction area, $N(\bar{t})$, obeys the probability continuity equation

$$\frac{d}{d\bar{t}}N(\bar{t}) = it\sum_{j'}\left(c^{\dagger}_{j',0}c_{j',1} - c^{\dagger}_{j',1}c_{j',0}\right)(\bar{t}), \tag{B.8}$$

where the right-hand side is the current operator between site 0 and site 1 of lead j', summed over all leads. Taking the expectation value in the state $\left|q_{j,k}\right\rangle$, we find

$$-(4t\sin k_1\sinh k_2)\,C_j(k)\,e^{4t\bar{t}\sin k_1\sinh k_2} = \sum_{j'}(2t\sin k_1)\,e^{-k_2}\left|S_{j'j}(k)\right|^2 e^{4t\bar{t}\sin k_1\sinh k_2}. \tag{B.9}$$

For the left-hand side we have used the form of the time evolution $e^{-i\varepsilon_k\bar{t}}$, and $C_j(k)$ is a positive time-independent constant proportional to the total probability in the junction area; $C_j(k)$ is divergent whenever $\left|S_{j'j}(k)\right|$ is divergent. For the right-hand side, we have used Eq. (B.7) at $n=0$ and $n=1$; the summation is over any j' where $\left|S_{j'j}(k)\right|$ is divergent.

Eq. (B.9) implies that either $\sin k_1 = 0$, in which case $k_1 = 0$ or π; or $\sinh k_2 < 0$, in which case $\left|e^{i(k_1+ik_2)}\right| > 1$. The poles of $S(k)$ on the $z = e^{ik}$ plane are therefore either outside the unit circle or located on the real axis. For the models we study in this chapter, the poles of $S(k)$ and those of $\Gamma(k)/(\sin k)$ coincide; in other words, the poles of $S(k)$ and $\Gamma(k)/(\sin k)$ on the $z = e^{ik}$ plane are either outside the unit circle or on the real axis.

We mention that similar results apply in the theory with a reduced bandwidth and a linearized dispersion in the leads. Eqs. (B.5) and (B.6) continue to hold; on the other hand, the probability current is proportional to v_F instead of $2t\sin k_1$, and all poles of $S(k)$ and $\Gamma(k)/(\sin k)$ are located in the lower half of the k plane.

B.2 Background transmission

This part is independent of the QD and the result should be the famous Landauer formula:

$$G'^{D}_{jj',00}(\Omega) = 2\int_0^{\pi}\frac{dk_1dk_2}{(2\pi)^2}\frac{f(\varepsilon_{k_1}) - f(\varepsilon_{k_2})}{\varepsilon_{k_1} - \varepsilon_{k_2} + \Omega^+}\,\mathrm{tr}\left(\mathbb{M}^{j}_{k_1k_2}\mathbb{M}^{j'}_{k_2k_1}\right). \tag{B.10}$$

Inserting Eq. (3.35), taking advantage of Eq. (B.5) and the unitarity of the $\mathbb{U}$ matrix, we find

$$G'^{D}_{jj',00}(\Omega) = 2\int_{-\pi}^{\pi} \frac{dk_1 dk_2}{(2\pi)^2} \frac{f(\varepsilon_{k_1}) - f(\varepsilon_{k_2})}{\varepsilon_{k_1} - \varepsilon_{k_2} + \Omega^+}$$
$$\times \left\{ \delta_{jj'} \frac{1}{1 - e^{i(k_1 - k_2 + i0)}} \frac{1}{1 - e^{i(k_2 - k_1 + i0)}} + S^*_{jj'}(k_1)\, \delta_{jj'} \frac{1}{1 - e^{-i(k_1 + k_2 - i0)}} \frac{1}{1 - e^{i(k_2 - k_1 + i0)}} \right.$$
$$\left. + \delta_{jj'} S_{jj'}(k_2) \frac{1}{1 - e^{i(k_1 + k_2 + i0)}} \frac{1}{1 - e^{i(k_2 - k_1 + i0)}} + S^*_{jj'}(k_1) S_{jj'}(k_2) \frac{1}{\left[1 - e^{i(k_2 - k_1 + i0)}\right]^2} \right\}. \tag{B.11}$$

By residue theorem we can perform the k_2 integral in the part proportional to $f(\varepsilon_{k_1})$ and the k_1 integral in the part proportional to $f(\varepsilon_{k_2})$. In the following we assume $\Omega > 0$; the case $\Omega < 0$ can be dealt with similarly.

We begin from the first term in curly brackets, which is proportional to $\delta_{jj'}$. For the part proportional to $f(\varepsilon_{k_1})$, making the substitution $z_2 = e^{ik_2}$, and calculating the contour integral on the counterclockwise unit circle, we find

$$\int_{-\pi}^{\pi} \frac{dk_2}{2\pi} \frac{f(\varepsilon_{k_1})}{\varepsilon_{k_1} - \varepsilon_{k_2} + \Omega^+} \frac{1}{1 - e^{i(k_1 - k_2 + i\eta)}} \frac{1}{1 - e^{i(k_2 - k_1 + i\eta)}}$$
$$= \frac{f(\varepsilon_{k_1})}{2it \sin p_1} \frac{1}{1 - e^{i(k_1 - p_1)}} \frac{1}{1 - e^{i(p_1 - k_1)}} + \frac{f(\varepsilon_{k_1})}{\Omega} \frac{1}{1 - e^{-2\eta}}, \tag{B.12a}$$

where $\eta \to 0^+$. (η corresponds to the rate of switching on the bias voltage in Kubo formalism, so the limit $\eta \to 0$ should be taken before the dc limit $\Omega \to 0$.) We have assumed $\varepsilon_{k_1} + \Omega \equiv \varepsilon_{p_1}$ where $0 \le p_1 \le \pi$ if p_1 is real; the poles of the integrand inside the unit circle are then $z_2 = e^{i(p_1 + i0)}$ and $z_2 = e^{i(k_1 + i\eta)}$. At the band edges, $2t - \Omega < \varepsilon_{k_1} < 2t$, and p_1 is purely imaginary; we can choose it to have a positive imaginary part so the above expression remains valid. Similarly

$$\int_{-\pi}^{\pi} \frac{dk_1}{2\pi} \frac{f(\varepsilon_{k_2})}{\varepsilon_{k_1} - \varepsilon_{k_2} + \Omega^+} \frac{1}{1 - e^{i(k_1 - k_2 + i\eta)}} \frac{1}{1 - e^{i(k_2 - k_1 + i\eta)}}$$
$$= \frac{f(\varepsilon_{k_2})}{2it \sin p_2} \frac{1}{1 - e^{i(-p_2 - k_2)}} \frac{1}{1 - e^{i(p_2 + k_2)}} + \frac{f(\varepsilon_{k_2})}{\Omega} \frac{1}{1 - e^{-2\eta}}, \tag{B.12b}$$

where $\varepsilon_{k_2} - \Omega = \varepsilon_{p_2}$, $0 \le p_2 \le \pi$ if p_2 is real, or $p_2 = -i|p_2|$ if p_2 is purely imaginary. Now combine the two parts. In the $\Omega \to 0$ limit, $p_1 \to k_1$ only for p_1 real and $k_1 > 0$, and $p_2 \to -k_2$ only for p_2 real and $k_2 < 0$; the most divergent contribution is therefore

$$\int_{-\pi}^{\pi}\frac{dk_1dk_2}{(2\pi)^2}\frac{f(\varepsilon_{k_1})-f(\varepsilon_{k_2})}{\varepsilon_{k_1}-\varepsilon_{k_2}+\Omega^+}\frac{1}{1-e^{i(k_1-k_2+i0)}}\frac{1}{1-e^{i(k_2-k_1+i0)}}$$
$$=\int_{-2t}^{2t-\Omega}\frac{d\varepsilon_{k_1}}{2\pi i}\left[f(\varepsilon_{k_1})-f(\varepsilon_{k_1}+\Omega)\right]\frac{1}{(2t\sin k_1)(2t\sin p_1)}\frac{1}{1-e^{i(k_1-p_1)}}\frac{1}{1-e^{i(p_1-k_1)}}+O(1). \tag{B.13}$$

We have substituted the dummy variables $k_2\to p_1$, $p_2\to k_1$, and noted that $\varepsilon_{p_1}=\varepsilon_{k_1}+\Omega$. Expanding various parts of the integrand in $\Omega\to 0$ limit, we find

$$\int_{-\pi}^{\pi}\frac{dk_1dk_2}{(2\pi)^2}\frac{f(\varepsilon_{k_1})-f(\varepsilon_{k_2})}{\varepsilon_{k_1}-\varepsilon_{k_2}+\Omega^+}\frac{1}{1-e^{i(k_1-k_2+i0)}}\frac{1}{1-e^{i(k_2-k_1+i0)}}$$
$$=\frac{1}{2\pi i\Omega}\int_{-2t}^{2t-\Omega}d\varepsilon_{k_1}\left[-f'(\varepsilon_{k_1})\right]+O(1). \tag{B.14}$$

The two terms in $G'^{D}_{jj',00}(\Omega)$ which are linear in the S-matrix do not contribute any terms of $O(1/\Omega)$ to $G'^{D}_{jj'}$: the difference of Fermi functions is proportional to Ω, but the denominators are also $O(\Omega)$, unlike the case for the $\delta_{jj'}$ terms whose denominators are $O\left(\Omega^2\right)$. This leaves us with the term quadratic in the S-matrix, which can be similarly evaluated. For the part proportional to $f(\varepsilon_{k_1})$,

$$\int_{-\pi}^{\pi}\frac{dk_2}{2\pi}\frac{f(\varepsilon_{k_1})}{\varepsilon_{k_1}-\varepsilon_{k_2}+\Omega^+}S^*_{jj'}(k_1)S_{jj'}(k_2)\frac{1}{\left[1-e^{i(k_2-k_1+i0)}\right]^2}$$
$$=\frac{f(\varepsilon_{k_1})}{2it\sin p_1}S^*_{jj'}(k_1)S_{jj'}(p_1)\frac{1}{\left[1-e^{i(p_1-k_1)}\right]^2}+\left(\text{contribution of poles of } S_{jj'}\right); \tag{B.15a}$$

the poles of $S_{jj'}$ inside the unit circle (on the real axis) may contribute to the contour integral, but these terms are regular in the $\Omega\to 0$ limit and do not contribute to the dc conductance. Similarly

$$\int_{-\pi}^{\pi}\frac{dk_1}{2\pi}\frac{f(\varepsilon_{k_2})}{\varepsilon_{k_1}-\varepsilon_{k_2}+\Omega^+}S^*_{jj'}(k_1)S_{jj'}(k_2)\frac{1}{\left[1-e^{i(k_2-k_1+i0)}\right]^2}$$
$$=\frac{f(\varepsilon_{k_2})}{2it\sin p_2}S^*_{jj'}(p_2)S_{jj'}(k_2)\frac{1}{\left[1-e^{i(k_2-p_2)}\right]^2}+\left(\text{contribution of poles of } S^*_{jj'}\right), \tag{B.15b}$$

Therefore

$$\int_{-\pi}^{\pi}\frac{dk_1dk_2}{(2\pi)^2}\frac{f(\varepsilon_{k_1})-f(\varepsilon_{k_2})}{\varepsilon_{k_1}-\varepsilon_{k_2}+\Omega^+}S^*_{jj'}(k_1)S_{jj'}(k_2)\frac{1}{\left[1-e^{i(k_2-k_1+i0)}\right]^2}$$
$$=\int_{-2t}^{2t-\Omega}\frac{d\varepsilon_{k_1}}{2\pi i}\frac{f(\varepsilon_{k_1})-f(\varepsilon_{k_1}+\Omega)}{(2t\sin k_1)(2t\sin p_1)}S^*_{jj'}(k_1)S_{jj'}(p_1)\frac{1}{\left[1-e^{i(p_1-k_1)}\right]^2}+O(1)$$
$$=-\frac{1}{2\pi i\Omega}\int_{-2t}^{2t-\Omega}d\varepsilon_{k_1}\left[-f'(\varepsilon_{k_1})\right]S^*_{jj'}(k_1)S_{jj'}(p_1)+O(1). \tag{B.16}$$

From Eqs. (B.14) and (B.16), we conclude that

$$G'^D_{jj',00}(\Omega)=\frac{1}{\pi i\Omega}\int_{-2t}^{2t-\Omega}d\varepsilon_{k_1}\left[-f'(\varepsilon_{k_1})\right]\left[\delta_{jj'}-S^*_{jj'}(k_1)S_{jj'}(p_1)\right]+O(1); \tag{B.17}$$

taking the $\Omega\to 0$ limit, noting that $p_1\to k_1$, we recover the Landauer formula, Eq. (3.47b).

B.3 Terms linear in T-matrix

We focus on $G'^D_{jj',0R}+G'^D_{jj',0A}$; the calculation of $G'^D_{jj',R0}+G'^D_{jj',A0}$ is analogous.

$$G'^D_{jj',0R}(\Omega)+G'^D_{jj',0A}(\Omega)$$
$$=2\int_0^{\pi}\frac{dk_1}{(2\pi)^2}\frac{dq_1dq_2}{(2\pi)^2}\int d\omega\frac{f(\omega)-f(\varepsilon_{q_1})}{\omega-\varepsilon_{q_1}+\Omega^+}\,\mathrm{tr}\left\{\mathbb{M}^j_{k_1q_1}\mathbb{M}^{j'}_{q_1q_2}\left(i\tau_\psi\right)\right.$$
$$\left.\times\left[g^R_{q_2}(\omega)V_{q_2}G^R_{dd}(\omega)V_{k_1}g^R_{k_1}(\omega)-g^A_{q_2}(\omega)V_{q_2}G^A_{dd}(\omega)V_{k_1}g^A_{k_1}(\omega)\right]\right\}. \tag{B.18}$$

Using Eqs. (3.22), (3.35), (B.5) and (B.6), a huge simplification takes place:

$$G'^D_{jj',0R}(\Omega)$$
$$=2\int_{-\pi}^{\pi}\frac{dk_1dq_1dq_2}{(2\pi)^4}\int d\omega\frac{f(\omega)-f(\varepsilon_{q_1})}{\omega-\varepsilon_{q_1}+\Omega^+}ig^R_{q_2}(\omega)G^R_{dd}(\omega)g^R_{k_1}(\omega)\sum_{r_1r_2}t^*_{r_1}t_{r_2}$$
$$\times\Gamma_{r_1j}(k_1)\left[\delta_{jj'}\frac{1}{1-e^{i(k_1-q_1+i0)}}+S_{jj'}(q_1)\frac{1}{1-e^{i(k_1+q_1+i0)}}\right]\Gamma^*_{r_2j'}(q_2)\frac{1}{1-e^{i(q_1-q_2+i0)}}, \tag{B.19a}$$

$$
\begin{aligned}
&G'^{D}_{jj',0A}(\Omega) \\
&= 2\int_{-\pi}^{\pi} \frac{dk_1 dq_1 dq_2}{(2\pi)^4} \int d\omega \frac{f(\omega)-f(\varepsilon_{q_1})}{\omega-\varepsilon_{q_1}+\Omega^+}(-i)\, g^A_{q_2}(\omega)\, G^A_{dd}(\omega)\, g^A_{k_1}(\omega) \sum_{r_1 r_2} t^*_{r_1} t_{r_2} \\
&\times \Gamma_{r_1 j}(k_1) \left[\delta_{jj'} \frac{1}{1-e^{i(k_1-q_1+i0)}} + S_{jj'}(q_1) \frac{1}{1-e^{i(k_1+q_1+i0)}}\right] \Gamma^*_{r_2 j'}(q_2) \frac{1}{1-e^{i(q_1-q_2+i0)}}.
\end{aligned} \tag{B.19b}
$$

Writing $\omega = \varepsilon_k$, where $0 \le k \le \pi$ or $k = i|k|$, we are now free to do the k_1 and q_2 integrals. The poles of $\Gamma(k_1)$ and $\Gamma^*(q_2)$ are again not important in the dc limit:

$$
\begin{aligned}
&G'^{D}_{jj',0R}(\Omega) \\
&= 2\int_{-\pi}^{\pi} \frac{dq_1}{(2\pi)^2} \int d\varepsilon_k \frac{f(\varepsilon_k)-f(\varepsilon_{q_1})}{\varepsilon_k-\varepsilon_{q_1}+\Omega^+} i \sum_{r_1 r_2} t^*_{r_1} t_{r_2} \frac{1}{2it\sin k} G^R_{dd}(\varepsilon_k) \frac{1}{2it\sin k} \\
&\times \Gamma_{r_1 j}(k) \left[\delta_{jj'} \frac{1}{1-e^{i(k-q_1+i0)}} + S_{jj'}(q_1) \frac{1}{1-e^{i(k+q_1+i0)}}\right] \Gamma^*_{r_2 j'}(-k) \frac{1}{1-e^{i(q_1+k+i0)}} + O(1),
\end{aligned} \tag{B.20a}
$$

$$
\begin{aligned}
&G'^{D}_{jj',0A}(\Omega) \\
&= 2\int_{-\pi}^{\pi} \frac{dq_1}{(2\pi)^2} \int d\varepsilon_k \frac{f(\varepsilon_k)-f(\varepsilon_{q_1})}{\varepsilon_k-\varepsilon_{q_1}+\Omega^+} (-i) \sum_{r_1 r_2} t^*_{r_1} t_{r_2} \frac{1}{-2it\sin k} G^A_{dd}(\varepsilon_k) \frac{1}{-2it\sin k} \\
&\times \Gamma_{r_1 j}(-k) \left[\delta_{jj'} \frac{1}{1-e^{i(-k-q_1+i0)}} + S_{jj'}(q_1) \frac{1}{1-e^{i(-k+q_1+i0)}}\right] \Gamma^*_{r_2 j'}(k) \frac{1}{1-e^{i(q_1-k+i0)}} + O(1).
\end{aligned} \tag{B.20b}
$$

Now do the ε_k and q_1 integrals. The $\delta_{jj'}$ terms are regular in the dc limit, so we only need to keep the $S_{jj'}$ terms. In the $0R$ term, while the q_1 integral in the $f(\varepsilon_k)$ part is straightforward, the ε_k integral

in the $f(\varepsilon_{q_1})$ part can be simplified by expanding around $k+q_1=0$:

$$\begin{aligned}
&G'^{D}_{jj',0R}(\Omega)\\
&=2\frac{1}{2\pi}\int_{-2t}^{2t-\Omega}d\varepsilon_k\frac{f(\varepsilon_k)}{2it\sin p}i\sum_{r_1r_2}t^*_{r_1}t_{r_2}\frac{1}{2it\sin k}G^R_{dd}(\varepsilon_k)\frac{\Gamma_{r_1j}(k)\Gamma^*_{r_2j'}(-k)}{2it\sin k}S_{jj'}(p)\\
&\times\frac{1}{\left[1-e^{i(k+p+i0)}\right]^2}-2\int_{-\pi}^{0}\frac{dq_1}{(2\pi)^2}(2t\sin q_1)S_{jj'}(q_1)\int_{-\infty}^{\infty}d\varepsilon_k\frac{f(\varepsilon_{q_1})}{(\varepsilon_k-\varepsilon_{q_1}+\Omega^+)}\\
&\times i\sum_{r_1r_2}t^*_{r_1}t_{r_2}G^R_{dd}(\varepsilon_k)\frac{\Gamma_{r_1j}(k)\Gamma^*_{r_2j'}(-k)}{2t\sin k}\frac{1}{(\varepsilon_k-\varepsilon_{-q_1}+i0)^2}+O(1)\\
&=O(1).
\end{aligned}\tag{B.21a}$$

Here, in the $f(\varepsilon_k)$ part, we have written $\varepsilon_k+\Omega\equiv\varepsilon_p$ $(0\le p\le\pi)$ assuming $\Omega>0$, integrated over q_1 using the complex variable e^{iq_1}, and again neglected $O(1)$ contributions from the poles of $S(q_1)$. Because $k+p$ is always positive and never close to 0, the denominator for the $f(\varepsilon_k)$ part is $O(1)$; thus the $f(\varepsilon_k)$ part is itself $O(1)$. Meanwhile, in the $f(\varepsilon_{q_1})$ part, we have used $(2t\sin k)(k+q_1+i0)\approx(2t\sin q_1)(k+q_1+i0)\approx\varepsilon_k-\varepsilon_{-q_1}+i0$ for $|k+q_1|\ll 1$. We then extend the ε_k domain of integration back to the entire real axis. Both $G^R_{dd}(\varepsilon_k)$ and $\Gamma_{r_1j}(k)\Gamma^*_{r_2j'}(-k)/(\sin k)$ are analytic in the upper ε_k half plane; thus, closing the ε_k contour above the real axis, the ε_k integral in the $f(\varepsilon_{q_1})$ part sees no pole and vanishes. Similarly, in the $0A$ term,

$$\begin{aligned}
&G'^{D}_{jj',0A}(\Omega)\\
&=2\frac{1}{2\pi i}\int_{-2t}^{2t-\Omega}d\varepsilon_k f(\varepsilon_k)(-i)\sum_{r_1r_2}t^*_{r_1}t_{r_2}G^A_{dd}(\varepsilon_k)\frac{\Gamma_{r_1j}(-k)\Gamma^*_{r_2j'}(k)}{2t\sin k}S_{jj'}(p)\frac{1}{\Omega^2}\\
&-2\int_{-2t+\Omega}^{2t}\frac{d\varepsilon_{q_1}}{2\pi i}S_{jj'}(q_1)f(\varepsilon_{q_1})(-i)\sum_{r_1r_2}t^*_{r_1}t_{r_2}G^A_{dd}(\varepsilon_{p_1})\frac{\Gamma_{r_1j}(-p_1)\Gamma^*_{r_2j'}(p_1)}{2t\sin p_1}\frac{1}{\Omega^2}+O(1)\\
&=-2\frac{1}{\pi\Omega}\int_{-2t}^{2t-\Omega}d\varepsilon_k\left[-f'(\varepsilon_k)\right]\sum_{r_1r_2}t^*_{r_1}t_{r_2}\Gamma_{r_1j}(-k)\Gamma^*_{r_2j'}(k)\pi\nu_kG^A_{dd}(\varepsilon_k)S_{jj'}(p)+O(1).
\end{aligned}\tag{B.21b}$$

We have adopted the shorthand $\varepsilon_{q_1}-\Omega\equiv\varepsilon_{p_1}$ $(0\le p_1\le\pi)$ and identified k with p_1 and p with q_1. This result, together with $G'^{D}_{jj',R0}+G'^{D}_{jj',A0}$ which yields its complex conjugate, leads to Eqs. (3.47c) and (3.47d).

B.4 Terms quadratic in T-matrix

We focus on $G'^{D}_{jj',RR}(\Omega)+G'^{D}_{jj',RA}(\Omega)$ first.

$$
\begin{aligned}
&G'^{D}_{jj',RR}(\Omega)+G'^{D}_{jj',RA}(\Omega)\\
&=2\int\frac{d\omega d\omega'}{(2\pi)^2}\frac{f(\omega)-f(\omega')}{\omega-\omega'+\Omega^+}\int_0^{\pi}\frac{dk_1dk_2}{(2\pi)^2}\frac{dq_1dq_2}{(2\pi)^2}\,\mathrm{tr}\Big\{\mathbb{M}^{j}_{k_1k_2}(i\tau_\psi)\,g^R_{k_2}(\omega')\,V_{k_2}G^R_{dd}(\omega')\,V_{q_1}g^R_{q_1}(\omega')\\
&\times\mathbb{M}^{j'}_{q_1q_2}(i\tau_\psi)\left[g^R_{q_2}(\omega)\,V_{q_2}G^R_{dd}(\omega)\,V_{k_1}g^R_{k_1}(\omega)-g^A_{q_2}(\omega)\,V_{q_2}G^A_{dd}(\omega)\,V_{k_1}g^A_{k_1}(\omega)\right]\Big\}. \qquad \text{(B.22)}
\end{aligned}
$$

Inserting Eqs. (3.22), (3.35) and using Eq. (B.6) again, we find

$$
\begin{aligned}
&G'^{D}_{jj',RR}(\Omega)+G'^{D}_{jj',RA}(\Omega)\\
&=2\int\frac{d\omega d\omega'}{(2\pi)^2}\frac{f(\omega)-f(\omega')}{\omega-\omega'+\Omega^+}\int_{-\pi}^{\pi}\frac{dk_1dk_2}{(2\pi)^2}\frac{dq_1dq_2}{(2\pi)^2}\sum_{r_1r_2r'_1r'_2}t^*_{r_1}t_{r_2}t^*_{r'_1}t_{r'_2}\Gamma_{r_1j}(k_1)\\
&\times\Gamma^*_{r_2j}(k_2)\,\frac{1}{1-e^{i(k_1-k_2+i0)}}ig^R_{k_2}(\omega')\,G^R_{dd}(\omega')\,g^R_{q_1}(\omega')\,\Gamma_{r'_1j'}(q_1)\,\Gamma^*_{r'_2j'}(q_2)\\
&\times\frac{1}{1-e^{i(q_1-q_2+i0)}}i\left[g^R_{q_2}(\omega)\,G^R_{dd}(\omega)\,g^R_{k_1}(\omega)-g^A_{q_2}(\omega)\,G^A_{dd}(\omega)\,g^A_{k_1}(\omega)\right]. \qquad \text{(B.23)}
\end{aligned}
$$

We can integrate over all four momenta. Let $\omega=\varepsilon_k$ where $0\le k\le\pi$ or $k=i|k|$, and $\omega'=\varepsilon_{k'}$ where $0\le k'\le\pi$ or $k'=-i|k'|$; integrating over k_2 and q_1,

$$
\begin{aligned}
&G'^{D}_{jj',RR}(\Omega)+G'^{D}_{jj',RA}(\Omega)\\
&=2\int\frac{d\varepsilon_k d\varepsilon_{k'}}{(2\pi)^2}\frac{f(\varepsilon_k)-f(\varepsilon_{k'})}{\varepsilon_k-\varepsilon_{k'}+\Omega^+}\int_{-\pi}^{\pi}\frac{dk_1dq_2}{(2\pi)^2}\sum_{r_1r_2r'_1r'_2}t^*_{r_1}t_{r_2}t^*_{r'_1}t_{r'_2}\Gamma_{r_1j}(k_1)\\
&\times\Gamma^*_{r_2j}(-k')\,\frac{1}{1-e^{i(k_1+k'+i0)}}i\frac{1}{2it\sin k'}G^R_{dd}(\varepsilon_{k'})\,\frac{1}{2it\sin k'}\Gamma_{r'_1j'}(k')\,\Gamma^*_{r'_2j'}(q_2)\\
&\times\frac{1}{1-e^{i(k'-q_2+i0)}}i\left[g^R_{q_2}(\varepsilon_k)\,G^R_{dd}(\varepsilon_k)\,g^R_{k_1}(\varepsilon_k)-g^A_{q_2}(\varepsilon_k)\,G^A_{dd}(\varepsilon_k)\,g^A_{k_1}(\varepsilon_k)\right]; \qquad \text{(B.24)}
\end{aligned}
$$

finally, integrating over k_1 and q_2, we find

$$
G'^{D}_{jj',RR}(\Omega)=O(1), \qquad \text{(B.25a)}
$$

$$
\begin{aligned}
&G'^{D}_{jj',RA}(\Omega) \\
&= 2\int \frac{d\varepsilon_k d\varepsilon_{k'}}{(2\pi)^2} \frac{f(\varepsilon_k) - f(\varepsilon_{k'})}{\varepsilon_k - \varepsilon_{k'} + \Omega^+} \sum_{r_1 r_2 r_1' r_2'} t^*_{r_1} t_{r_2} t^*_{r_1'} t_{r_2'} \Gamma_{r_1 j}(-k) \Gamma^*_{r_2 j}\left(-k'\right) \Gamma_{r_1' j'}\left(k'\right) \\
&\times \Gamma^*_{r_2' j'}(k) \frac{1}{(2t\sin k')^2} \frac{1}{(2t\sin k)^2} \frac{1}{\left[1 - e^{i(k'-k+i0)}\right]^2} G^R_{dd}(\varepsilon_{k'}) G^A_{dd}(\varepsilon_k). \qquad \text{(B.25b)}
\end{aligned}
$$

Expanding around $k = k'$ and integrating over ε_k and $\varepsilon_{k'}$, assuming $\Omega > 0$, we obtain

$$
\begin{aligned}
&G'^{D}_{jj',RA}(\Omega) \\
&= 2\int_{-2t}^{2t-\Omega} \frac{d\varepsilon_k}{2\pi i} \Omega\left[-f'(\varepsilon_k)\right] \sum_{r_1 r_2 r_1' r_2'} t^*_{r_1} t_{r_2} t^*_{r_1'} t_{r_2'} \frac{\Gamma_{r_1 j}(-k) \Gamma^*_{r_2' j'}(k)}{2t\sin k} \\
&\times \frac{\Gamma^*_{r_2 j}(-p) \Gamma_{r_1' j'}(p)}{2t\sin p} \frac{1}{-\Omega^2} G^R_{dd}(\varepsilon_p) G^A_{dd}(\varepsilon_k) + O(1), \qquad \text{(B.26)}
\end{aligned}
$$

where we have written $\varepsilon_k + \Omega \equiv \varepsilon_p$. A similar calculation can be performed on $G'^{D}_{jj',AR}(\Omega)$ and $G'^{D}_{jj',AA}(\Omega)$; both are $O(1)$ for the same reason that $G'^{D}_{jj',RR}(\Omega)$ is $O(1)$. Therefore, $G'^{D}_{jj',RA}$ is the only term quadratic in the T-matrix which contributes to the linear dc conductance. Note that this is not the case in Ref. [66], where the *RA* term and the *AR* term are complex conjugates as a result of taking the δ-function part in Eq. (3.38). It is easy to see that Eq. (B.26) reproduces Eq. (3.47e).

We mention in passing that Eq. (3.47a) can be derived in the wide band limit with essentially the same method, although the pole structure is much simpler in that case.

Appendix C

Details of weak-coupling and FL perturbation theory

This appendix contains technical details related to the perturbation theory calculation[112] in Section 3.4.

C.1 Weak-coupling perturbation theory

In this subsection, we present the details for the perturbation theory in the weak-coupling regime. These include the calculations of the T-matrix and the connected contribution, both to the third order in the Kondo coupling J.

C.1.1 T-matrix

The object of interest is imaginary time two-point Green's function of the screening basis. Keeping all terms up to $O\left(V^4\right)$ and only the divergent terms at $O\left(V^6\right)$, the Fourier transformed Green's function has the form

$$
\begin{aligned}
&-\int_0^\beta d\tau e^{i\omega_n\tau}\left\langle T_\tau \psi_k(\tau)\,\psi_{k'}^\dagger(0)\right\rangle_{\mathrm{H}} \\
&= 2\pi\delta\left(k-k'\right)g_k(i\omega_n)+K_{kk'}g_k(i\omega_n)\,g_{k'}(i\omega_n)+\int\frac{dq}{2\pi}\int_0^\beta d\tau e^{i\omega_n\tau}\int_0^\beta d\tau_1 d\tau_2 g_k(\tau-\tau_1)\,g_q(\tau_1-\tau_2)\,g_{k'}(\tau_2) \\
&\times\left[K_{kq}K_{qk'}+\frac{1}{4}\sum_{ab}J_{kq}J_{qk'}\sigma^a\sigma^b\left\langle T_\tau S_d^a(\tau_1)\,S_d^b(\tau_2)\right\rangle\right]+\int\frac{dq_1dq_2}{(2\pi)^2}\int_0^\beta d\tau e^{i\omega_n\tau}\int_0^\beta d\tau_1 d\tau_2 d\tau_3 J_{kq_1}J_{q_1q_2}J_{q_2k'} \\
&\times g_k(\tau-\tau_1)\,g_{q_1}(\tau_1-\tau_2)\,g_{q_2}(\tau_2-\tau_3)\,g_{k'}(\tau_3)\,\frac{1}{8}\sum_{abc}\sigma^a\sigma^b\sigma^c\left\langle T_\tau S_d^a(\tau_1)\,S_d^b(\tau_2)\,S_d^c(\tau_3)\right\rangle, \qquad \text{(C.1)}
\end{aligned}
$$

where the subscript H stands for Heisenberg picture,

$$g_p(i\omega_n) = \frac{1}{i\omega_n - \varepsilon_p} \tag{C.2}$$

is the Fourier transform of the free Matsubara Green's function Eq. (3.53), $\omega_n = (2n+1)\pi/\beta$, and we have used the fact that the free propagators are proportional to identity in spin space and therefore commute with the Pauli matrices. Recalling Eq. (3.69), the imaginary time integrals in the third term are trivial after Fourier transform. In the $O\left(J^3\right)$ term, the τ integral is also easy after Fourier transform, but integrals over τ_1, τ_2 and τ_3 are best calculated in the time domain. The time-ordered product of spins evaluates to

$$\begin{aligned}
&\left\langle T_\tau S_d^a(\tau_1) S_d^b(\tau_2) S_d^c(\tau_3) \right\rangle \\
&= \frac{1}{8} i\varepsilon^{abc} \left[\theta(\tau_1,\tau_2,\tau_3) - \theta(\tau_1,\tau_3,\tau_2) - \theta(\tau_2,\tau_1,\tau_3) + \theta(\tau_2,\tau_3,\tau_1) + \theta(\tau_3,\tau_1,\tau_2) - \theta(\tau_3,\tau_2,\tau_1)\right] \\
&= \frac{1}{8} i\varepsilon^{abc} \left\{2\left[\theta(\tau_1,\tau_2,\tau_3) + \theta(\tau_2,\tau_3,\tau_1) + \theta(\tau_3,\tau_1,\tau_2)\right] - 1\right\},
\end{aligned} \tag{C.3}$$

where ε^{abc} is the 3D Levi-Civita symbol and $\theta(\tau_1,\tau_2,\tau_3) = \theta(\tau_1-\tau_2)\,\theta(\tau_2-\tau_3)$. The non-trivial time-ordering is known to produce a logarithmic divergence. Straightforward algebra yields

$$\begin{aligned}
&\int_0^\beta d\tau_1 d\tau_2 d\tau_3 e^{i\omega_n\tau_1} g_{q_1}(\tau_1-\tau_2)\, g_{q_2}(\tau_2-\tau_3)\, g_{k'}(\tau_3) \left(2\left[\theta(\tau_1,\tau_2,\tau_3) + \theta(\tau_2,\tau_3,\tau_1) + \theta(\tau_3,\tau_1,\tau_2)\right] - 1\right) \\
&= g_{k'}(i\omega_n) \frac{1}{\varepsilon_{q_2} - \varepsilon_{q_1}} \left\{ g_{q_1}(i\omega_n)\left[f(\varepsilon_{q_2}) - f(-\varepsilon_{q_2})\right] - g_{q_2}(i\omega_n)\left[f(\varepsilon_{q_1}) - f(-\varepsilon_{q_1})\right] \right\};
\end{aligned} \tag{C.4}$$

therefore, using $\sigma^a\sigma^b\sigma^c = i\varepsilon^{abc}$ and $\sum_{abc}\varepsilon^{abc}\varepsilon^{abc} = 6$, we can write

$$-\int_0^\beta d\tau e^{i\omega_n\tau} \left\langle T_\tau \psi_k(\tau)\, \psi_{k'}^\dagger(0) \right\rangle_{\mathrm{H}} = 2\pi\delta\left(k-k'\right) g_k(i\omega_n) + g_k(i\omega_n)\, \mathrm{T}_{kk'}(i\omega_n)\, g_{k'}(i\omega_n), \tag{C.5}$$

where

$$\begin{aligned}
\mathrm{T}_{kk'}(i\omega_n) = K_{kk'} &+ \int \frac{dq}{2\pi} g_q(i\omega_n) \left(K_{kq}K_{qk'} + \frac{3}{16} J_{kq}J_{qk'} \right) - \frac{3}{32} \int \frac{dq_1 dq_2}{(2\pi)^2} J_{kq_1} J_{q_1q_2} J_{q_2k'} \\
&\times \frac{1}{\varepsilon_{q_2} - \varepsilon_{q_1}} \left\{ g_{q_1}(i\omega_n)\left[f(\varepsilon_{q_2}) - f(-\varepsilon_{q_2})\right] - g_{q_2}(i\omega_n)\left[f(\varepsilon_{q_1}) - f(-\varepsilon_{q_1})\right] \right\}.
\end{aligned} \tag{C.6}$$

Upon analytic continuation, we find the retarded T-matrix

$$\nu \mathrm{T}_{kk'}(\Omega) = \left[\nu K_{kk'} + \nu^2 \int d\varepsilon_q \frac{1}{\Omega^+ - \varepsilon_q} \left(K_{kq} K_{qk'} + \frac{3}{16} J_{kq} J_{qk'} \right) \right.$$
$$\left. - \nu^3 \int d\varepsilon_q d\varepsilon_{q'} \frac{3}{16} \frac{J_{kq} J_{qq'} J_{q'k'}}{\Omega^+ - \varepsilon_q} \frac{f(\varepsilon_{q'}) - f(-\varepsilon_{q'})}{\varepsilon_{q'} - \varepsilon_q} \right], \tag{C.7}$$

where ν is the Fermi surface density of states. We have used Eqs. (3.25b) and (3.25d), noticing that j_k and κ_k are essentially independent of k in the Kondo limit; the dummy variables q_1 and q_2 are then interchangeable, and are rewritten as q and q'.

If we imagine that our Kondo model were defined for dilute impurities rather than a single mesoscopic device, then translational invariance would be recovered after impurity averaging, and the imaginary part of the on-shell self-energy would represent the single particle lifetime, which is a physical observable. Therefore, when we reduce the momentum cutoff of the continuum Kondo model, the imaginary part of the on-shell self-energy per unit impurity concentration, or equivalently the imaginary part of the on-shell T-matrix, should be cutoff independent. It is given by

$$\mathrm{Im}\,\mathrm{T}_{kk}(\varepsilon_k) = \left(-\pi \nu V_k^2\right) V_k^2 \left\{ \frac{1}{4}\kappa^2 + \frac{3}{4} \left[j - \nu j^2 \int d\varepsilon_q V_q^2 \frac{f(\varepsilon_q) - f(-\varepsilon_q)}{\varepsilon_q - \varepsilon_k} \right]^2 \right\}. \tag{C.8}$$

As the running energy cutoff is reduced from D to $D - \delta D$, we recover Eq. (3.27) [or equivalently Eq. (3.26)], the RG equation for the coupling constant j (or $J_{kk'}$).

C.1.2 Connected contribution to the conductance

The second order calculation has been discussed previously so we focus on the third order. Two non-zero diagrams exist at this order:

$$\mathscr{G}^{C(3)}_{k_1 k_2 q_1 q_2}(i\omega_p) = \int_0^\beta d\tau e^{i\omega_p \tau} \int_0^\beta d\tau_1 d\tau_2 d\tau_3 \frac{1}{8} \mathrm{tr}\left(\sigma^a \sigma^b \sigma^c\right) \sum_{abc} \left\langle T_\tau S_d^a(\tau_1) S_d^b(\tau_2) S_d^c(\tau_3) \right\rangle \int \frac{dq}{2\pi}$$
$$\times \left[J_{q_2 q} J_{q k_1} J_{k_2 q_1} g_{q_2}(-\tau_1) g_q(\tau_1 - \tau_2) g_{k_1}(\tau_2 - \tau) g_{k_2}(\tau - \tau_3) g_{q_1}(\tau_3) \right.$$
$$\left. + J_{q_2 k_1} J_{k_2 q} J_{q q_1} g_{q_2}(-\tau_1) g_{k_1}(\tau_1 - \tau) g_{k_2}(\tau - \tau_2) g_q(\tau_2 - \tau_3) g_{q_1}(\tau_3) \right]. \tag{C.9}$$

The τ integral becomes trivial in the frequency domain. By Eq. (C.3),

$$\mathscr{G}^{C(3)}_{k_1k_2q_1q_2}(i\omega_p) = -\frac{3}{16}\frac{1}{\beta}\sum_{\omega_{n_1}} g_{k_1}(i\omega_{n_1})\, g_{k_2}(i\omega_{n_1}+i\omega_p)\int\frac{dq}{2\pi}\int_0^\beta d\tau_1 d\tau_2 d\tau_3$$
$$\times\{2[\theta(\tau_1,\tau_2,\tau_3)+\theta(\tau_2,\tau_3,\tau_1)+\theta(\tau_3,\tau_1,\tau_2)]-1\}$$
$$\times\Big[J_{q_2q}J_{qk_1}J_{k_2q_1}g_{q_2}(-\tau_1)\, g_q(\tau_1-\tau_2)\, e^{-i\omega_{n_1}\tau_2}e^{i(\omega_{n_1}+\omega_p)\tau_3}g_{q_1}(\tau_3)$$
$$+J_{q_2k_1}J_{k_2q}J_{qq_1}g_{q_2}(-\tau_1)\, e^{-i\omega_{n_1}\tau_1}e^{i(\omega_{n_1}+\omega_p)\tau_2}g_q(\tau_2-\tau_3)\, g_{q_1}(\tau_3)\Big]. \tag{C.10}$$

These two terms contribute equally and we show the details for the first term only. Integrate over τ_1, τ_2 and τ_3:

$$\int_0^\beta d\tau_1 d\tau_2 d\tau_3\{2[\theta(\tau_1,\tau_2,\tau_3)+\theta(\tau_2,\tau_3,\tau_1)+\theta(\tau_3,\tau_1,\tau_2)]-1\}\, g_{q_2}(-\tau_1)\, g_q(\tau_1-\tau_2)\, e^{-i\omega_{n_1}\tau_2}e^{i(\omega_{n_1}+\omega_p)\tau_3}g_{q_1}(\tau_3)$$
$$=\frac{1}{\varepsilon_{q_1}-\varepsilon_{q_2}-i\omega_p}\left\{\frac{f(\varepsilon_q)-f(-\varepsilon_q)}{\varepsilon_{q_2}-\varepsilon_q}\frac{1}{i\omega_{n_1}-\varepsilon_{q_2}}-\frac{f(\varepsilon_q)-f(-\varepsilon_q)}{\varepsilon_{q_1}-\varepsilon_q-i\omega_p}\frac{1}{i\omega_{n_1}+i\omega_p-\varepsilon_{q_1}}\right.$$
$$\left.-\left[\frac{f(\varepsilon_{q_2})-f(-\varepsilon_{q_2})}{\varepsilon_{q_2}-\varepsilon_q}-\frac{f(\varepsilon_{q_1})-f(-\varepsilon_{q_1})}{\varepsilon_{q_1}-\varepsilon_q-i\omega_p}\right]\frac{1}{i\omega_{n_1}-\varepsilon_q}\right\}; \tag{C.11}$$

this allows us to do the ω_{n_1} summation, e.g.

$$-\frac{1}{\beta}\sum_{i\omega_{n_1}}\frac{1}{i\omega_{n_1}-\varepsilon_{k_1}}\frac{1}{i\omega_{n_1}+i\omega_p-\varepsilon_{k_2}}\frac{1}{i\omega_{n_1}-\varepsilon_q}$$
$$=-f(\varepsilon_{k_2})\frac{1}{\varepsilon_{k_2}-\varepsilon_{k_1}-i\omega_p}\frac{1}{\varepsilon_{k_2}-\varepsilon_q-i\omega_p}+\int\frac{d\omega}{2\pi i}f(\omega)$$
$$\times\frac{1}{\omega+i\omega_p-\varepsilon_{k_2}}\left(\frac{1}{\omega^+-\varepsilon_{k_1}}\frac{1}{\omega^+-\varepsilon_q}-\frac{1}{\omega^--\varepsilon_{k_1}}\frac{1}{\omega^--\varepsilon_q}\right). \tag{C.12}$$

Analytic continuation gives the retarded four-point function,

$$
\begin{aligned}
&G^{C(3)}_{k_1k_2q_1q_2}(\Omega)\\
&=\frac{3}{16}\int\frac{dq}{2\pi}J_{q_2q}J_{qk_1}J_{k_2q_1}\frac{1}{\varepsilon_{q_1}-\varepsilon_{q_2}-\Omega^+}\left\{\frac{f(\varepsilon_q)-f(-\varepsilon_q)}{\varepsilon_{q_2}-\varepsilon_q}\left[-f(\varepsilon_{k_2})\frac{1}{\varepsilon_{k_2}-\varepsilon_{k_1}-\Omega^+}\frac{1}{\varepsilon_{k_2}-\varepsilon_{q_2}-\Omega^+}\right.\right.\\
&\left.+\int\frac{d\omega}{2\pi i}f(\omega)\frac{1}{\omega+\Omega^+-\varepsilon_{k_2}}\left(\frac{1}{\omega^+-\varepsilon_{k_1}}\frac{1}{\omega^+-\varepsilon_{q_2}}-\frac{1}{\omega^--\varepsilon_{k_1}}\frac{1}{\omega^--\varepsilon_{q_2}}\right)\right]\\
&-\frac{f(\varepsilon_q)-f(-\varepsilon_q)}{\varepsilon_{q_1}-\varepsilon_q-\Omega^+}\left[-f(\varepsilon_{k_1})\frac{1}{\varepsilon_{k_1}+\Omega^+-\varepsilon_{k_2}}\frac{1}{\varepsilon_{k_1}+\Omega^+-\varepsilon_{q_1}}\right.\\
&+\int\frac{d\omega}{2\pi i}f(\omega)\frac{1}{\omega-\Omega^+-\varepsilon_{k_1}}\left(\frac{1}{\omega^+-\varepsilon_{k_2}}\frac{1}{\omega^+-\varepsilon_{q_1}}-\frac{1}{\omega^--\varepsilon_{k_2}}\frac{1}{\omega^--\varepsilon_{q_1}}\right)\Big]\\
&-\left[\frac{f(\varepsilon_{q_2})-f(-\varepsilon_{q_2})}{\varepsilon_{q_2}-\varepsilon_q}-\frac{f(\varepsilon_{q_1})-f(-\varepsilon_{q_1})}{\varepsilon_{q_1}-\varepsilon_q-\Omega^+}\right]\left[-f(\varepsilon_{k_2})\frac{1}{\varepsilon_{k_2}-\varepsilon_{k_1}-\Omega^+}\frac{1}{\varepsilon_{k_2}-\varepsilon_q-\Omega^+}\right.\\
&\left.\left.+\int\frac{d\omega}{2\pi i}f(\omega)\frac{1}{\omega+\Omega^+-\varepsilon_{k_2}}\left(\frac{1}{\omega^+-\varepsilon_{k_1}}\frac{1}{\omega^+-\varepsilon_q}-\frac{1}{\omega^--\varepsilon_{k_1}}\frac{1}{\omega^--\varepsilon_q}\right)\right]\right\}+\text{equivalent contribution.}
\end{aligned}
\tag{C.13}
$$

Substituting Eq. (C.13) into Eq. (3.73), we can perform many of the integrals over k_1, k_2, q_1 and q_2 using contour methods. We should be careful how the contours are closed: for instance, the $i/(k_1-k_2+i0)$ term in Eq. (3.73) (which derives from the particle number operator in a lead) should be interpreted as $\int_0^\infty dx e^{i(k_1-k_2+i0)x}$, and forces the k_1 contour to close on the upper half plane and the k_2 contour to close on the lower half plane. When the smoke clears

$$
\begin{aligned}
&G'^{C(3)}_{jj'}(\Omega)\\
&\to\frac{1}{\Omega}\frac{3}{16}\int\frac{dk_1dq_2}{(2\pi)^2}\left[-f'(\varepsilon_{k_1})\right](2i\pi)\,\delta(\varepsilon_{k_1}-\varepsilon_{q_2})\sum_{r_1r_2r_1'r_2'}t^*_{r_1}t_{r_2}t^*_{r_1'}t_{r_2'}\Gamma'^*_{r_1,j,k_1}\Gamma'_{r_2,j,k_1+\frac{\Omega}{v_F}}\Gamma_{r_1',j',q_2+\frac{\Omega}{v_F}}\Gamma^*_{r_2',j',q_2}\\
&\times\int\frac{dq}{2\pi}V_q^2(2j)^3\frac{f(\varepsilon_q)-f(-\varepsilon_q)}{\varepsilon_{q_2}-\varepsilon_q}+\text{equivalent contribution}+O(1)\\
&=\frac{1}{i\pi\Omega}\int d\varepsilon_p\left[-f'(\varepsilon_p)\right]\frac{3\pi^2\nu^3J_{pp}}{16}\mathscr{Z}_{2,jj'}(\varepsilon_p)\int d\varepsilon_qJ_{pq}J_{qp}\frac{f(\varepsilon_q)-f(-\varepsilon_q)}{\varepsilon_p-\varepsilon_q}+O(1).
\end{aligned}
\tag{C.14}
$$

Therefore, we can combine the second and the third order results as follows:

$$
G^C_{jj'}=-\frac{2e^2}{h}\int d\varepsilon_p\left[-f'(\varepsilon_p)\right]\mathscr{T}^C_{jj'}(\varepsilon_p),
\tag{C.15}
$$

where the connected transmission probability is

$$\mathscr{T}^{C}_{jj'}(\varepsilon_p) = \mathscr{Z}_{2,jj'}(\varepsilon_p)\frac{3\pi^2}{16}\left[\nu J_{pp} - \frac{1}{2}\nu^2\int d\varepsilon_q J_{pq}J_{qp}\frac{f(\varepsilon_q)-f(-\varepsilon_q)}{\varepsilon_q-\varepsilon_p}\right]^2 + O\left(J^4\right). \tag{C.16}$$

This is formally similar to the $O\left(J^2\right)$ result Eq. (3.78) but with a renormalized coupling constant J; the renormalization is again consistent with Eq. (3.26).

C.2 FL perturbation theory

In this subsection, we discuss the perturbation theory in the FL regime $T \ll T_K \ll E_V$ (also assuming $E_V \sim E_{\text{conn}}$; see Table 3.1). We first present an alternative derivation of Eq. (3.88), the $O\left(1/T_K^2\right)$ retarded T-matrix obtained in Ref. [3]. Then we perform an additional consistency check on our formalism of eliminating the connected contribution to the dc conductance at low temperatures: we directly compute the connected contribution to $O\left(T^2/T_K^2\right)$, and show that Eq. (3.62) is indeed satisfied.

In momentum space, the leading irrelevant operator Eq. (3.87) takes the form

$$\begin{aligned} H_{int} = &\frac{2\pi v_F^2}{T_K}\int d\eta H(\eta)\int \frac{dq_1dq_2dq_3dq_4}{(2\pi)^4}e^{i(q_1-q_2+q_3-q_4)\eta}:\tilde{\psi}^\dagger_{q_1\alpha}\tilde{\psi}_{q_2\alpha}\tilde{\psi}^\dagger_{q_3\beta}\tilde{\psi}_{q_4\beta}: \\ &-\frac{v_F^2}{T_K}\int d\eta H(\eta)\int\frac{dq_1dq_2}{(2\pi)^2}(q_1+q_2)e^{i(q_1-q_2)\eta}:\tilde{\psi}^\dagger_{q_1\alpha}\tilde{\psi}_{q_2\alpha}:. \end{aligned} \tag{C.17}$$

(We measure all momenta relative to the Fermi wavevector k_F hereafter.) Here η is the location of the operator; the weight function $H(\eta)$ is peaked at the origin and can be approximated as a δ-function above the length scale v_F/T_K. To lighten notations, we take $H(\eta) = \delta(\eta)$ whenever it is unambiguous to do so.

At $O\left(1/T_K^2\right)$ both terms in Eq. (C.17) contribute to the T-matrix, but only the first term plays a role in the connected 4-point function.

C.2.1 T-matrix

To find the retarded T-matrix of the phase-shifted screening channel $\tilde{\psi}$, we begin from the imaginary time 2-point Green's function

$$\tilde{\mathscr{G}}_{kk'}(\tau) \equiv -\left\langle T_\tau \tilde{\psi}_k(\tau)\,\tilde{\psi}^\dagger_{k'}(0)\right\rangle_{\text{H}}. \tag{C.18}$$

This object is diagonal in spin indices. The three diagrams in Fig. 3.4 panel b) evaluate to

$$\tilde{\mathscr{G}}_{kk'}(\tau) = 2\pi\delta\left(k-k'\right)g_k(\tau) - \frac{v_F^2}{T_K}\left(k+k'\right)\int d\tau_1 g_k(\tau-\tau_1)\,g_{k'}(\tau_1) + \left(\frac{v_F^2}{T_K}\right)^2\int\frac{dq}{2\pi}(k+q)$$
$$\times\left(q+k'\right)\int d\eta_1 d\eta_2 H(\eta_1)H(\eta_2)\,e^{i(k\eta_1-k'\eta_2)}e^{iq(\eta_2-\eta_1)}\int d\tau_1 d\tau_2 g_k(\tau-\tau_1)\,g_q(\tau_1-\tau_2)$$
$$\times g_{k'}(\tau_2) - 4\left(\frac{2\pi v_F^2}{T_K}\right)^2\int\frac{dq_2dq_3dq_4}{(2\pi)^3}\int d\eta_1 d\eta_2 H(\eta_1)H(\eta_2)\,e^{i(k\eta_1-k'\eta_2)}$$
$$\times e^{i(q_2-q_3+q_4)(\eta_2-\eta_1)}\int d\tau_1 d\tau_2 g_k(\tau-\tau_1)\,g_{q_2}(\tau_1-\tau_2)\,g_{q_3}(\tau_2-\tau_1)\,g_{q_4}(\tau_1-\tau_2)\,g_{k'}(\tau_2). \tag{C.19}$$

Going to the Fourier space, we identify the imaginary time T-matrix as

$$\tilde{\mathrm{T}}_{kk'}(i\omega_n) = -\frac{v_F^2}{T_K}\left(k+k'\right) + \left(\frac{v_F^2}{T_K}\right)^2\int\frac{dq}{2\pi}(k+q)\left(q+k'\right)\int d\eta_1 d\eta_2 H(\eta_1)H(\eta_2)\,e^{i(k\eta_1-k'\eta_2)}$$
$$\times e^{iq(\eta_2-\eta_1)}g_q(i\omega_n) - 4\left(\frac{2\pi v_F^2}{T_K}\right)^2\int\frac{dq_2dq_3dq_4}{(2\pi)^3}\int d\eta_1 d\eta_2 H(\eta_1)H(\eta_2)\,e^{i(k\eta_1-k'\eta_2)}$$
$$\times e^{i(q_2-q_3+q_4)(\eta_2-\eta_1)}\frac{1}{\beta}\sum_{\omega_{n_2}}\frac{1}{\beta}\sum_{\omega_{n_4}}g_{q_2}(i\omega_{n_2})\,g_{q_3}(i\omega_{n_2}+i\omega_{n_4}-i\omega_n)\,g_{q_4}(i\omega_{n_4}). \tag{C.20}$$

where all Matsubara frequencies are fermionic, e.g. $\omega_n = (2n+1)\pi/\beta$. Both frequency summations are standard,[74] and analytic continuation $i\omega_n \to \omega^+$ yields

$$\tilde{\mathrm{T}}_{kk'}(\omega) = -\frac{v_F^2}{T_K}\left(k+k'\right) + \left(\frac{v_F^2}{T_K}\right)^2\int\frac{dq}{2\pi}(k+q)\left(q+k'\right)\int d\eta_1 d\eta_2 H(\eta_1)H(\eta_2)\,e^{i(k\eta_1-k'\eta_2)}$$
$$\times\frac{e^{iq(\eta_2-\eta_1)}}{\omega^+-\varepsilon_q} - 4\left(\frac{2\pi v_F^2}{T_K}\right)^2\int d\eta_1 d\eta_2 H(\eta_1)H(\eta_2)\,e^{i(k\eta_1-k'\eta_2)}\int\frac{dq_2dq_3dq_4}{(2\pi)^3}$$
$$\times e^{i(q_2-q_3+q_4)(\eta_2-\eta_1)}\frac{\left[-f_B(\varepsilon_{q_3}-\varepsilon_{q_4})-f(\varepsilon_{q_2})\right]\left[f(\varepsilon_{q_4})-f(\varepsilon_{q_3})\right]}{\omega^+-\varepsilon_{q_3}-\varepsilon_{q_4}-\varepsilon_{q_2}}, \tag{C.21}$$

where $f_B(\omega) = 1/\left(e^{\beta\omega}-1\right)$ is the Bose function.

In the q integral we close the contour in the upper half plane for $\eta_2 > \eta_1$, and in the lower half plane for $\eta_2 < \eta_1$; this leads to

$$\int\frac{dq}{2\pi}(k+q)\left(q+k'\right)\frac{e^{iq(\eta_2-\eta_1)}}{\omega^+-\varepsilon_q} = -\frac{i}{v_F}\left(k+\frac{\omega}{v_F}\right)\left(\frac{\omega}{v_F}+k'\right)e^{i\frac{\omega^+}{v_F}(\eta_2-\eta_1)}H(\eta_2-\eta_1). \tag{C.22}$$

For the on-shell T-matrix $\tilde{\mathrm{T}}_{pp}(\varepsilon_p)$, the phase factors involving η_1 and η_2 cancel, and the η integrals become $\int d\eta_1 d\eta_2 H(\eta_1) H(\eta_2) H(\eta_2-\eta_1) = 1/2$. We can simplify the triple integral over q_2, q_3 and q_4 by the contour method in a similar fashion, before using the following identity,

$$\int_{-\infty}^{\infty} d\varepsilon_{q_2} d\varepsilon_{q_3} d\varepsilon_{q_4} \left[f_B(\varepsilon_{q_3}-\varepsilon_{q_4}) + f(\varepsilon_{q_2})\right] \left[f(\varepsilon_{q_4}) - f(\varepsilon_{q_3})\right] \delta(\omega + \varepsilon_{q_3} - \varepsilon_{q_4} - \varepsilon_{q_2}) = \frac{1}{2}\left(\pi^2 T^2 + \omega^2\right), \tag{C.23}$$

which has been given in Ref. [89] in the context of an inelastic scattering collision integral. Collecting all three terms, we recover Eq. (3.88).

C.2.2 Connected contribution to the conductance

Inserting Eqs. (3.72) and (3.85) into the 4-point function Eq. (3.73), and performing the k_1, k_2, q_1 and q_2 integrals, we obtain

$$\begin{aligned}
\mathscr{G}'^{C}_{jj'}(i\omega_p) = \int \frac{dp_1 dp_2 dp_3 dp_4}{(2\pi)^4} \tilde{\mathscr{G}}^{C}_{p_1 p_2 p_3 p_4}(i\omega_p) \sum_{j_1 j_2} \sum_{j_1' j_2'} \mathbb{U}_{1,j_1} \mathbb{U}^*_{1,j_2} \mathbb{U}_{1,j_1'} \mathbb{U}^*_{1,j_2'} \\
\times \left(\delta_{jj_1}\delta_{jj_2} \frac{i}{p_1 - p_2 + i0} + S^*_{jj_1} S_{jj_2} \frac{i}{p_2 - p_1 + i0} \right) \\
\times \left(\delta_{j'j_1'}\delta_{j'j_2'} \frac{i}{p_3 - p_4 + i0} + S^*_{j'j_1'} S_{j'j_2'} \frac{i}{p_4 - p_3 + i0} \right);
\end{aligned} \tag{C.24}$$

we have ignored the momentum dependence of $\mathbb{U}$ and S in the Fermi liquid regime (which is justified at $T_K \ll E_{\mathrm{conn}}$). Here the δ_P-independent connected four-point correlation function for $\tilde{\psi}$ is defined as

$$\tilde{\mathscr{G}}^{C}_{p_1 p_2 p_3 p_4}(i\omega_p) \equiv -\int_0^\beta d\tau e^{i\omega_p \tau} \sum_{\sigma\sigma'} \left\langle T_\tau \tilde{\psi}^\dagger_{p_1\sigma}(\tau) \tilde{\psi}_{p_2\sigma}(\tau) \tilde{\psi}^\dagger_{p_3\sigma'}(0) \tilde{\psi}_{p_4\sigma'}(0) \right\rangle_C. \tag{C.25}$$

We observe that $\delta_{\psi\psi}$ drops out of $\mathscr{G}'^{C}_{jj'}$ completely, which reflects the inelastic nature of the connected contribution.

To $O\left(1/T_K^2\right)$, there are three diagrams resulting in nonzero connected contributions to the linear dc conductance, depicted in Fig. C.1. The corresponding 4-point functions read

$$\begin{aligned}
\tilde{\mathscr{G}}^{C,\mathrm{BCS}}_{p_1 p_2 p_3 p_4}(i\omega_p) = -4\left(\frac{2\pi\nu_F^2}{T_K}\right)^2 \int_0^\beta d\tau e^{i\omega_p\tau} \int_0^\beta d\tau_1 d\tau_2 \sum_{\sigma\sigma'} \delta_{\sigma\bar{\sigma}'} \int \frac{dq_1 dq_3}{(2\pi)^2} \\
\times g_{p_1}(\tau_1 - \tau) g_{p_2}(\tau - \tau_2) g_{p_3}(\tau_1) g_{p_4}(-\tau_2) g_{q_1}(\tau_2 - \tau_1) g_{q_3}(\tau_2 - \tau_1),
\end{aligned} \tag{C.26a}$$

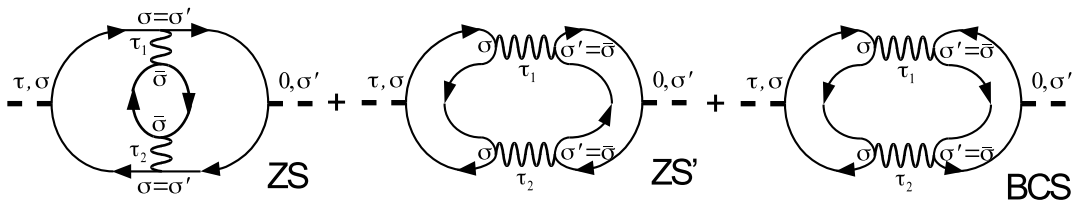

Figure C.1: The three connected diagrams at $O\left(T^2/T_K^2\right)$ contributing to the conductance. ZS, ZS' and BCS label only the topology of the diagrams and not necessarily the physics.

$$\tilde{\mathscr{G}}^{C,\mathrm{ZS}}_{p_1p_2p_3p_4}(i\omega_p) = -4\left(\frac{2\pi\nu_F^2}{T_K}\right)^2 \int_0^\beta d\tau e^{i\omega_p\tau}\int_0^\beta d\tau_1 d\tau_2 \sum_{\sigma\sigma'}\delta_{\sigma\sigma'}\int\frac{dq_3dq_4}{(2\pi)^2}$$
$$\times g_{p_1}(\tau_1-\tau)\,g_{p_2}(\tau-\tau_2)\,g_{p_3}(\tau_2)\,g_{p_4}(-\tau_1)\,g_{q_3}(\tau_2-\tau_1)\,g_{q_4}(\tau_1-\tau_2), \qquad \text{(C.26b)}$$

$$\tilde{\mathscr{G}}^{C,\mathrm{ZS'}}_{p_1p_2p_3p_4}(i\omega_p) = -4\left(\frac{2\pi\nu_F^2}{T_K}\right)^2 \int_0^\beta d\tau e^{i\omega_p\tau}\int_0^\beta d\tau_1 d\tau_2 \sum_{\sigma\sigma'}\delta_{\sigma\bar{\sigma}'}\int\frac{dq_1dq_4}{(2\pi)^2}$$
$$\times g_{p_1}(\tau_1-\tau)\,g_{p_2}(\tau-\tau_2)\,g_{p_3}(\tau_2)\,g_{p_4}(-\tau_1)\,g_{q_1}(\tau_2-\tau_1)\,g_{q_4}(\tau_1-\tau_2). \qquad \text{(C.26c)}$$

Here the terminology of BCS, ZS and ZS′ is borrowed from Ref. [109] and refers only to the topology of the diagrams.

We illustrate the calculation with the BCS diagram; ZS and ZS' again turn out to be completely analogous. Going to the Fourier space,

$$\tilde{\mathscr{G}}^{C,\mathrm{BCS}}_{p_1p_2p_3p_4}(i\omega_p)$$
$$= -\left(\frac{2\pi\nu_F^2}{T_K}\right)^2 8\int\frac{dq_1dq_3}{(2\pi)^2}\frac{1}{\beta}\sum_{\omega_{n_1}}\frac{1}{\beta}\sum_{\omega_{n_3}}\frac{1}{\beta}\sum_{\omega_{n_5}} g_{p_1}(i\omega_{n_1})\,g_{p_2}(i\omega_{n_1}+i\omega_p)$$
$$\times g_{p_3}(i\omega_{n_3})\,g_{p_4}(i\omega_{n_3}-i\omega_p)\,g_{q_1}(i\omega_{n_5})\,g_{q_3}(i\omega_{n_1}+i\omega_{n_3}-i\omega_{n_5}); \qquad \text{(C.27)}$$

the ω_{n_5} summation is standard, whereas the ω_{n_1} and ω_{n_3} summations require the following identities:

$$\begin{aligned}
&\frac{1}{\beta}\sum_{\omega_{n_3}}\frac{1}{i\omega_{n_3}-\varepsilon_{p_3}}\frac{1}{i\omega_{n_3}-i\omega_p-\varepsilon_{p_4}}\frac{1}{i\omega_{n_1}+i\omega_{n_3}-\varepsilon_{q_1}-\varepsilon_{q_3}}\\
&=f(\varepsilon_{p_3})\frac{1}{\varepsilon_{p_3}-i\omega_p-\varepsilon_{p_4}}\frac{1}{i\omega_{n_1}+\varepsilon_{p_3}-\varepsilon_{q_1}-\varepsilon_{q_3}}+f(\varepsilon_{p_4})\frac{1}{i\omega_p+\varepsilon_{p_4}-\varepsilon_{p_3}}\frac{1}{i\omega_{n_1}+i\omega_p+\varepsilon_{p_4}-\varepsilon_{q_1}-\varepsilon_{q_3}}\\
&-f_B(\varepsilon_{q_1}+\varepsilon_{q_3})\frac{1}{\varepsilon_{q_1}+\varepsilon_{q_3}-i\omega_{n_1}-\varepsilon_{p_3}}\frac{1}{\varepsilon_{q_1}+\varepsilon_{q_3}-i\omega_{n_1}-i\omega_p-\varepsilon_{p_4}},
\end{aligned}\tag{C.28a}$$

and

$$\begin{aligned}
&-\frac{1}{\beta}\sum_{\omega_{n_1}}\frac{1}{i\omega_{n_1}-\varepsilon_{p_1}}\frac{1}{i\omega_{n_1}+i\omega_p-\varepsilon_{p_2}}\frac{1}{i\omega_{n_1}+i\omega_p+\varepsilon_{p_4}-\varepsilon_{q_1}-\varepsilon_{q_3}}\\
&=\int_{-\infty}^{\infty}\frac{d\varepsilon}{2\pi i}f(\varepsilon)\frac{1}{\varepsilon-i\omega_p-\varepsilon_{p_1}}\left(\frac{1}{\varepsilon^+-\varepsilon_{p_2}}\frac{1}{\varepsilon^++\varepsilon_{p_4}-\varepsilon_{q_1}-\varepsilon_{q_3}}\right.\\
&\left.-\frac{1}{\varepsilon^--\varepsilon_{p_2}}\frac{1}{\varepsilon^-+\varepsilon_{p_4}-\varepsilon_{q_1}-\varepsilon_{q_3}}\right)-f(\varepsilon_{p_1})\frac{1}{\varepsilon_{p_1}+i\omega_p-\varepsilon_{p_2}}\frac{1}{\varepsilon_{p_1}+i\omega_p+\varepsilon_{p_4}-\varepsilon_{q_1}-\varepsilon_{q_3}},
\end{aligned}\tag{C.28b}$$

where $\varepsilon^{\pm}\equiv\varepsilon\pm i0^+$. The second identity can be derived by allowing the complex plane contour to wrap around the line $\mathrm{Im}\,z=\omega_p$[74].

After applying the identities above, performing analytic continuation $i\omega_p\to\Omega^+$, and performing all p integrals that are approachable by the contour method in Eq. (C.24), we find

$$\begin{aligned}
&G'^{C,\mathrm{BCS}}_{jj'}(\Omega)\\
&=-\left(\frac{2\pi v_F^2}{T_K}\right)^2 8\sum_{j_1j_2}\mathbb{U}_{1,j_1}\mathbb{U}^*_{1,j_2}\mathbb{U}_{1,j'}\mathbb{U}^*_{1,j'}S^*_{jj_1}S_{jj_2}\frac{1}{\Omega}\int\frac{dq_1dq_3}{(2\pi)^2}\left[f(-\varepsilon_{q_1})-f(\varepsilon_{q_3})\right]\\
&\times\left\{\int\frac{dp_1dp_4}{(2\pi)^2}\left[f(\varepsilon_{p_4})+f_B(\varepsilon_{q_1}+\varepsilon_{q_3})\right]\frac{f(\varepsilon_{p_1}+\Omega)-f(\varepsilon_{p_1})}{\Omega}\frac{1}{\varepsilon_{p_1}+\Omega^++\varepsilon_{p_4}-\varepsilon_{q_1}-\varepsilon_{q_3}}\right.\\
&\left.-\int\frac{dp_2dp_3}{(2\pi)^2}\left[f(\varepsilon_{p_3})+f_B(\varepsilon_{q_1}+\varepsilon_{q_3})\right]\frac{f(\varepsilon_{p_2}-\Omega)-f(\varepsilon_{p_2})}{-\Omega}\frac{1}{\varepsilon_{p_2}-\Omega^++\varepsilon_{p_3}-\varepsilon_{q_1}-\varepsilon_{q_3}}\right\}.
\end{aligned}\tag{C.29}$$

In the dc limit, the principal value parts of the integrands cancel to $O(1/\Omega)$, while the δ-function parts remain:

$$G'^{C,\mathrm{BCS}}_{jj'}(\Omega) = -\frac{(2\pi)^2}{T_K^2} 8 \sum_{j_1 j_2} \mathbb{U}_{1,j_1} \mathbb{U}^*_{1,j_2} \mathbb{U}_{1,j'} \mathbb{U}^*_{1,j'} S^*_{jj_1} S_{jj_2} \frac{1}{\Omega} \frac{2i\pi}{(2\pi)^4} \int d\varepsilon_{p_1} \left[-f'(\varepsilon_{p_1})\right]$$
$$\times \int d\varepsilon_{p_4} d\varepsilon_{q_1} d\varepsilon_{q_3} \left[f(\varepsilon_{p_4}) + f_B(\varepsilon_{q_1} + \varepsilon_{q_3})\right] \left[f(-\varepsilon_{q_1}) - f(\varepsilon_{q_3})\right] \delta(\varepsilon_{p_1} + \varepsilon_{p_4} - \varepsilon_{q_1} - \varepsilon_{q_3}) + O(1)$$
$$= -\frac{4}{T_K^2} \sum_{j_1 j_2} \mathbb{U}_{1,j_1} \mathbb{U}^*_{1,j_2} \mathbb{U}_{1,j'} \mathbb{U}^*_{1,j'} S^*_{jj_1} S_{jj_2} \frac{1}{\Omega} \frac{i}{2\pi} \int d\varepsilon_{p_1} \left[-f'(\varepsilon_{p_1})\right] \left(\pi^2 T^2 + \varepsilon_{p_1}^2\right) + O(1). \quad \text{(C.30)}$$

In the second step we have again invoked Eq. (C.23).

Each of the ZS and ZS' contributions ends up being the opposite of the BCS contribution,

$$G'^{C,\mathrm{ZS}}_{jj'}(\Omega) = G'^{C,\mathrm{ZS'}}_{jj'}(\Omega) = -G'^{C,\mathrm{BCS}}_{jj'}(\Omega). \quad \text{(C.31)}$$

therefore, using Eq. (3.22) for the $\mathbb{U}$ matrix elements, we can express the total connected contribution to the conductance to $O\left(1/T_K^2\right)$ as

$$G^C_{jj'} = \frac{e^2}{h} \lim_{\Omega \to 0} (2\pi i \Omega) G'^{C,\mathrm{BCS}}_{jj'}(\Omega) = -\frac{2e^2}{h} \int d\omega \left[-f'(\omega)\right] \mathscr{T}^C_{jj'}(\omega), \quad \text{(C.32)}$$

where

$$\mathscr{T}^C_{jj'}(\omega) = -\frac{2}{V_{k_F}^4} \left[S(k_F) \Gamma^\dagger(k_F) \lambda \Gamma(k_F) S^\dagger(k_F)\right]_{jj} \left[\Gamma^\dagger(k_F) \lambda \Gamma(k_F)\right]_{j'j'} \frac{\pi^2 T^2 + \omega^2}{T_K^2}. \quad \text{(C.33)}$$

We have reintroduced the coupling matrix Eq. (3.20). The ω integral can be done explicitly:

$$G^C_{jj'} = \frac{2e^2}{h} \frac{8}{3V_{k_F}^4} \left| \left[S(k_F) \Gamma^\dagger(k_F) \lambda \Gamma(k_F)\right]_{jj'} \right|^2 \left(\frac{\pi T}{T_K}\right)^2, \quad \text{(C.34)}$$

i.e. the lowest order connected contribution to the conductance is $O\left(T^2/T_K^2\right)$, characteristic of a FL.

Eq. (C.33) is in explicit agreement with Eq. (3.62). We can also check its consistency with the Eq. (3.48) and single-particle T-matrix inelasticity. Recall that, by virtue of Eq. (3.65), we should have the following approximate identity for $\omega \approx 0$ in the FL regime:

$$\mathscr{T}^C_{jj'}(\omega) = -\frac{1}{V_{k_F}^2} \left[S(k_F) \Gamma^\dagger(k_F) \lambda \Gamma(k_F) S^\dagger(k_F)\right]_{jj} \sum_{j''} \mathscr{T}^D_{j''j'}(\omega). \quad \text{(C.35)}$$

On the other hand, Eqs. (3.86) and (3.88) yield for the on-shell T-matrix

$$\mathrm{Im}\left[-\pi\nu \mathrm{T}(\omega)\right] - \left|-\pi\nu \mathrm{T}(\omega)\right|^2 = \frac{\pi^2 T^2 + \omega^2}{2T_K^2}; \quad \text{(C.36)}$$

therefore, plugging Eq. (C.36) into Eq. (3.48), we find that for $\omega \approx 0$,

$$\sum_{j''} \mathscr{T}^{D}_{j''j'}(\omega) = \frac{\pi^2 T^2 + \omega^2}{2T_K^2} \frac{4}{V_{k_F}^2} \left[\Gamma^{\dagger}(k_F)\,\lambda\,\Gamma(k_F)\right]_{j'j'}. \tag{C.37}$$

Eqs. (C.35) and (C.37) are fully consistent with Eq. (C.33).